SYNTHESIS AND SPECTRAL CHARACTERIZATION OF TYROSINE BASED PEPTIDE NANOSTRUCTURES

A THESIS SUBMITTED FOR THE DEGREE OF DOCTOR OF PHILOSOPHY IN THE FACULTY OF SCIENCE, JADAVPUR UNIVERSITY

2021

BY

Mrs. LEENA MAJUMDER

CSIR-INDIAN INSTITUTE OF CHEMICAL BIOLOGY
ORGANIC AND MEDICINAL CHEMISTRY DIVISION
4, RAJA S. C. MULLICK ROAD, JADAVPUR
KOLKATA-700 032, INDIA

INDIAN INSTITUTE OF CHEMICAL BIOLOGY
CSIR-IICB, 4, RAJA S.C.MULLICK ROAD, JADAVPUR,KOLKTA 700032, INDIA
PHONE:+91-33-24730492/3491/3493/6793, FAX: 033-2473 5197/ 2472 3967

Dr. Biswadip Banerji, Senior Principal Scientist
Ph.D (IIT - Kanpur), M.Sc.(Calcutta University)
2009 – Onwards: CSIR-IICB, Kolkata, India
2008: Team Lead, Chembiotek-Kolkata
2006 – 2008: Postdoctoral Research Fellow, (Prof. K.C. Nicolaou); CSL@ICES-A*-STAR
2003 – 2006: Postdoctoral Research Fellow, (Prof. C.J. Schofield); Oxford Centre for Molecular Science (OCMS) & Chemistry-Research Laboratory (CRL), Oxford University, UK.

Office address:
Room No. 17 &12 (Ground Floor)
Phone No. +91-33-24735709
Hand Phone No. 09903752881
Email: biswadip@iicb.res.in
biswadip.banerji@gmail.com

CERTIFICATE FROM THE SUPERVISER

This is to certify that the thesis entitled "SYNTHESIS AND SPECTRAL CHARACTERIZATION OF TYROSINE BASED PEPTIDE NANOSTRUCTURES" submitted by LEENA MAJUMDER, who got her name registered on 19.06.2017 [Registration no. D-7/SC/234/17, Index no. 52/17/Chem./25] for the award of Ph.D. (Science) degree of Jadavpur University, is absolutely based upon her own work under the supervision of Dr. BISWADIP BANERJI and neither this thesis nor any part of it has been submitted for either any degree/diploma or any other academic award anywhere before.

Biswadip Banerji 22/11/21.

(Dr. Biswadip Banerji)

Signature of the supervisor date with official Seal

Dr. Biswadip Banerji
M.Sc (Cal), PhD (IIT-K)
Senior Scientist,
Dept. of Chemistry
Indian Institute of Chemical Biology, CSIR-IICB
4, Raja S. C. Mulick Road, Kolkata-700 032, INDIA

DECLARATION

I, Leena Majumder hereby declare that the work emphasized in this thesis entitled "SYNTHESIS AND SPECTRAL CHARACTERIZATION OF TYROSINE BASED PEPTIDE NANOSTRUCTURES" is my own work and carried under the guidance of Dr. Biswadip Banerji, senior principal scientist, CSIR-Indian Institute of Chemical Biology, Jadavpur, Kolkata, India.

I have duly acknowledged all the sources of information which have been used in this thesis. This thesis has not been submitted in part or full, in any degree or diploma of this or any other university.

Leena Majumder

LEENA MAJUMDER

Organic and Medicinal Chemistry Division

CSIR-Indian Institute of Chemical Biology

Jadavpur, Kolkata-700032

India.

DEDICATED TO MY GOD AND MY PARENTS

Acknowledgement

Today as I am penning down my thesis. This may be my only opportunity to thank these individuals in writing; I may be a bit more verbose in my thanks than necessary.

It gives me a great pleasure to express my gratitude towards all the people who contributed to the completion of this thesis. First and foremost, I would like to express my deepest gratitude to Dr. Biswadip Banerji, for his excellent guidance and support which enabled me to reach this day of thesis completion. I am very lucky to have such a caring, patient, encouraging and experienced supervisor who ensured all the positive inputs to cross all the toughest of the hurdles during this eventful journey. He provided the combination of necessary freedom and control for fulfilling the desired research objectives. I am greatly indebted to him for being my best teacher ever. I will always remember his encouraging stories and brain storming discussions that changed my way of doing science and exploring out of box ideas.

I sincerely thank CSIR-Indian Institute of Chemical Biology for giving me the platform to carry on my research. I take this opportunity to sincerely acknowledge the University Grant Commission under Council of Scientific & Industrial Research, Government of India, New Delhi, for providing financial assistance in the form of Fellowship which buttressed me to perform my work comfortably. I would like to thank Prof. Samit Chattopadhyay, ex director of IICB for allowing me to be a part of this institute. I would like to thank the present director Dr. Arun Bandopadhyay for providing me necessary facilities to carry out my research work. I am also thankful to Dr. Nakul C. Maiti for giving me the opportunity to collaborate with his lab members and his continuous support help me to do some successful research works. I would like to thank each and every

member and staffs of Central Instrumentation Department of CSIR-IICB for helping me with conducting a variety of experiments and processing the data.

I am indebted to my lab seniors. Firstly, thanks to Dr. Moumita Chatterjee, our dearest Moumita di, for her unconditional help throughout my research work. I would like to thank other senior lab members Dr. Chandrasekhar Kadaigadi, Dr. Kill Sunil Kumar, Dr. Satadru Chatterjee and Dr. Saswati Adhikary for their kind support and help. I would like to thank all my lab friends Saswati Ghosh (chotu), Ravuri Srinath (G2), Krishnendu Khamaru, Debabrata Sarkar, Abhudyay Guin, Arindam Manna, Suvankar shee, Saurav Pakrashi and Kaushik Seal, thank you all for maintaining positive environment in the lab and immense support on work bench, without your support it will not possible to complete this journey in such a smooth manner. Their valuable comments, comprehensive exchange of ideas during the research work and creating friendly environment that helped me to handling the difficult situations. I wish all of them every success in their days ahead.

Within this course of PhD, CSIR-IICB has become my family; I would like to thank my fellow doctoral students for their feedback and cooperation. Special thanks to Dr. Moumta Jash, Dr. Amrita Mondal and Dr. Dipendu Patra for being such a good friend. I would like to thank Dr. Kaushik Bera for supporting me all the time whenever needed.

I would like to express my deepest gratitude to my beloved family: my parents Mr. Ranjit Majumder and Mrs. Suparna Majumder for supporting me, my elder brother Mr. Sangram Majumder for his tremendous belief in me, my parents in law Mr. Monoj Kumar Mukhopadhyay, Mrs. Ratna Mukherjee for their encouragement and support. I thank my husband Mr. Mitrabarun Mukhopadhyay for his support and help. I would like to thank some family members Brijesh

Karmakar and Ganesh Patra, for making this journey smooth. Their silent blessings, constant support and encouragement enabled me to reach my destiny.

Above all, I would like to thank my Lord, for giving me the intelligence to understand and resolving the problem arising during the experiment and giving me strength to complete this research.
Thank you.

Leena Majumder
Organic and Medicinal Chemistry Division
CSIR-Indian Institute of Chemical Biology, Kolkata, India

CONTENTS

LIST OF ABBREVATIONS

AFM:	Atomic Force Microscopy
FE-SEM:	Field Emission Scanning Electron Microscopy
TEM:	Transmission Electron Microscopy
FT-IR:	Fourier Transform Infrared
UV-vis:	Ultraviolet visible
Powder XRD:	Powder X-Ray Diffraction
NMR:	Nuclear Magnetic Resonance
ESI:	Electron Spray Ionization
DFT:	Density Functional Theory
CD:	Circular Dichroism
TLC:	Thin Layer Chromatography
BOC:	Tertiary butoxy carbonyl
EDC.HCl:	1-Ethyl-3-(3-dimethylaminopropyl)carbodiimide hydrochloride
HOBt:	Hydroxybenzotriazole
MGC:	Minimum Gelation Concentration
ThT:	Thioflavin T
K_{app}:	Apparent rate constant value
^{o}C:	Temperature in degrees centigrade
G′:	Storage modulus
G″:	Loss modulus

mL:	Milli litre
ppm:	Parts per million
exp:	Experimental
theo:	Theoretical
h:	Hour
min:	Minute
g:	Gram
mg:	Milligram
mM:	Millimolar
μM:	Micromolar
DCM:	Dichloromethane
DMF:	Dimethyl formamide
DMSO:	Dimethyl sulfoxide
TEA:	Triethyl amine
rt:	Room temperature
HOMO:	Highest occupied molecular orbital

GENERAL REMARKS

- ^{1}H NMR and ^{13}C NMR were measured on a Bruker DPX 300 MHz and Bruker DRX 600 MHz NMR instrument. Generally, $CDCl_3$, DMSO-d_6 and MeOD have been used for NMR sample solutions preparation. Chemical shifts (δ) were reported in parts per million (ppm) and tetramethylsilane (δ = 0.00) used as the internal standard. The standard abbreviations s, d, t, q, m, J refers to singlet, doublet, triplet, quartet, multiplet, and the coupling constant respectively.

- Analytical thin layer chromatography (TLC) was obtained via standard Merck TLC silica gel 60 F254 aluminium sheets. Visualization of the spots on TLC plate was achieved through exposure of UV light, iodine vapour etc. Progress of the reaction was monitored via TLC checking. Moisture sensitive reactions were carried out using standard syringe-septum techniques. Column chromatography was carried out with silica gel 60-120 and 100-200 mesh.

- Unless otherwise mentioned, petroleum ether refers to fraction boiling in the range 60-80^{0}C. All reagents and solvents were purified and dried by conventional protocol.

- All evaporation of solvents was carried out under reduced pressure in Heidolph Rotary Evaporator of Cat. No: P/N Hei-VAP Value/G3: 560-01300-001.

- CD spectra (190-400 nm) were recorded at 200 nm/min scan speed, with 1 nm bandwidth on a Jasco J-810 spectrometer using a 10 mm quartz cell.

- AFM images were obtained on Pico Plus 5500 AFM (Agilent Technologies, Inc., Santa Clara, CA, USA) with the piezo scanner range of 9 μm. The images (256 × 256 pixels) were captured with a scan size between 0.5 and 5 μm at the scan speed rate of 0.5 rpm. The images were processed through flattening via Pico view software (Molecular Imaging Inc., Ann Arbor, MI, USA). For this purpose, sample solutions were incubated at room temperature for required time, and then the solution was applied to a mica foil, after drying the sample solution placed at mica foil, the specimen was observed through atomic force microscopy.

- UV−Vis absorption spectra of the samples were acquired using a JASCO V-630 spectrophotometer (JASCO International Co. Ltd., Japan) within the wavelength range of 200−500 nm. A high-quality quartz cuvette having path length 1 cm was used for spectral measurement.

- Fluorescence spectra were measured with the Cary Eclipse (Agilent Technology) fluorescence spectrophotometer.

- Powder XRD study of the dipeptides was carried out by placing the solid sample on a glass plate. Experiments were carried out by using an X-ray diffractometer (Bruker AXS, Model No. D8 Advance).

- The rheological measurement of the gel obtained from dipeptide TP1 in methanol-water solvent system (at a ratio 1:1) was performed using Modular Compact Rheometer (Anton Parr, MCR 102, Austria). The instrument was equipped with an air compressor unit which maintained the air pressure at 7 kg/cm2. Standard cone-plate geometry (CP-40, 40 mm outer diameter, angle 1◦) was employed in the

study. Frequency sweep (G, G versus angular sweep) was measured in oscillation mode. The data was analysed using Rheoplus software (US 200, version 3.62).

- Raman spectra were measured with triple Raman spectrometer (Model: T64000, Make: J-Y Horiba) equipped with 1800 grooves/mm grating, TE cooled synapse CCD and with an open stage Olympus microscope with 50x objective. Each Raman spectra of the solid sample were collected using 533 nm wavelength laser from DPSS laser (Make: spectra physics) excitation 2mW laser power, and 10 s of data acquisition time with each spectral data having average of 4 accumulations. Data analyses with baseline correction were performed using Origin Pro 8.0 SRO software (OriginLab Corporation).

- The FT-IR spectra of the samples were recorded on a Bruker TENSOR27 spectrometer. The KBr disc technique was used to record the spectra of the solid sample. Solid sample was mixed with KBr in a clean glass pestle and compressed to obtain a pellet. Background spectra were obtained for KBr pellet for each sample. Bruker software was used for data processing. Experimental data obtained were analysed using Origin Pro 8.0 SRO software (OriginLab Corporation).

- The formations of self-assembly by peptides were monitored by ThT fluorescence assay measurements. ThT is a normally used dye that emits a strong fluorescence signal upon binding to the cradle of ß-sheet structures often found in fibrillary network produced from proteins/peptides. The more ThT fluorescence (intensity) in the presence of protein sample suggests higher amount of fibril with β-sheet conformation. The peptide solution was prepared by dissolving the solid peptides in methanol and incubated for required hours at ambient temperature (25 ^{o}C). A stock ThT solution was prepared in water. Before spectral measurement, certain volume of peptide solution was added to 1 ml of ThT solution and mixed thoroughly so that

the desired final concentration of the peptide was prepared. The fluorescence measurement was done using Cary Eclipse fluorescence spectrophotometer (Agilent Technology) in a quartz cuvette of 1 cm path length. The excitation and emission slit widths were fixed at 5 nm each and the emission range was 455-600 nm. The chosen excitation wavelength was 445 nm.

. Fluorescence peak intensity values at 485 nm were plotted against time and fitted to the sigmoidal curve equation

$$Y = \frac{y_1 + m_1 x + (y_f + m_f x)}{1 + e^{-[(x - x_0)/\tau]}}$$

ThT fluorescence intensity is denoted by Y, x denotes time, x_0 is the time required to achieve 50% of maximum fluorescence intensity, the apparent rate constant is k_{app}, fibrillar growth is $1/\tau$, and the time period in lag phase is derived by $x_0 - 2\tau$.

PRELUDE

The world is so much larger than we can comprehend, especially without a good microscope! Beyond the limits of our perception, there exists a micro-cosmos so different from our macroscopic world, yet so integrated into our reality. In the nano-regime, the true wonders of life take place and it is here where atoms assemble into molecules and molecules into living organisms. This thesis work, on "Synthesis and Spectral Characterization of Tyrosine Based Peptide Nanostructures" aims to give a glimpse of idea into this captivating world, and in an effort to understand and explain the underlying mechanisms and phenomenon participating there.

In the past few decades, several research efforts were performed on peptide based self-assembling systems. Among them, short peptides have emerged as an interesting research field due to its wide range of applications. The underlying advantages of selecting short peptides lie in the facts that they are easy to design and synthesize. High yield product can be achieved through simple laboratory procedures and peptides are considered as outstanding model systems for studying biological self-assembly. Self-assembly is defined as a spontaneous organization of individual components into well-ordered structures using non-covalent interactions. Short peptide based self-assembled nanostructures have been systematically studied by several research groups. This class of biomaterials has significant potential in a number of applications including nanomedicine, catalysis, light-harvesting, tissue engineering, sensing, templating and nanoelectronics. Thus in this thesis *de-novo* tyrosine based short peptides have been synthesized, their self-assembly pattern and physicochemical properties have been characterized through AFM, FE-SSEM and several vibrational spectroscopic analysis such as FT-IR, NMR, powder XRD, UV-vis

and Fluorescence spectroscopy. This thesis is divided into four chapters. A brief description of each chapter is discussed below, as a snap shot.

Chapter 1

This part contains brief background on peptide based self-assembled nanostructures and their potential applications in industries and academia. As discussed earlier, self-assembly involves low-energy especially non-covalent interactions that are combined to form well-defined and stable supramolecular architechtures. The use of short and simple peptide based derivatives are now considered as a versatile building blocks which offers a suitable platform due to chemical versatility of amino acid motif combined with simplicity and chemical accessibility of peptides. Several studies have already been employed using amphiphilic peptides, cyclic peptides, amyloid inspired peptides and aromatic peptides that can self-assemble into wide range of nano to micro supramolecular architechtures. Therefore, self-recognition of peptide molecules and their applications in modern nanotechnology owing to their specific molecular recognition patterns and the feasibility to manipulate them for specific functions have been discussed here.

Chapter 2

Over the past few decades, short peptide based self-assembled supramolecular gel has gained significant interest due to their special self-assembly and various potential applications in drug delivery, molecular sensing, oil spill recovery and as environmental pollutant removing agents. In this chapter, a small tyrosine based dipeptide was designed and synthesized. Surprisingly, this dipeptide was able to form gel in various solvent mixture. The structural insights of these gels were characterized by FE-SEM, AFM, FT-IR analysis, and X-ray diffraction studies. The mechanical strength of these gels was investigated through rheological experiments. Moreover, the gel obtained from this dipeptide had

potential application for waste water treatment by removing toxic dyes and was used as a phase selective gelator for oil-spillage recovery.

Chapter 3

This section provides detail study of assembly formation and structural intricacy of two *de-novo* tyrosine based dipeptides by NMR and vibrational spectroscopic analysis. In this work, a thorough investigation was carried out on the ability of self-assembly pattern of two benzyl protected tyrosine and different side chain protected glutamic acid residues. The small variation of the substituent groups in the peptide moieties caused significant difference in their self-assembly formation and structural alignment. One of the peptide produced fibrillar network whereas another formed spherical/ oligomeric assembly in the same solvent. The nature of self-assembly pattern of these peptides was both concentration and time dependent. This difference in morphological behaviour motivated us to study them in detail by FT-IR, NMR and Raman spectroscopic analyses. Furthermore, these spectroscopic results were verified by DFT calculation. ThT fluorescence study confirmed that the fibrillary network produced by peptide showed compact ß-sheet formation. Whereas another one with spherical/oligomeric assembly showed no compact ß-sheet formation in ThT study. Interestingly, the fibrillary network produced from one peptide showed gelatinous nature in methanol-water solvent mixture. Rheological experiment was also carried out to understand the flow behaviour and rigidity of the gel.

Chapter 4

In this chapter, efforts were made to synthesize and analyse the self-assembly pattern of di-tyrosine based dipeptide. This dipeptide C-terminally protected by ester group and N-terminally protected by tert-butoxy carbonyl (BOC) group. Furthermore, the side chain of tyrosine residue was protected through benzyl groups. The purpose of synthesizing O-benzyl protected tyrosine dipeptide was

to determine whether this could alter the triggering force for molecular self-assembly and affect the ultimate self-assembled pattern compared to other peptides. The single crystal X-ray analysis of this peptide confirmed that this peptide exhibited in a parallel ß-sheet pattern which further self-assembled to form ß-sheet promoted helical architectures by various non-covalent interactions in the crystalline state. Atomic force microscopy and FE-SEM analyses were carried out to understand the morphological pattern of this dipeptide. FT-IR and NMR analyses employed to find the molecular forces responsible for self-assembly. Furthermore, the experimental result of circular dichroism (CD) spectroscopy gave an idea of nature of self-assembly associated with this dipeptide. Hirshfeld surface analysis and DFT study also carried out for this dipeptide which concluded the same result as obtained from single crystal X-ray, AFM, FE-SEM, and CD analyses.

Chapter 1

General Introduction and Scope of the Present Work

1.1 Brief History of Nanotechnology

Nanoparticles and nanostructures have been used by humans, specifically by the Roman in the fourth century AD. The colorful secret of a 2400 years old Roman chalice (Lycurgus Cup) from the British Museum collection represents a supersensitive new technology that might help diagnose human disease or pinpoint biohazards at security checkpoints (Figure 1). This masterpiece demonstrated an ancient and powerful example of nanotechnology of early civilization. It is one of the oldest examples of dichroic glass, which means the Lycurgus Cup changes its color in certain lighting conditions. The cup appears green in direct light and red-purple when light shines through it.

***Figure 1**. The Lycurgus Cup, the appearance of green is due to reflected light and red-purple is due to transmitted light. Source of picture: British Museum Webpage. The pictures are used for presentation only.*

Later in 1990, scientists analysed the secret behind the changing color of Lycurgus Cup by performing several experiments. First a group of scientists performed transmission electron microscopy to explain the phenomenon of dichroism.[1] This showed the presence of nanoparticles with diameter 50-100 nm is responsible for the observed two colors. After that, X-ray analysis performed which showed that these nanoparticles are silver-gold (Ag-Au) alloy, with a ratio of Ag: Au (7:3), in addition about 10% of copper in a dispersed matrix.[2,3] The red color appears as a result of light absorption by Au nanoparticles (bigger particles). The green color is attributed due to scattering effect by colloidal dispersion of Ag nanoparticles with a size > 40 nm. It is considered as one of the oldest synthetic nanomaterials. A very familiar effect is seen in late medieval church windows. It is also showing luminous red and yellow color due to presence of Ag-Au alloy into the glass. During 9^{th} to 17^{th} century, Islamic world and Europe used glowing glittering "luster" ceramic glazes that contained Ag, Cu and other nanoparticles.[4] The Italians also used nanoparticles in making of Renaissance Pottery in 16^{th} century.[5] This piece of art also influenced by Ottoman techniques, to produce "Damascus" saber blades, cementite nanowires and carbon nanotubes to provide strength, resilience, and the ability to hold a keen edge in 13^{th} – 18^{th} century.[6] These colors and material properties were produced for hundred years however; medieval artists did not know the cause behind these surprising effects. In 1857, Michael Faraday studied the preparation and properties of colloidal suspension of Ruby gold. He prepared brightly ruby colored gold nanoparticle solutions that are still being displayed in Royal Institution's Faraday Museum in London.[7] The revolution in nanotechnology was started with the famous seminar talk "There is a plenty of room in the bottom" given by American physicist and noble prize laureate Richard Feynman in 1959 during the annual meeting organised by American Physical Society. In this meeting, Feynman first proposed the general ideas of nanotechnology – to manipulate individual atoms and molecules in order to construct devices with

nanoscale dimensions.[8] Here Feynman anticipated the inevitable miniaturization of devices into nanometer size with enhanced performance. For these reason he is considered the father of modern nanotechnology. After fifteen years, in 1974 a Japanese scientist Norio Taniguchi was the first person to use and define the term "Nanotechnology" by describing as: "nanotechnology mainly consists of the processing of separation, consolidation, and deformation of materials by one atom or one molecule".[9]

1.2 General Introduction to nanotechnology and nanoscience

According to National Nanotechnology Initiative (NNI), the definition of nanotechnology is: "*Research and technology development at the atomic, molecular, or macromolecular scale, leading to the controlled creation and use of structures, devices, and systems with a length scale of 1-100 nanometers (nm).*" Nanoscience contributes in almost every field of science and nanotechnologies make life easier in this era. The word 'nano' originated from a Greek prefix meaning 'dwarf' or something which are very small and deals with the material of 10^{-9} meter scale. By definition nanoscience refers to the study of structures and molecules ranging from 1-100 nm scale and nanotechnology define the utilization of nanoscience in practical application such as- devices etc.[10] The objects at this nanoscale contain noble properties and functions that differ markedly from those seen in macro scale. Nanomaterials are lighter, stronger, can be used as conductor of heat and electricity in a different way and possess various optical properties as compared to bulk materials. It can make materials more chemically reactive. Therefore, in recent years, many research organizations are currently working on the development of nanomaterial applications. Most significantly, nanomaterials can be self-assembled in completely different way, exploiting the same principles as occurred in living

organisms. Generally the most complex nanostructures can be found in nature; therefore it is not strange that all amazing processes involving in living organisms, has been the source of motivation for many researchers working in this field. Here Jean Marie Lehn used the famous line made by Leonardo da Vinci, "*Where Nature finishes producing its own species, man begins, using natural things and with the help of this nature, to create an infinity of species*" to give the future perspective and outlook based on nanotechnology.[11]

There are two approaches developed describing the different possibilities for the synthesis of nanostructures. These manufacturing approaches fall under the two categories, one is top down and another one is bottom up, these two processes differ in degrees of quality, speed and cost.

The top-down approach is nothing but the breaking down of bulk material to achieve nano-sized particle. This approach can be applied by using advanced technologies for example precision engineering and lithography which have been developed and optimised by industry in recent years. Precision engineering mainly focuses on the microelectronics industry during the entire production process and the high performance can be attained by virtue of combination of improvements. Whereas lithography is the modelling of a surface through the exposure of light, ions or electrons, and the deposition of the material on to that surface to generate that materials.[12]

The bottom-up approach involves building up of nanostructures from bottom such as- atom by atom or molecule by molecule with the help of chemical and physical processes which are in nano-scale range (1nm-100nm) using controlled manipulation of self-assembly of atoms or molecules. Chemical synthesis is a

process of producing rough materials which can be used as the building blocks of more advanced ordered materials or can be used directly in product in their bulk ordered form. Our very known self-assembly process is a bottom-up approach in which atoms or molecules organize themselves into ordered nanostructures by chemical and physical interactions between them. Positional assembly is the only technique where single atom, molecule or cluster can be positioned freely one by one.[12]

The general techniques involve in top-down and bottom-up processes are schematically represented in Figure 2.

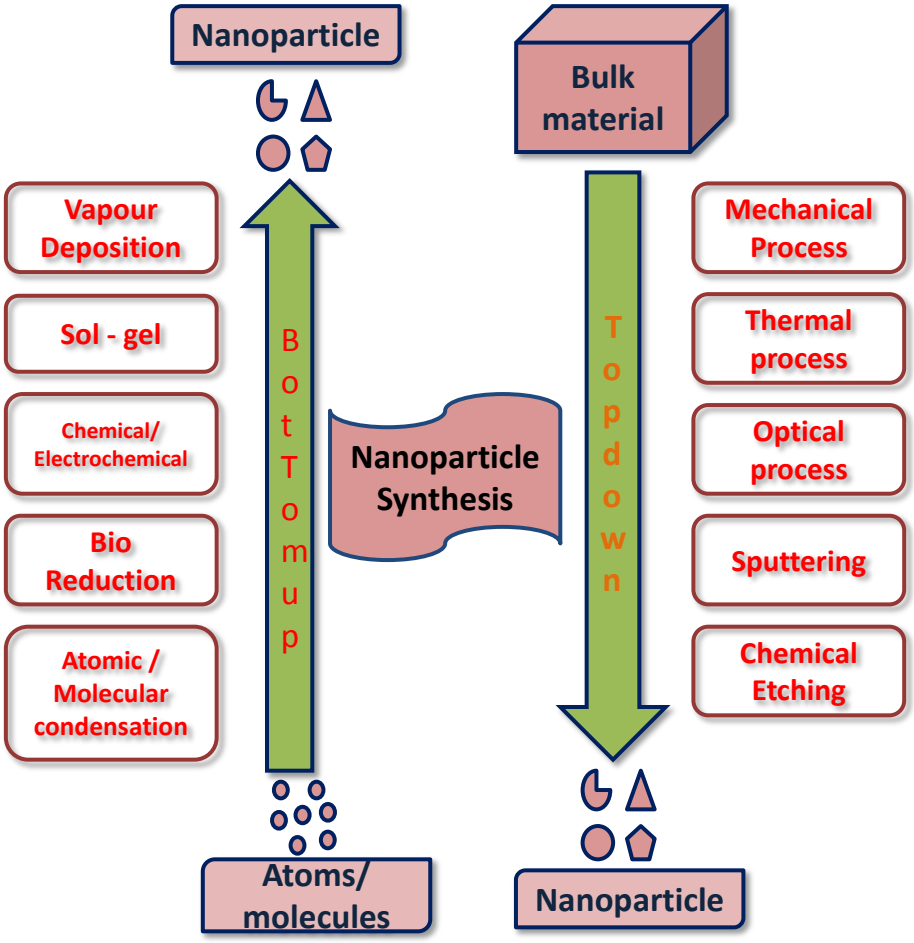

***Figure 2**. The schematic representation of top down and bottom up technology: different methods for nanoparticle synthesis.*

As the applications of inorganic, metallic, semiconductor, and polymer based nanoparticles has become versatile approach in modern nanotechnology, there is also increasing apprehension about its toxological properties. Such as- carbon nanoparticles have some biological limitations.[13,14] It has been shown to induce lipid per-oxidation in the brain cell of fish and pulmonary inflammation in rats. Therefore, a group of people started thinking about an alternative approach by using peptides and proteins as building unit to generate nanoparticles. This opened up a new field called – Bionanotechnology. Moreover, peptide and protein based self-assembled nanostructures have received significant attention due to their potential application in nanomedicine, drug delivery, tissue engineering, oil spillage recovery and environmental pollutant removing adsorbents.[15–29] Self-assembly is one of the significant areas of nanoscience and nanotechnologies. Self-assembly has been testified as one of the most powerful and efficient method to design nanostructures at the molecular and atomic level.

1.3 General introduction of Self-assembly

Self-assembly involves autonomous aggregation of components into ordered patterns or structures.[30] It plays an important role in various biological systems either to achieve its biological function or as a part of a pathogenic processes. For example – the development of biological membranes upon self-assembly of phospholipids, DNA double helix formation through specific hydrogen bonding interactions, the formation of amyloid fibrils applicable to a variety of generic disorder and as well as protein microtubules and microfilaments as functional unit of intracellular interplay. Inspired from these biological processes, a variety of biological and biomimetic materials have been developed via previously mentioned "Bottom-up" approach called molecular self-assembly.[31–37] Molecular self-assembly is an impulsive and spontaneous process of forming ordered nanostructures under certain thermodynamic and kinetic conditions based on specific and local molecular interactions. [11,38,39]The self-assembly process is facilitated by various non-covalent

interactions including hydrogen bonds, π-π stacking interactions, hydrophobic interactions, electrostatic interactions, non-specific Van der Waals forces and dipole-dipole interactions.[38,40–42] However, individually these interactions are relatively weak but when combined as a whole they can govern the self-assembly process.

1.4 Advantages of using peptide as a molecular building blocks in self-assembly process

The global trend is growing towards the biomolecules based fabricated nanostructures. Among the different biomolecules, peptides have become one of the most promising building blocks because of their unmatched biocompatibility, biodiversity, chemical diversity and most significantly resembles with proteins. Inspired from protein self-assembly in living organisms, several self-assembled structures have been developed using different amino acid sequence. [16,43–45] The self-assembled nanostructures originated from peptide are the gait of 20 amino acids. The formation of nanostructures can be controlled or tuned in terms of numbers, type, sequence and side chain of amino acid residues. The peptide based self-assembled nanostructures not only limited to natural amino acids; it can be customized by incorporating modified amino acid in the peptide design to have superior self-assembling properties. This bottom-up approach mainly inspired from the wonders of nature functioning on nanoscale that can generate many biological nanostructures for example proteins, DNA/RNA etc. The top-down method, which is superior to bottom-up science, help to discover new peptide sequence depending on the specific binding site on bio macromolecules based on their structural properties. Therefore, these specific advantages of peptides convincing the scientists to reach after these macromolecules and discover new molecular self-assemblies. Furthermore, the peptide synthesis is simple and cost-effective synthetic chemical approach via conventional

procedures, in solution or solid phase. The inherent biological properties of peptides make them constructive for many medical and biological applications.[46–48] They can also mimic the functions and behaviour of proteins, presenting an alternative model for gaining insight into the self-assembly and protein function. Again, the unique self-assembling properties of designed or extracted peptide building blocks enable them to undergo into well-defined nanostructures with various applications. Over the past few decades, significant progress has been emerged in this field. A number of peptide-derived building units such as- cyclic peptides, dendritic peptides, amphiphile peptides, surfactant-like oligopeptides, copolypeptides, and aromatic dipeptides, have been designed and developed for the creation of functional supramolecular architectures and the exploration of their possible applications in biology, nanotechnology and supramolecular chemistry.[49–51]

1.5 Peptide based self-assembled nanostructures

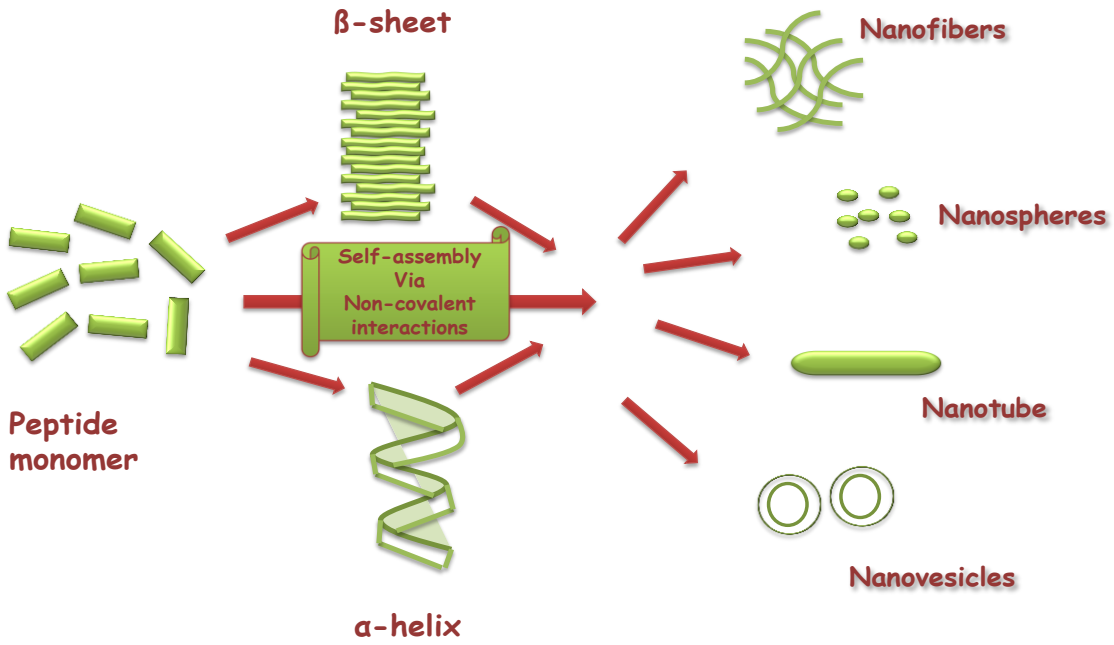

Figure 3. *Different nanostructures produced due to self-assembly of peptides.*

Peptide can be self-assembled into a variety of nanostructures including nanofibers, nanotubes, nanospheres, vesicles, coil, ribbon and twisted ribbons depending on their type, sequence and self-assembling condition.[52–58] To generate these nanostructures different types and structure of peptides are responsible including dipeptides, cyclic peptides, amphiphilic peptides, α-helical peptides, ß-sheet peptides etc.[59–62]

Recently, researchers tried to explore the self-assembly pattern of short peptides as small as dipeptides. In general dipeptides have the ability to self-assemble into different nanostructures by minimizing the difficulty and the cost of fabrication process and increasing the stability of the system.[63,64] The first investigation of dipeptide self-assembly came from Gorbitz's group, they reported the self-assembly pattern of diphenylalanine (FF) moiety.[65] This moiety has recognised the core motif of the amyloid ß (Aß) polypeptide segment and the driving force for the self-assembly of Alzheimer's disease. Many studies revealed that this FF dipeptide moiety can self-assemble into different nanostructures including nanoparticles, nanotubes, nanovesicles and nanowires etc.[66–70] Kim and his group demonstrated FF self-assembled into nanotubes by dissolving the dipeptide into water after inducing sonication followed by heating. FF also generated nanowires in water at high ionic strength.[71] They also showed the fascinating morphological transformation between nanowires and nanotubes found from self-assembly of FF moiety[71] and later several mechanical applications including biosensors, nanodevices, conducting nanomaterials were carried out using these two nanostructures.[54,72] Gorbitz et al further showed hydrophobic dipeptides like LL, LF, IL and FL can also self-assemble into nanotubes by forming head to tail hydrogen bonds.[73–76] Gazit and his co-workers further modified the FF moiety by incorporating thiol group.[77] Surprisingly, this fabrication led to the formation of tubular to spherical nanostructures. This group further showed the self-assembly pattern of other aromatic homodipeptide into nanofibrils, nanoplates, nanospheres and hydrogels.[78] Later, several applications were carried out using these

nanostructures. They can be applied for casting mold for the fabrication of metallic nano-wires and other different biomedical applications including biosensing, tissue-engineering, drug-delivery and bioimaging etc.[79–83] Modified dipeptides have also been explored by the scientists as templates for making biologically functional self-assembled nano or microstructures .[84,85] The modified dipeptide having N-terminal ω amino acid residue could undergo self-organization by forming nanotubes in solid as well as in aqueous state.[86] The morphological analysis revealed that the nanotubes were uniform and well-organized with various dimensions. The self-assembled nanostructures generated from these modified dipeptides were significantly different in solid as well as in solution state. This observation proved that the self-assembling mechanisms of these modified dipeptides were different in these two self-assembling conditions.[87] The hydrogen bonding capacity of water molecules played an important role in the self-assembly and even in the stabilization of the nanotubes. Due to the beautiful nanostructures obtained from phenylalanine peptide, several investigations were carried out by modifying the phenylalanine residue. For example, BOC-protected diphenylalanine residue formed tubular like nanostructures whereas Fmoc-protected and Cbz-protected diphenylalanine residue formed fibrillar structure very similar to amyloid fibril.[78] Further exploration on modified diphenylalanine analogue by using amine and carboxyl group revealed that these dipeptides formed ordered tubular structures at nanomeric scale.[88] Another investigation by ujin and co-worker demonstrated that Fmoc-dipeptide made from the combination of four different amino acid residues namely glycine, alanine, leucine and phenylalanine formed hydrogels depending on the nature, sequence and type of amino acid present in the peptide building block.[25] Generally, peptides containing aromatic residue like Fmoc, benzyl, naphthyl, pyrene have been proven good templates that tend to form fibrillar network due to the presence of aromatic π-π stacking and hydrophobic interactions .[85,89–95] Another interesting observation found when the dipeptide

(D)-F-(D)-F dissolved in water. Both nanotubes and vesicles were found upon diluting the solution with appropriate volume of water, suggesting that concentration of medium played a pivotal role in forming these nanostructures.[96] Apart from dipeptide self-assembled nanostructures, other short linear peptide nanostructures have been studied for biomedical applications including drug delivery.[97,98] A short peptide KLVFF from amyloid- beta peptide self-assembled to form nanofibrous structure and could also form hydrogel in a concentrated phosphate-buffer saline solution.[97] Irrespective of dipeptides and linear peptides other interesting type of peptides has become an interesting area of research i.e cyclic peptides, amphiphilic peptides and surfactant like peptides etc. Cyclic peptides formed from alternating D- and L- number of amino acids can self-assemble into nanotubular structure.[99] The nanotubular pattern is formed by aggregating the cyclic peptide as basic building blocks to form a flat conformation structure where the amino and the carbonyl side chain are perpendicular to the ring.[100] The structure is stabilized by hydrogen bonding between amide groups.[101] This unique nanotubular structure of cyclic peptide has some advantages over other peptides such as- precise diameter controls and could also be tuned by modifying the peptide sequence and length.[100] Amphiphilic peptides are special type of peptide that contains hydrophilic peptide head group and hydrophobic peptide tail. These peptides could undergo in forming various secondary and tertiary conformations.[102,103] Numerous self-assembled nanostructures were formed from these types of peptides nanotubular, nanovesicles and nanomicelle.[104] The electrostatic and hydrophobic interactions are the main participating driving force in forming the self-assembly pattern of amphiphilic peptides.[105] Therefore, peptide self-assembled well-defined nanostructures are stabilized through various non-covalent interactions as discussed earlier. The self-assembled nanostructures can be manipulated or tuned by changing the type, sequence or by applying external triggers such as temperature, pH value, concentration, medium, solvent, ionic strength etc. One

peptide self-assembled nanostructures can also be used in multiple functions including cell-penetration, drug-delivery, tissue engineering and environmental pollutant adsorbents etc. Biocompatibility, biodegradability and biodiversity make peptide building blocks superior to other organic moieties. Furthermore, its preparation in large scale attributed peptide as a promising target in modern nanotechnology. Among the different types of peptides discussed earlier, aromatic peptides have received considerable attention for the bottom-up construction of several important nanostructures.

1.6 Scope of the thesis

In recent times, many studies were carried out using phenyl alanine based self-assembly system but less is known about other aromatic amino acids. In this thesis, we mainly focus on the self-assembled nanostructures obtained from tyrosine based dipeptide moiety. Tyrosine is a versatile amino acid having significant role in living organism. It acts as a building block of proteins, a precursor of melanin and several neurotransmitters and hormones. Some tyrosine residues can participate equally in signal transduction processes in proteins and function as a receiver. Tyrosinemia is a generic disorder characterized by disruptions in the multistep process that breaks down the amino acid- tyrosine. It falls into the category of amyloid like metabolic diseases. Alkaptonuria, a typical amyloidogenic disorder occurs due to the accumulation of metabolite tyrosine and homogentisic acid. Here, in this thesis five different types of benzyl protected tyrosine based dipeptides were synthesized, characterized and one of the peptide based gel material was used for waste water treatment. Second chapter mainly focused on two dipeptides where terminally benzyl protected tyrosine residue was coupled with phenyl alanine and pentafluorinated phenyl alanine moiety. The structural insight of these dipeptides was characterized by AFM, FE-SEM, FT-IR, NMR and powder XRD study. Surprisingly, one of the dipeptide was showing gelatinous nature in different solvent mixture. This gel was further

utilized for waste water treatment by removing three different dyes from water and can act as a PSOG (phase selective organogelator).

Next a comparative study was performed between two dipeptides where terminally benzyl protected tyrosine residue was coupled with different side chain protected glutamic acid residues. Interestingly, a small variation in the substituent groups became responsible for significant changes in their morphological behaviour. The different in morphological pattern and characteristic details of these two dipeptides were discussed using AFM, NMR and several vibrational spectroscopic analyses. Further the 3-dimensional geometric structure, UV-Vis spectrum, HOMO-LUMO energy, FT-IR and Raman spectra were also calculated using Density Functional Theory. Molecular dynamic simulations also carried out for both the peptides.

Very rare and interesting ß-sheet promoted helical structure produced by di-tyrosine di-peptide was reported in the last chapter. The self-assembly pattern of this dipeptide was explored in various solvents. This novel dipeptide readily undergoes fibrillar network with ß-sheet and helical like hydrogen bonding pattern in solution. Morphology of this dipeptide was elucidated by Atomic force microscope (AFM) and Field emission scanning electron microscope (FE-SEM). Deuterium exchange proton NMR study, temperature dependent proton NMR study and FT-IR spectroscopy revealed the key molecular forces behind the benzyl protected tyrosine dipeptide assembly. In addition, CD spectroscopy also established the self-assembly phenomenon associated with this dipeptide. The single crystal X-ray analysis of this dipeptide further revealed that this peptide exhibited in a parallel ß-sheet pattern but this further self-assembled to form ß-sheet promoted helical architectures by various non-covalent interactions in the crystalline state. Hirshfeld surface analysis and DFT study were also performed for this dipeptide which also supported the result obtained from single crystal X-ray analysis.

CHAPTER 2

SOLVENT ASSISTED TYROSINE BASED LOW MOLECULAR WEIGHT EFFICIENT GELATOR AND ITS APPLICATION IN WATER PURIFICATION

2.1 Aim of the present work

Low molecular weight gelators from short synthetic peptides are rapidly expanding area of research interest due to their wide range of applications from biology to nanochemistry. Peptides are particularly an important class of organic materials for studying self-assembly and gelation propensity as these molecules are biocompatible and biodegradable and incorporation of a diversity of amino acids make them useful for several applications. In this chapter, an O-benzyl-tyrosine- pentafluoro-phenyl alanine based gelator molecule was synthesized and characterized. This dipeptide showed gelatinous property in a mixture of solvents. In one category, a translucent gel was formed in water – methanol (1:1) solvent system. Other polar protic solvents (DMF, DMSO, acetonitrile, ethanol etc.) were found to be useful instead of methanol to make this gel. In another category, aromatic solvents (toluene, benzene etc.) and long chain hydrocarbon (petroleum ether, kerosene, and diesel) mixtures were used to make gel. This gel was also translucent in nature and stable for several weeks. Morphology of these gel materials were characterized through AFM and FE-SEM analysis. NMR, FT-IR, XRD and rheological study were also carried out for these gel materials. Both the gels prepared from different solvent systems are used for waste water treatment by removing toxic dyes and acting as phase selective organo gelator (PSOG).

2.2 Introduction

In the past two decades, the peptide and amino acid derived supramolecular gels arising from hierarchical self-assembly of low molecular weight organic compounds is of increasing interest of current research area due to their unique properties.[106–113] Self-assembled supramolecular gels have gained significant attention in drug delivery matrices, molecular sensing, advance material science, pharmaceutical preparation, oil spill recovery and as environmental pollutant removing agents.[114–122] Gels can be described as soft materials in which solvent molecules are entrapped into one dimensional structure and cross link to constitute a network provided by the gelator molecules under suitable conditions.[123,124] Most of the gels belong to polymeric materials and hyper branched dendritic molecules. These gelator molecules are associated with various non-covalent interactions such as- hydrogen bonds, vander waals forces, π-π stacking, dipole-dipole, charge-transfer coordination interactions, and solvophobic effects.[125–132] These interactions play a great role during the organization of small molecular assemblies into three dimensional architecture that has the ability to immobilise solvent molecules which is trapped under appropriate conditions to form gels. Commonly used natural bio-polymers for example - Long chain hydrocarbons, saccharides, peptides, amides, ureas, nucleobase, steroids, and two component systems belong to low molecular weight gelators (LMWGs). In contrast to these naturally occurring biopolymers "engineered" peptide based low molecular weight gelators in organic and aqueous solvents were explored, having ample applications in nanomedicine, catalysts, light-harvesting, tissue engineering scaffolds, sensing, templating and nanoelectronics.[111,133,134] In most of the cases these gelator molecules involve hydrogen bonding and /or π-π interactions for self-assembly in their respective gel state. Peptides are particularly useful candidates to study self-assembly and

gelation due to their biocompatibility and biodegradability as well as incorporating a diverse range of amino acids to control the peptide sequence.

Water is the most essential resource for survival on our planet – Earth. With the development and industrialization of human civilization, water pollution has now become a great threat to us. Water pollution mainly occurs due to the degradation and contamination of water by harmful chemicals. Disposal of harmful chemicals into water not only exert negative effects on species living in water but also on the broader biological community. Nowadays water purification has become a matter of supreme importance in contemporary environmental research. Industries like textile, printing, plastic, leather, and food used various synthetic dyes and pigments.[135,136] Dyes are the specific class of organic compounds composed of conjugated phenyl units. Presence of these phenyl units in dye molecules is responsible for their non-degradability and high toxicity.[137,138] Therefore, contamination of dye molecules in water has become a great problem as they cause extensive damage to natural ecosystems and human health. In addition, marine pollution through accidental or intentional discharge of crude oil and petrochemicals has become serious environmental issue. The annual disposal of millions tons of petroleum across waterways worldwide and contamination of water with dyes are very much toxic to biological systems when their levels exceed cellular need.[139] Therefore many conventional approaches, such as – ion-exchange, membrane filtration, adsorption procedures, chemical precipitation and biological degradation have been employed for removing these environmental effluents.[140,141] However, these processes suffer many disadvantages like incomplete removal, high cost and high energy requirements.[142] In this respect, the development of an approach which is cheaper and more potent is highly beneficial and promising task. Previous investigation in our laboratory described that benzyl protected amino acid residue like cysteine was able to generate various self-assembled structures including sphere, protofibril, fibril via hydrogen

bonding through amide linkage and π-π stacking through aromatic ring of the substituted amino acid.[143,144] Due to the important feature of tyrosine moiety an investigation was carried out by developing a dipeptide composed of benzyl protected tyrosine residue. In this chapter, two dipeptides were designed and synthesized composed of *N*-(*tert*-butoxycarbonyl)-L-phenylalanine-O-benzyl-L-tyrosine methyl ester and *N*-(*tert*-butoxycarbonyl)pentafluoro-L-phenylalanine-O-benzyl-L-tyrosine methyl ester. Among these two, the dipeptide composed of pentafluoro substituent can able to form gel in polar protic solvent- water mixture and as well as in aromatic solvent-long chain hydrocarbon (such as petroleum ether, kerosene, diesel) mixture. The morphology of the dipeptide containing O-benzyl tyrosine and phenyl alanine was investigated by atomic force microscopy and observed fibrillar network in mixture of solvents. Unfortunately, this dipeptide was failed to form gel in pure as well as mixture of solvents rather it generated suspension in mixture of solvents (Figure 20). The structural insights of these gels were characterized through Field emission scanning electron microscopy, Atomic Force Microscopy, FT-IR analysis, X-ray diffraction studies and their mechanical strength were investigated by Rheological experiments. Both the gels had potential application for the treatment of waste water. The gel obtained from methanol-water mixture has the efficiency to adsorb toxic dyes (crystal violet, Eriochrome black T and Rhodamine B) and gel obtained from another solvent system can be used as phase selective gelator (PSG) for oil-spill recovery. UV-Vis spectroscopy was used to investigate the dye adsorption propensity of the gelator molecule.

2.3 Results and discussion

The inclination of '*N-(tert*-butoxycarbonyl)pentafluoro-L- phenylalanine O-benzyl-l-tyrosine' (TP1, Scheme 1) dipeptide towards gelation was studied in different versatile solvent systems including methanol, ethanol, dimethyl sulfoxide, dimethylformamide, acetonitrile, acetone, petroleum ether, kerosene,

diesel, toluene, benzene, xylene and water etc. The dipeptide (TP1) was failed to show any gelatinous ability in single solvent among the above mentioned solvents. Due to this reason, the gelation of this dipeptide was tested in a mixture of solvent system. Water is miscible with polar protic solvent. Therefore, a solvent system was developed where water was used with polar protic solvent to investigate the gelation propensity of this dipeptide in this solvent mixture. Surprisingly, when water was added to the methanolic solution of the dipeptide, a white coloured suspension appeared and then keeping the solution without any disturbance formed a translucent gel within few seconds. The gelation test was carried out in a tube by tube inversion method (Figure 14 and 15). The gel formed from methanol-water solvent system was thermoreversible in nature. Heating the gel gave a clear solution then keeping the solution without any disturbance translucent gel reappeared. The minimum gelation concentration (MGC) of the dipeptide in methanol-water system at a ratio 1:1 was 0.25% w/v and the calculated Tgel of the corresponding MGC was found to be 72^{o}C. The gel-to-sol transition temperature (Tgel) was determined by placing the organogel containing inverted screw-capped glass vial into a thermostatted water bath and raising the temperature at a rate of 2^{o}C min^{-1}. The T_{gel} was defined as the temperature ($\pm$0.5^{o}C) at which the gel melted and showed gravitational flow. It was observed that the gelation appeared immediately in 50% methanol-water system. Further increasing methanol amount, less amount of gel formation was observed. Other protic solvents such as- DMF, DMSO, acetonitrile and ethanol were tested instead of methanol. Interestingly, this dipeptide also formed gel in these solvents in assistance with water. From this observation, it can be concluded that water is essential for gelation due to water assisted hydrogen bonding. The importance of water in this solvent mixture was further confirmed from D_2O exchange proton NMR study. The gel formed from polar protic solvent and water mixture was translucent, thermoreversible, stable for several weeks without any noticeable change under ambient condition. Apart from the mixture

of polar protic solvent and water, this dipeptide was shown to form translucent gel in the mixture of aromatic solvent i.e. toluene and nonpolar solvent like petroleum ether. The translucent gel formed by this dipeptide (TP1) in accordance with the mixture of toluene and petroleum ether is thermoreversible in nature and stable for several weeks at ambient temperature. The minimum gelation concentration (MGC) of the dipeptide in (1:20) toluene-petroleum ether system was 0.2% w/v and Tgel at this MGC was found to be 48^{o}C. The gelation test was also successful when benzene, xylene used along with petroleum ether instead of toluene. The gel prepared from toluene and long chain hydrocarbon (such as- petroleum ether, kerosene and diesel) was prepared in absence of water. This dipeptide had better gelation tendency in 50% methanol-water solvent system with 0.25% w/v MGC. This gel was further tested in water purification by removing three different toxic dyes. Surprisingly, the gel obtained from toluene-petroleum ether solvent system was found to act as a phase selective gelator which can selectively gelate the oil part in oil-water mixture keeping the water part fixed. This phase selective gelation was again investigated using kerosene, diesel instead of petroleum ether (Figure 17 and 18).

2.3.1 Synthesis of the dipeptides

All chemicals were purchased from Sigma-Aldrich and used without further purification unless otherwise stated. Solvents were freshly distilled by the standard procedures prior to use. Column chromatography was performed on silica gel (Merck, 60–120 mesh) with the required eluent. Finally, compounds were characterized by ^{1}H-NMR, ^{13}C-NMR and mass spectrometry**.**

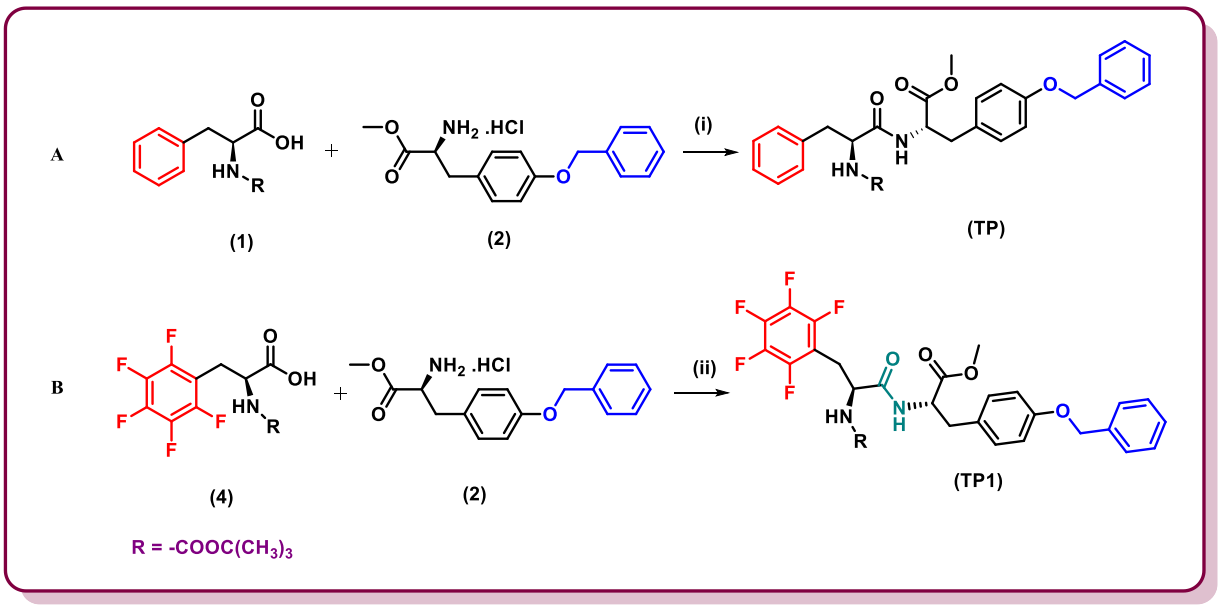

Scheme 1. Structure and schematic presentation of the synthesis of the dipeptides. *Reagents and condition (i) EDC.HCl, HOBt, TEA, .0°C to RT, 8h.*

Synthesis of dipeptide (TP)

To a well stirred solution of N-(tert-butoxycarbonyl) - L - phenylalanine(1, 1g, 3.77 mmol) dissolved in N,N-dimethylformamide (15 mL), was added anhydrous hydroxybenzotriazole (HOBT; 611 mg 4.52 mmol) slowly followed by 1-ethyl-3,3-(dimethylamino) propyl carbodiimide hydrochloride (EDC•HCl; 1g ,5.65mmol) in cooled condition under nitrogen atmosphere. Then the stirring was continued for 10 minutes at ice-cooled condition and to this mixture triethylamine (TEA; 2.6 mL ,18.85mmol) was added along with O-benzyl-L-tyrosine methyl ester (2, 900mg, 3.77 mmol;), subsequently the reaction was further continued for 8 h at room temperature (monitoring via TLC). The reaction mixture was then concentrated to dryness and extracted with ethyl acetate from aqueous layer. Evaporation of solvent under reduced pressure produced the crude product, which was further purified by column chromatography over silica gel (hexane/ethyl acetate) to afford the intermediate compound 'TP' as white solid (yield = 78%).

Synthesis of dipeptide (TP1)

To a well stirred solution of N-(tert-butoxycarbonyl)pentafluoro- L - phenylalanine(4, 1g, 2.81mmol) dissolved in N,N-dimethylformamide (15 mL), was added anhydrous hydroxybenzotriazole (HOBT; 455 mg 3.37mmol) slowly followed by 1-ethyl-3,3-(dimethylamino) propyl carbodiimide hydrochloride (EDC•HCl; 1g ,5.62mmol) in cooled condition under nitrogen atmosphere. Then the stirring was continued for 10 minutes at ice-cooled condition and to this mixture triethylamine (TEA; 2mL ,14.05mmol) was added along with O-benzyl-L-tyrosine methyl ester (2, 900mg, 2.81mmol;), subsequently the reaction was further continued for 8 h at room temperature (monitoring via TLC). The reaction mixture was then concentrated to dryness and extracted with ethyl acetate from aqueous layer. Evaporation of solvent under reduced pressure produced the crude product, which was further purified by column chromatography over silica gel (hexane/ethyl acetate) to afford the intermediate compound 'TP1' as white solid (yield = 80%).

2.3.2 Morphological studies

FE-SEM study

Morphologies of the gel materials were investigated using field emission scanning electron microscopy (FE-SEM). For FE-SEM study, dilute solutions of gel materials were dried and platinum coating was carried out. Then the micrographs were taken in an FE-SEM apparatus (Jeol Scanning Microscope-JSM-7600F). Another FE-SEM study of the gel after adsorption of the dye was performed in an FE- SEM apparatus Hitachi S-4800**.**

The effect of solvents on the morphology of this dipeptide (TP1) was investigated by Field emission scanning electron microscopic (FE-SEM) experiment. FE-SEM investigation helped to understand the morphological pattern of the xerogel prepared from their respective solvent systems at their MGC. All the xerogels

showed highly cross-linked entangled structure. An intertwined fibrillar network was observed when methanol-water system (Figure 1A) was taken. In this case it was observed that two or more fibres were linked to each other to obtain a thicker fibre. Highly cross linked, entangled sheets like structures were obtained in case of toluene-petroleum ether solvent system (Figure 1B). Generally for the formation of the gel such fibrillar network were responsible for the entrapment of large number of solvent molecules and also restricted the free movement of solvent molecules.[145]

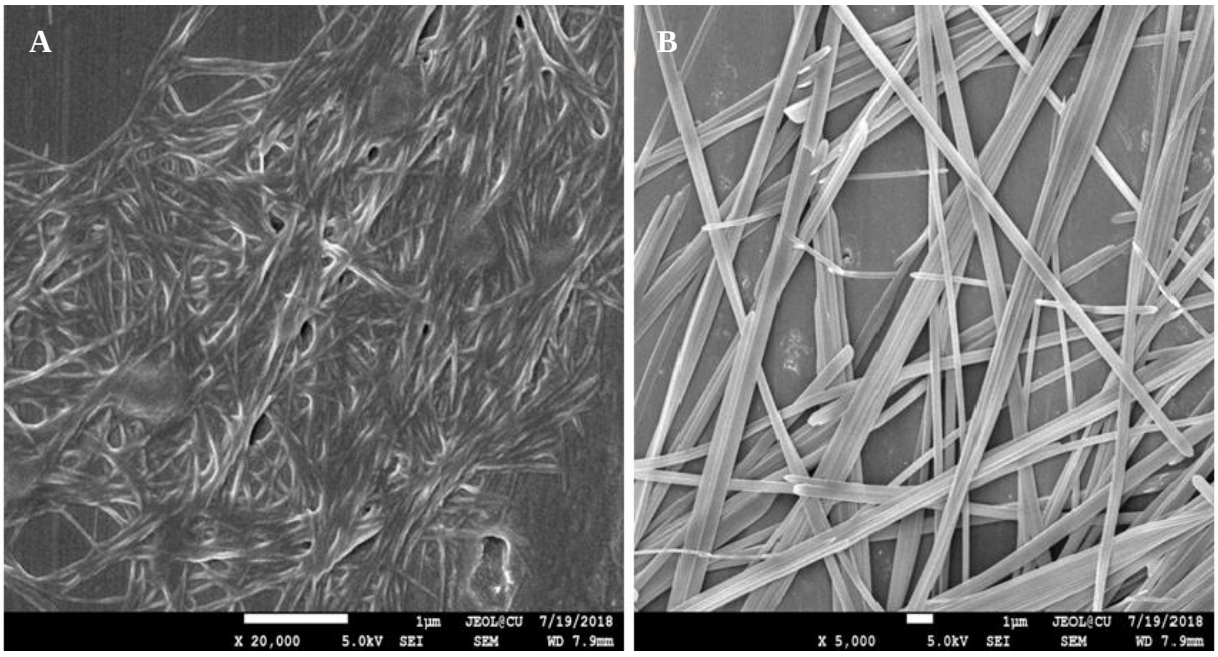

Figure 1. *Field emission scanning electron microscopic images of the dipeptide in (A) Methanol-water system (B) Toluene-Petroleum ether system.*

AFM study

Dipeptide (TP1) suspended in their respective solvent was aged at room temperature for 24h separately and then this solution was drop casted in freshly cleaved muscovite Ruby mica sheet (ASTM V1 Grade Ruby Mica, Micafab India Pvt. Ltd., Chennai, India). After drying the sample solution coated on mica foil, the specimen was observed through atomic force microscope. AFM images were obtained on Pico Plus 5500 AFM (Agilent Technologies, Inc., Santa Clara, CA, USA) with the piezo scanner range of 9 μm. The images (256 × 256 pixels) were

captured with a scan size between 0.5 and 5 μm at the scan speed rate of 0.5 rpm. The images were processed through flattening via Pico view software (Molecular Imaging Inc., Ann Arbor, MI, USA).

The morphology adapted by this dipeptide (TP1) in their dilute solutions was investigated by Atomic Force Microscopy. For AFM imaging, stock solutions were prepared by dissolving TP1 separately in methanol, toluene and their respective solvent mixtures for required hours and deposited on freshly cleaved mica surface. The images were recorded under the microscope after drying the sample. In methanol and toluene solvents, TP1 showed fibrillar like assembly network. The widths of the fibres obtained from dipeptide dissolved separately in methanol and toluene solution were 60-90 nm and 70-90 nm respectively (Figure 2A and 2B). Therefore, the conclusion can be drawn that TP1 generated dispersed fibrils from dilute solution (5 μM). Moreover the result obtained from the AFM images of this dipeptide were also in agreement with the cross-linked entangled structure accounting for further aggregation of the discrete fibrils with the assistance of solvent molecules in the corresponding gel state. The morphology of the dipeptide in mixture of solvents also showed fibrils from dilute solution in their respective solvent system (Figure 2C and 2D). This observation also corroborated with the result obtained from FE-SEM analysis.

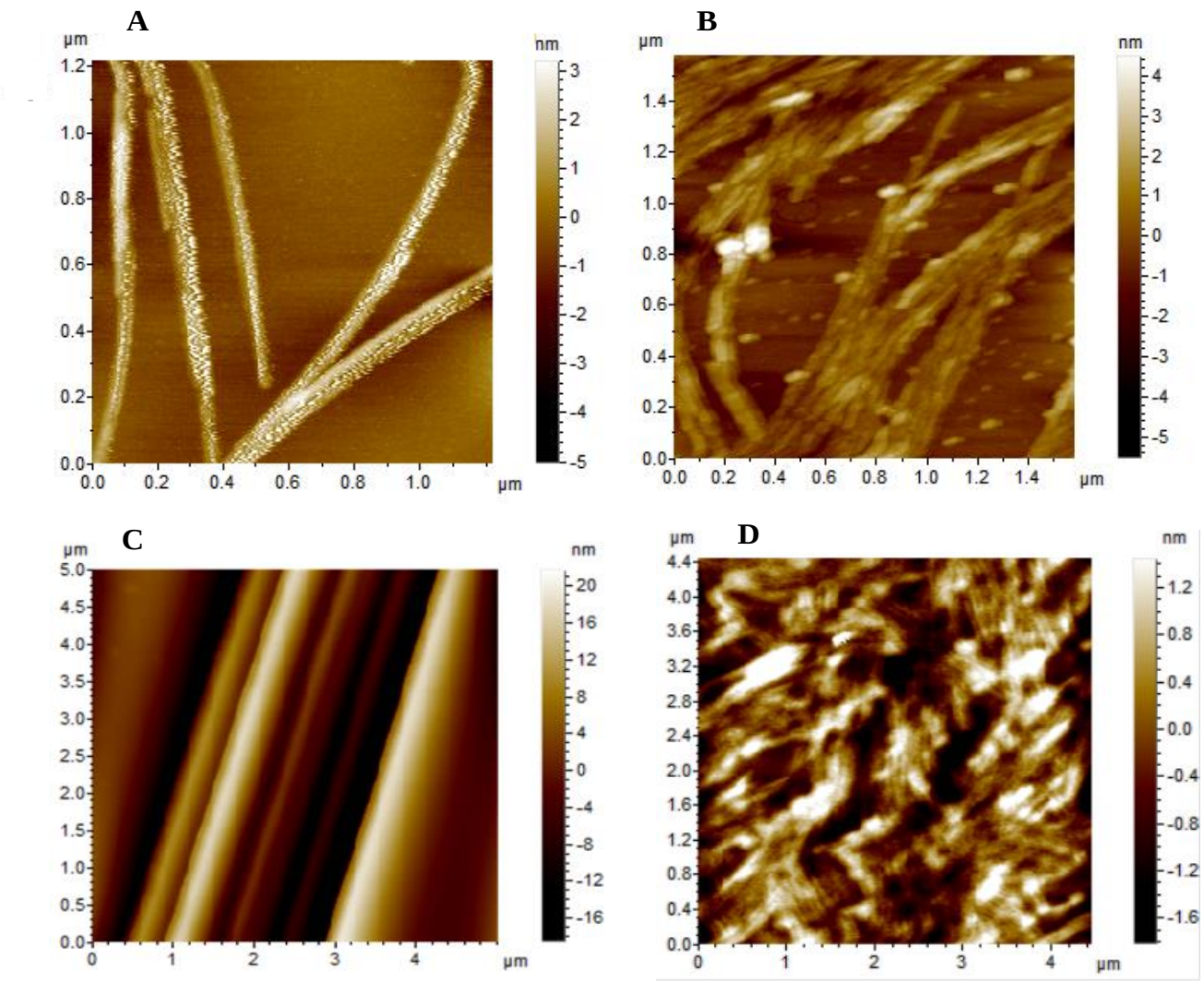

***Figure 2**. Atomic Force microscopic images of the dipeptide(TP1). Panel (A) and panel (B) indicate fibrillar aggregates produced from dipeptide in their dilute methanolic and toluene solution respectively. Lower panels indicate AFM images of the gelator dipeptide in mixture of solvents (C). in methanol-water and (D). in toluene-petroleum ether.*

2.3.3 Deuterated (H/D) exchange proton NMR study

Deuterated (H/D) exchange proton NMR study of the dipeptide (TP1) provided important insights about the hydrogen bonding patterns of the two amide protons in solution state.[146] This experiment was performed by dissolving the dipeptide (TP1) in DMSO-d_6 solvent and ^{1}H-spectrum was taken in this pure solvent. After

that certain volume of D_2O was added and spectrums were taken at different time point of incubation.

Investigating H/D exchange proton NMR study, it was found that two doublet peaks appeared around δ 8.50 and 6.94 ppm for peptide NH and BOC NH respectively in absence of D_2O because of two different chemical environments of two amine groups. The total 9 aromatic protons arose at δ 7.40 (2H), 7.34 (2H), 7.29-7.27 (1H), 7.08 (2H) and 6.87 (2H) ppm respectively for this dipeptide (TP1)in the NMR spectrum (Figure 3A). Addition of 10μL D_2O to a 10 mM dipeptide solution in DMSO-d_6, the intensity of proton arose at δ 6.94 ppm (BOC NH) diminished rapidly (within 1min.) and shifted from 6.94 to 6.90 ppm as shown in (Figure 3B). The shielding effect of this BOC NH may be due to the fact that, this proton involved in strong hydrogen bonding with DMSO, when D_2O was added interaction pattern of the hydrogen may be altered depending on its position and orientations.[147] The intensity of the other proton appeared at δ 8.50 ppm for peptide NH diminished slowly. The D_2O (H/D) exchange proton NMR spectrum was taken after different time point of incubation as shown in (Figure 3C and 3D). From this NMR study it can be concluded that both the protons are solvent exposed and participated in intermolecular H-bonding with another dipeptide molecules and the solvent molecules.

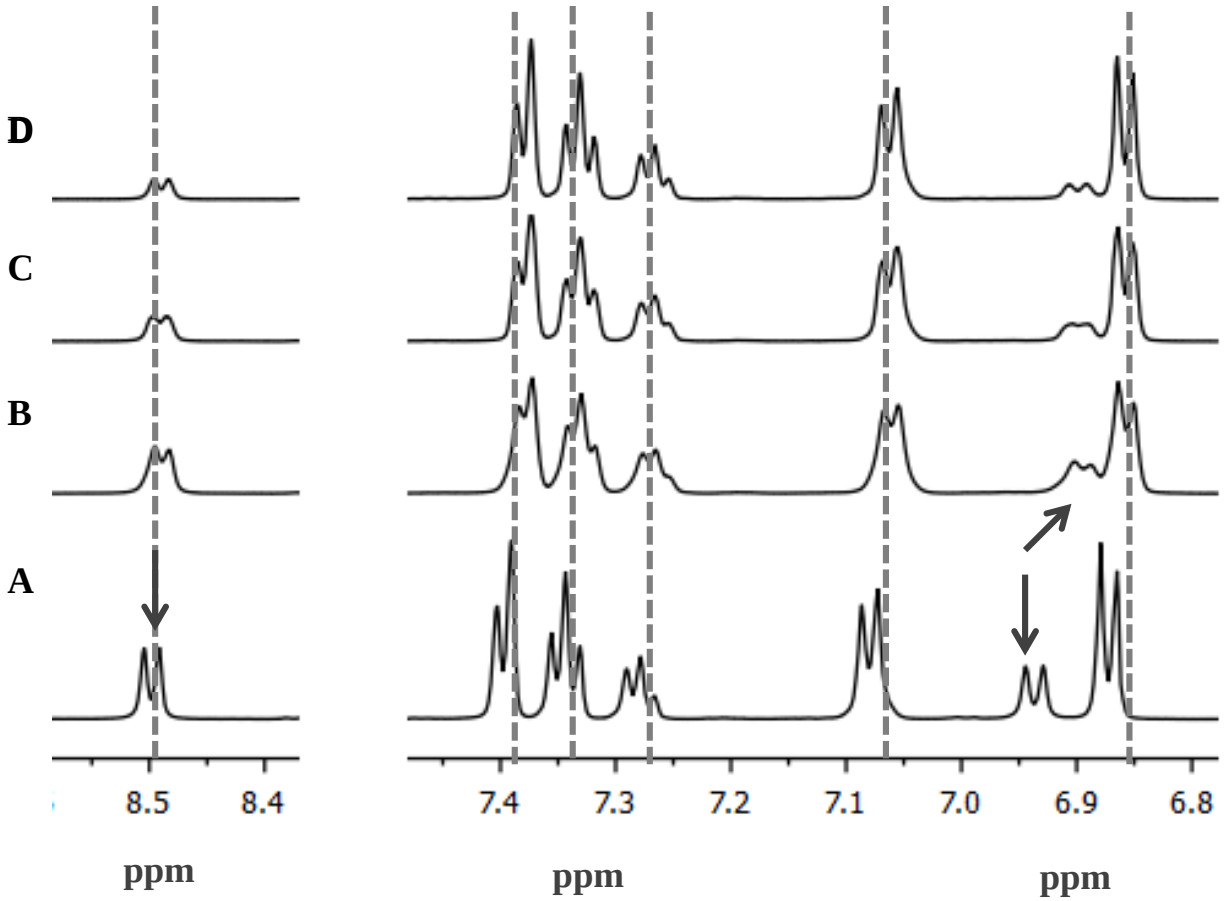

Figure 3. *H/D exchange NMR experiment of dipeptide (10 mM) in DMSO-d_6.*

(A) ^{1}H-NMR spectra of dipeptide (TP1) in absence of D_2O in solution. Upper panels show the perturbation of the spectra in presence of D_2O (D_2O: DMSO-d_6 = 1:50) at different point after addition of D_2O: (B) 0h, (C) 2h and (D) 4h. For presentation clarity only peak regions are shown and the bottom axis is broken. Dashed lines and arrows are to highlight the perturbation of the peak positions and intensities.

2.3.4 FT-IR analysis

The FT-IR spectra of the dipeptide were recorded on a PerkinElmer Spectrum Two spectrometer. For recording the FT-IR in wet gel state, the gels were prepared in their respective solvents at their MGC. The spectra were scanned from 400–4000 cm^{-1} at 4 cm^{-1} resolution. Spectrum 10 software was used for data processing.

Infrared spectroscopy was most often used to determine the molecular arrangement of the peptide backbone along with the structural orientation in aggregated state by analysing the most sensitive bands like amide I, amide II and amide III which are mainly originating from backbone vibrations. FT-IR spectroscopy studies were performed to compare the secondary structures of the peptide both in solid and self-assembled structures in greater detail. For recording the FT-IR spectra of the dipeptide (TP1) in their wet gel state; the gels were prepared in their respective solvent system at their MGC according the procedure given above. The important FT-IR band positions are marked in the Figure 4 and assignment of these bands are placed in supporting information (Figure 16 and Table 1). The molecular interactions were influenced by the amide backbone configuration. In most cases, the characteristic amide I, amide II and amide III bands are mainly originating from backbone vibrations, those appeared at 1600–1690 cm^{-1}, 1480–1580 cm^{-1} and 1230–1300 cm^{-1} respectively.[148] In order to get the molecular interactions associated with the gelation of the dipeptide, we measured the FTIR spectra of the dipeptide in their solid and wet gel state (Figure 4). In the solid state of TP1 (Figure 4A), one sharp peak appeared at 1666 cm^{-1} along with a hump at 1655 cm^{-1} corresponding to amide I vibrational mode of the carbamate carbonyl and the amide carbonyl respectively. In addition, Sharp peak appeared at 1740 cm^{-1} for the ester carbonyl in the solid state of the dipeptide (TP1). However for the gel state of TP1 in methanol-water solvent system

(Figure 4B), the characteristics peak appeared at 1628 cm^{-1}, 1666 cm^{-1} and 1740 cm^{-1} with broadening nature compared to solid state. These broadening of the amide peaks and the appearance of the peak at 1628 cm^{-1} indicated that in the gel state this dipeptide (TP1) become hydrated through the water and methanol solvent system. The amide (-CONH) group may be involved in hydrogen bond formation with water. Thus the associated water molecules contribute to the broadness at 1628 cm^{-1}. Similarly for the gel state of this dipeptide (TP1) in toluene petroleum ether (Figure 4C), shifting of the amide peak from1666 cm^{-1} to1658 cm^{-1} along merged with the hump at 1655 cm^{-1} was observed. This result suggested a strong hydrogen bonding in gel state compared to solid state.

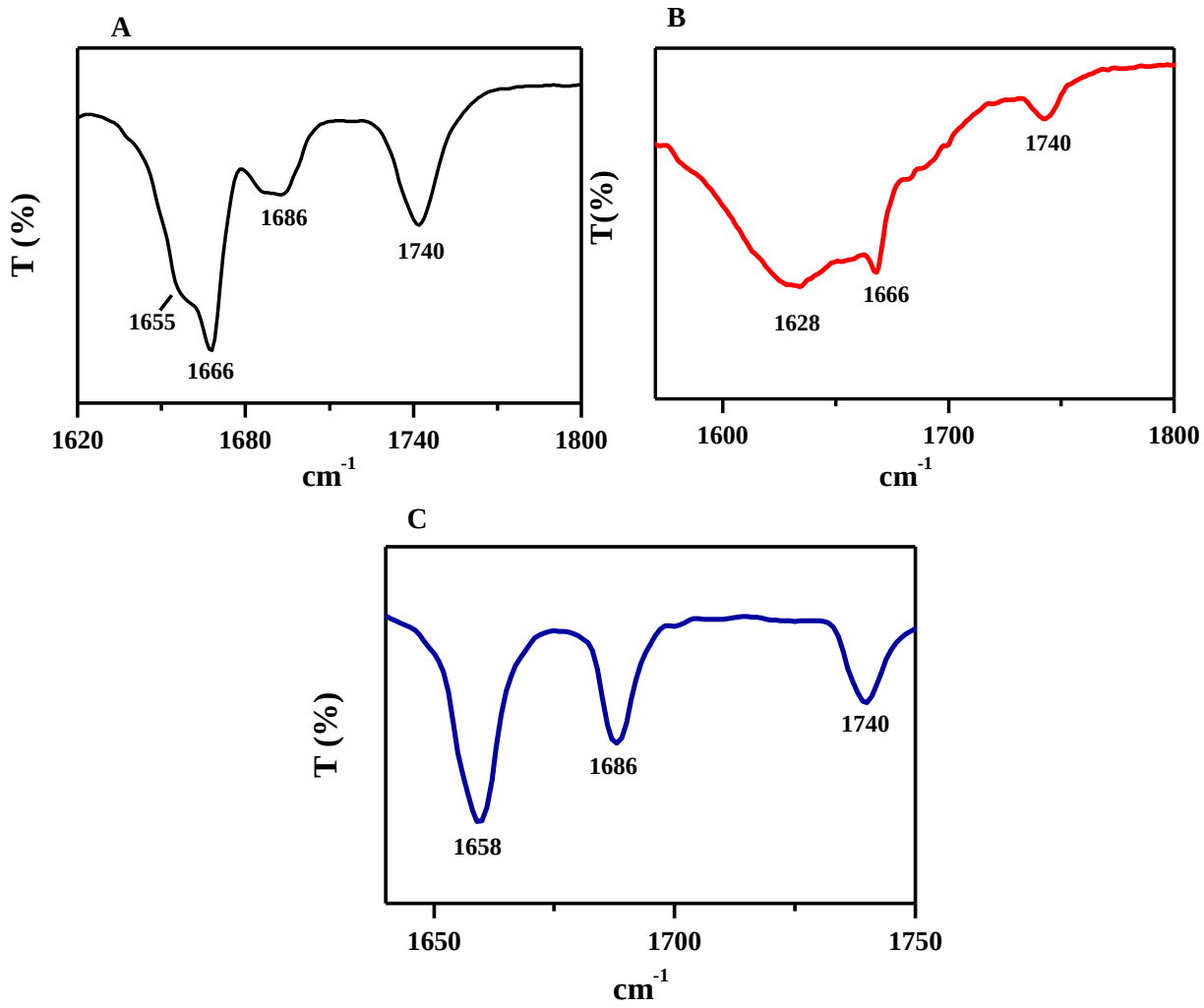

Figure 4. *FT-IR spectra of the dipeptide(TP1) in three different conditions.*
(A) indicates solid state (B) represents wet gel state prepared from methanol-water and (C) indicates wet gel state prepared from toluene-petroleum ether system.

2.3.5 X-ray diffraction study

XRD study of the xerogel was carried out by placing the sample on a glass plate. Experiments were carried out by using an X-ray diffractometer (Bruker AXS, Model No. D8 Advance).

To determine the solid state molecular arrangement and packing of dipeptide (TP1) at the atomic level, powder X-ray diffraction (XRD) experiment were carried out in both gel state obtained from two different solvent system and its solid state, as represented in Figure 5. The xerogel form showed sharp reflections appeared in the 5–40^{o} (2θ value) range and was therefore inferred to be crystalline in nature. Xerogel obtained from the dipeptide in toluene-petroleum ether solvent system showed a peak (Figure 5B) corresponding to d-spacing 4.73 Å (2θ ~ 18.7°) accompanied by the other peak at 9.71 Å (2θ ~ 9.1°), which were indicative of a ß-sheet-like arrangement of these gelator molecules. The peak at 4.73 Å represented the spacing between peptide chains within a ß-sheet. Additionally, the peak at 9.71 Å was approximately doubled the ß-sheet spacing. This may be due to either, the repeating unit of ß-sheet type hydrogen bonding or the 'side-chain' spacing between two interacting parallel sheets.[149] Moreover, a peak at 2θ ~ 26.29° (3.38 Å) was observed for the xerogel obtained from toluene-petroleum ether solvent system, indicating the presence of π-π stacking interactions.[150–152] In the case of solid state the broad peaks (Figure 5A) were due to the heavy scatterings, which represented semi-crystalline characteristics of the dipeptide. Despite of the fact that the dipeptide partially lost its crystalline property in the dry state, the low intense peaks at 2θ ~ 9.8° (9.01 Å), 18.2° (4.86 Å) and 25.3° (3.51 Å) were still present, which indicated the presence ß-sheet-like arrangement and π-π stacking interaction in the dry state although these values are slightly shifted from the xerogel obtained from toluene-petroleum ether solvent system. Further, few strong intense lines are also observed in the wet-gel state which may be due to pure phenylalanine or tyrosine as reported

earlier.[153–156] Unlike the sharp reflection in toluene-petroleum ether solvent system, the XRD spectrum of the dipeptide in methanol-water solvent system (Figure 5C) showed broad peaks which indicated that the crystalline property of the dipeptide is less in this medium. It suggested that the xerogel state of the dipeptide significantly depended on the polarity of the environment. It showed peaks at 2θ ~ 18.67° (4.74 Å) and 29.51° (3.02 Å), which may be due to ß-sheet like arrangement and π-π stacking interactions as obtained from the toluene-petroleum ether medium.

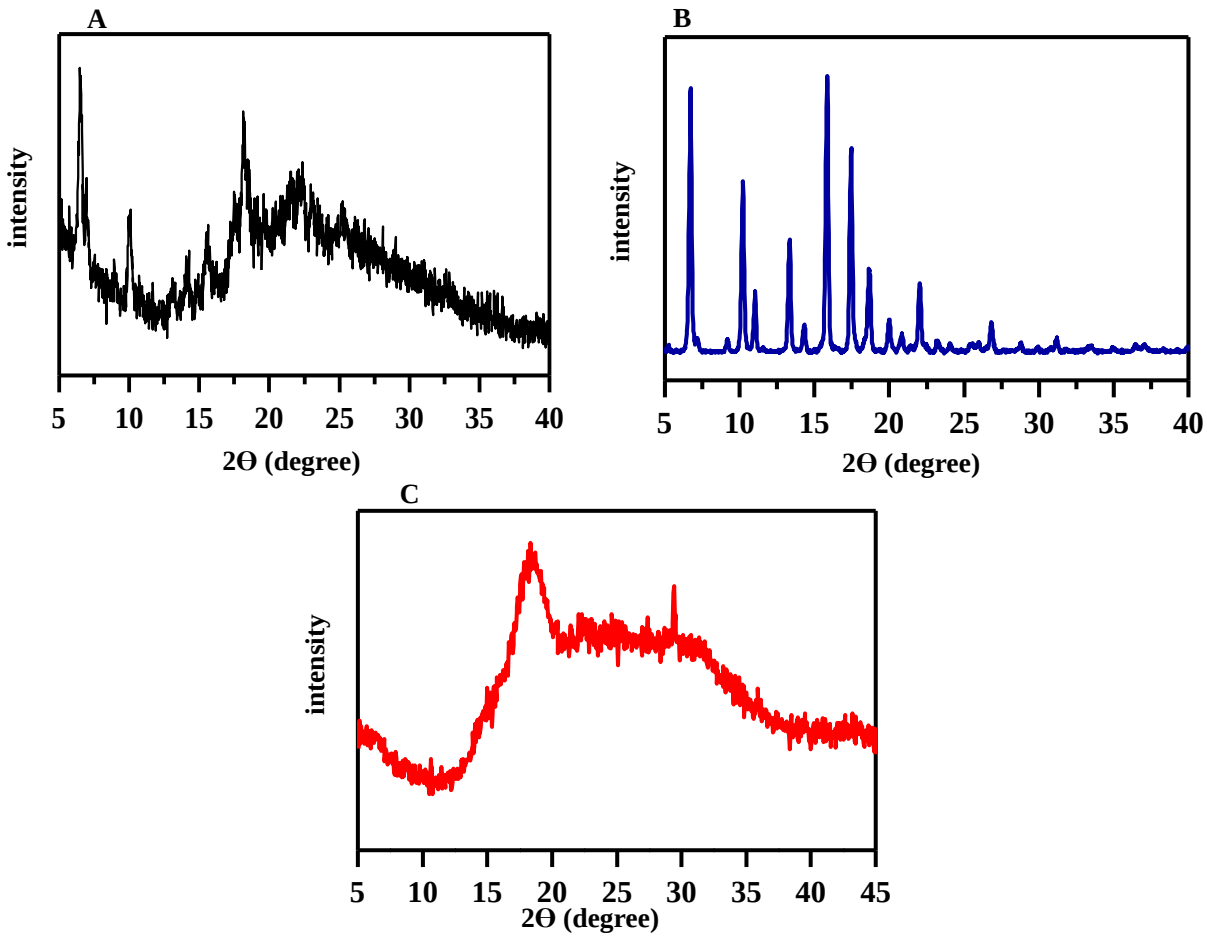

Figure 5. *(A) X-ray diffraction patterns of the dipeptide (TP1) in its solid state. (B) X-ray diffraction patterns of the dipeptide in its xerogel state (toluene – petroleum ether system). (C) X-ray diffraction patterns of the dipeptide in its xerogel state (methanol-water system).*

2.3.6 Rheological experiment

The rheological measurement of the gel obtained from toluene-petroleum ether solvent system was performed using Modular Compact Rheometer (Anton Parr, MCR 102, Austria). The instrument was equipped with an air compressor unit which maintained the air pressure at 7 kg/cm2. A standard cone-plate geometry (CP-40, 40 mm outer diameter, angle 1◦) was employed in the study. Frequency sweep (G, G versus angular sweep) was measured in oscillation mode. The data was analysed using Rheoplus software (US 200, version 3.62). Another rheology experiment of the gel obtained from methanol-water solvent system was performed in SDT Q Series Advanced Rheometer AR 2000.

Rheological experiments were performed in order to examine the mechanical strength of the gel in their respective solvent system. The storage modulus (G′) and loss modulus (G″) were measured in a typical frequency sweep experiment under a constant (0.1%) strain as a function of applied angular frequency and were represented in Figure 6. It is evident from the fact that if storage modulus (G′) is greater than the loss modulus (G″) and no cross-over point is found throughout the entire range of frequency the material is likely to be considered as gel. In this experiment, it was found that for gelatinous material in both solvent systems the storage modulus (G′) remained greater than the loss modulus (G″) and no cross-over point was found in the entire range of frequency. This result is in agreement with the fact that a soft solid like gel phase material was present.

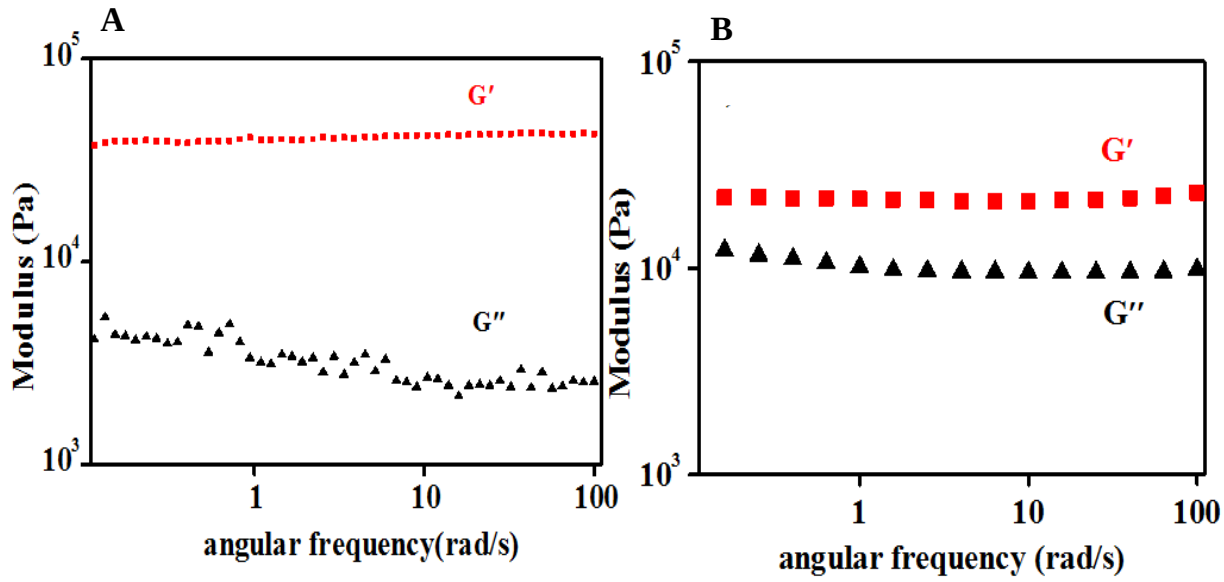

.

Figure 6. *Frequency sweep experiment of the dipeptide at 0.1% constant strain (A) Methanol-water system (B) Toluene- petroleum ether system.*

2.3.7 Dye adsorption study

Dye adsorption study was monitored by adding 1mL of dye (0.01 mM) to a sample tube together with 2 mg of TP1. This solution was left for 24 h at RT to adsorb the dye. The final concentration of the dye in the solution was determined by UV/Vis spectroscopy. UV−vis absorption spectra were recorded using a JASCO V-630 spectrophotometer. A high-quality quartz cuvette was used for measuring the absorbance.

Since the last two decades, water pollution has become a matter of great concern to nature due to the textile industry and organic dyes.[40] These dyes are discharged into the river, oceans in large amount by these industries which contaminated our natural sources. Nowadays, low molecular weight gelators offer an alternative appealing for removal of these toxic dyes quite efficiently. The gel obtained from methanol-water solvent system was tested for absorbing these hazardous dyes by adding aqueous solution of the dye to the gel. Three different dyes crystal violet, Eriochrome black T and Rhodamine B were adsorbed rapidly over a period of time by this supramolecular adsorbent. The concentration of the dyes used for

this investigation was 0.01 mM. After 24 h more than 90% of the dyes were adsorbed for crystal violet and Eriochrome black T and more than 80% dye was adsorbed for Rhodamine B (Figure 7). For Rhodamine B, dye adsorption study was further investigated and found that 92% adsorption was done after 48h (Figure 21)**.** UV-Vis spectroscopy was further performed to understand the adsorption of these dyes from aqueous solution. Surprisingly, it was found that the dye was adsorbed by the gel leaving behind the clear water (Figure 8A, 8B and 8C). The morphological analysis was performed for these dye adsorbed gel through FE-SEM analysis. The hydrogen bonding, and/ or π-π stacking between the dye molecules and the gelator molecule may be responsible for the morphological change of this gelator molecule after dye adsorption.

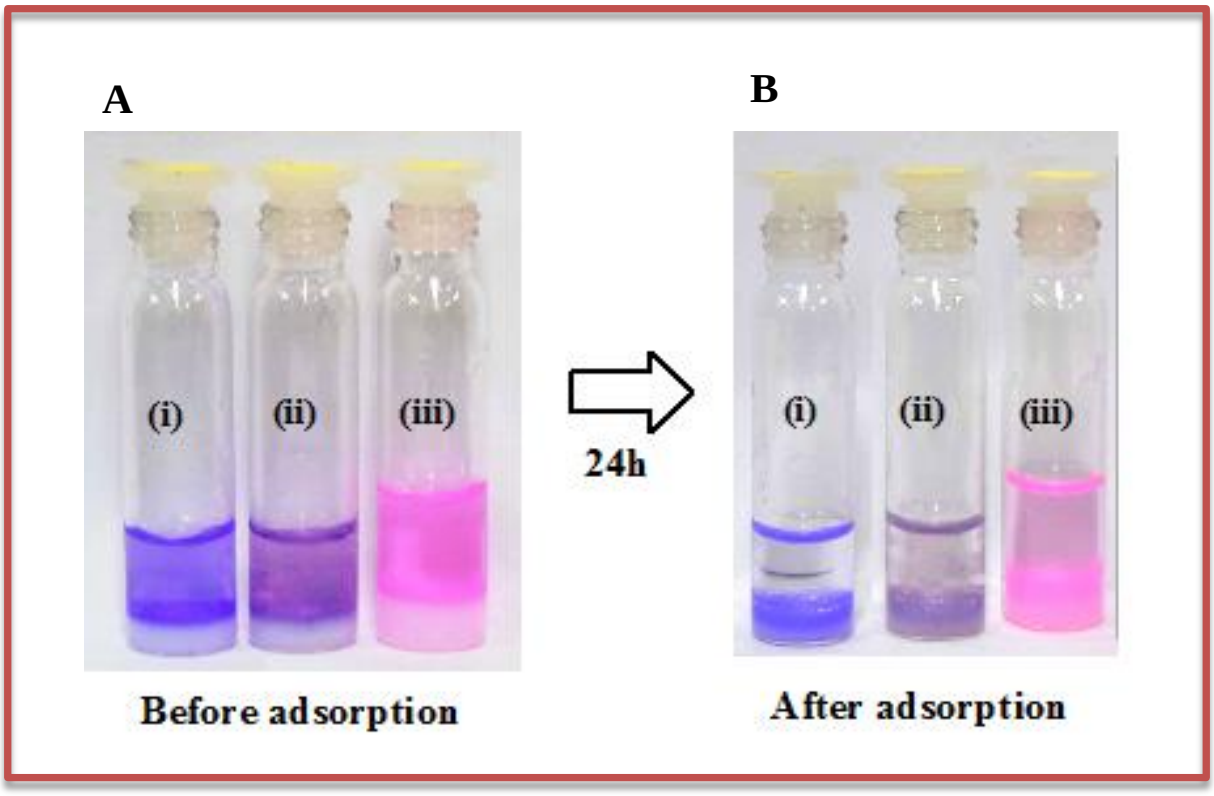

Figure 7*. Photographic images of the gel obtained from the gelator dipeptide i) Crystal violet ii) Eriochrome black T iii) Rhodamine B; (A) Before adsorption, (B) After adsorption.*

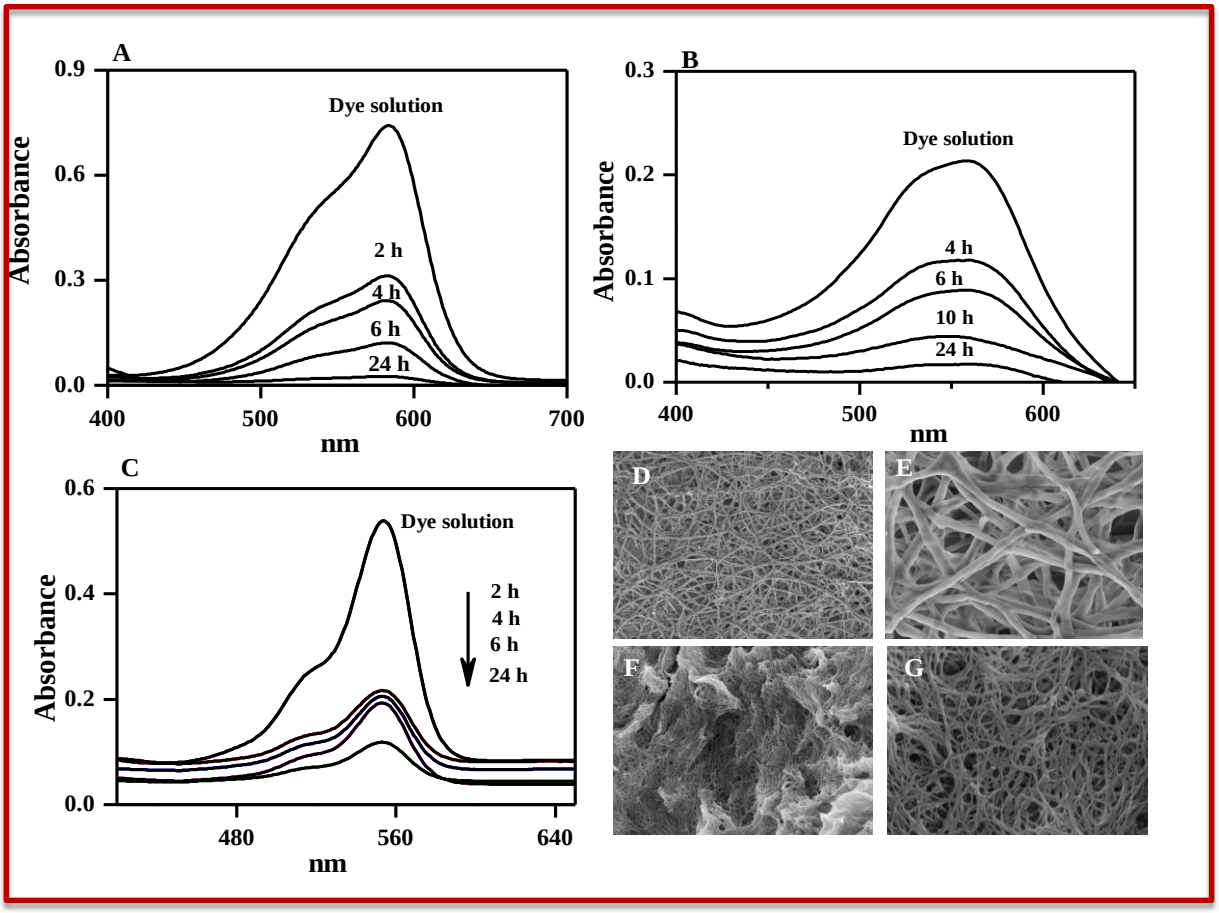

Figure 8. *UV data for time dependant adsorption for aqueous dye solution (A) Crystal violet (B) Eriochrome black T (C) Rhodamine B; (D), (E) represent FE-SEM images of the crystal violet adsorbed gel. (F) and(G) represent FE-SEM images of the Rhodamine B adsorbed gel.*

2.3.8 Selective organogelation

Phase selective organogelator (PSOG) are capable gelling organic solvents in the presence of second, immiscible solvents, which is typically water and they are being explored for a range of environmental remediation applications including oil spill containment. In recent times, low molecular weight supramolecular gels (LMWG) offer a unique application through selective gelation of oil products having molecular weight larger than their own molecular weight. This property can be used as oil-spill remediation-so called 'bio-refinery design'. The insoluble behaviour of the organogel in water and good gelation ability in many organic solvents make them suitable for selective gelation of oil in oil water mixture. To

carry out this experimental procedure, 5 mg compound was added to the mixture of 1 mL of toluene-pet-ether mixture (1:20) and 1 mL of water in a glass vial in Figure 9. Then the glass vial was heated to solubilise the compound in this two-phase and shaken vigorously to make it homogeneous. After cooling to room temperature the organic layer was gelated and water layer remained intact in its liquid state. Further, experiments were carried out for toluene-kerosene and toluene-diesel system and surprisingly, this dipeptide was capable of forming gel in these solvent systems keeping water part intact (Figure 17 and 18).

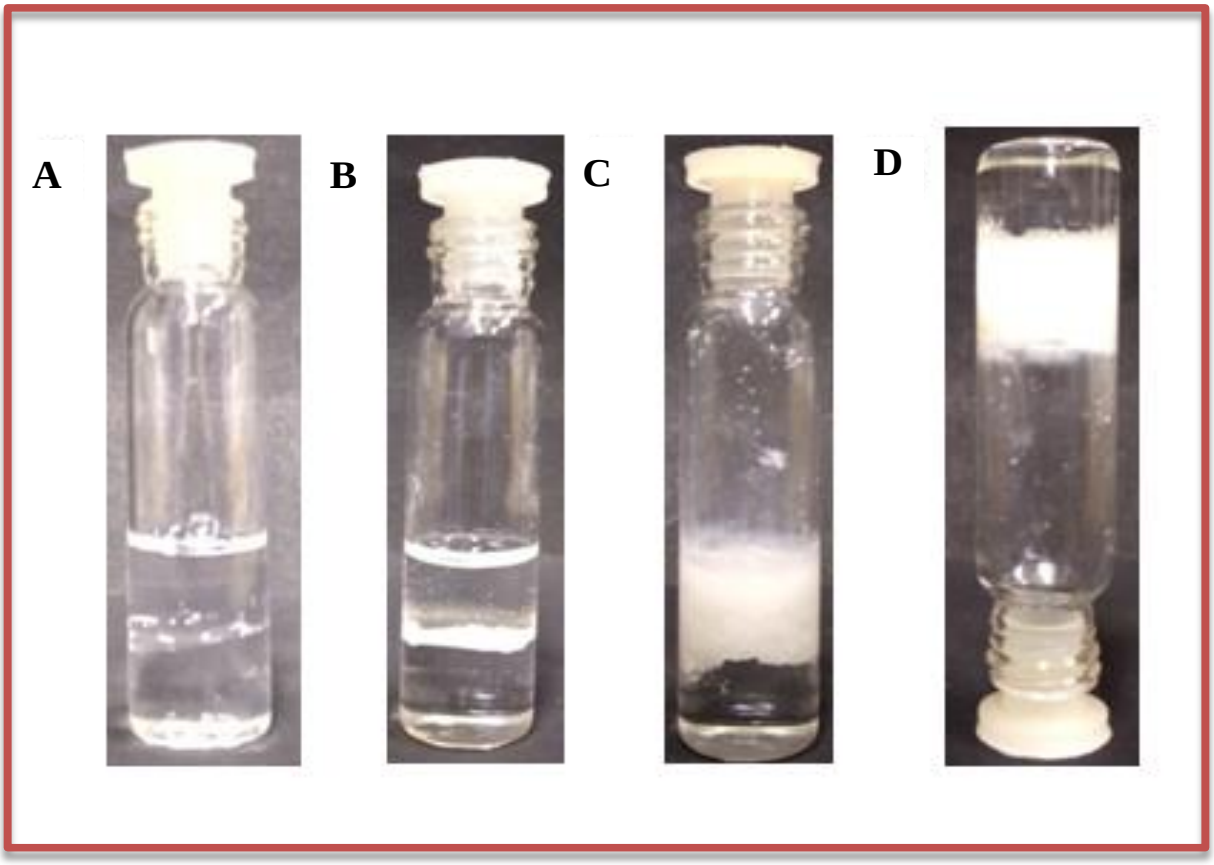

Figure 9. *Photographic images of the phase selective gelation of the gelator dipeptide. (A) 1 mL of toluene- pet ether mixture (1:20) and 1 mL of water with the gelator. (B) Gelator was dissolved in by heating. (C) Selective gelation of toluene-pet ether layer at room temperature. (D) Inversion test was performed with this phase selective gelator.*

2.4 Conclusions

This work represented here vividly demonstrated the formation of a new low molecular weight gelator peptide consisting of N-(*tert*-butoxycarbonyl) pentafluoro- L – phenylalanine and O-benzyl-L-tyrosine. The gelation propensity of this dipeptide was investigated in various mixtures of solvents. Water is found to be an essential component along with polar protic solvent systems for gelation of this dipeptide. In addition, long chain hydrocarbon unit is found to be important in assistance with aromatic solvents for gelation of this dipeptide. Both the gels obtained from these two solvent systems were thermoreversible and translucent in nature. These gelator molecules had the potential application in waste-water treatment. Interestingly, the gel obtained from methanol-water solvent system had been used to adsorb three different toxic dyes (Crystal violet, Eriochrome black T and Rhodamine B) from aqueous solution. The gel prepared from aromatic solvent and long chain hydrocarbon was effectively active as a PSG (phase selective gelator) in oil spill recovery. The relatively low-cost starting materials to synthesize the gelator, the low amount required for the formation of the gel and the higher amount of absorption capacity of the gel hold future promise for using this soft material in waste-water management.

2.5 Supporting information

2.5.1 Characterization of the dipeptides

^{1}H and ^{13}C NMR spectra of N-(*tert*-butoxycarbonyl)pentafluoro-L-phenylalanine - O-benzyl-L-tyrosine methyl ester

^{1}H NMR (600 MHz, DMSO-d_6): δ (in ppm) 8.50 (1H, d, *J* = 6Hz, NH of amide), 7.40 (2H, d, *J* = 12Hz, Ar-H), 7.34 (2H, t, *J* = 12Hz, Ar-H), 7.29-7.27 (1H, m, Ar-H), 7.08 (2H, d, *J* = 12Hz, Ar-H), 6.94 (1H, d, *J* = 6Hz, NH of BOC group), 6.87 (2H, d, *J* = 6Hz, Ar-H), 5.03 (2H, s, -O-CH_2-Ar), 4.39-4.35 (1H, m, CαH), 4.29-4.25 (1H, m, CαH), 3.58 (3H, s, -CH_3 of ester group), 2.94-2.88 (2H, m, -CH_2-), 2.80-2.77 (1H, m), 2.74-2.70 (1H, m), 1.27 (9H, s, -CH_3 of tertiary butyl group).

^{13}C NMR (150 MHz, DMSO-d_6): δ (in ppm) 172.16, 170.18, 157.55, 155.27, 137.61, 130.58, 129.46, 128.84, 128.20, 128.03, 114.91, 78.88, 69.51, 60.24, 54.31, 53.10, 52.36, 36.29, 31.44, 28.33, 26.26, 22.55, 14.56.

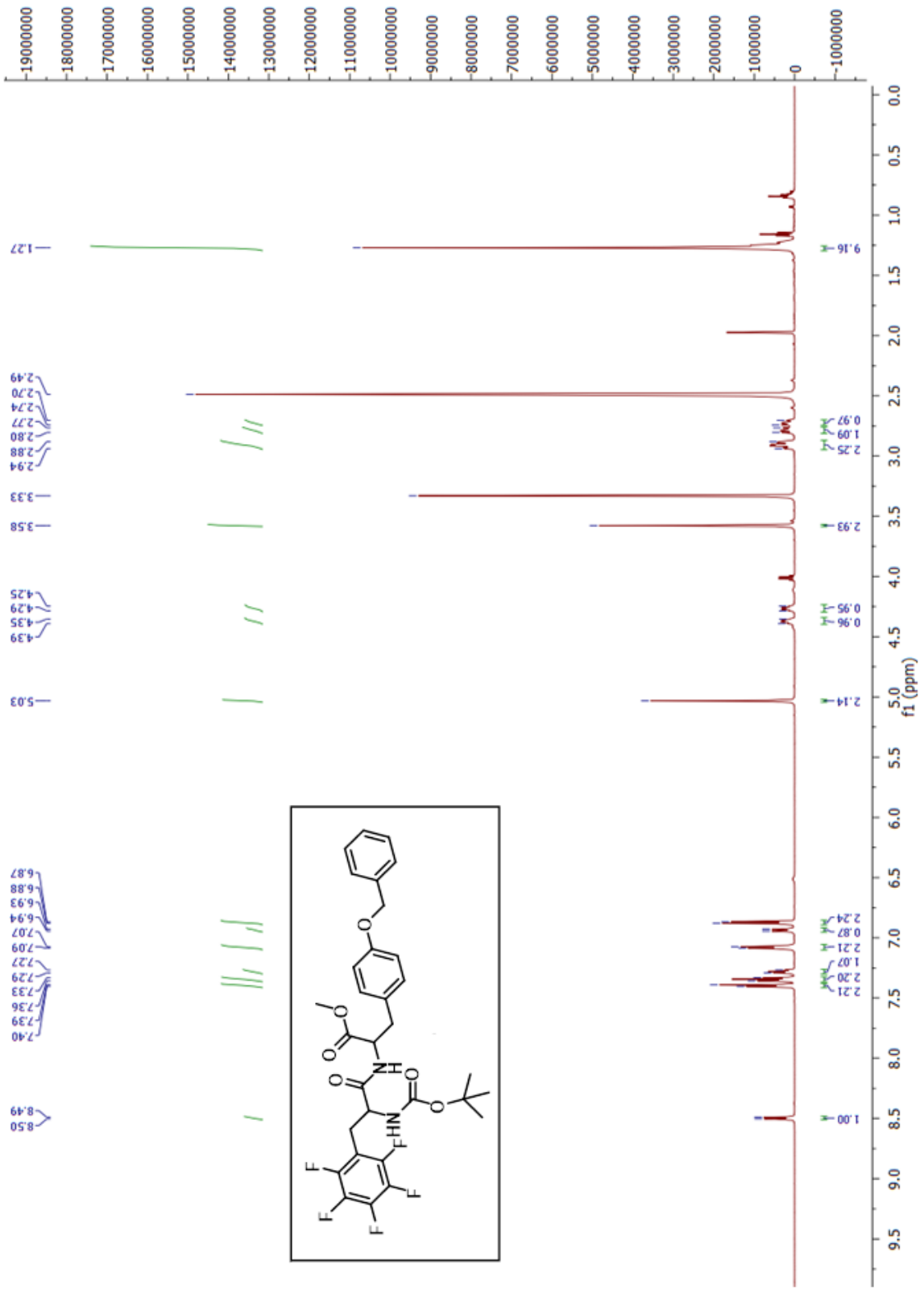

Figure 10. *^{1}H NMR spectra of N-(tert-butoxycarbonyl) pentafluoro-L-phenylalanine - O-benzyl-L-tyrosine methyl ester*

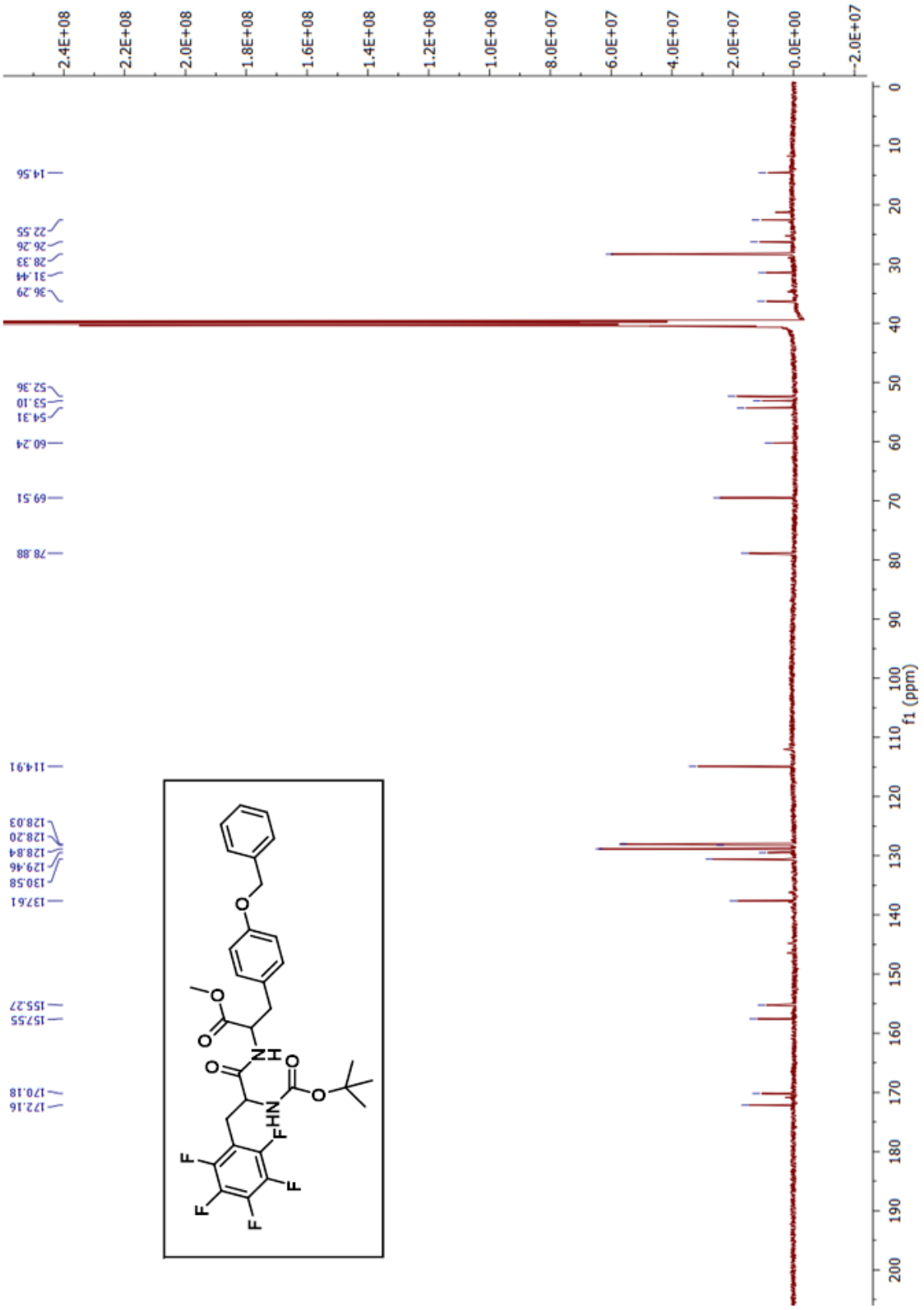

Figure 11. *^{13}C NMR spectra of N-(tert-butoxycarbonyl) pentafluoro-L-phenylalanine - O-benzyl-L-tyrosine methyl ester.*

^{1}H and ^{13}C NMR spectra of N-(tert-butoxycarbonyl)-L-phenylalanine - O-benzyl-L-tyrosine methyl ester

^{1}H NMR (600 MHz, DMSO-d_6): δ (in ppm) 8.28 (1H, d, *J* = 12Hz, NH of amide), 7.40 (2H, d, *J* = 6 Hz, Ar-H), 7.36 (2H, t, *J* = 6 Hz, Ar-H) , 7.31-7.29 (1H, m, Ar-H), 7.25-7.20 (4H, m, Ar-H), 7.17 (1H, d, *J* = 6 Hz, Ar-H), 7.13 (2H, d, *J* = 12 Hz, Ar-H), 6.90 (2H, d, *J* = 6 Hz, Ar-H), 6.84 (1H, d, *J* = 6 Hz, NH of BOC group), 5.04 (2H, s, -O-CH_2-Ar), 4.46-4.42 (1H, m, CαH), 4.19-4.15 (1H, m, CαH), 3.56 (3H, s, -CH_3 of ester group), 2.98-2.94 (1H, m), 2.90-2.87 (2H, m), 2.68-2.64 (1H, m), 1.27 (9H, s, -CH_3 of tertiary butyl group).

^{13}C NMR (150 MHz, DMSO-d_6): δ (in ppm) 172.29, 157.55, 155.52, 138.46, 137.98, 130.61, 129.59, 128.82, 128.39, 128.19, 128.04, 126.58, 114.99, 78.43, 69.54, 55.91, 54.16, 52.24, 37.83, 36.33, 28.54.

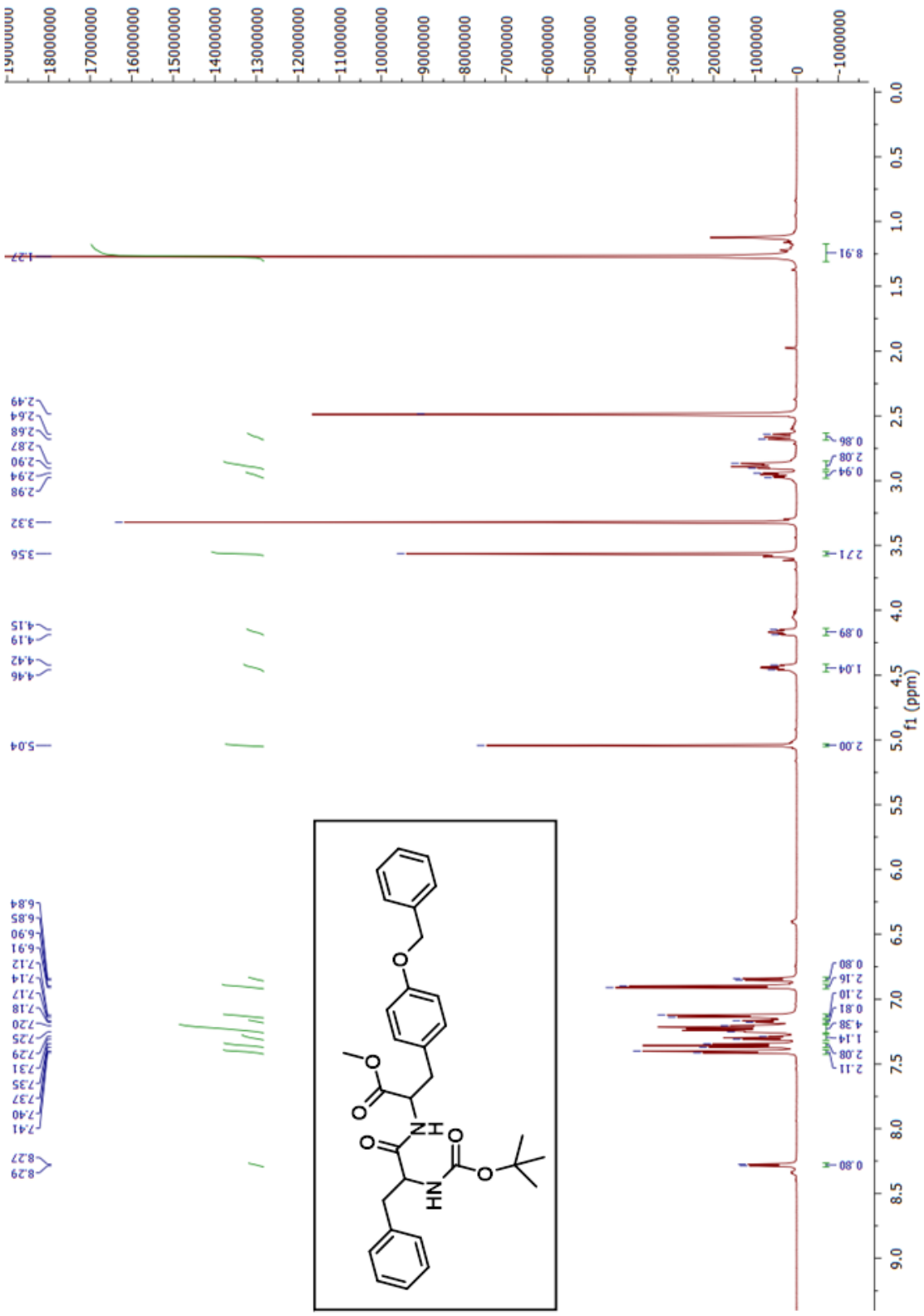

Figure 12.*[1]H spectra of N-(tert-butoxycarbonyl)-L-phenylalanine - O-benzyl-L-tyrosine methyl ester.*

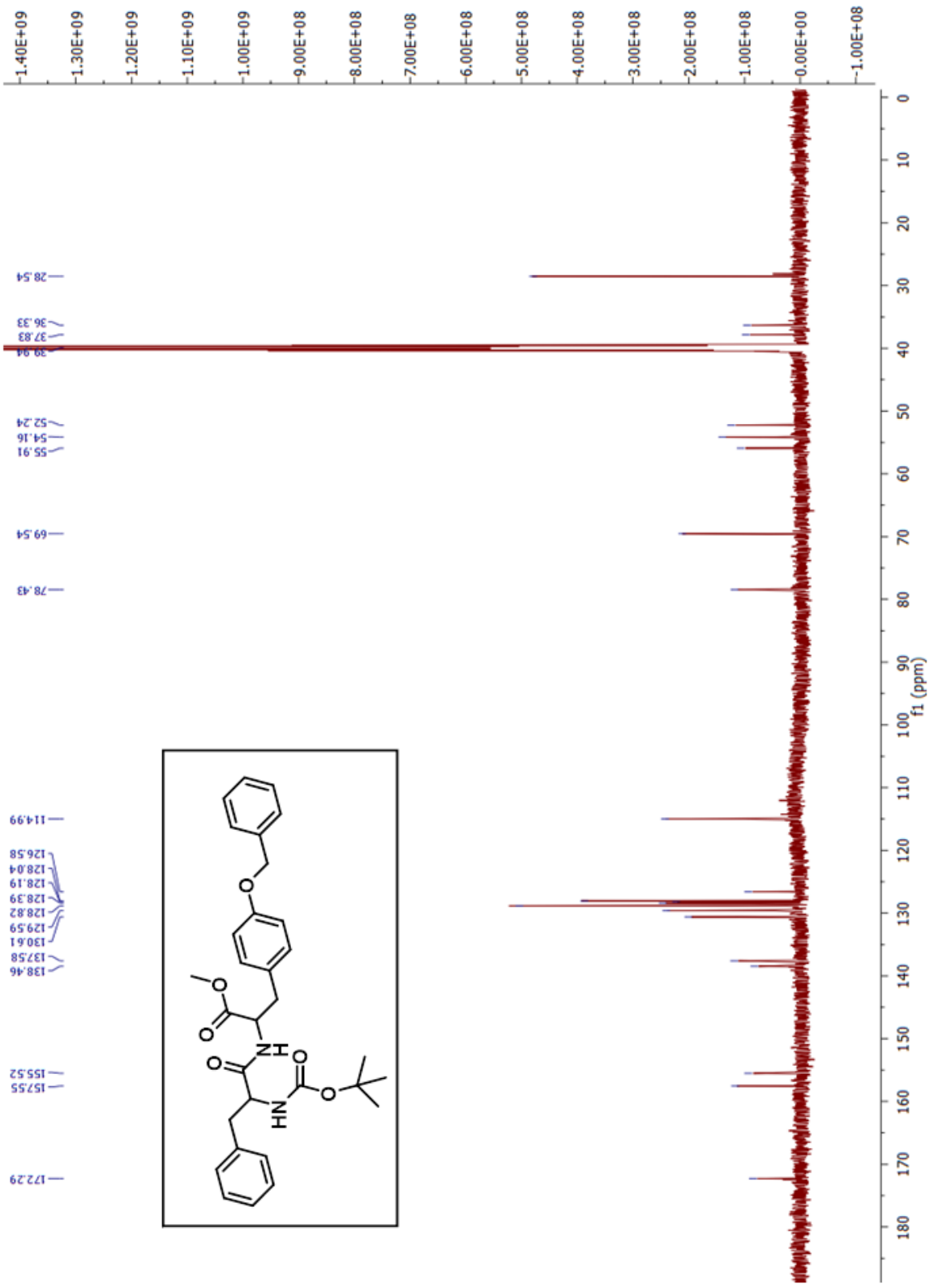

Figure 13. *^{13}C NMR spectra of N-(tert-butoxycarbonyl)-L-phenylalanine - O-benzyl-L-tyrosine methyl ester.*

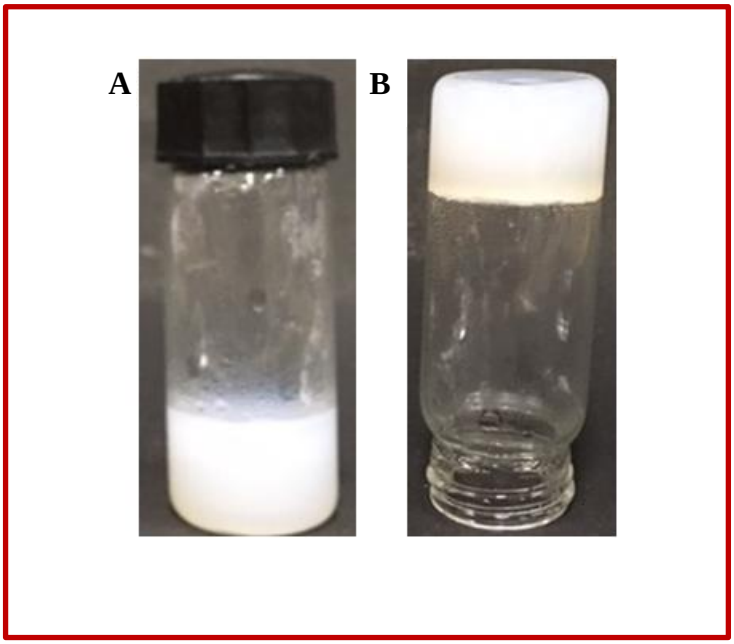

Figure 14. *Images of the gel obtained from gelator peptide (A) gel obtained from methanol-water mixture. (B) Tube inversion test of this gel.*

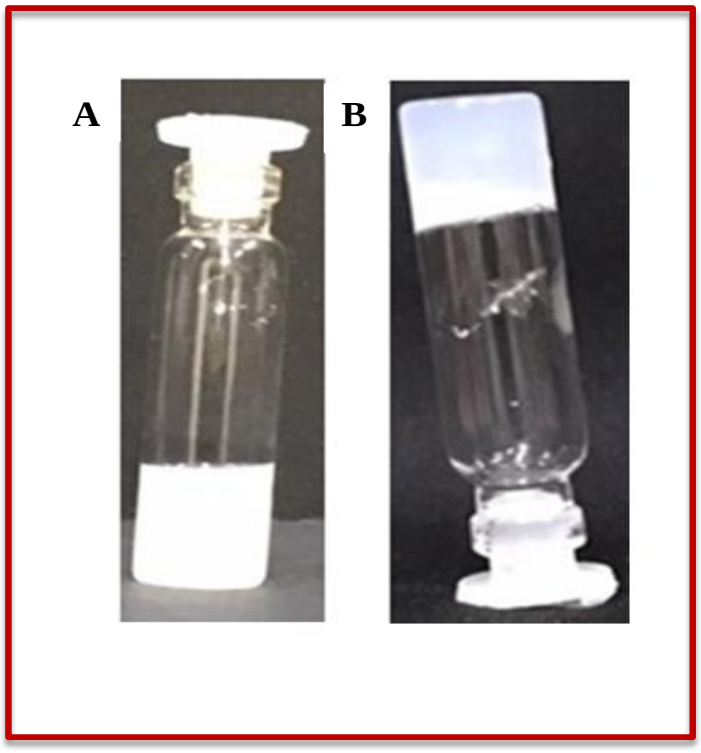

Figure 15. *Images of the gel obtained from gelator peptide (A) from toluene-petroleum ether mixture. (B) Tube inversion test of this gel.*

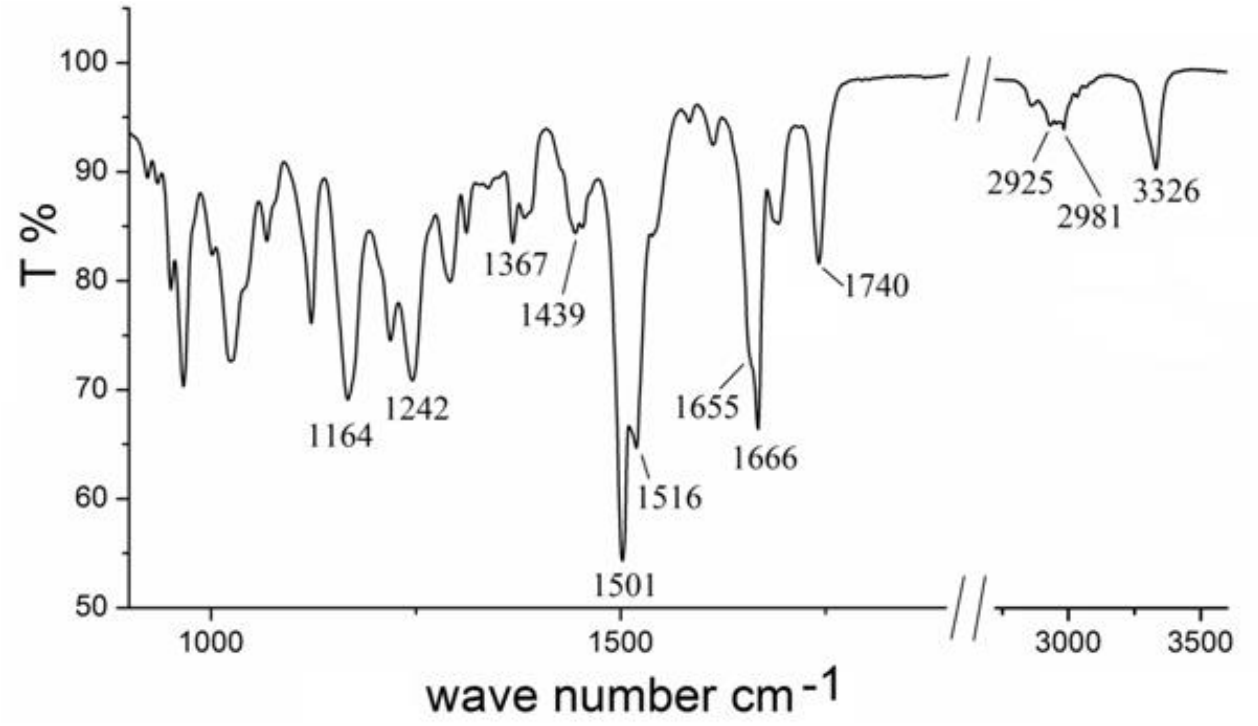

Figure 16. *Full range of FT-IR spectra of the dipeptide (TP1).*

Table 1: Assignments of the FT-IR bands in the solid state of TP1.

IR frequency (cm^{-1})	Modes of assignments	IR frequency (cm^{-1})	Modes of assignments
3326	amide NH asymmetric stretching	1516	amide II (N–H bend in plane and C–N stretch)
2981	CH_3antisymmetric stretching of tertiary butyl group	1501	aromatic C-C vibration
2925	CH_2 antisymmetric stretching	1439	CH_2 bending
1740	C=O stretching of the ester	1367	CH_3 of tertiary group symmetric bending
1666	amide C=O stretching (amide I) of carbamate carbonyl	1242	amide III (N-H bend in plane and C-N stretch)
1655	amide C=O stretching (amide I)	1164	Ester C–O asymmetric stretch

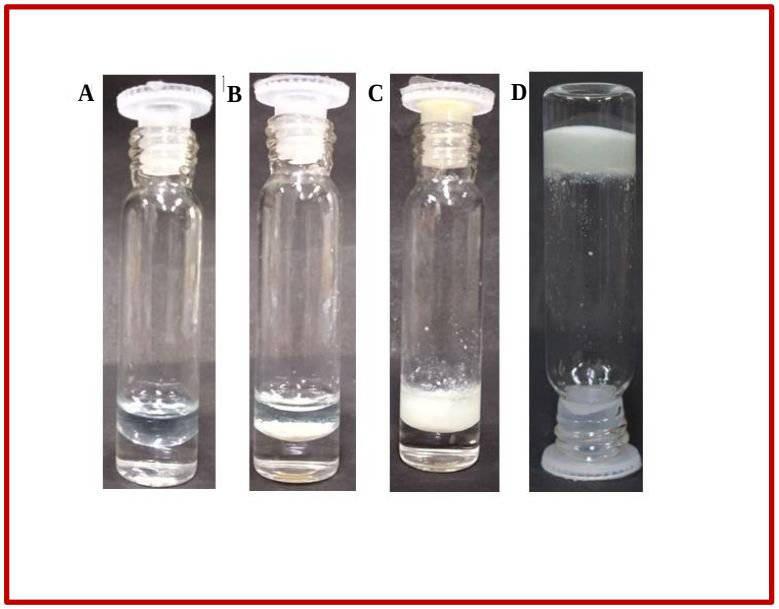

Figure 17. *Photographic images of the phase selective gelation of the gelator dipeptide (TP1): (A) 500µL of toluene- kerosene mixture and 500µ L of water with the gelator. (B) gelator was dissolved in by heating. (C) Selective gelation of toluene-kerosene layer at room temperature. (D) Inversion test was performed with this phase selective gel*

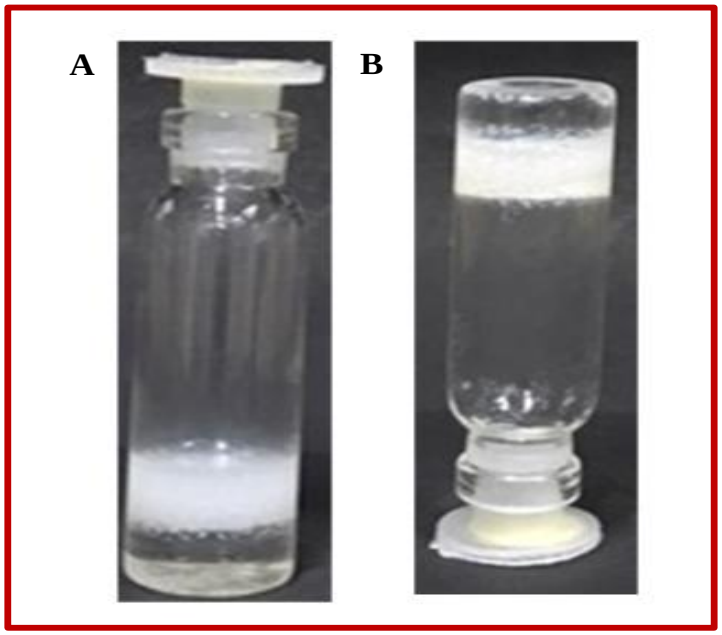

Figure 18. *Photographic images of the phase selective gelation of the gelator dipeptide(TP1): (A) Selective gelation of toluene-diesel layer at room temperature. (B) Inversion test was performed with this phase selective gel.*

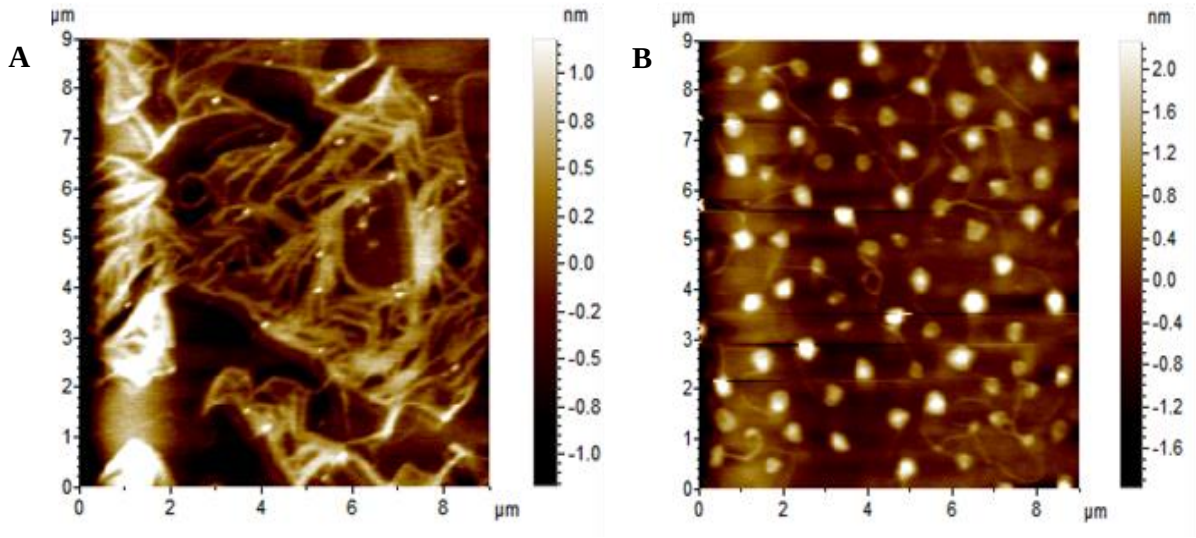

***Figure 19**. Atomic force microscopic images N-(tert-butoxycarbonyl)-L-phenylalanine- O-benzyl-L-tyrosine methyl ester dipeptide (A) Methanol-water (B) Toluene-petroleum ether.*

2.4.8. Gelation study of N-(tert-butoxycarbonyl) -L-phenylalanine-O-benzyl-L-tyrosine methyl ester in different solvent system.

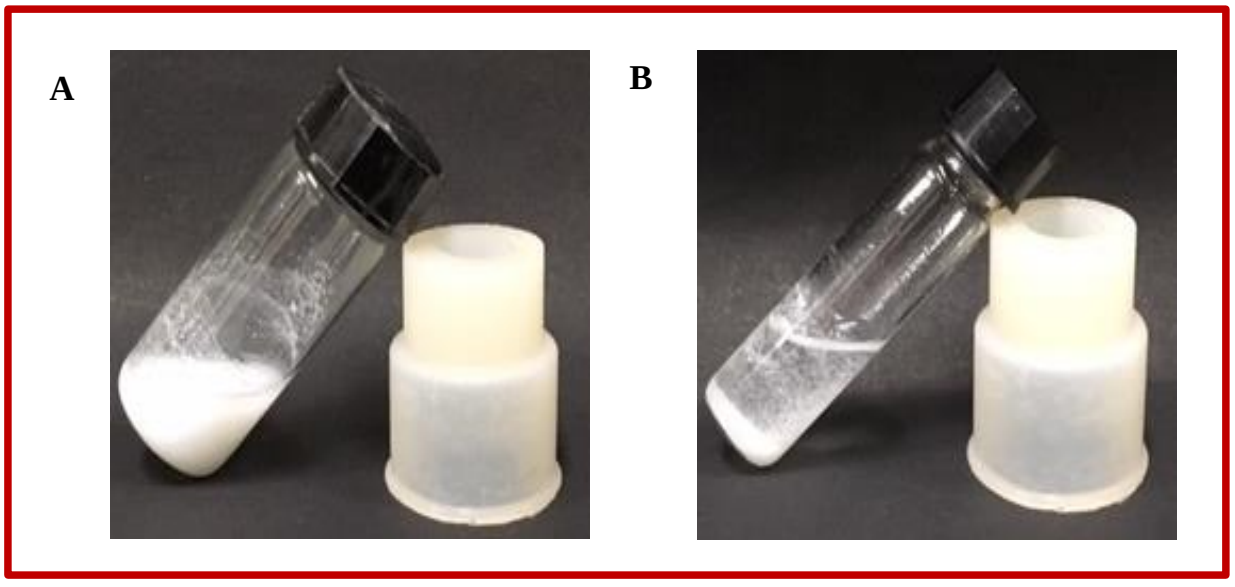

***Figure 20**. Gelation study of N-(tert-butoxycarbonyl) -L-phenylalanine-O-benzyl-L-tyrosine methyl ester in different solvent system : N-(tert-butoxycarbonyl)-L-phenylalanine - O-benzyl-L-tyrosine methyl ester formed suspension in (A) methanol-water and (B) toluene-petroleum ether solvent system.*

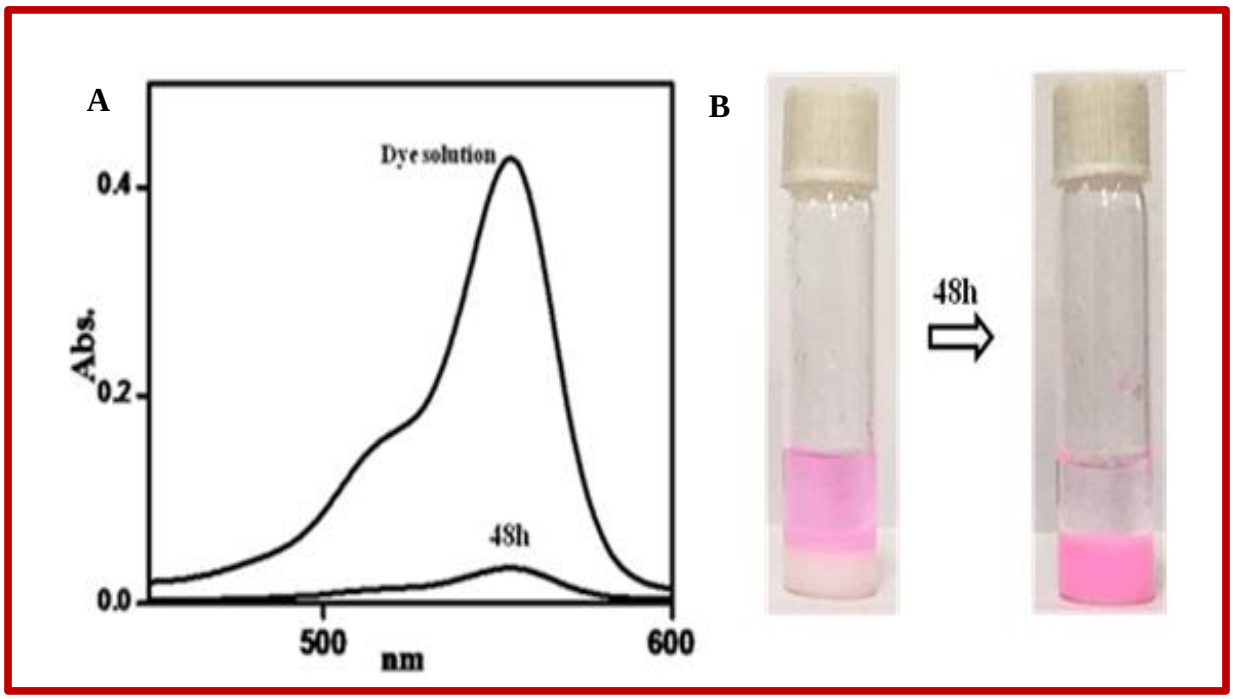

***Figure 21**. (A) UV data for time dependant adsorption for (~0.01mM) Rhodamine dye solution (B) photographic images of the dye adsorption solution of TP1.*

CHAPTER 3

STRUCTURE AND SELF-ASSEMBLY OF TWO de-novo DIPEPTIDES IN METHANOL: MOLECULAR DETAILS BY NMR AND VIBRATIONAL SPECTROSCOPIC ANALYSES

3.1 Aim of the present work

The evolving interest in nanotechnology has enthused the development and discovery of new materials that can self-assemble into well-ordered structures at the nanometer size. However, such ordered and reproducible structures are very common motif in biological systems; they are a tremendous challenge for material science. In the past few decades, research efforts were carried out on peptide based self-assembled systems due to their diverse applications. Short peptides are easy to design, synthesize and making them excellent model systems for biological systems. In this chapter, investigations were performed on the self-assembly pattern of two dipeptides composed of O-benzyl-L-tyrosine and differently protected (substituted) side chain of glutamic acid residue. A small change in the side chain variation of the peptide residues caused significant difference in morphological pattern of the aggregates produced in MeOH. The difference in the structure of two peptides was linked to mainly side chain variation. TBP1 contained methyl ester of glutamic acid part and TBP2 contained benzyl group protected glutamic acid residue. This small variation was responsible for the formation of aggregates of two distinct morphologies: TBP1 produced elongated fibrillar network and TBP2 produced oligomeric assembly in methanol. The difference in self-assembly pattern of these dipeptides enhanced our interest to study in detail the key molecular forces responsible for generation of these morphology. Several spectroscopic analyses such as- UV, NMR, FT-IR and Raman analyses were carried out. Not only the experimental methods, The UV-Vis, FT-IR and Raman spectra were recorded and compared with the computational spectra obtained by density functional method (DFT/B3LYP) with 6 31G (d) basis set. Molecular dynamic simulation study was carried out for both the peptides. Further investigation on dipeptide which underwent to produce fibrillar aggregates can form gel in methanol-water solvent system at 1:1 ratio.

3.2 Introduction

Synthesis of short peptides gained momentum in last two decades due to their biocompatibility, biodegradability and some resemblance with proteins.[125,157] They were also known to form self-organized nano-architechtures which show various applications in bio-interface engineering, biosensors, advance material science and therapeutics etc.[158–162] Therefore, several studies have been carried out using peptide based materials ranging from three-dimensional (3D) cell culture scaffolds to artificial enzymes, antibacterial, anticancer agents, hemostasis treatments, optical waveguides, and semiconductors.[51,161,163] Potential strategies are taken for the in-vitro fabrication of higher ordered structures from nano to supramolecular architectures from these small peptides.[164,165] Many of these molecules are considered as amazing building blocks for developing self-assembled nanostructures.[43,166,167] Recently, the nanostructure based supramolecular architectures are evolving its interest beyond constructing complex morphologies towards the potential applications of self-assemblies.[168–173] The self-assembled nanostructures produced from these small peptides however depends on the constituent of amino acids and the selection of appropriate solvent.[51,174] The available twenty amino acids control various physicochemical and structural features to the overall morphology of the peptide due to the presence of variety in charge, hydrophobicity, size, and polarity in side chains. Several physicochemical parameters such as pH, ionic strength, solvents, light, temperatures, time, peptide concentration, surrounding media, and its processing route are responsible for the phase and morphological transition of peptides to gain different nanostructures.[174–180] Apart from other parameters involved in the self-recognition process the polarity of the solvent present in the incubation medium plays a significant role for the formation of these self-assemble structures via peptide-solvent interactions. The self-assembly pattern of di-phenyl alanine in binary solvent system was examined by Huang et al. Where

it was found that this dipeptide formed microtubes and nanofibers in this solvent system.[174] Rissanou et al. examined the morphological changes associated with di-alanine and di-phenylalanine peptides in methanol and water solvent respectively. Where they found different nanostructures like fibers, tubes, amorphous in different solvent condition and temperature.[181] Another research group examined morphological pattern of tri-phenylalanine in various solvent mixtures. A wide range of nanostructures like helical fibrils, grouped needle, doughnut-like hollow shapes, micro-bottles and leaves like dendrimers etc. were obtained from these investigation.[182] The solvent controlled structural transition of a symmetric amphiphilic peptide KI_4K was described by Zhao et al. [183]

Previous investigations mainly focused on the structural intricacy and self-assembly pattern obtained from benzyl protected amino acid residues like cysteine, tyrosine etc. The morphological behaviour of two side chain benzyl protected cysteine dipeptide revealed nanotubular structure in aqueous media. The non- covalent interactions involving hydrogen bonding and π-π stacking helped to provide the orientation of nanotubular self-assembly of this benzyl protected cysteine dipeptide in aqueous medium.[184] Next investigation performed with terminally benzyl protected cysteine tripeptide moiety. Surprisingly, this tripeptide generated annular and proto-fibrillar assemblies in methanol solvent. The weak forces such as- hydrogen bonding, π-π stacking, vander waals and hydrophobic interactions cooperatively provide the generation of intact and well-ordered three dimensional structures upon aging the tripeptide in methanol.[143] Interestingly, spherical assemblies were generated when one phenyl alanine was incorporated into cysteine dipeptide moiety. The morphological behaviour of this tripeptide was examined in different organic solvent under concentration dependant manner.[144] Moreover, this tripeptide exhibited significant cytotoxicity toward different cancer cell lines and induced apoptosis to promote cancer cell. Apart from the effect of solvent present in the incubation media, the

concentration of peptide plays a significant role in self-organization process. Naskar et al. described transition of an oligo-peptide from nanovesicles to nanotubes at neutral pH under concentration dependent manner.[185]

3.3 Results and Discussion

In this work, the ability of self-assembly pattern of two dipeptides that contain benzyl protected tyrosine and different side chain protected glutamic acid residues were thoroughly examined (Figure 1). The investigation was performed by synthesizing two *de novo* peptides TBP1 (*N*-Boc-(O-benzyl)-tyro-(di-methyl)-glutamate) and TBP2 (*N*-Boc-(O-benzyl)-glu-(O-benzyl)-tyrosine-methyl ester (Figure 1). The small changes in the substituent groups in the peptide residues caused a significant difference in their structural alignment and the self-assembly formation that produced nano size aggregates of two distinct morphologies. The peptide TBP1 which contains methyl ester of glutamic acid formed highly cross-linked fibrillar network where TBP2 having benzyl protected glutamic acid residue formed oligomers in MeOH. The morphological transition of these two peptides depends on the concentration as well as the incubation time of peptide solution. This difference in morphological behaviour of two peptides encouraged to study them in detail by NMR and vibrational spectroscopic analyses. Furthermore, the HOMO-LUMO energies as well as their energy gap and vibrational spectroscopic results were computed by density functional theory calculation. The calculated and experimental electronic absorption spectra of the peptides showed no significant difference in their electronic transition behaviour. FT-IR and Raman spectra of both TBP1and TBP2 in solid state showed peptide amide I band at ~1650 $cm^{-1}$and indicated similar conformation state of the amide group in the peptide bonds. However, molecular interactions of the peptides in methanol differed and caused formation of assembly structure of different morphologies. It was confirmed by D_2O exchange proton NMR measurements that the peptide NH of TBP1 was more exposed and rapidly exchanged with D_2O

compared to peptide NH in TBP2 which showed slower deuterium/proton exchange in DMSO solvent. Both thioflavin T fluorescence measurement and FT-IR analysis indicated that fibrillar assembly produced by TBP1 and compact ß-sheet conformation while TBP2 produced no fibrillary network with compact sheet structure. The blue shift of the peptide carbonyl Raman frequency to~1657 cm^{-1} indicating more ordered structure of TBP1 due to fibrillation. Interestingly it was also observed that fibrillary network produced by TBP1 showed gel properties and oligomers of TBP2 failed to do this gel forming unique properties. This chapter describes an interesting study in detail to show how protecting groups in small dipeptide controls the three dimensional morphologies of the molecules in their nanoformulations.

3.3.1 Synthesis of two dipeptides

The current investigation illustrated the synthesis of two novel peptides and showed how the presence of an additional phenyl group resulted formation of different type of self-assembly structure in methanol. Two dipeptide molecules were chemically synthesized in the laboratory: In one peptide O-benzyl-L-tyrosine linked to methyl ester of glutamic acid residue and produce N-Boc-(O-benzyl)-tyro-(di-methyl)-glutamate abbreviated as TBP1 and in another molecule O-benzyl-L-tyrosine coupled with benzyl protected glutamic acid residue generated N-Boc-(O-benzyl)-glu-(O-benzyl)-tyrosine-methyl ester abbreviated as TBP2. The molecular architectures of the peptides are shown in Figure1.

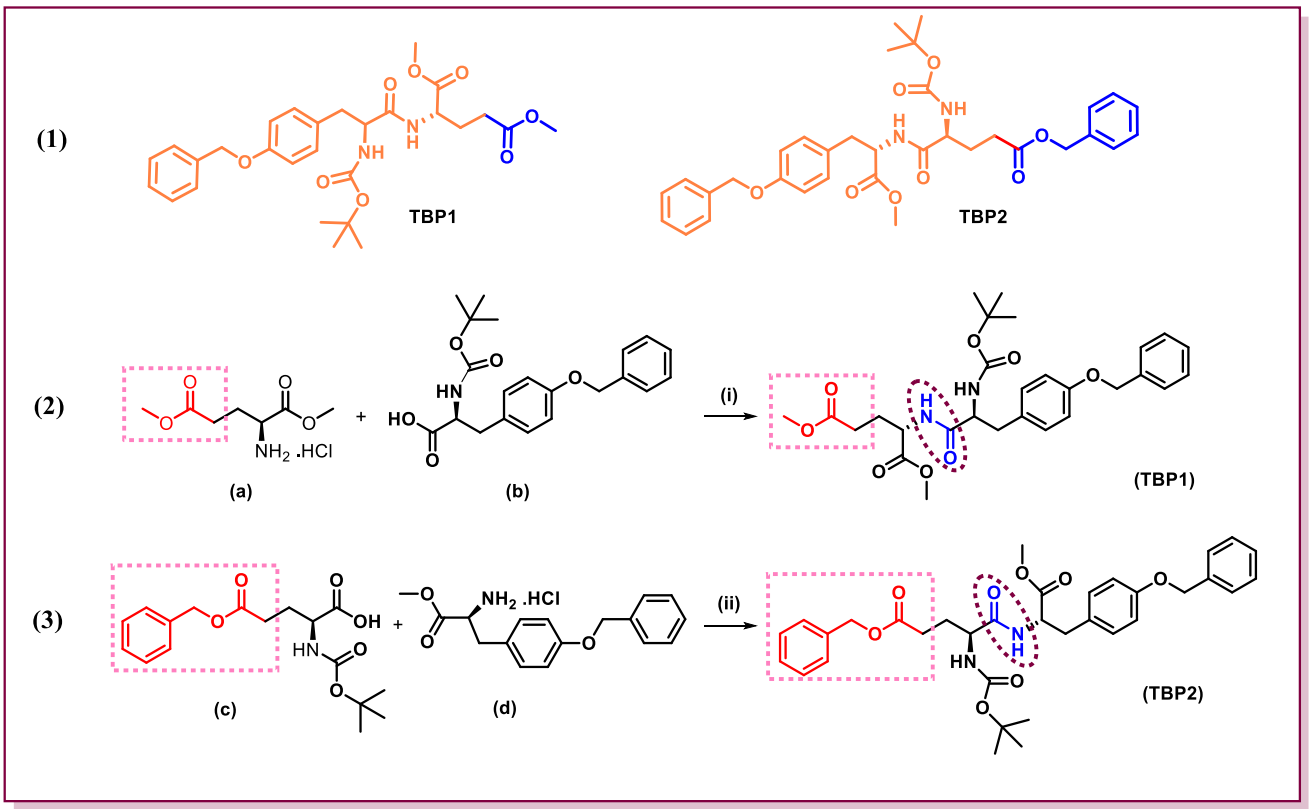

Figure 1. *Structure and schematic presentation of synthesis of two novel dipeptides.*

(1) Structure of the two peptides: N-Boc-(O-benzyl)-tyro-(di-methyl)-glutamate (TBP1) and N-Boc-(O-benzyl)-glu-(O-benzyl)-tyrosine-methyl ester (TBP2). (2) Substrates for synthesis of TBP1: methyl ester of glutamic acid (a), N-(tert-butoxycarbonyl)-O-benzyl-L-tyrosine (b). (3) Substrates for synthesis of TBP2: N-(tert-butoxycarbonyl)-O-benzyl-L-glutamic acid (c), methyl ester of O-benzyl-L-tyrosine (d). (i) and (ii) are marked for experimental conditions, the reaction was done with EDC.HCl (1-ethyl-3,3-(dimethylamino) propyl carbodiimide hydrochloride), HOBT (hydroxylbenzotriazo le), TEA (triethylamine), 0^{o}C to RT, reaction duration 8h.

Synthesis of TBP1

To a well-stirred solution of N-(tert-Butoxycarbonyl)-O-benzyl-L-tyrosine (b ; 500 mg, 1.34 mmol) dissolved in N,Ndimethylformamide (8 mL), was added anhydrous hydroxybenzotriazole (HOBt; 218 mg, 1.6 mmol) followed by 1- ethyl-3,3-(dimethylamino) propyl carbodiimide hydrochloride (EDC•HCl; 387 mg, 2.01 mmol) under cold condition and nitrogen atmosphere. The stirring was continued for 10 min under ice-cooled condition and then triethylamine (TEA; 1 mL, 10 mmol) was added to this mixture along with methyl ester of glutamic acid (a; 340

mg, 1.6 mmol); subsequently, the reaction was further continued for 8 h at room temperature and completion of the reaction was monitored via thin-layer chromatography (TLC). The reaction mixture was then concentrated under reduced pressure, diluted with water and extracted with ethyl acetate from aqueous layer. The crude product was obtained after evaporation of the solvent and purified by column chromatography over silica gel (petroleum ether /ethyl acetate 70:30) to afford peptide "TBP1" as white solid (yield = 75 %).

Synthesis of TBP2

To a well-stirred solution of N-(tert-Butoxycarbonyl)-O-benzyl-L-glutamic acid (c ; 500 mg, 1.48 mmol) dissolved in N,Ndimethyl formamide (8 mL), was added anhydrous hydroxybenzotriazole (HOBt; 240mg, 1.77 mmol) followed by 1- ethyl-3,3-(dimethylamino) propyl carbodiimide hydrochloride (EDC·HCl; 426 mg, 2.22 mmol) under cold condition and nitrogen atmosphere. The stirring was continued for 10 min under ice-cooled condition and then triethylamine (TEA; 1.5 mL, 10 mmol) was added to this mixture along with methyl ester of O-benzyl –L-tyrosine (d; 571 mg, 1.48 mmol); subsequently, the reaction was further continued for 8h at room temperature and completion of the reaction was monitored via thin-layer chromatography (TLC). The reaction mixture was then concentrated under reduced pressure, diluted with water and extracted with ethyl acetate from aqueous layer. The crude product obtained after evaporation of the solvent was purified by column chromatography over silica gel (petroleum ether /ethyl acetate 75:25) to afford peptide "TBP2" as white solid (yield = 70 %).

3.3.2 Electronic (absorption) behaviour

UV-Vis study

UV−Vis absorption spectra of the dipeptides TBP1 and TBP2 (dissolved in methanol) were acquired using a JASCO V-630 spectrophotometer (JASCO

International Co. Ltd., Japan) within the wavelength range of 200−500 nm. A high-quality quartz cuvette having path length of 1 cm was used for spectral measurement. Concentration of the peptide was kept ~ 10 µM.

DFT study

Gaussian 09, Revision E.01 program was used for quantum chemical calculations.[186] The calculations were carried out for both peptides (TBP1 & TBP2) using the density functional theory (DFT) with B3LYP[187,188] functional and 6-31G (d) basis set.[189,190] UV-vis spectra and electronic properties such as HOMO and LUMO energies were calculated using time-dependent DFT with self-consistent field (TD-SCF/DFT), B3LYP functional using 6-31G (d) basis set in methanol under Polarizable Continuum Model (PCM).[191,192]

A dilute solution (~ 10µM) of TBP1 in methanol showed a broad absorption spectrum (Figure 2A) in the UV region. The dipeptide showed absorption maxima at λ_{max} = 273 nm. The absorption was assigned to π−π* transition. The dipeptide TBP2 also showed similar absorption behaviour like TBP1 (Figure 2C). Figure 2B present the calculated UV-vis spectra of TBP1in methanol solvent under Polarizable Continuum Model (PCM) using TD-B3LYP (SCF) level of theory and 6-31G (d) basis set. It exhibited absorption bands at λ = 247.91 nm (ΔE ≈ 5.0012 eV), 237.07 (ΔE ≈ 5.2299 eV), 231.51 (ΔE ≈5.3555 eV) (Table 1) for first three excited states. Maximum transition probability was associated with electronic state 141 (HOMO) to 143 (LUMO+2). The UV−vis spectra (Figure 2D) of TBP2 was also simulated in the methanol solvent using the same method. The calculated excitation energies, oscillator strengths of the simulated UV−Vis spectra are represented in Table 1. The dipeptide exhibited absorption bands at λ = 250.69 (ΔE ≈ 4.9458 eV), 240.51 (ΔE ≈ 5.1550 eV), 236.37 (ΔE ≈5.2454 eV) for first three excited states respectively in the methanol solvent. Each of the excited states was composed of several electronic transitions. Transition probability found to be maximum from electronic state 161 (HOMO) to 164

(LUMO+2). The oscillator strength was maximum for the absorption band with the first excited states. No major differences found in the absorption behaviour of these two dipeptides in the experimental or in theoretical analysis. However, non-covalent molecular interaction with self or solvent molecules were substantially differed and generated different type of association in methanol and methanol/water mixed solution condition as discussed below.

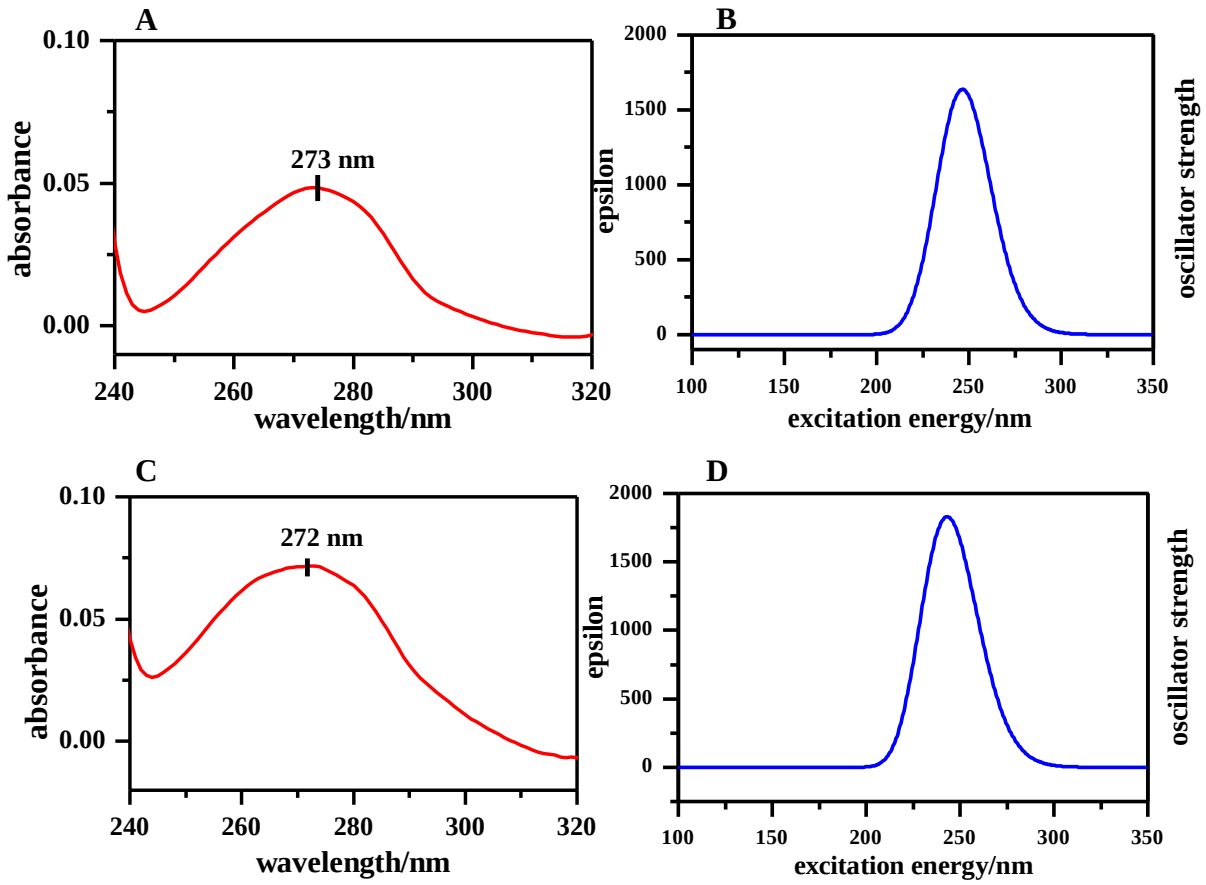

Figure 2. *Experimental and theoretical absorption spectra of TBP1 and TBP2.*

(A) and (C) are experimental UV-Vis spectra of TBP1 and TBP2, respectively, in methanol, for each peptide solution concentration was 10 μM. (B) and (D) are calculated absorption spectra of TBP1 and TBP2 respectively, for the calculation MeOH was chosen as solvent. The peak positions are marked.

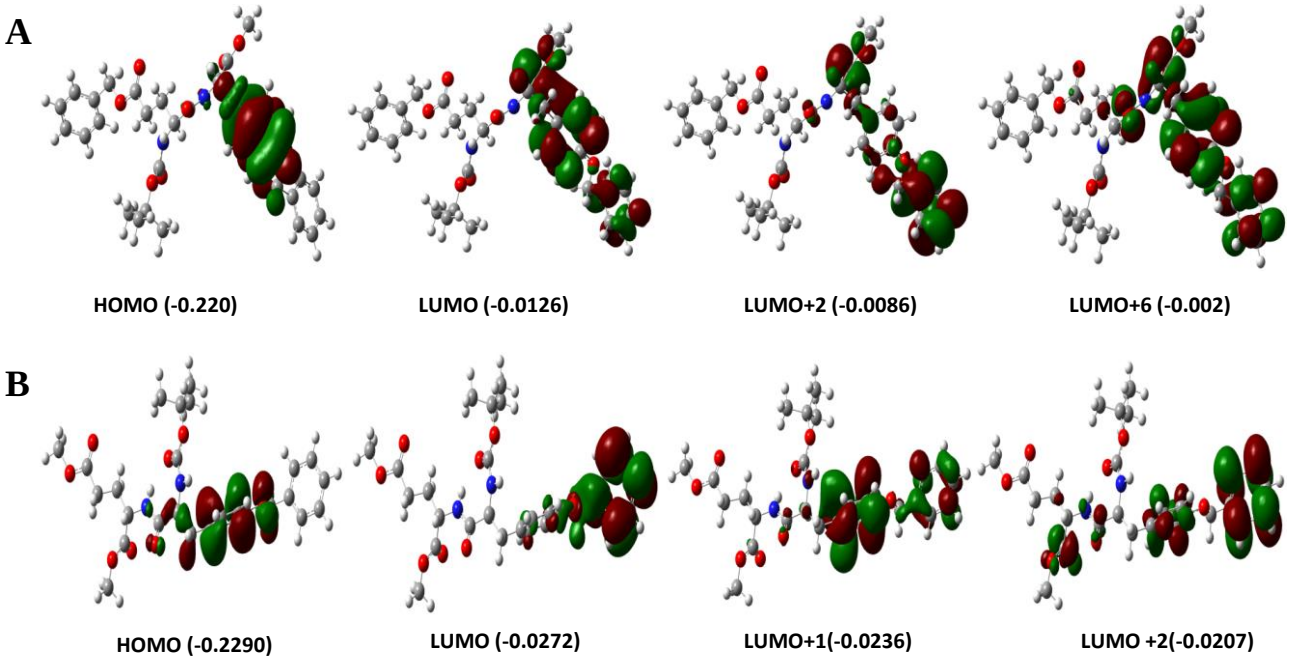

Figure 3. *Pictorial presentation of some key molecular orbitals of dipeptides, TBP1 & TBP2.*

(A) Key molecular orbitals (MOs) of dipeptide TBP2 obtained upon DFT analysis using TD-B3LYP(SCF) /6-31G (d) level involved in the electronic transitions generating absorption bands in methanol solvent. (B) Key molecular orbitals (MOs) of TBP1 using TD-B3LYP(SCF) /6-31G (d) level involved in the electronic transitions generating absorption bands in methanol solvent.

Table 1: Calculated wavelength absorption band (λ_{calc}/nm), oscillator strength, and probability and excitation energy of the simulated UV-Vis spectra of the dipeptides using TD-B3LYP (SCF) /6-31G (d) level for TBP1 & TBP2.

system	excited state	transition	wavelength λ_{calc}(nm)	oscillator strength	probability	excitation energy (eV)
TBP1	1	141 ->142	247.91	0.0371	0.61675	5.0012
	2	141 ->143	237.07	0.0014	0.63714	5.2299
	3	141 ->144	231.51	0.0047	0.63525	5.3555
TBP2	1	161->162	250.69	0.0196	0.6571	4.9458
	2	161 ->164	240.51	0.0175	0.6759	5.1550
	3	161 ->167	236.37	0.0127	0.5354	5.2454

3.3.3 Molecular Dynamics Simulations

Molecular dynamics (MD) simulations were performed with Desmond as implemented in Schrodinger Maestro (Academic release 2020-3) following previously published protocol.[193] In brief, monomers of the peptides were placed inside of an orthorhombic periodic boundary box with at least 10 Å buffer region on each side and solvated with explicit methanol. Simulations were run under isothermal–isobaric conditions in OPLS (optimized potentials for liquid simulations) force field. Systems were equilibrated with default relaxation protocol prior to the production run.[193] The (φ, ψ) angles were perturbed in the free peptides using an umbrella potential of width 5° and height 0.03 kcal/mol to obtain the complete potential energy profiles of the backbone torsion. Gas phase simulations were performed in a canonical ensemble without solvent.

Structural propensity of the peptides

Secondary structural propensity of a peptide backbone can be derived from the dihedral angle (φ, ψ) parameters (Figure 4). Therefore, the (φ, ψ) angle disposition in TBP1 and TBP2 was probed by free energy perturbation method using classical

molecular dynamics simulation. The dihedral angle φ is defined by the atoms C-N-Cα-C and is a measure of rotation over N-Cα bond, whereas the dihedral angle ψ is defined by N-Cα-C-N atoms and is a measure of rotation over Cα-C bond. The peptide bond -C-N- is rigid with the carbonyl O and amide H lying in a trans configuration in the amide plane. Thus, in peptide TBP1 and TBP2, there are two sets of dihedral angle as shown in Figure 4 and designated by (φ_1, ψ_1) and (φ_2, ψ_2). It is evident from this figure that the value of ψ_1 gives the orientation of two amide-NH groups (BOC-NH and peptide-NH) and the value of φ_2 gives the orientation of two peptide-CO groups. The lowest energy configurations as observed in the potential energy surface obtained by perturbation of (φ_1, ψ_1) and (φ_2, ψ_2) dihedral angles in TBP1 and TBP2 are shown in Figure 5 and the approximate values of the most probable torsions are listed in Table 2. The data indicates that in comparison to gas phase, structural heterogeneity increases in methanol in both the peptides. Low energy dihedral angle configurations indicate vastly different backbone geometries of TBP1 and TBP2.

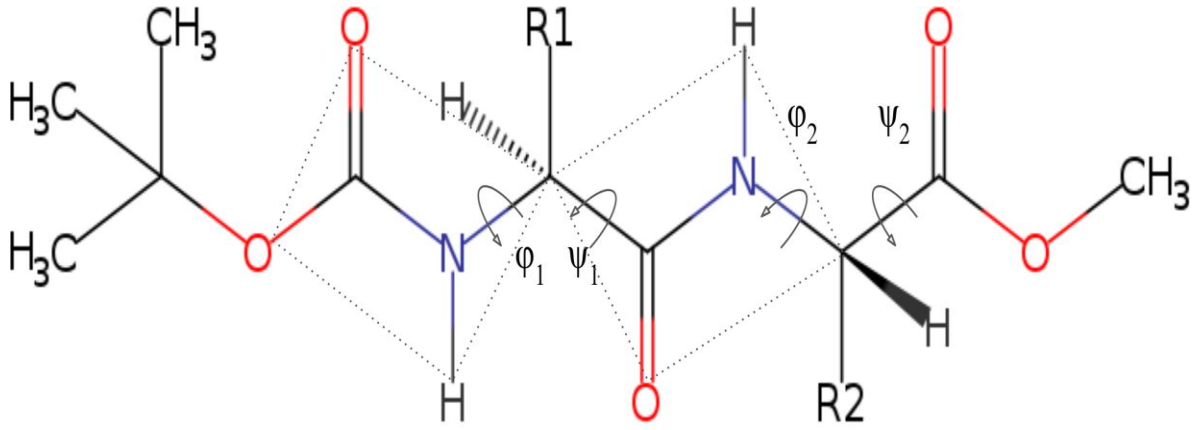

	TBP1	TBP2
R1	O-benzyl-tyrosyl side chain	O-benzyl-glutamic acid side chain
R2	methyl-glutamic acid side chain	O-benzyl-tyrosyl side chain

Figure 4. *The peptide backbone in the dipeptide. The dihedral angles (φ1, ψ1) and (φ2, ψ2) are marked. Amide planes are marked with dotted lines.*

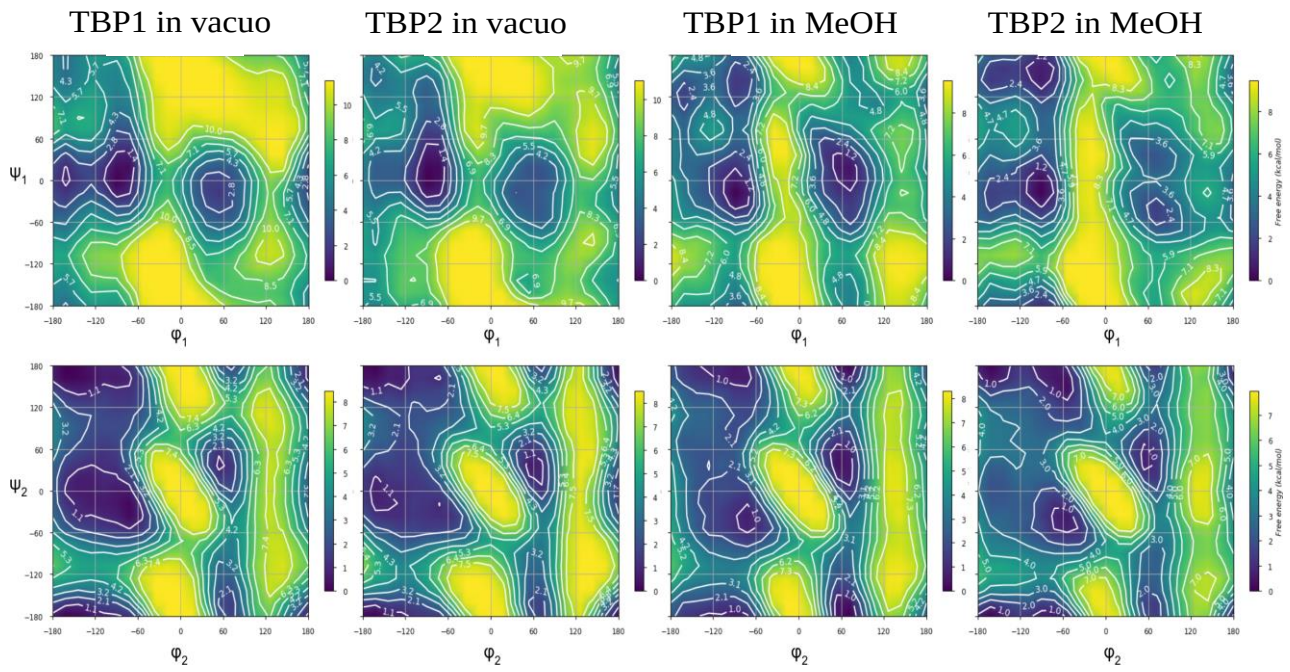

Figure 5. *Free energy profiles of dihedral angle perturbation of TBP1 and TBP2. φ_1, ψ_1 values range from -180 to 180 degrees. Free energies calculated with respect to the lowest energy conformations. Iso-energy lines are drawn at specific intervals and labeled with ΔG values in kcal/mol.*

Table 2: Dihedral angle distribution of TBP1 and TBP2 backbone as obtained by free energy perturbation.

	(φ_1, ψ_1)	(φ_2, ψ_2)
TBP1 (in vacuo)	(-90,0) or (-160,0)	(-120,0) or (-120,175) or (55,40)
TBP2 (in vacuo)	(-90,0)	(-160,0) or (-160,180) or (60,60)
TBP1 (in MeOH)	(-90,-20) or (60,20)	(-75,-45) or (-90,170) or (60,-170) or (60,45)
TBP2 (in MeOH)	(-90,-10) or (-90,160)	(-60,-45) or (-75,160) or (-160, 175) or (60,50)

3.3.4 Self-assembly of the peptides in MeOH

AFM study

AFM images were obtained on Pico Plus 5500 AFM (Agilent Technologies, Inc., Santa Clara, CA, USA) with the piezo scanner range of 9 μm. The images (256 × 256 pixels) were captured with a scan size between 0.5 and 5 μm at the scan speed rate of 0.5 rpm. The images were processed through flattening via Pico view software (Molecular Imaging Inc., Ann Arbor, MI, USA). For this purpose, dipeptide solution was incubated at room temperature for required time, and subsequently the solution was applied to a mica foil. After drying the sample under air, the sample on mica substrate was observed through atomic force microscopy.

Several research groups studied that the peptides those contained aromatic groups in their architechtures have a generic ability to self-assemble in protic solvent and produced different nano-size aggregates. To gain visual insight into the self-assembly and aggregation properties of TBP1 and TBP2, both the peptides were dissolved in methanol to make final concentration of the peptide ~ 0.03 mM and 0.3 mM respectively. The prepared solution was incubated for 24h and deposited on freshly cleaved mica surface. After drying, AFM imaging technique was used to examine morphological pattterns of the assembly structures produced in MeOH. Figure 6 shows the fiber bundles produced from TBP1. However, TBP2 produced spherical assembly structure of nano-sphere after 24h incubation as shown in Figure 7. The width of the fiber (obtained from TBP1) varied in the range of 20-50 nm (Figure 6A) and several micrometres in length. At higher concentration (~0.3 mM), the fiber morphologies were diversified, showing dense cross-linked fibrillar network structure, having width in the range of 30-60 nm (Figure 6C). It indicated that the diameter of fibers was dependent on the concentration of TBP1 solution. Moreover, the width of the dense fibers decreases to 10-30 nm upon sonication (Figure 6D). This suggested that the dense fibrillar network was assembled of

several mini-fibers and the lateral association was disturbed by the sonication. AFM study showed that TBP2 in dilute condition (0.03 mM in methanol) produced nano-spheres like assemblies with diameter of 60-110 nm (Figure 7A). Surprisingly, with increasing concentration (~10 times), higher diameter oligomer/spheroidal aggregates were formed having size in the range of 250-500 nm (Figure 7B). The sonication caused the size reduction of the oligomers from 250-500 nm to 75-200 nm (Figure 7D). Incubating the peptide solution for a longer period, the size of the oligomers became larger (Figure 31).

To check the incubation time dependency of TBP1 & TBP2 assembly formation, the dipeptide was dissolved in methanol and AFM images were taken at several time intervals. (Figure 9). Due to the fast fibrillation and higher dependency on the concentration of peptide TBP1 in methanol, the peptide concentration was kept low at ~ 75 µM. AFM analysis showed that TBP1 showed nanospherical assembly structure after 5min of incubation (Figure 9A). After 1h, TBP1 produced like fibrillar aggregates (Figure 9C). In case of TBP2, the aggregation properties at this concentration was slow, nanospheres with diameter 20-30 nm could be observed after 2 h of incubation (Figure 9D). The size of nanospheres increased to 30-60 nm after 8h (Figure 9E). After 24 h of incubation, TBP2 generated larger spherical assemblies with diameter 60-120 nm (Figure 9F). Hence it can be concluded that the morphology of the assembled structures adapted by both TBP1 and TBP2 was time as well as concentration dependent. This time dependent morphological analysis also correlated with the result obtained from ThT fluorescence study.

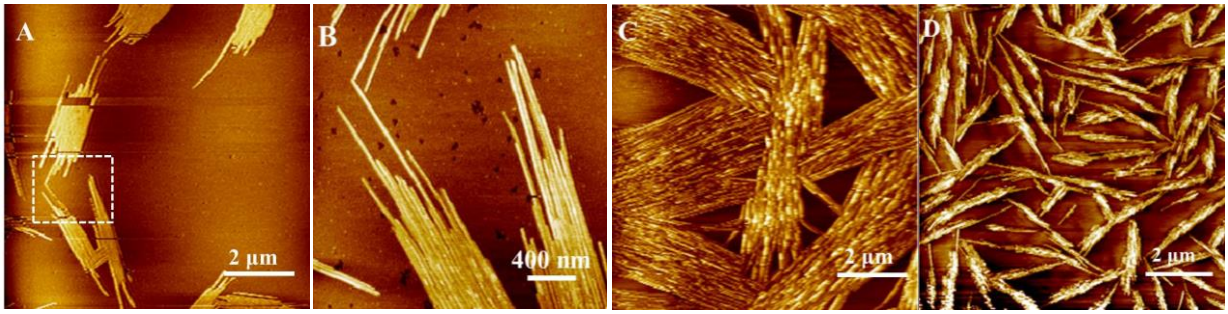

Figure 6. *Atomic force microscopy (AFM) images of aggregates produced from TBP1 as incubated in methanol for 24h at RT (25^{0}C).*

(A) Fibrillar aggregates produced from dilute solution of TBP1 (0.03 mM) (B) Shows the enlarged portion of the area enclosed by white dotted line in (A).(C) Highly cross-linked dense fibers produced from TBP1 incubated at higher concentration (~0.3 mM). (D) Sonication induced fibrils obtained from concentrated solution of TBP1.

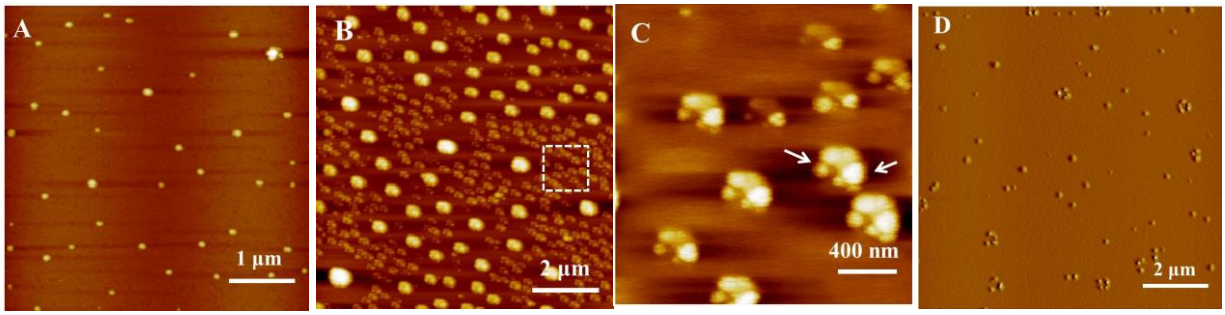

Figure 7. *Atomic force microscopy (AFM) images of oligomeric aggregates produced from TBP2 as incubated in methanol for 24h at RT (25^{0}C).*

Panel (A) shows nanosphere structure produced from dilute (0.03 mM) TBP2 solution and (B) shows bigger size (~ 200-500 nm) aggregates produced when the peptide concentration was ~0.3 mM, (C) is the expanded form of marked portion of (B). (D) shows smaller size aggregates produced upon sonication of aggregates shown in panel (B).

3.3.5 Thioflavin T (ThT) fluorescence assay:

ThT fluorescence assay was measured to investigate the formation of self-assembly by TBP1 & TBP2. ThT is a routinely used dye to check the formation of well-ordered ß-sheet rich fibrillary network produced from proteins/peptides.[194,195] The more ThT fluorescence (intensity) in the presence of protein sample suggests higher amount of fibril with ß-sheet conformation. The peptide solution was prepared by dissolving the solid peptides in methanol and incubated for required hours at ambient temperature (25 ^{o}C). A stock ThT solution (~75 μM) was prepared in water. Before spectral measurement, 150 μl of peptide solution was added to 1 ml of ThT solution (~75 μM) and mixed thoroughly so that the final concentration of the peptide was ~ 75 μM. The fluorescence measurement was done using Cary Eclipse fluorescence spectrophotometer (Agilent Technology) in a quartz cuvette of 1 cm path length. The excitation and emission slit widths were fixed at 5 nm each and the emission range was 455-600 nm. The chosen excitation wavelength was 445 nm.

To measure the time dependent aggregation of the peptide, the peptide solution was prepared by dissolving the solid sample in MeOH. 150 μl of the freshly prepared peptide solution (500 μM) was added to 1 ml of ThT solution (~75 μM) and mixed thoroughly so that the final concentration of the peptide was ~ 75 μM. ThT fluorescence spectra were recorded at different time point of incubation keeping other measurement conditions similar as stated above. Fluorescence peak intensity values at 485 nm were plotted against time and fitted to the sigmoidal curve equation (equation 1).[195]

$$Y = \frac{y_1 + m_1 x + (y_f + m_f x)}{1 + e^{-[(x - x_0)/\tau]}} \ldots\ldots\ldots (1)$$

ThT fluorescence intensity is denoted by Y, x denotes time, x_0 is the time required to achieve 50% of maximum fluorescence intensity, the apparent rate constant is k_{app}, fibrillar growth is $1/\tau$, and the time period in lag phase is derived by $x_0 - 2\tau$.

Based on thioflavin T (ThT) fluorescence measurement the nature of the secondary structure and growth kinetics of aggregation/fibril formation was thoroughly examined. The fluorescence spectra of ThT in the presence of TBP1 and TBP2 were represented in Figure 8A. From the figure, it was observed that the ThT fluorescence signal of TBP1 (solution in methanol) was significantly higher than that of TBP2. Moreover, incubated TBP2 solution did not show any major change in ThT fluorescence intensity. This result suggested the presence of fibrillary network with ß-sheet conformation in case of TBP1, whereas TBP2 did not favour the formation of fiber like assembly structure with compact ß-sheet structure. AFM analysis also supported the result obtained from ThT study.

Next, growth kinetics of fiber/oligomer formation by TBP1 and TBP2 were also investigated by ThT fluorescence measurements at different time point of incubation (Figure 8B). The nature of the fibril formation growth followed sigmoidal curve (Figure 8B). Based on the fluorescence enhancement and incubation time the fitted data showed that a lag phase of fibrillation of TBP1 was 11 min followed by a growth phase of 11-50 min. The apparent rate constant (k_{app} value) of fibrillation is calculated as ~ 0.125 min^{-1}. Due to the morphological transformation from nanospherical to protofibril-assembly state which was further confirmed from AFM analysis, there was an elevation in the curve. The structural elevation came to an equilibrium state after 50 min of incubation. Therefore, within 1h the fibril formation reached its static equilibrium state. This result indicated that TBP1 rapidly self-assembled in methanol solution to form fibrillar aggregate. Interestingly, no additional increment in the ThT fluorescence intensity was observed for TBP2 (Figure 8B), indicating the absence of fibrillar aggregates in methanol solvent. The similar conclusion inferred from

morphological study. Further morphological transition of self-assembly pattern of TBP1 and TBP2 aggregates were examined through AFM study. At the initial lag phase i.e. after 5 min of incubation in methanol TBP1 showed nanospherical assembly structure (Figure 9A). However, during growth phase (after 35 min of incubation) protofibril was observed (Figure 9B) and fibrils with width 20 nm diameter were obtained after 60 min of incubated TBP1 solution. These results inferred that the equilibrium state was achieved after 1h (Figure 9C) .Whereas nanospherical assembly structure obtained from TBP2 even after 2h of incubation and no structural elevation was observed (Figure 9D). Thus the peptide conformation in the produce fibrillary network was beta sheet rich, however TBP2 failed to attain similar structure and confined in a spherical nanostructure.

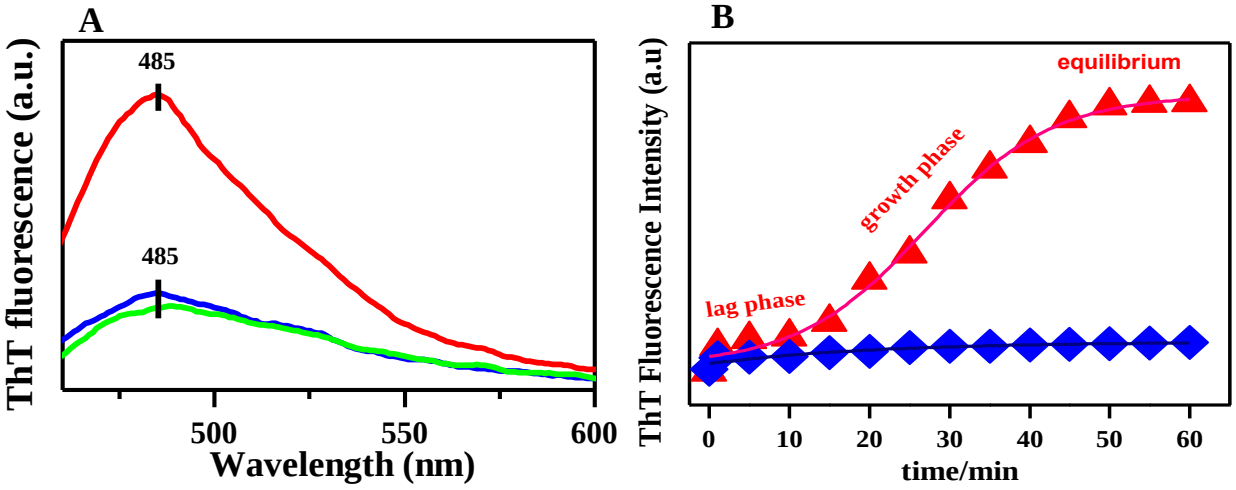

Figure 8. *Thioflavin T (ThT) fluorescence assay for the formation of aggregates by the two peptides, TBP1 & TBP2 in methanol solvent.*
(A) ThT fluorescence spectra spectrum in the absence and presence of peptides (~ 75 μM) in methanol incubated for 1h at 25^0C (RT): green trace, without any peptide; blue trace, in the presence TBP2; red trace, in the presence of TBP1. (B) ThT fluorescence intensity at 485 nm recorded at different time point of incubation of ThT and peptide in MeOH: red triangle, for TBP1 and blue rhombus, for TBP2. The points are connected via straight line.

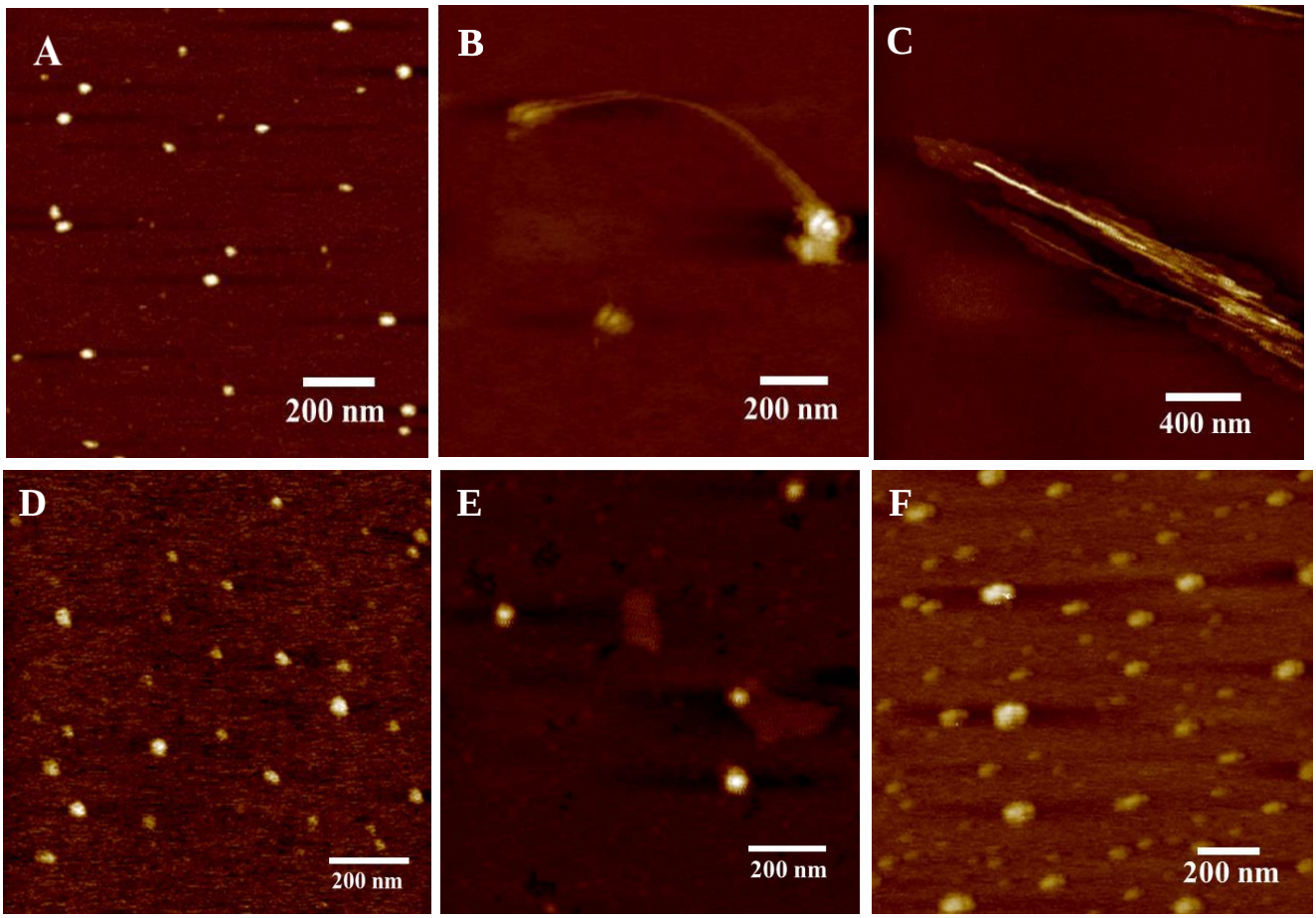

Figure 9. *AFM images of aggregates produced at different time point of incubation from dilute (~ 75 μM) TBP1 solution in MeOH at 25^{0}C (RT) :(A)after 5 min,(B) after 35 min and (C) after 60 min . Lower three panels (D, E, F) show the AFM images of aggregates produced from TBP2 solution in same solution condition, however at incubation time of (D)2h, (E) 8h and (F)24h. Scale bar is given for the size measurement.*

3.3.6 H/D exchange proton NMR analysis:

H/D exchange experiment provides information about the hydrogen bonding pattern of the respective protons in their solution state. To carry out this experiment blank ^{1}H- NMR spectrums were taken for both peptides (concentration~10 mM) in DMSO-d_6 solvent. After that 10 µl D2O was added to it and spectrums were taken at different time points of incubation. Rate constant values were calculated by plotting intensity vs time and fitted to an exponential curve. Rate constant values for both TBP1 and TBP2 were calculated according to the following equation.

Aggregation of TBP1 follows first order kinetics. The equation describing the kinetics is given below (equation 2):

$A/A_0 = e^{-kt}$…….. ….(2)

Where A is the NMR peak intensity at time t, A_0 is the initial intensity and k is the rate constant.

The equation 3 describing the kinetics for TBP2 is given below.

$A/A_0 = 1/(1+e^{k(t-t_{1/2})})$ …. …. ….(3)

Where $t_{1/2}$ is the half time when NMR peak intensity reached 50%; k is the apparent growth rate. The lag time or t_{lag} can be computed as (equation 4):

$t_{lag} = t_{1/2} - 2/k$… ……. ….(4)

Molecular self-assembly process is guided by several non-covalent interactions, such as- vander Waals force, hydrophobic, ionic, hydrogen bonding and π-π stacking interactions etc. These low energy interactions cooperatively provide intact and well-ordered three dimensional architechtures. To get an idea about the molecular force promoting the self-aggregation process, NMR analysis of both the dipeptides TBP1 and TBP2 was done. Among them, H/D exchange

experiment resolved the hydrogen bonding pattern of the two amide protons in their respective solution state. Figure 10 displays the proton NMR spectra of TBP1 in DMSO and in the presence of D_2O/DMSO (1:50 V/V) mixed solvent. In the absence of D_2O, two doublet peaks appeared around δ 8.27 and 6.87 ppm, respectively, for –NH proton of -CONH, and tert-butoxycarbonyl (BOC) group (Figure 10A). The other peaks appeared at δ 7.40-7.39 (2H), 7.37- 7.34 (2H), 7.30-7.28(1H), 7.13 (2H), 6.87 (2H) were responsible for aromatic protons inTBP1 (Figure 10A). After adding D_2O to a 10mM solution of TBP1 in DMSO-d_6, the intensity of the proton at δ 8.27 ppm diminished rapidly and ultimately disappeared as time passed (Figure 10B, 10C and 10D). The proton signal appeared at δ 6.87 diminished relatively slowly and slightly shifted from δ 6.87 to 6.80 ppm as shown in Figures 10B, 10C and 10D.The initial shifting of the proton in the NMR spectrum may be due to changing of the solvent condition (from pure DMSO to DMSO/D_2O mixture); In DMSO medium, the dipeptide (TBP1) formed strong H-bonding with DMSO. The addition of D_2O, -NH of tert-butoxycarbonyl (BOC) proton weakened and it resulted chemical shift towards higher shielding region.[147] However subsequent changes in the intensity of NH protons were due to exchange of the N-H group with deuterium.

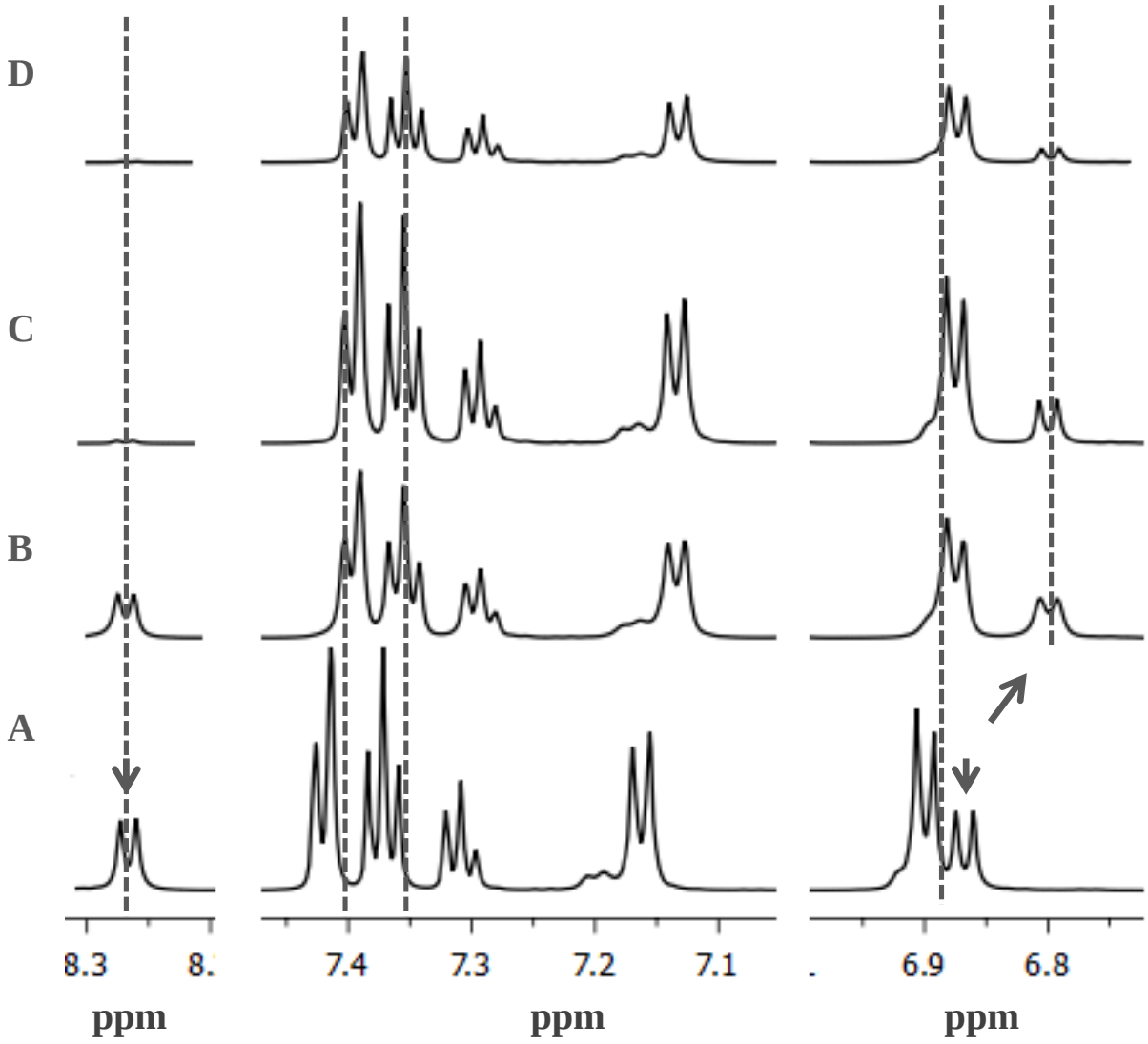

Figure 10. *H/D exchange NMR experiment on TBP1 (10 mM) in DMSO-d_6.*

(A) ^{1}H-NMR spectra of TBP1 in absence of D_2O in solution. Upper panels show the perturbation of the spectra in presence of D_2O (D_2O: DMSO-d_6 = 1:50) at different point after addition of D_2O: (B) 0h, (C)3h and (D)6h. For presentation clarity only peak regions are shown and the bottom axis is broken. Dashed lines and arrows are to highlight the perturbation of the peak positions and intensities.

H/D exchange study with TBP2 revealed two doublet proton peaks in the NMR spectra (Figure11): the doublet at ~ 8.18 ppm was due to –NH of CONH and the doublet at 6.88 ppm for -NH of BOC group (Figure 10A) because of the different chemical environment of the amide groups in the peptide. The amide peak appears at δ 6.88 ppm was merged with another two aromatic protons. The other aromatic protons appear at 7.42-7.40 ppm (2H), 7.38-7.33 ppm (6H), 7.32-7.29 ppm (2H), 7.11 ppm (2H), 6.88 (2H) (Figure 11A). After addition of D_2O, the intensity for both protons NMR signals at δ 8.18 ppm and 6.88 ppm were reduced slowly compared to rapid exchange of NH protons of TBP1 (Figure 11). After 6h of addition of D_2O, the peak intensity of -NH of peptide amide and -NH of BOC were not changed significantly (Figure 10B and 10C). Interestingly, however, after 10h the peak appeared at δ 8.18 ppm disappeared completely and the intensity of other proton at δ 6.88 ppm also decreased to a certain level. Thus the NMR results suggested that for TBP1 both the amide NHs are solvent exposed and may be engaged in intermolecular H-bonding with the surrounding solvent molecules and, were capable to exchange rapidly with solvent molecules. Whereas for dipeptide TBP2, the amide protons may be participated in intermolecular H-bonding and get exchanged with D_2O at a slower rate compared to dipeptide TBP1. Rate constant values for the amide proton exchange with the solvent D_2O for both TBP1 and TBP2 were calculated by plotting proton intensity vs time (Figure 34). The rate constant for TBP1 was 0.93 h^{-1}. However, TBP2 showed a lag phase and the apparent growth rate for TBP2 aggregation was found to be 1.28 h^{-1}. The peptides were soluble in DMSO and therefore, H/D exchange proton NMR study was carried out in DMSO/ D_2Osolvent to understand the participation/accessibility of peptide amide (-CONH) hydrogen in hydrogen bonding with surrounding solvent molecules. However, aggregation behaviour of the peptides was investigated in methanol solvent. In methanol both the peptides very quickly produced aggregates. This resulted slow tumbling of

the peptide assembly and, consequent rapid T2 relaxation resulted loss of NMR signals of amide protons. (Figure 35 and 36 for clear comparison)

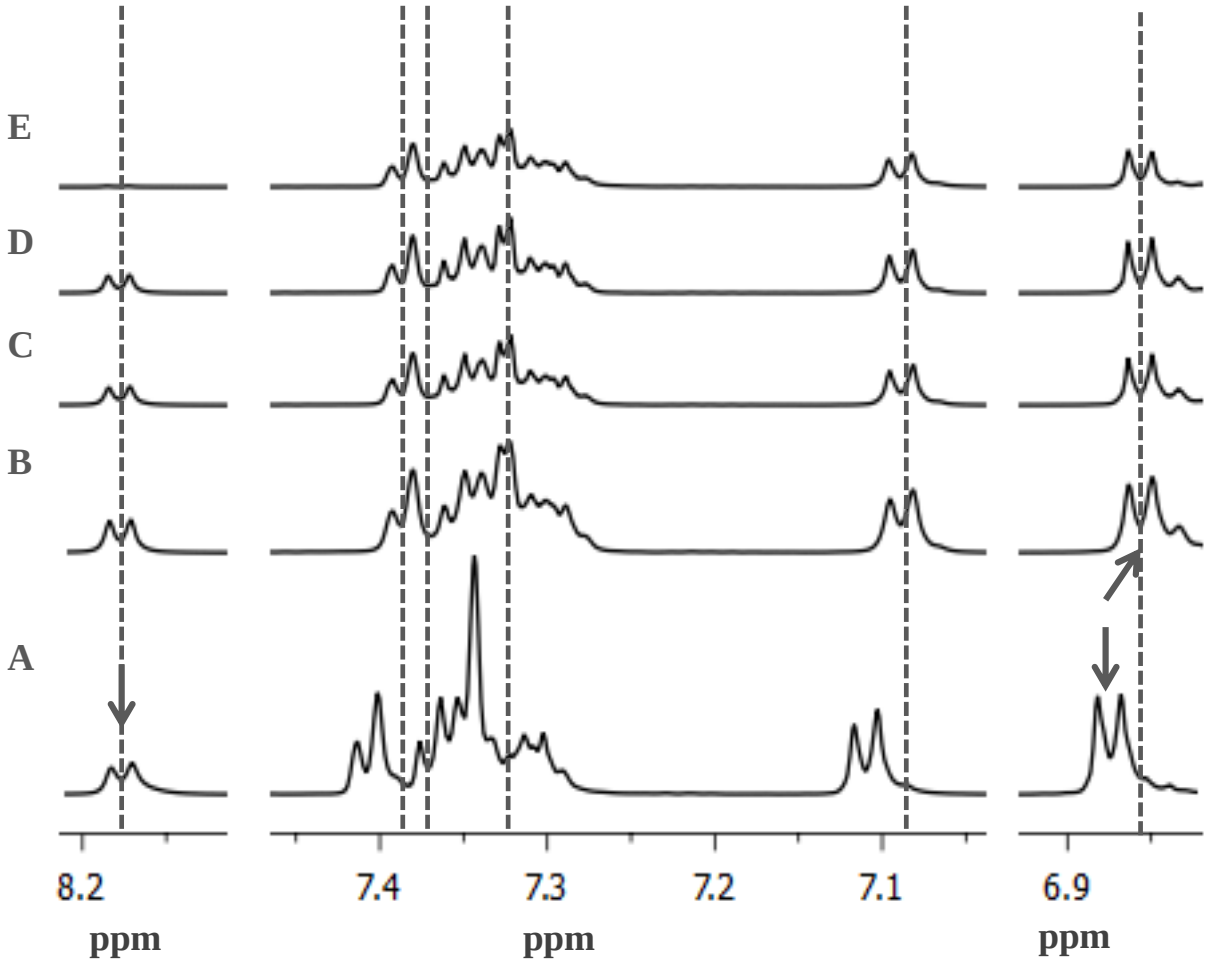

Figure 11. *H/D exchange NMR experiment on TBP2 (10 mM) in DMSO-d_6.*

(A) ^{1}H-NMR spectra of TBP2 in absence of D_2O. Upper panels shows the effect of addition of D_2O (D_2O: DMSO-d_6 = 1:50) at different points:(B)0h, (C)3h, (D)6h and (E)10h. For presentation clarity only peak regions with broken axis are shown. Dashed lines and arrows are to highlight the perturbation of the peak positions and intensities.

3.3.7 FT-IR analysis

The FT-IR spectra of the samples were recorded on a Bruker TENSOR27 spectrometer. The KBr disc technique was used to record the spectra of the solid sample. Solid sample was mixed with KBr in a clean glass pestle and compressed to obtain a pellet. Background spectra were obtained for KBr pellet for each sample. For recording the FT-IR spectra in solution state, dipeptide solution of 200 μM concentration in methanol/DMSO was used. The spectra were scanned from 600 to 4000 cm^{-1}. Bruker software was used for data processing. Experimental data obtained were analysed using Origin Pro 8.0 SRO software (Origin Lab Corporation).

Structure sensitive amide I and III modes of vibration in FT-IR spectra of proteins and peptides are often used to derive structural aspects (amide bond configuration) of the peptide chain. We measured FT-IR spectra of both the peptides (TBP1 and TBP2) in solid and solution states. Further theoretical FT-IR spectra were calculated by applying the density functional theory (DFT) with the B3LYP functional and 6-31G (d) basis set in the gas phase. Figure 12A shows the calculated FT-IR spectrum of TBP1 and Figure 12B shows different vibration modes associated with amide groups present in the peptide. Gauss View 09 was used to generate visual presentations and verify the normal mode assignments. As expected the peptide produced multiple bands related to several functional groups and CH bonds. The band positions are listed in Table 3. The assignment of most of the bands were guided by the calculated frequency as obtained by theoretical analysis and by the survey of values reported in literature.[192,193,196,197]

Our analysis was largely focused on carbonyl –C=O stretching frequencies of amide group (-CONH) and ester (-COOMe) groups present in both peptides. For TBP1 peptide, the calculated -C=O stretching bands for the amide of the main chain peptide bond (marked as ‘a’ in Figures 12A and 12B) and BOC-amide (marked as

‘a′’ in Figures 12A and 12B), respectively, appeared at 1754 and 1774 cm^{-1}. The two carbonyl groups as a part of the ester shows vibration signature significantly at higher frequencies: 1836 cm^{-1} band was assigned to main chain –COOMe marked as ‘b’ in Figures 12A and 12B and 1826 cm^{-1} for another similar ester group as side chain -COOMe marked as ‘b′’ in Figures 12A and 12B. Two amide II modes of vibration bands associated with two amide groups i.e. main chain peptide and BOC-amide appeared at respectively, 1587 cm^{-1} (marked as ‘c’ in Figures 12A and 12B) and 1546 cm^{-1} (marked as ‘d’ in Figures 12A and 12B). The other major band frequency positions are enlisted in Table 3. Some changes in band positions were observed in the FT-IR spectra calculated using methanol as solvent (Table 3). Lower three panels in Figures 12 present the experimental FT-IR spectra of peptide TBP1 in the solid as well as in solution states at room temperature (~24 ^{o}C). Four major FT-IR bands for solid TBP1 were noted at 1650, 1687, 1730 and 1746 cm^{-1} (Figure 12C) and linked to stretching vibrations of -C=O groups present in the molecule. The band at 1650 cm^{-1} represented the carbonyl stretch of the main chain peptide bond and the amide II region appeared at 1523 cm^{-1}. This region also overlapped with the phenyl ring vibrations. The band at 1687 cm^{-1} was assigned to the carbonyl group of the BOC-amide group. The 1730 cm^{-1} and 1746 cm^{-1} bands were assigned for main chain and side chain ester carbonyl stretching frequencies. The calculated vibrational frequencies were significantly higher than the experimental FT-IR frequencies and it could be due to systematic error caused by basis set incompleteness and anharmonicity factor associated with vibrational motion.

Further FT-IR measurement was carried out in DMSO. In DMSO the peptide remained soluble and did not produce detectable aggregates or higher order assembly structures. Significant changes in FT-IR spectra were observed as the peptide was dissolved in DMSO (Figures 12D). Most of the carbonyl vibration band positions were blue shifted (compared to solid state) due to formation of H-bond with the sulfoxide oxygen of DMSO and amide protons of the peptides.[198] In

addition, the reduction in dielectric constant, due to addition of DMSO also caused the enhancement of the amide I band vibration and shifting to a higher frequency. Homogeneous broadening and solvation resulted in the overlapping of four bands associated with the amide and ester groups.

However, in methanol, the peptide TBP1 quickly transformed into fibrillar aggregates (as confirmed by AFM and ThT fluorescence assay measurement) and noticeable sifting of C=O stretching band position occurred (Figure 12E). The main chain amide band was red shifted (compared to the monomeric band in DMSO) to 1660 cm^{-1} (Figure 12E) and it was about 10 cm^{-1} higher in frequency compared to the solid state band frequency. This shifting indicated the weakening of the –NHC=O bond due to the involvement of the carbonyl oxygen in H-bonding with methanol. This change may also involve geometrical changes in the conformation/configuration surrounding the amide groups. However, it is pertinent to mention that the main chain amide band overlapped with the band of BOC amide group.

Similarly, Figure 13 display the theoretical and experimental FT-IR spectra of TBP2 peptide. Table 4 lists the FT-IR band positions of different groups and bonds of the peptide. The major vibrations associated with carbonyl groups are also marked in (Figure 13B). Due to homogeneous and heterogeneous broadening of the spectra caused by aggregated peptide solution, amide band positions were quite overlapped. The amide I bands for the main chain peptide and the BOC-amide groups appeared at 1758 and 1784 cm^{-1}, respectively (Figure 13A). The amide II bands appeared at 1562 cm^{-1} for the peptide amide group and the BOC amide produced the band at 1531 cm^{-1}. Two overlapping bands at 1818 cm^{-1} were assigned to carbonyl stretching frequencies for two ester groups. Figure 13C shows the FT-IR spectra of TBP2 in solid state .The vibration band of carbonyl groups for the peptide and BOC amide groups appeared at 1649 and 1689 cm^{-1}, respectively, and two

carbonyl groups as a part of the ester showed vibration signature at significantly higher frequencies of ~1741 cm^{-1} and 1730 cm^{-1}, respectively. Figures 22 and 23 provide the full range FT-IR spectra for both the peptides in the solid state. TBP2 peptide was also soluble in methanol and showed multiple and overlapped FT-IR bands associated with four carbonyl groups present in the molecule. TBP2 in methanol produced oligomeric aggregates and showed the main chain amide band position at 1665 cm^{-1} (Figure 13E). However, it was broader than the band at 1660 cm^{-1} that appeared for fibrillar aggregates produced by TBP1 in MeOH. It was possible that the oligomeric assembly state of the peptide TBP2 maintained slightly different configuration and it may not be as compact as the fibrillar structure produced by TBP1.

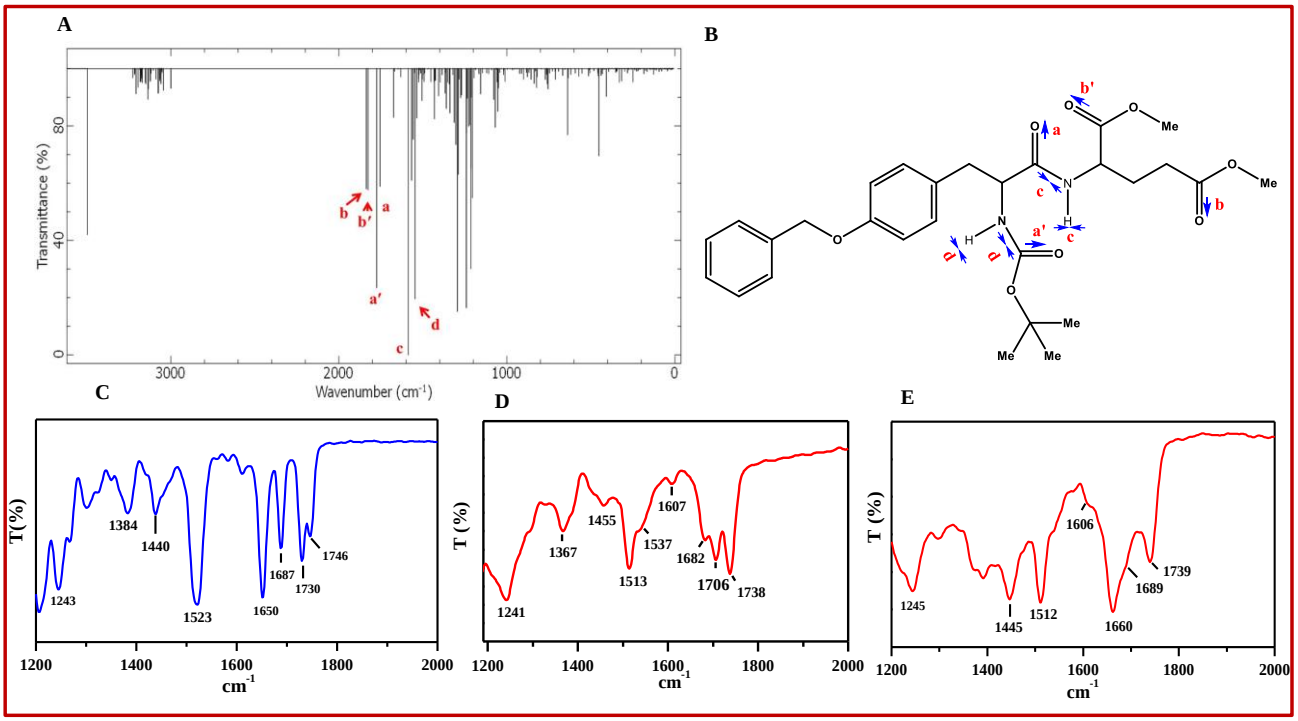

Figure 12. *Calculated and Experimental Fourier transform infrared (FT-IR) spectra of TBP1. (A) Calculated FT-IR spectra of TBP1 usingTD-B3LYP (SCF) level of theory and 6-31G (d) basis set. (B) The modes of vibration of different groups of TBP1. (C) Solid state FT-IR spectra of TBP1. (D) Solution state FT-IR spectra of TBP1 in DMSO. (E) FT-IR spectra of the peptide in methanol. For each peptide solution the concentration was~200 µM. Major bands are marked.*

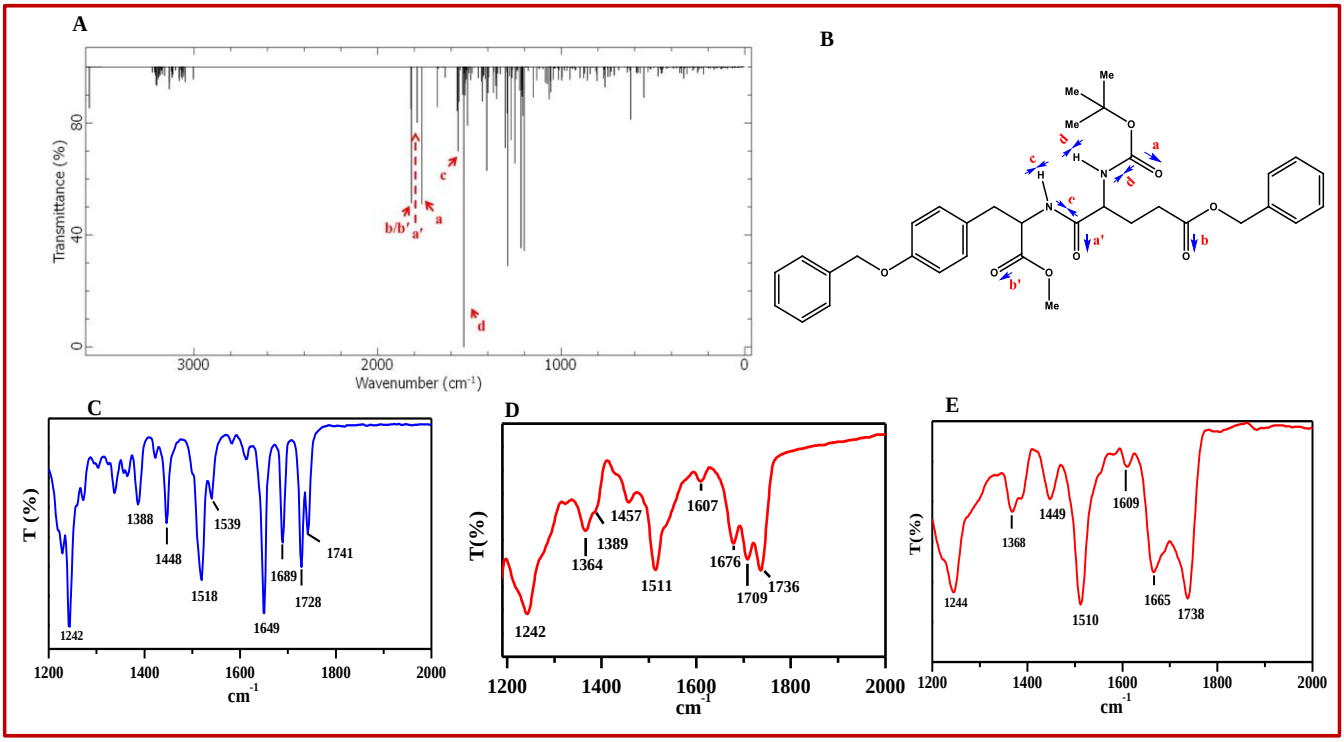

Figure 13. *Calculated and Experimental Fourier transform infrared (FT-IR) spectra of TBP2.(A)Calculated FT-IR spectra of TBP2 usingTD-B3LYP (SCF) /6-31G (d) level. (B) The modes of vibration of different groups of TBP2. (C) Solid state FT-IR spectra of TBP2. (D) Solution state FT-IR spectra of TBP2 in DMSO. (E) Aggregated FT-IR spectra of TBP2 in methanol. For each peptide solution the concentration was~200 µM. Major peaks are marked.*

Table 3. Experimental and Calculated Prominent FT-IR Bands (cm^{-1}) of TBP1at TD-B3LYP (SCF) /6-31G (d) level

$\nu_{(exp)}$, cm^{-1} (experimental, solid)	$\nu_{(theo)}$, cm^{-1} (calculated, MeOH)	$\nu_{(theo)}$, cm^{-1} (calculated in gas phase)	$\nu_{(exp)}$, cm^{-1} (MeOH)	$\nu_{(exp)}$, cm^{-1} (DMSO)	Vibration Assignment
1207 ,1243	1199, 1238	1204 ,1238	1242	1241	Ester C-O asymmetric stretch
1384	-	-	1370,1390	1367	CH_3 of tertiary group symmetric bending
1440	-	-	1445	1455	CH_2 bending
1523	1548,1577	1546,1587	1512	1513	N-H bend in plane and C-N stretch (amide II)
1650, 1687	1724, 1744	1754, 1774	1660	1682	Amide C=O stretching (amide I)
1730, 1746	1797, 1809	1826, 1836	1739	1738,1706	C=O stretching of the ester
3326	3498, 3624	3496, 3619	3323	-	N-H stretching

Table 4. Experimental and Calculated Prominent FT-IR Bands (cm^{-1}) of TBP2 at TD-B3LYP (SCF) /6-31G (d) level

$\nu_{(exp)}$, cm^{-1} (experimental, solid)	$\nu_{(theo)}$, cm^{-1} (calculated, MeOH)	$\nu_{(theo)}$, cm^{-1} (calculated in gas phase)	$\nu_{(exp)}$, cm^{-1} (MeOH)	$\nu_{(exp)}$, cm^{-1} (DMSO)	Vibration Assignment
1242	1251,1274	1201, 1219	1245	1243	Ester C-O asymmetric stretch
1388	-	-	1367	1364	CH_3 of tertiary group symmetric bending
1448	-	-	1449	1447	CH_2 bending
1518	1560,1563	1531, 1562	1510	1511	N-H bend in plane and C-N stretch (amide II)
1649, 1689	1731,1759	1758, 1784	1665	1676	Amide C=O stretching (amide I)
1728, 1741	1788,1795	1818	1738	1709, 1736	C=O stretching of the ester
3330, 3334	3574,3594	3570, 3590	3303, 3355	-	N-H stretching

3.3.8 Raman analysis

Raman spectra were measured with triple Raman spectrometer (Model: T64000, Make: J-Y Horiba) equipped with 1800 grooves/mm grating, TE cooled synapse CCD and with an open stage Olympus microscope with 50x objective. Each Raman spectrum was collected using 533 nm wavelength laser from DPSS laser (Make: spectra physics) excitation 2mW laser power, and 10 s of data acquisition time with each spectral data having average of 4 accumulations. Data analyses with baseline correction were performed using Origin Pro 8.0 SRO software (OriginLab Corporation).

Raman spectroscopic measurement was further engaged to derive the overall peptide backbone configuration via the Raman band positions of different carbonyl groups. For TBP1, in solid state the Raman amide I band appeared at 1651 cm^{-1} for the carbonyl group present in the main chain peptide part and another band at 1688 cm^{-1} for the carbonyl group present in the BOC part of the peptide (Figure 14A). The appearance of the bands at 1735 and 1748 cm^{-1} were due to stretching frequencies for ester carbonyls. Raman bands at 1004, 1034, 1612 cm^{-1} (Figure 28C) were assigned to several vibrations associated with the phenyl ring of the peptide. The appearance of the peak at 864 cm^{-1} was also due to the presence of phenyl moiety. The amide III band region appeared with peaks at 1220, 1244 cm^{-1} respectively. Figure 28A presents the calculated Raman vibrational spectrum of TBP1. This result predicted the presence of amide I band at 1680 cm^{-1}, amide III bands at 1238 and 1291 cm^{-1} with ester carbonyl bond vibration at 1778 and 1831 cm^{-1}. Table 5 shows some of the Raman vibrational frequencies with their assignments based on literature and the calculation. The calculated vibrational frequencies were comparatively higher than the experimental values due to encounter of systematic error caused by basis set incompleteness, and anharmonicity factor associated with vibrational motion.

Figure 14B shows the Raman spectra of TBP1 in methanol and the band positions are given in Table 5. The C=O stretching vibration bands associated with the peptide amide group shifted to 1658 $cm^{-1}$and the frequency position of the carbonyl of the amide group in the BOC part was broadened and remained at ~ 1686 cm^{-1}. The ester carbonyls also produced a broad vibrational band at 1737 cm^{-1}. The broadness may be due to fibril formation of the peptide as it was confirmed by the AFM analysis and ThT fluorescence assay measurements. Similarly, Figure 15A shows the Raman spectrum of TBP2 in solid state. Two Raman bands at 1653 and 1693 cm^{-1} were assigned to C=O stretching of amide carbonyl in the peptide bond and amide carbonyl of the BOC group, respectively. The ester carbonyl bond vibration appeared at 1731 and 1744 cm^{-1}. The bands 1220, 1242 and 1262 cm^{-1} represented Raman amide III vibrational modes of two amide groups present in the peptide. Figure 29A shows the calculated Raman spectrum of TBP2 using the same level of theory. Table 6 represents the Raman vibrational frequencies of TBP2 with band assignments. TBP2 oligomers produced in methanol showed four C=O stretching bands associated with four different carbonyl groups in the peptide molecule. Interestingly, we observed that the main peptide carbonyl bands appeared at 1649 cm^{-1} and no major shift in the band position was observed (Figure 15B).

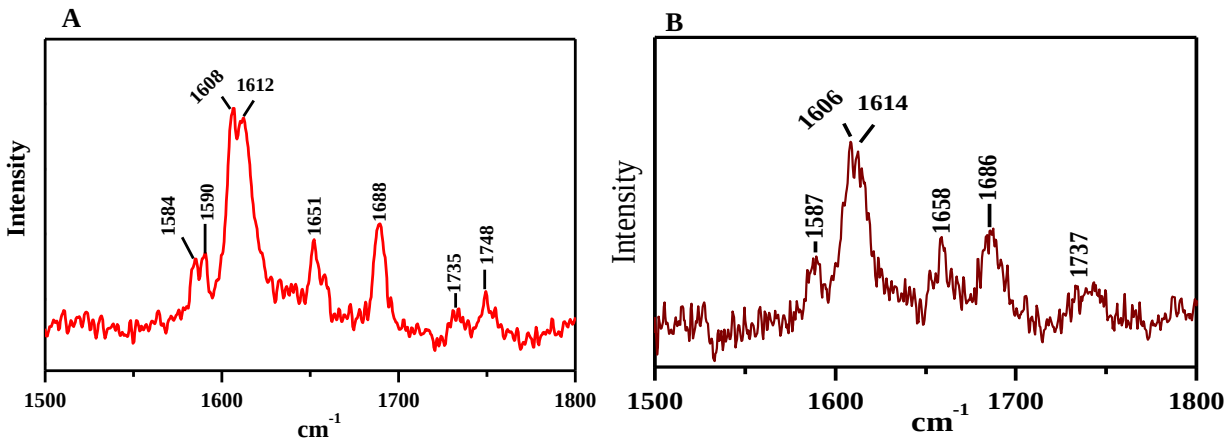

Figure 14: *Raman spectra of TBP1 in two different sample conditions.*

Panel (A) indicates experimental Raman spectra of TBP1 in solid state. Panel (B) shows experimental Raman spectra of TBP1 in methanol.

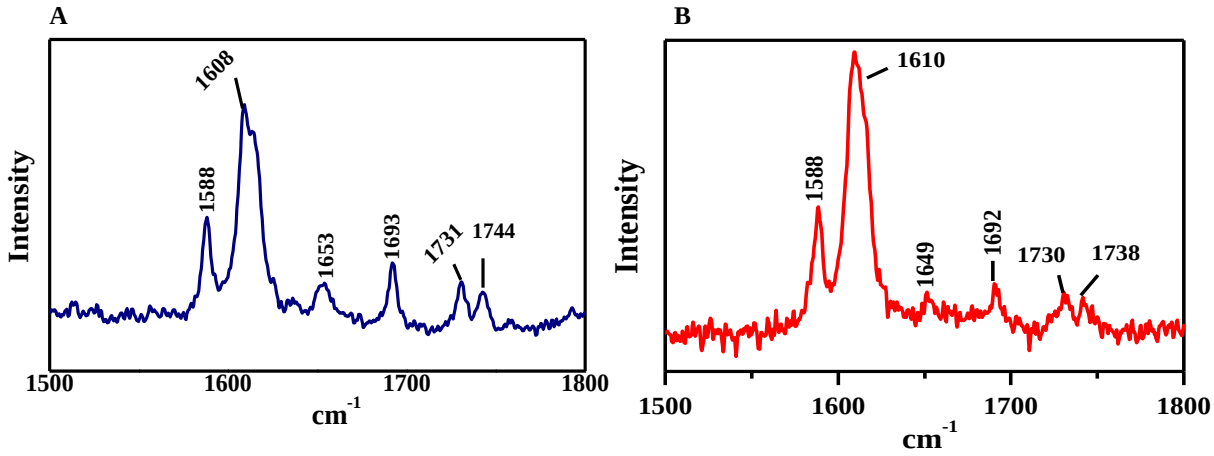

Figure 15: *Raman spectra of TBP2 in two different sample conditions.*

(A) shows Raman spectra of TBP2 in solid state. (B) represents Raman spectra of TBP2 in methanol. For each peptide solution the concentration was~100 µM.

Table 5: Prominent Raman Bands (cm^{-1}) of TBP1:

$\nu_{(theo)}$, cm^{-1} (calculated)	$\nu_{(exp)}$, cm^{-1} (experimental)	$\nu_{(exp)}$, cm^{-1} (MeOH)	Vibration Assignment
875	864	864	Tyr
933, 971	927	922	Cα-C stretching
1020	1004	1001	Phe
1058	1034	1028	Phe
1164	1137, 1182	1178	CH_2 symmetric rock+, Cα-C stretching
1206	1210	1209	Tyr, Phe
1238, 1274	1220, 1244	1248	Amide III
1398	1389	1380	Cα-H def, ν_{C-N} stretch
1516	1469	1466	CH_2, CH_3& CH deformation and scissoring
1623	1607	1606	Tyr aromatic vibration
1658	1651, 1688	1658, 1686	Amide I
1730	1733	1737	ν_{CO} at C terminal
1804	1749	-	ν_{CO} at C terminal

Table 6: Prominent Raman Bands (cm^{-1}) of TBP2:

$\nu_{(theo)}$, cm^{-1} (calculated)	$\nu_{(exp)}$, cm^{-1} (experimental)	$\nu_{(exp)}$, cm^{-1} (MeOH)	Vibration Assignment
875	860	858	Tyr
938, 964, 986	937	922	Cα-C stretching
1021	1004	1002	Phe
1059	1035, 1048	1032	Phe
1083	1066	-	Phe
1191	1157, 1178	1160, 1176	CH_2 symmetric rock+,Cα-C stretching
1237	1220	1215	Amide III
1263	1242	1249	Amide III
1287	1262	-	Amide III
1354	1359	-	Cα-H def
1401	1386	1384	Cα-H def, ν_{C-N} stretch.
1423	1424, 1451	1451	ν_{COO} symmetric stretch.
-	1608	1610	Amide I
1668	1653	1649	Amide I
1759	1693	1692	Amide I
1788, 1817	1731,1744	1738	ν_{CO}at C terminal

3.3.9 Structural analysis of the peptides and their aggregates based on sensitive amide I vibration band

The appearance of amide I band is directly linked to carbonyl (-CO) stretching motion of the bond along with the coupling of C-N stretching and N-H in-plane bending. Thus the amide I band is influenced by the geometry of the amide backbone configuration and hydrogen bonding pattern. The quantum chemical FT-IR analysis of both the peptides in the gas phase showed the main chain amide I band vibrations at 1754 and 1758 cm^{-1}, respectively, for TBP1 and TBP2. Theoretical analysis shows that the vibration of the backbone amide groups did not differ significantly in two peptides. FT-IR spectra of both TBP1and TBP2 in solid state showed main chain amide I band at ~1650 cm^{-1}. Thus one important piece information we derived from the solid state and theoretical FT-IR spectra is that both the amide groups in TBP1 and TBP2 possess similar structural configuration in their solid state/gas phase.

Both the peptides, however, quickly attained aggregate structure in MeOH. The spectra (bands) became quite broad and vibration bands associated with different carbonyl groups overlapped and deriving the secondary structure/ configuration of the amide bond became difficult. Aggregation also caused some heterogeneous broadening of the band positions. However, close inspection indicated that the TBP2 in methanol showed the main chain amide band position at 1665 cm^{-1} (Figure 13E) and it was broader than TBP1 amide I band at 1660 cm^{-1} that appeared for fibrillar networks produced by TBP1 in MeOH (Figure 12E). It was possible that the oligomeric assembly state of the peptide TBP2 maintained a different configuration and it may not be as compact as the fibrillar structure produced by TBP1. The presence of multiple C=O stretching modes hindered measuring of the exact shift and band widths of individual amide I bands associated with main chain peptide and

BOC amide groups. Therefore attempt to measure the Raman signature of the peptides both in the solid state and aggregates produced in methanol.

Raman spectroscopic measurement was engaged to derive the overall peptide backbone configuration via the Raman band position of amide mode of vibrations. The most significant bands related with amide linkage (- CONH) are amide I (1600−1690 cm^{-1}), amide II (1480−1580 cm^{-1}), amide III (1230−1300 cm^{-1}), amide IV (625−770 cm^{-1}), amide V (640− 800 cm^{-1}) and amide VI (540−600 cm^{-1}). Among them, amide I and amide III provide important structural insight about peptide or protein conformation. The amide I vibration mode of CONH group appeared in the spectral range of 1600-1690 cm^{-1} is, however, most sensitive to specific secondary structure/conformation of the peptide group.

Carbonyl group present in the main chain peptide showed the band positions at ~1650 $cm^{-1}$and another band at 1688 cm^{-1} for the carbonyl group present in the BOC part of the peptide (Figure 14A). The appearance of the bands at 1735 and 1748 cm^{-1} were due to stretching frequency for ester carbonyls. Thus the configuration of the main chain amide group of the two peptides may not differ significantly in the solid state. However, upon aggregation, the C=O stretching vibration band associated with the main chain amide group of TBP1 spectra shifted to 1658 cm^{-1} in methanol (the peptide instantly attained fibrillary structure) and the band became narrower. It indicated structural alteration towards ß-sheet conformation. TBP2 oligomers produced in methanol produced Raman amide band for main peptide group at 1649 cm^{-1} and no major shift in the band position compared to the solid state was observed (Figure 15B). The band was also broader. This result suggested that TBP2 peptide in its oligomeric state preserved most of its original configuration. TBP2 oligomers also failed to produce ThT fluorescence enhancement and it further suggested that TBP2 lacked ß-sheet conformation in its oligomeric state.

3.2.10 Powder X-ray diffraction (PXRD)

Powder XRD study of the dipeptides was carried out by placing the solid sample on a glass plate. Experiments were carried out by using an X-ray diffractometer (Bruker AXS, Model No. D8 Advance). The d-spacing was calculated from Bragg's equation.

$$n\lambda = 2dsin\theta \dots\dots\dots (5)$$

Where d is the interplanar spacing of the crystal, λ is the wavelength of the incident X-rays, θ is the angle of incidence, and n is the order of reflection close to unity.

To determine the solid-state molecular packing and orientation of the molecules in the self-assembled state, powder X-ray diffraction (PXRD) experiment of both molecules were carried out in the dry state and represented in Figure 16. The powder form showed sharp distinct peaks within the 2θ range 5-40^{o} which clearly indicated that the materials are crystalline in nature. TBP1 shows a peak corresponding to d-spacing ~ 4.32 Å (2θ = 20.5°) accompanied by the other peak at ~ 8.86 Å (2θ = 9.97°) (Figure 16A). This indicates the cross-ß-structure of the peptide chain present in the powdered state.[21,152,199] The peak at 4.32Å can be assigned for the inter strand distance of assembled peptide backbones forming a ß-sheet type arrangement, while the peak at 8.86 Å can be characterized as the distance between two stacked ß-sheets. The diffraction pattern of the TBP1 also shows peaks at 4.54 Å (2θ= 19.5°) and 11.83 Å (2θ = 7.46°). This also suggests its anti-parallel cross ß-packing arrangement in the powder state. Another peak at ~ 3.54 Å (2θ = 25.06°) signifies the π−π stacking interaction between the phenyl rings of the molecules in the three-dimensional network structure. For the aggregates of TBP2, these features are bit different, the peaks corresponding to stacked ß-sheet is completely absent and very weak intense peak corresponding to ß-strand distance appears at 4.35 Å (Figure 16B). Moreover, the π−π -stacking distance appears at

3.42 Å. From these above stated observations it can be concluded that both TBP1 and TBP2 form ordered arrangement, however the nature of their arrangements are slightly different.

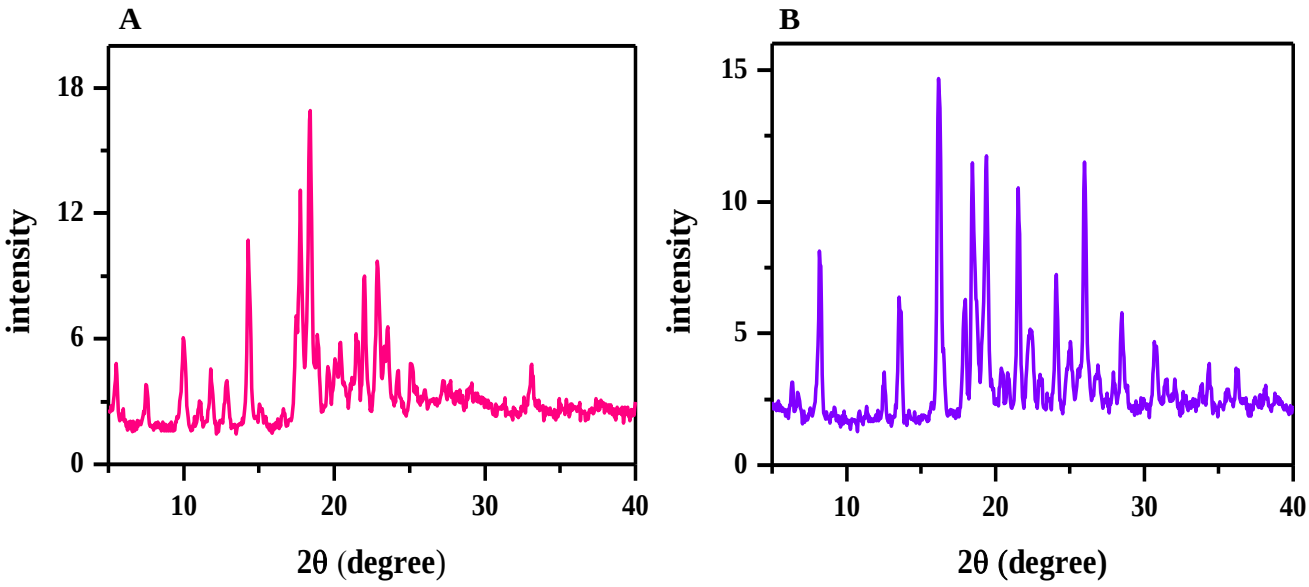

Figure 16. *Powder XRD patterns of dipeptide TBP1 (A), and TBP2 (B) in solid state.*

3.2.11 Rheological study

The rheological measurement of the gel obtained from dipeptide TBP1 in methanol-water solvent system (at a ratio 1:1) was performed using Modular Compact Rheometer (Anton Parr, MCR 102, Austria). The instrument was equipped with an air compressor unit which maintained the air pressure at 7 kg/cm^2. Standard cone-plate geometry (CP-40, 40 mm outer diameter, angle 1°) was employed in the study. Frequency sweep (G, G″ versus angular sweep) was measured in oscillation mode. The data was analysed using Rheoplus software (US 200, version 3.62).

The fundamental mechanical properties of a gel can be expressed through two main rheological tests such as – amplitude/strain sweep, and frequency sweep tests. These experiments represent the flow behaviour and viscoelastic properties of a gel. The

gel (Figure 30) obtained from dipeptideTBP1 in methanol-water (1:1) solvent system was investigated using strain sweep and frequency sweep experiments. The result obtained from strain sweep test is shown in Figure 17A. The test demonstrated the linear viscoelastic range (LVE) and the dependence of G′ and G″ on strain amplitude. G′ data was linear with a constant value up to a critical strain of 0.1%, beyond this critical strain G′ declined. At 0.1% strain G′ was 8 times greater than G″, at 1% strain G′ was 3 times greater than G″, and at 10% strain G′ was 1.65 times greater than G″. At 65% strain cross-over point found (where G′=G″), therefore before the cross-over point G′ remained greater than G″.Next, with this gel frequency sweep experiment was performed at a constant strain of 0.1% to monitor the storage modulus (G′) and the loss modulus (G″) as a function of applied angular frequency. It is evident from Figure 17B that G′ was higher than the G″ and no cross-over point was noticed within the experimental frequency regions (0.1-100 rad/s). For this gel, G′ was an order of magnitude (8.71 times) greater than G″at an applied angular frequency (10 rad/s). These results suggested the presence of soft ‘solid-like’ gel phase material was present.

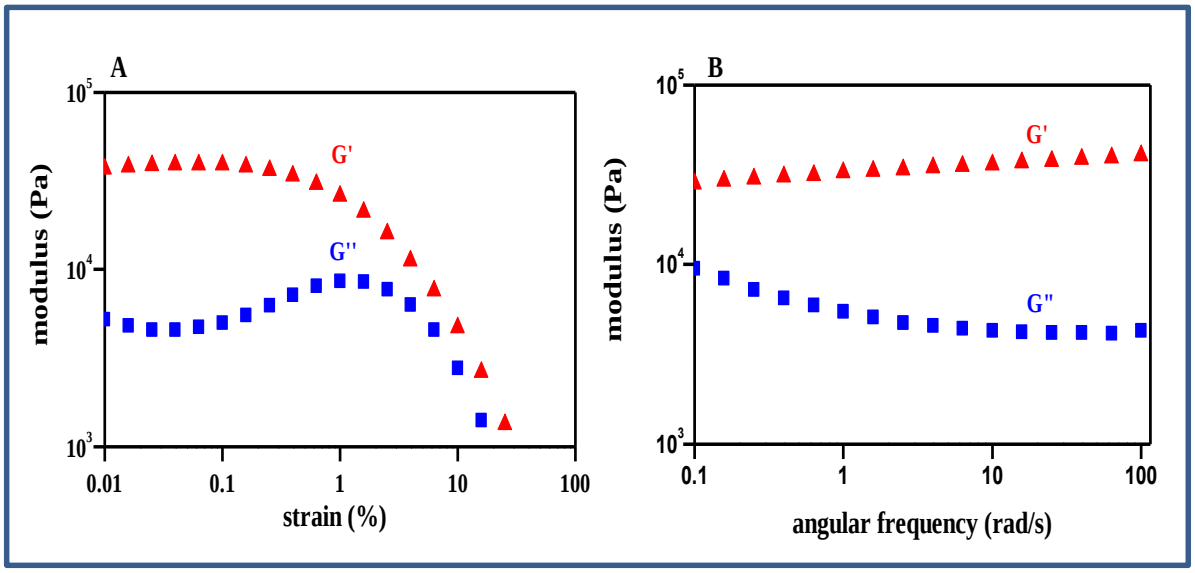

Figure 17. *Rheological analysis of the gel obtained from TBP1 in methanol-water solvent (1:1). Panel (A) shows the modulus plot against strain in a strain-sweep experiment (G'>G''). Panel (B) shows the frequency sweep result of the gel.*

3.4 Conclusion

Several investigations indicated that proteins and peptides have a generic ability to aggregate into elongated nano-scale structures commonly known as amyloid aggregates.[200] These nanometer size aggregates differ in their morphology. The conformation state of the involved peptide chains may also significantly altered compared to their native structure. Substituted tyrosine can produce aggregates of different morphologies and, these could have several applications in nanotechnology. The current investigations illustrate a robust change in physico-chemical behaviour of a dipeptide due to small change in the substitutions. The presence of extra phenyl ring in the peptide TBP2 added a significant hydrophobic microenvironment to promote the oligomerization of the peptide. D_2O exchange proton NMR measurement suggested that the two amide protons of dipeptide TBP1 can undergo easy proton exchange at much faster rate than the amide protons of dipeptide TBP2. This further suggested stronger hydrophobic encapsulation of the dipeptide TBP2 enriched with phenyl ring moiety as an extra substituent. The shifting and weakening of the amide I band vibration positions were due to H-bonding network among the peptide/solvent molecules. The cross ß-sheet structure in the fibrillar network in TBP1 peptide was due to strong intermolecular H- bonding network among the peptides. However, the hydrogen bonding pattern may be significantly different due to hydrophobic twist by the added phenyl group.

Additional interesting observation was that the fibrillar assembly structure of the peptide at a certain concentration can produce gel like structure encapsulating solvent ($MeOH/H_2O$) molecules in the fibrillar network. Thus it indicated that easily available fibrillar protein aggregates may be used in gel making formulation and may be potentially used for technological and commercial purposes.

3.5 Supporting information

3.5.1 Characterization of the dipeptides

^{1}H and ^{13}C NMR spectroscopy of *N*-Boc-(O-benzyl)-tyro-(di-methyl)-glutamate (TBP1)

^{1}H NMR (600 MHz, DMSO-d_6): δ (in ppm) 8.28 (1H, d, *J* = 12Hz, NH of amide), 7.42 (2H, d, *J* = 6Hz, Ar-H), 7.37 (2H, t, *J*= 6Hz, Ar-H), 7.31 (1H, t, *J* = 6Hz, Ar-H), 7.17`(2H, d, *J* = 6Hz, Ar-H), 6.91(2H, d, *J* = 6Hz, Ar-H), 6.87 (1H, d, *J* = 12Hz, NH of BOC group), 5.06 (2H, s, -O-CH_2-Ar), 4.35-4.31 (1H, m, CαH), 4.13-4.09 (1H, m, CαH), 3.60 (3H, s, -CH_3 of ester group), 3.57 (3H, s, -CH_3 of another ester group), 2.87-2.86(1H, m), 2.68-2.64(1H, m), 2.39-2.37 (2H, m, -CH_2-), 2.04-1.99 (1H, m), 1.86-1.80(1H, m), 1.30 (9H, s, -CH_3 of tertiary butyl group).

^{13}C NMR (150 MHz, DMSO- d_6): δ (in ppm) 173.09, 172.53, 172.40, 157.34, 155.68, 137.67, 130.64, 128.82, 128.17, 128.02, 114.75, 78.43, 69.55, 56.24, 52.35, 51.76, 51.40, 36.77, 29.83, 28.53, 26.56.

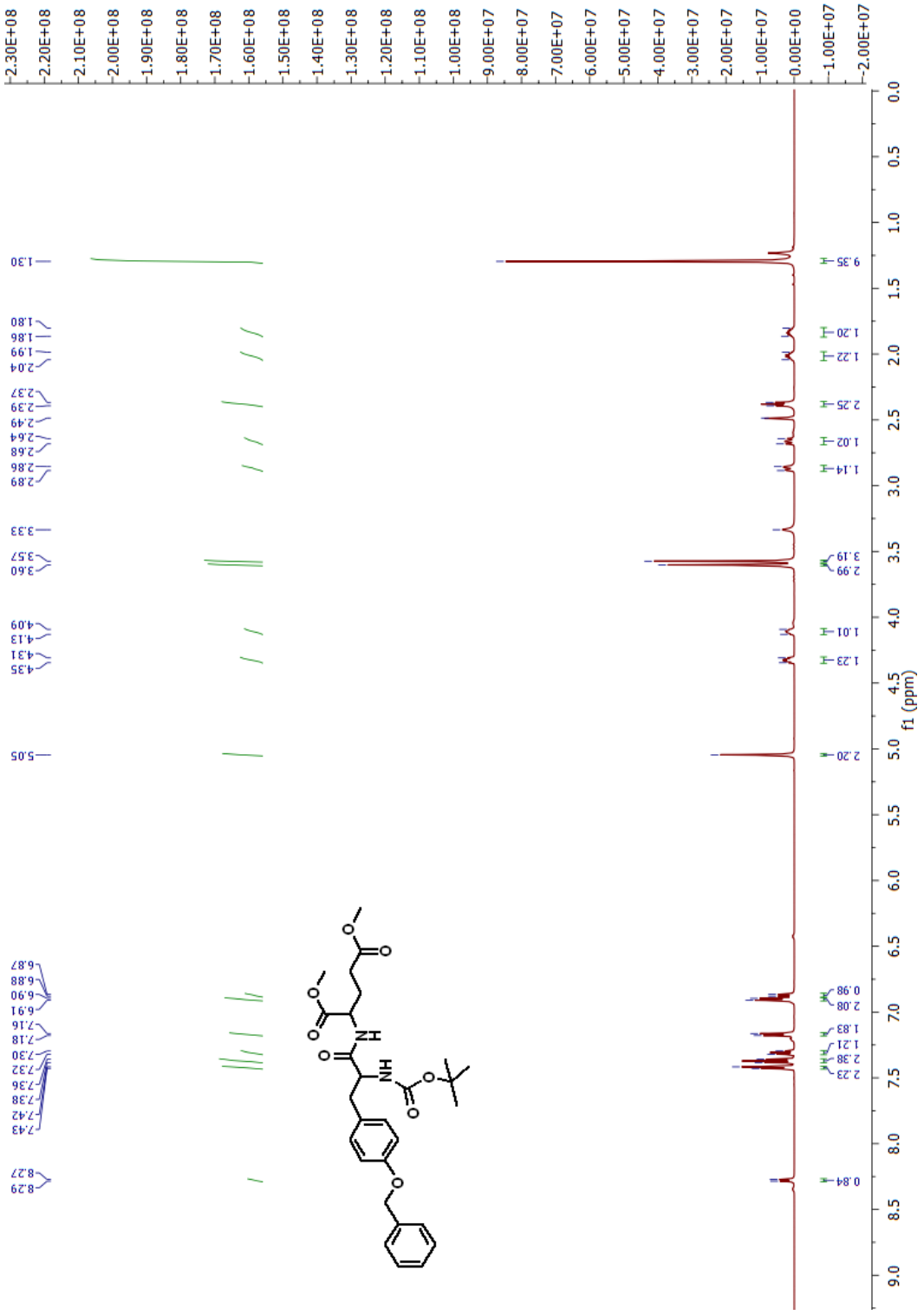

Figure 18. ^{1}H-NMR spectra of the dipeptide TBP1 dissolved in DMSO-d_6 solvent.

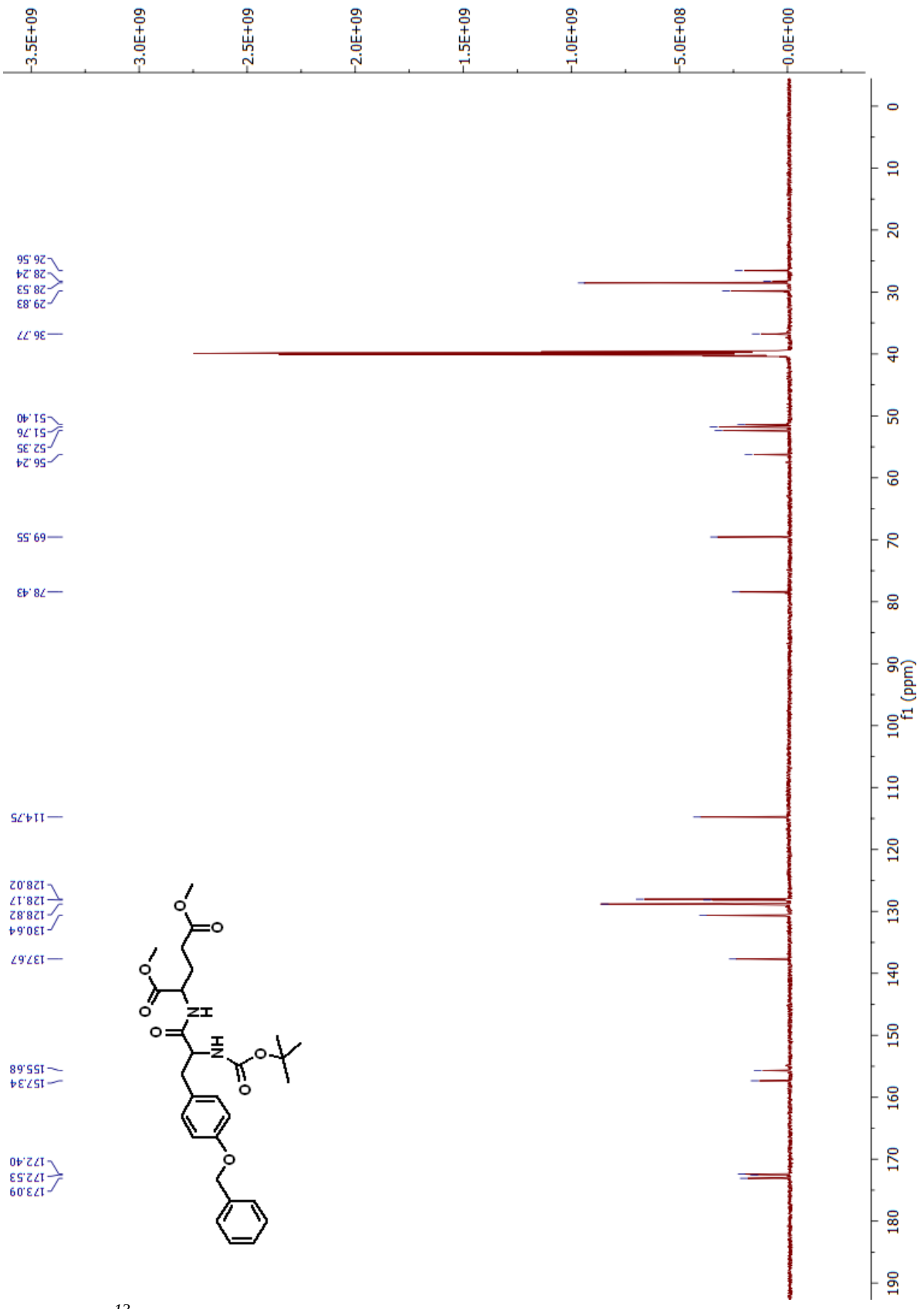

Figure 19. ^{13}C-NMR spectra of the dipeptide TBP1 dissolved in DMSO-d_6 solvent.

^{1}H and ^{13}C NMR spectroscopy *N*-Boc-(O-benzyl)-glu-(O-benzyl)-tyrosine-methyl ester (TBP2):

^{1}H NMR (600 MHz, DMSO-d_6): δ (in ppm) 8.18 (1H, d, *J* = 6Hz, NH of amide), 7.41 (2H, t, *J*=12Hz Ar-H), 7.38-7.33 (6H, m, Ar-H), 7.32-7.29 (2H, m, Ar-H), 7.11 (2H, d, *J* = 6Hz, Ar-H), 6.88 (3H, d, *J* = 12Hz), 5.08 (2H, s, -O-CH_2-Ar), 5.03 (2H, s, -O-CH_2-Ar), 4.44-4.40 (1H, m, CαH), 3.98-3.95 (1H, m, CαH), 3.54 (3H, s, -CH3 of ester group), 2.96-2.93 (1H, m), 2.88-2.84 (1H, m), 2.34-2.31 (2H, m, -CH_2-), 1.87-1.81 (1H, m), 1.77-1.70 (1H, m), 1.35 (9H, s, -CH_3 of tertiary butyl group).

^{13}C NMR (150 MHz, DMSO- d_6): δ (in ppm) 172.64, 172.28, 172.03, 157.53, 155.55, 137.58, 136.63, 130.57, 129.50, 128.84, 128.40, 128.27, 128.19, 114.94, 78.59, 69.53, 65.85, 54.07, 53.66, 52.21, 36.18, 30.38, 28.57, 27.68.

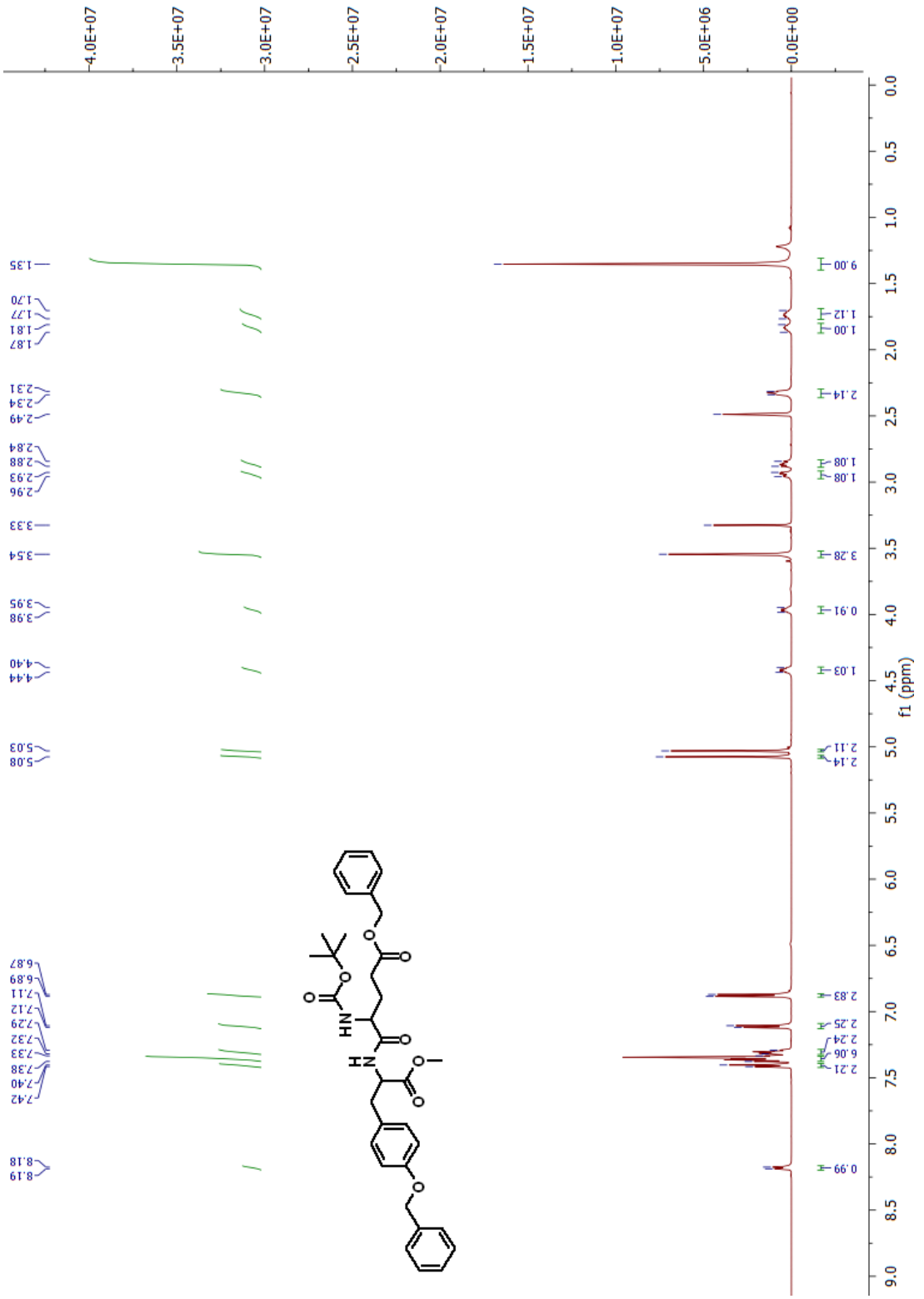

Figure 20. ^{1}H-NMR spectra of the dipeptide TBP2 dissolved in DMSO-d_6 solvent.

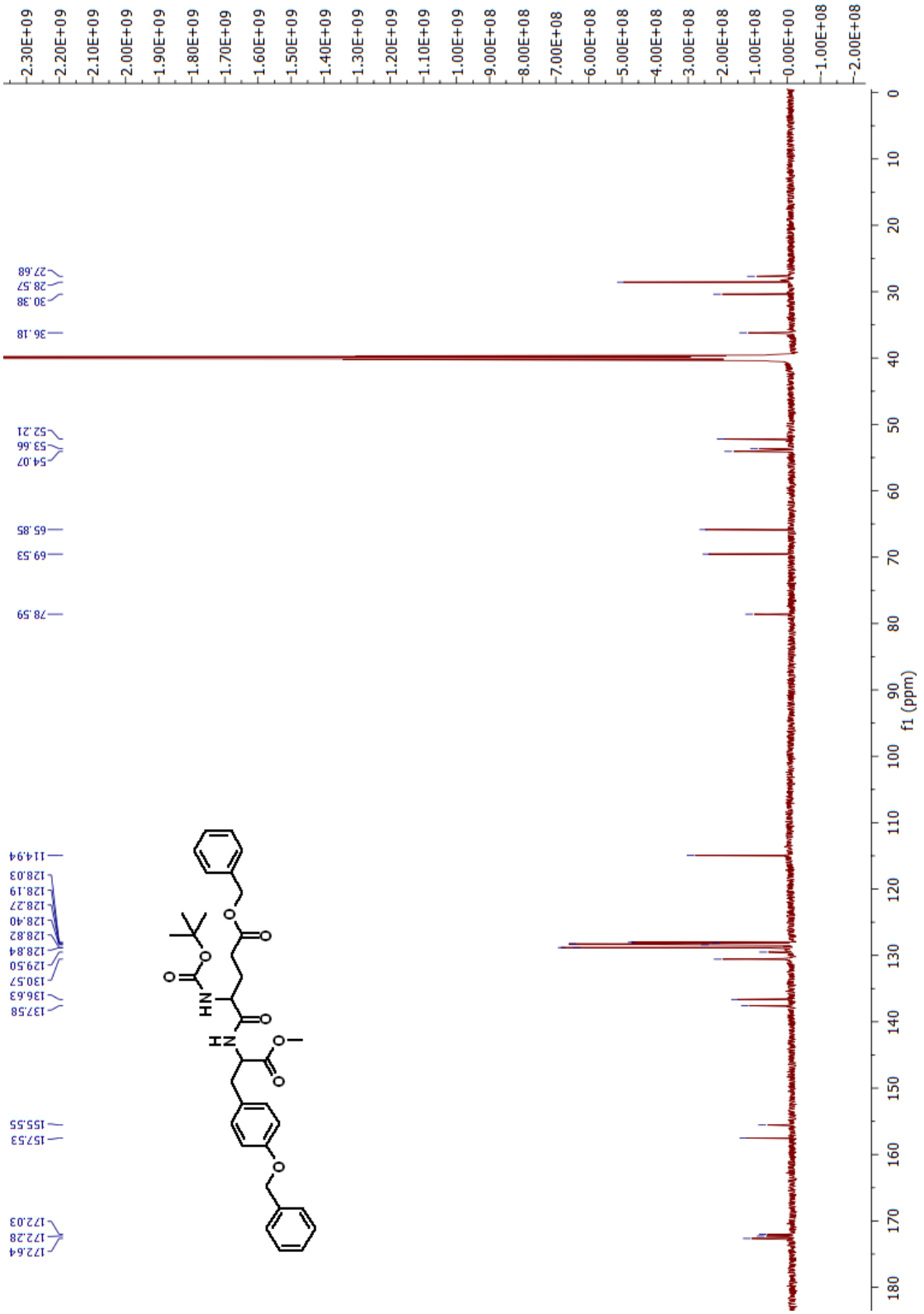

Figure 21. ^{13}C-NMR spectra of the dipeptide TBP2 dissolved in DMSO-d_6 solvent.

3.5.2 Assignment of the FT-IR spectra of the dipeptides.

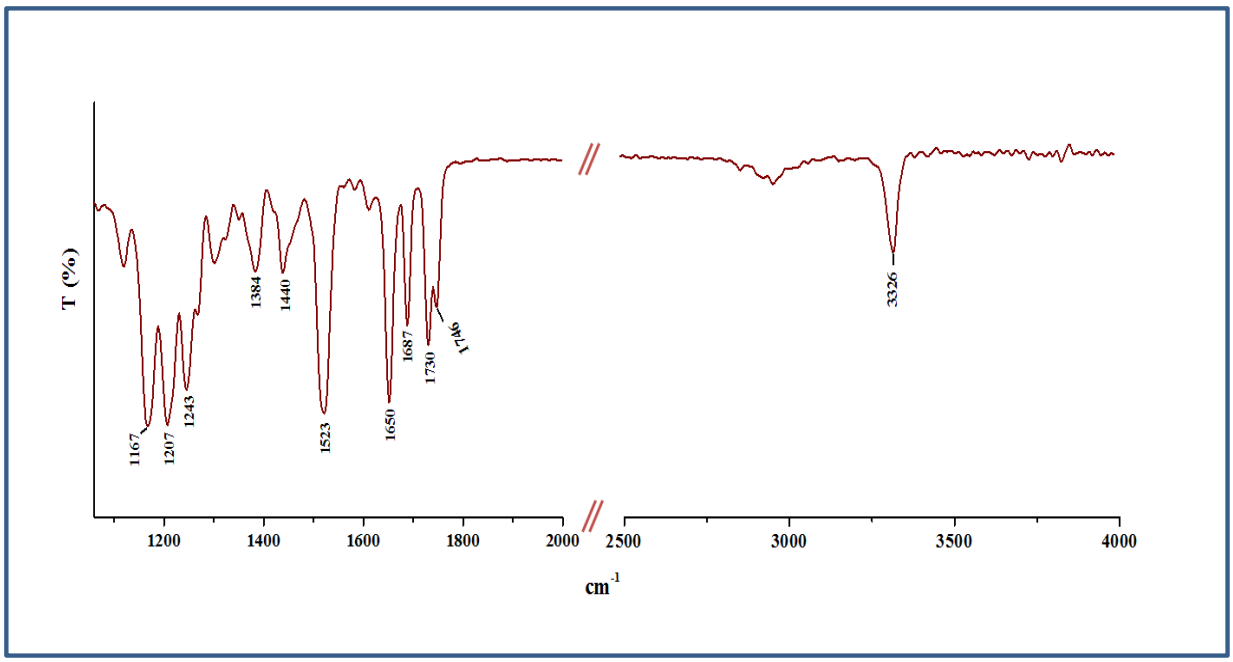

Figure 22. FT-IR spectra of TBP1 in its solid state.

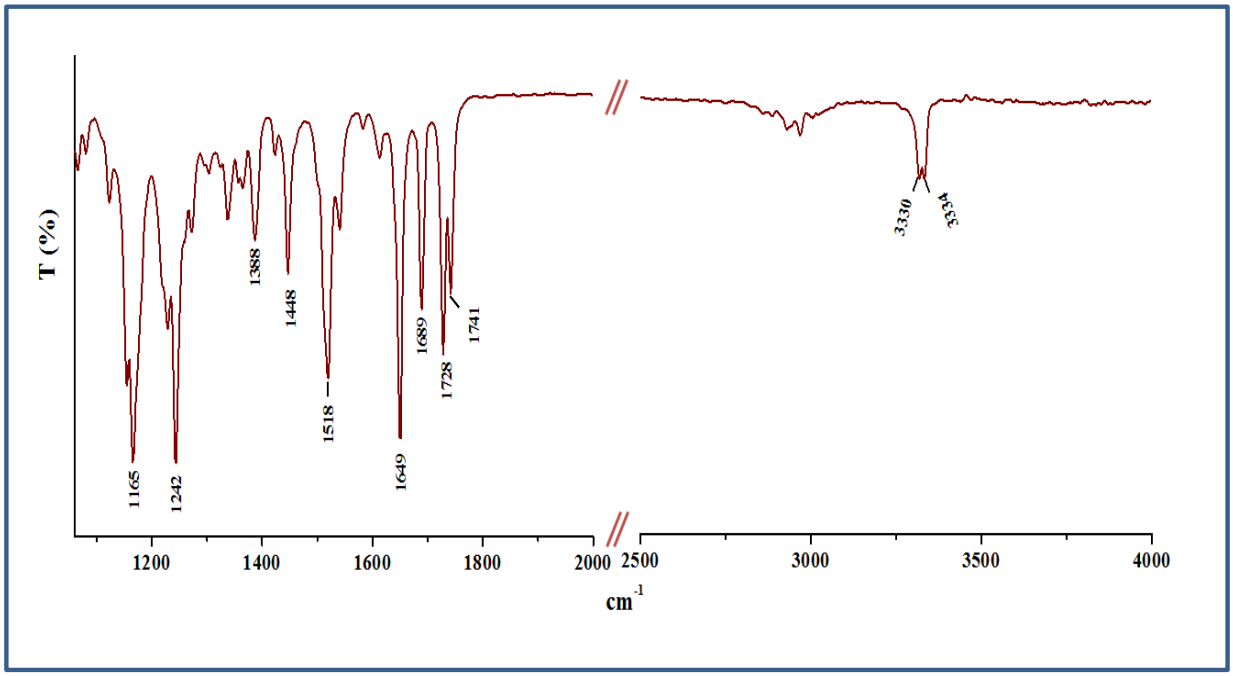

Figure 23. FT-IR spectra of TBP2 in its solid state.

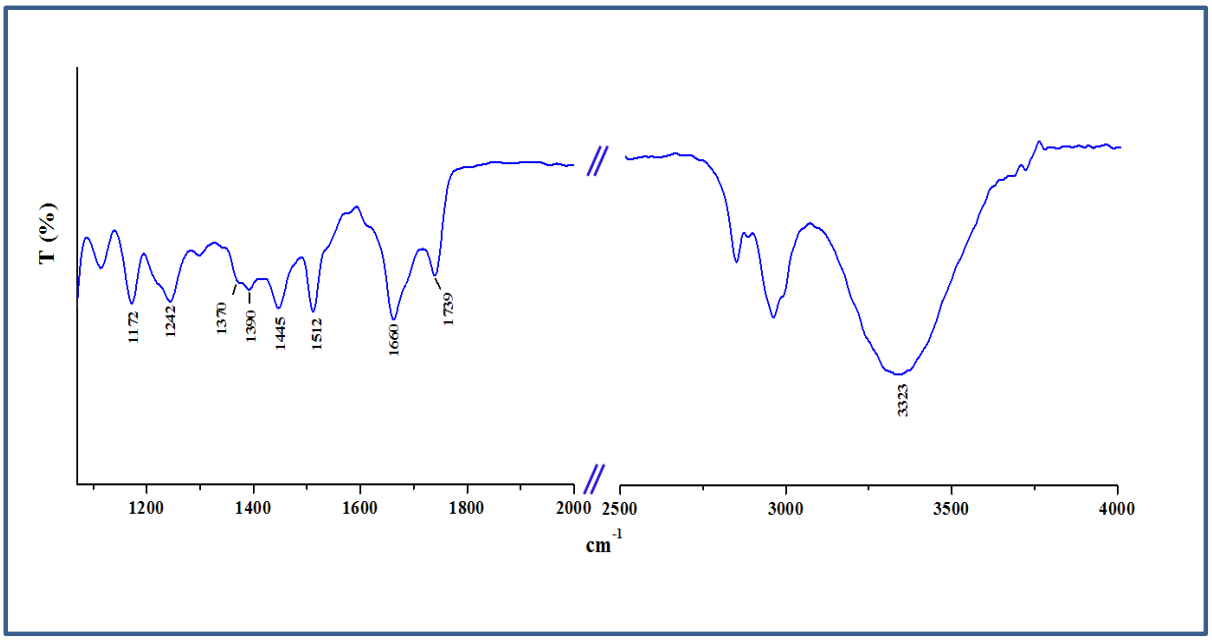

Figure 24. FT-IR spectra of TBP1 in Methanol. For peptide solution the concentration was~ 200 μM.

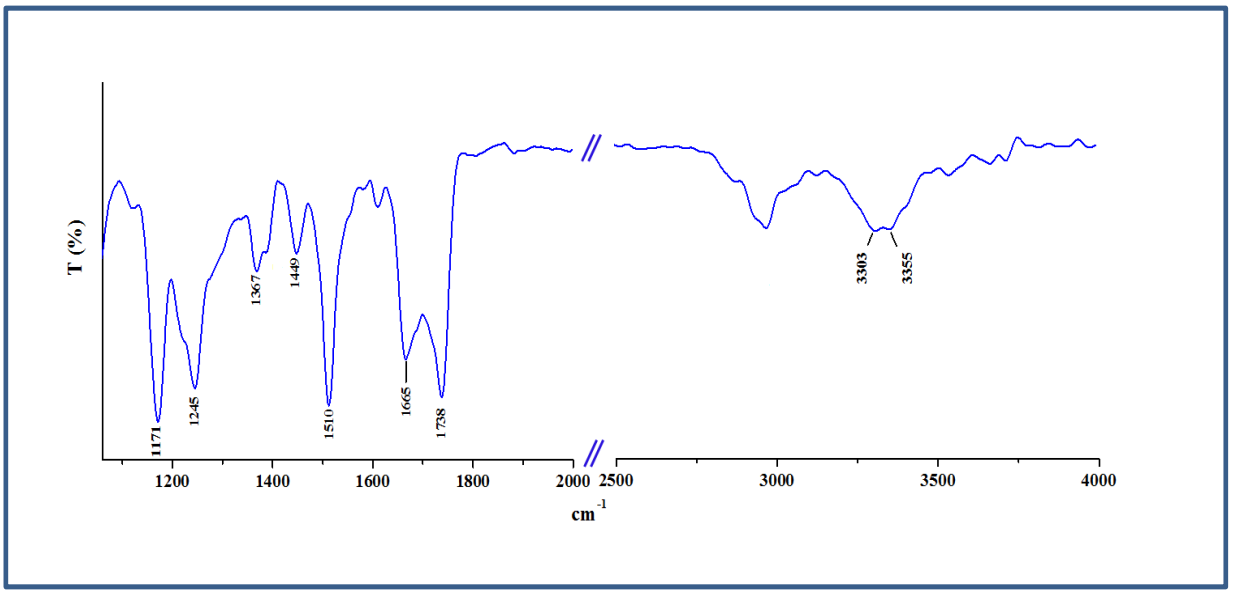

Figure 25. FT-IR spectra of TBP2 in Methanol. For peptide solution the concentration was~ 200 μM.

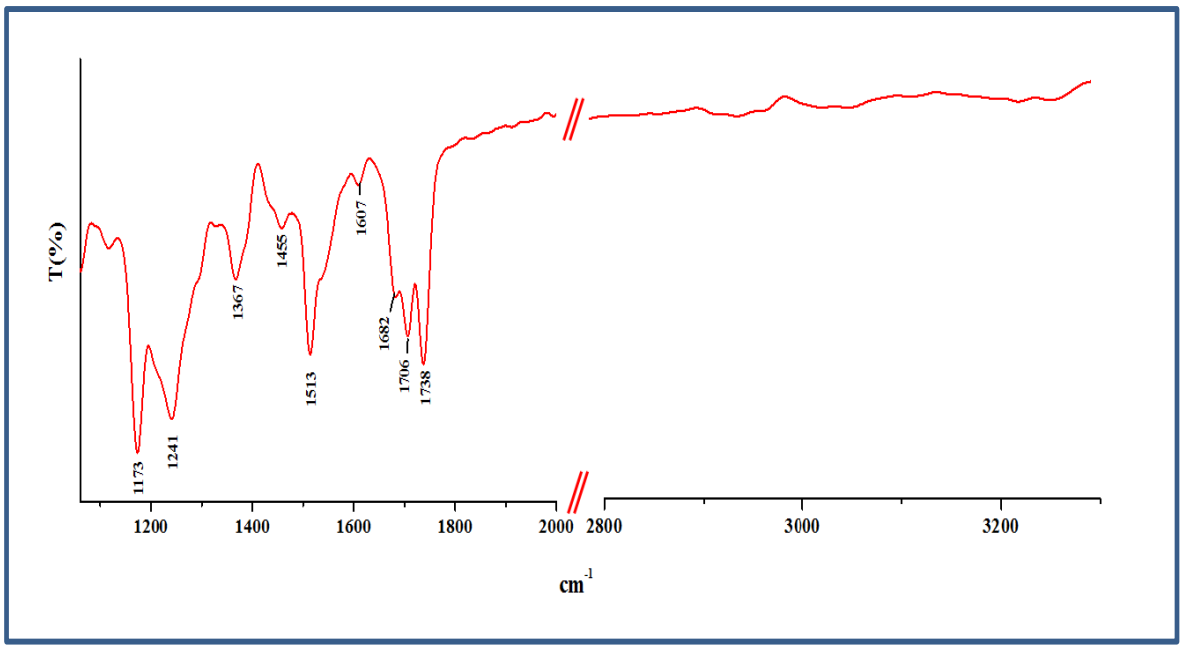

Figure 26. FT-IR spectra of TBP1 in DMSO. For peptide solution the concentration was~200 µM.

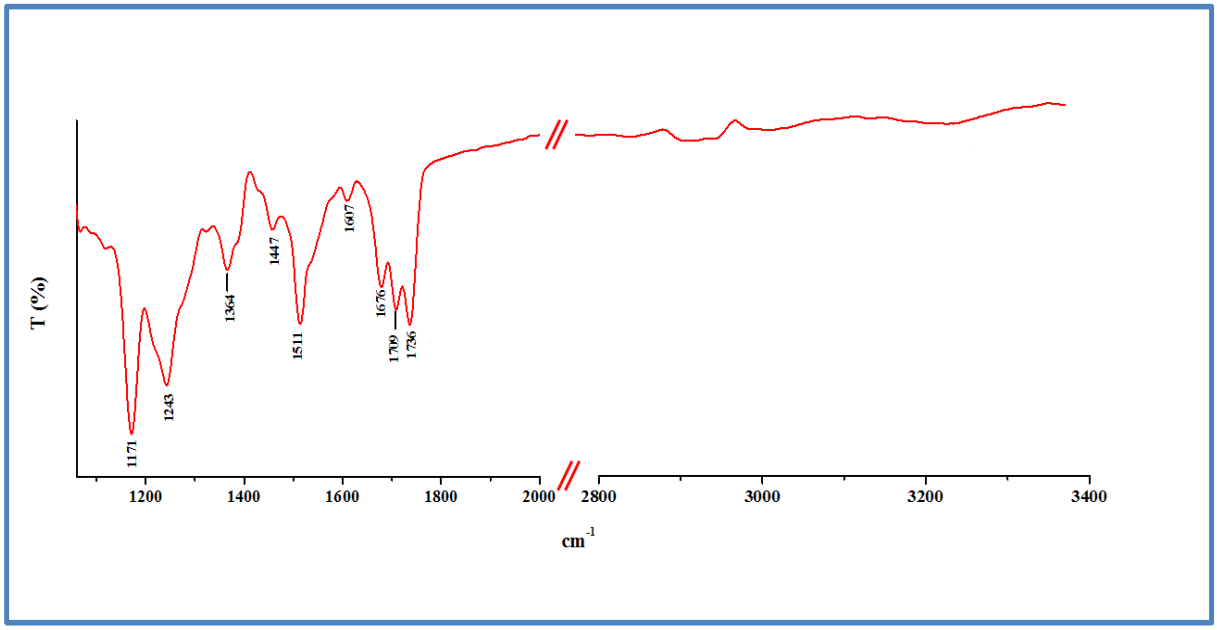

Figure 27. FT-IR spectra of TBP2 in DMSO. For peptide solution the concentration was~200 µM.

3.5.3 Raman spectras of the dipeptides in three different conditions

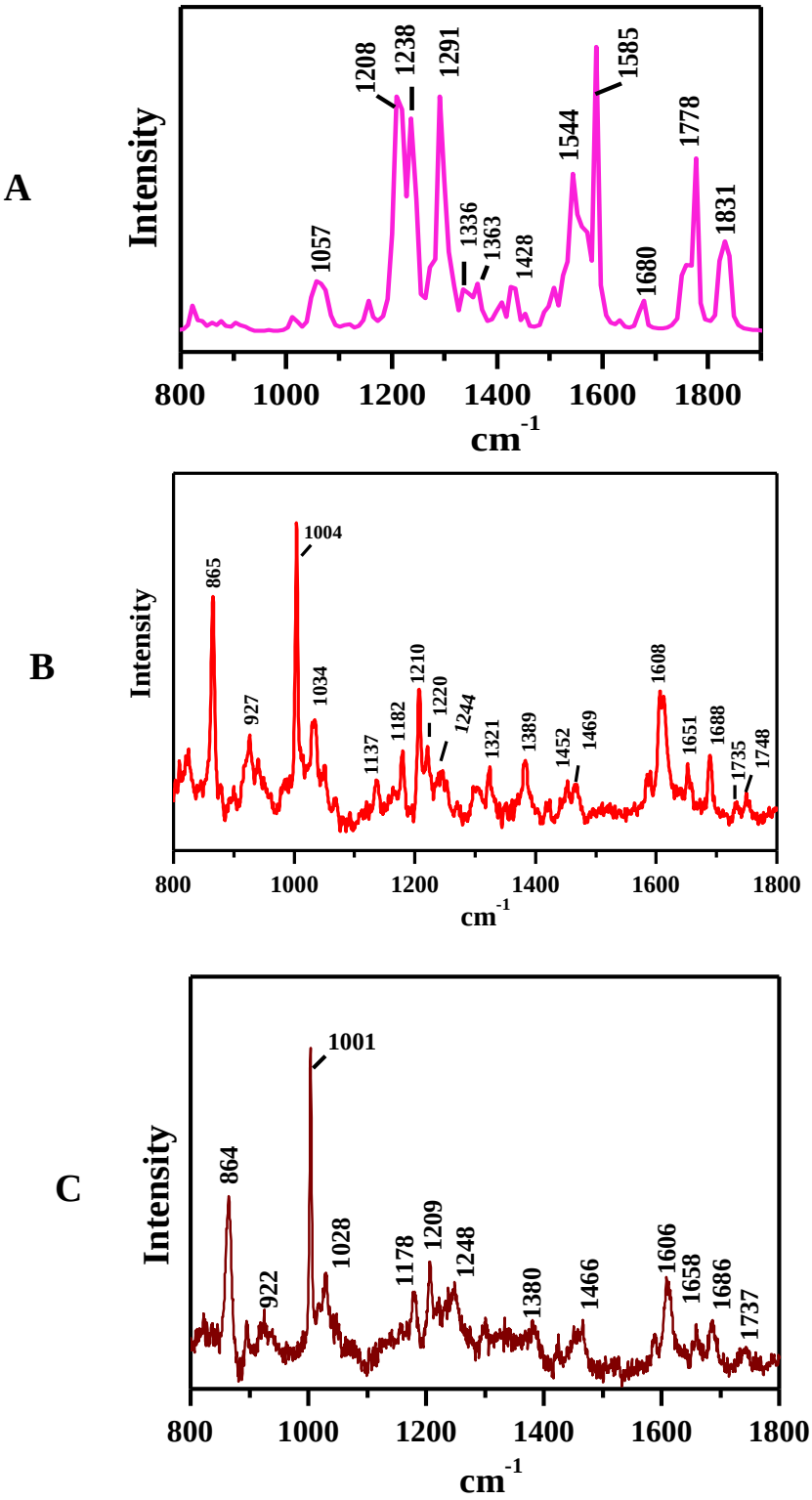

Figure 28. Raman spectra of TBP1 in three different sample conditions.

(A) Calculated Raman spectra of TBP1, (B) and (C) represent experimental Raman spectra of TBP1 in solid as well as in methanol.

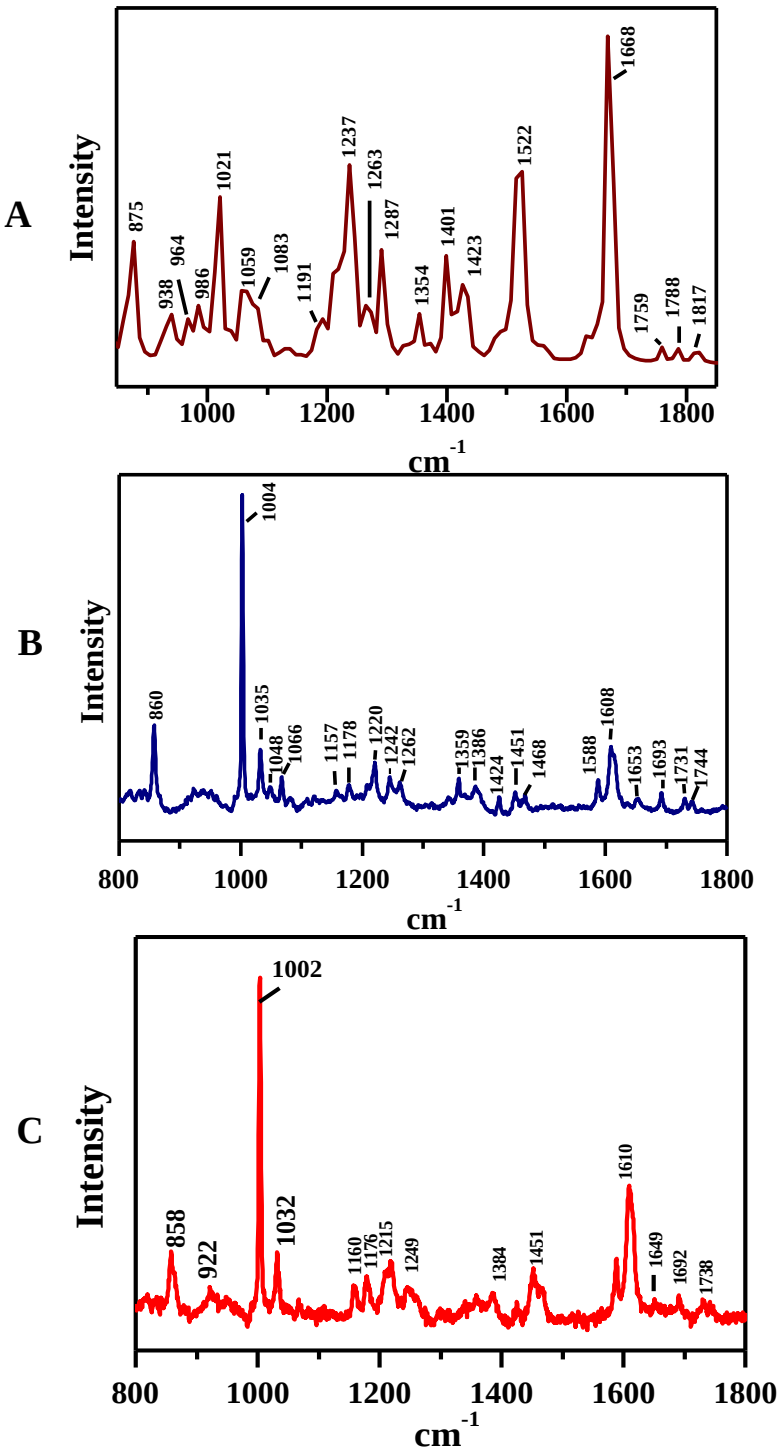

Figure 29. Raman spectra of TBP2 in three different sample conditions.

(A) Calculated Raman spectra of TBP2, (B) and (C) represent experimental Raman spectra of TBP2 in solid as well as in methanol.

3.5.4 Tube inversion test of the gelator peptide, TBP1 and AFM images of TBP2 aggregates after longer incubation.

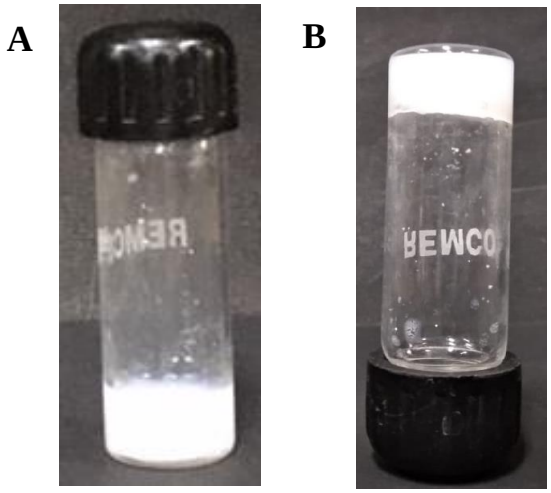

Figure 30. Images of the gel obtained from gelator peptide TBP1 (A) Gel obtained from methanol-water (1:1) solvent mixture. (B) Tube inversion test of this gel.

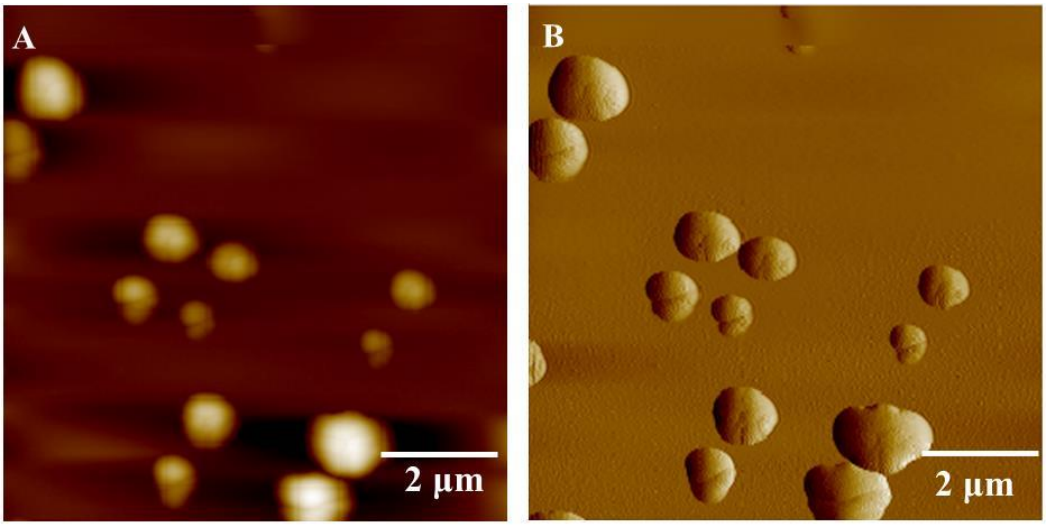

Figure 31. AFM images of the aggregates produced from TBP2 after 48h incubation in methanol.

3.5.5 ^{1}H NMR spectras of TBP1 and TBP2 in MeOD solvent.

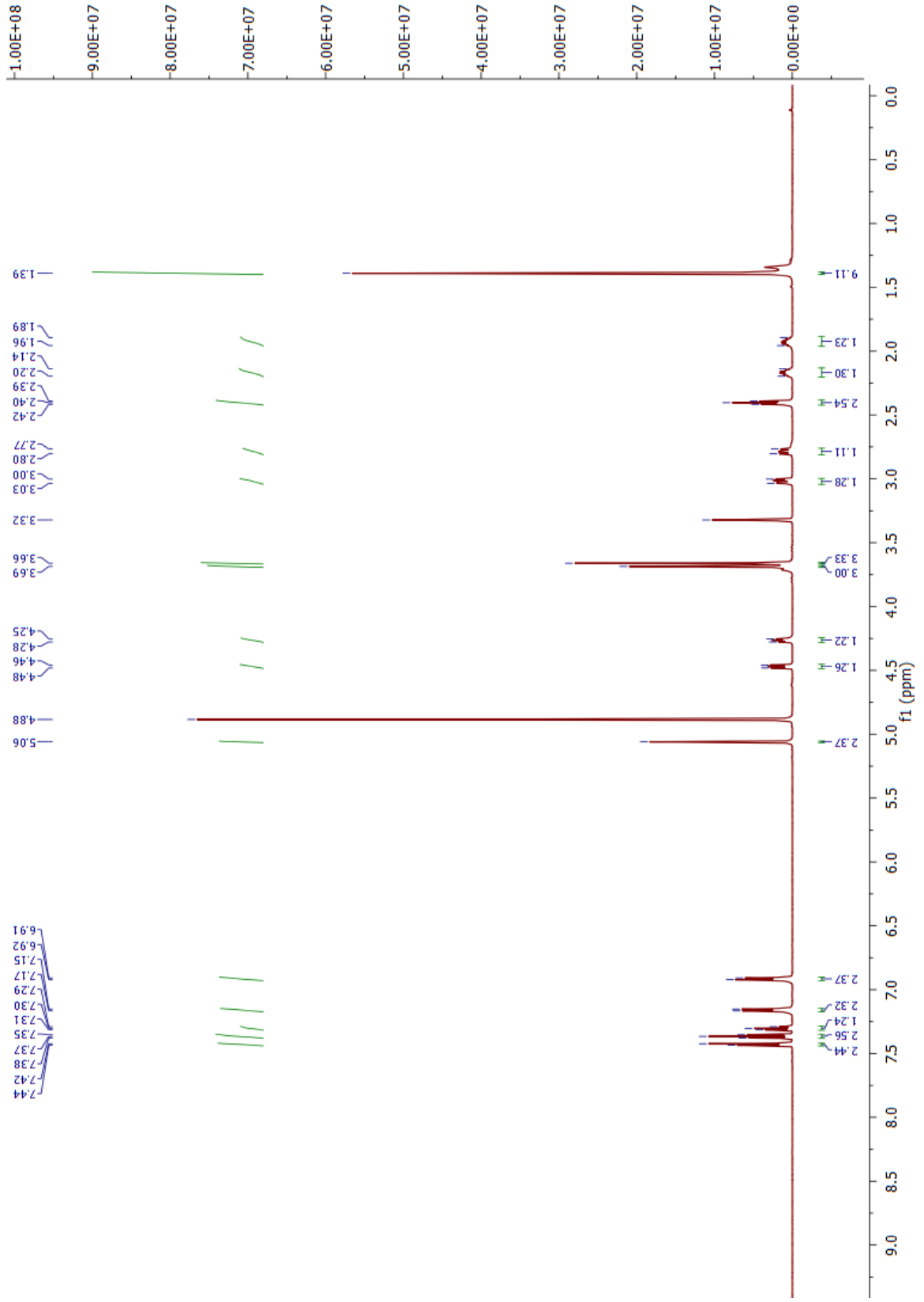

Figure 32. ^{1}H NMR spectra of TBP1 in MeOD solvent.

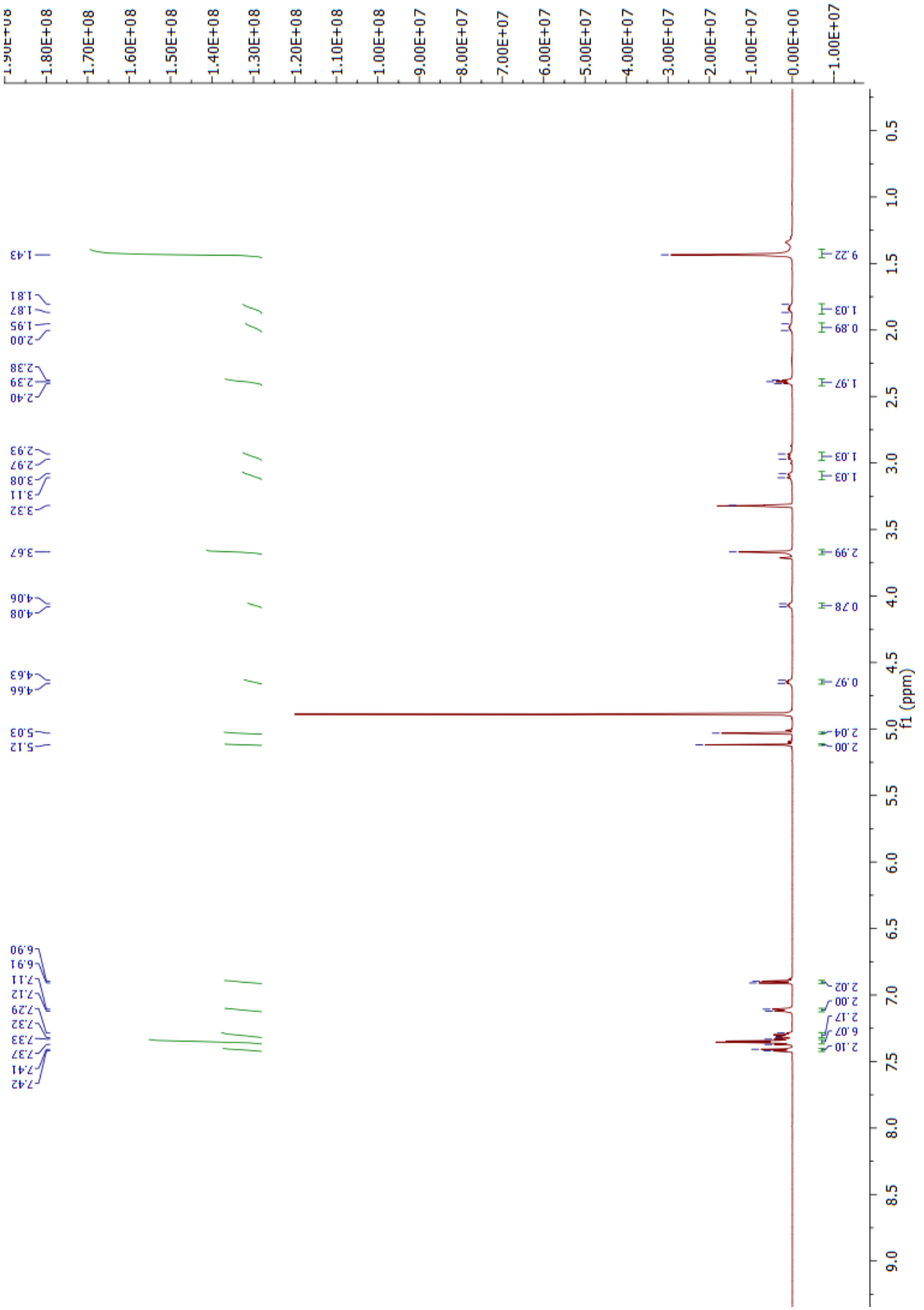

Figure 33. ^{1}H *NMR spectra of TBP2 in MeOD solvent.*

3.5.6 Reaction kinetics plot of both the dipeptides

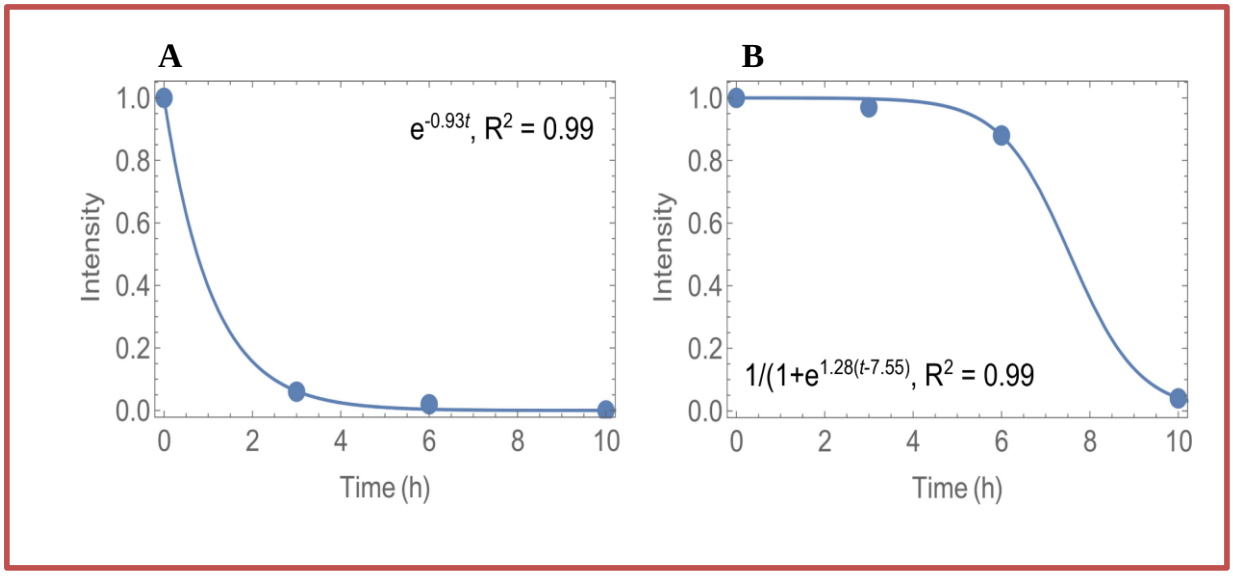

Figure 34. Reaction kinetics of TBP1 (A); reaction kinetics of TBP2 (B).

3.5.7 Expanded form of proton NMR spectra of both the peptides in MeOH.

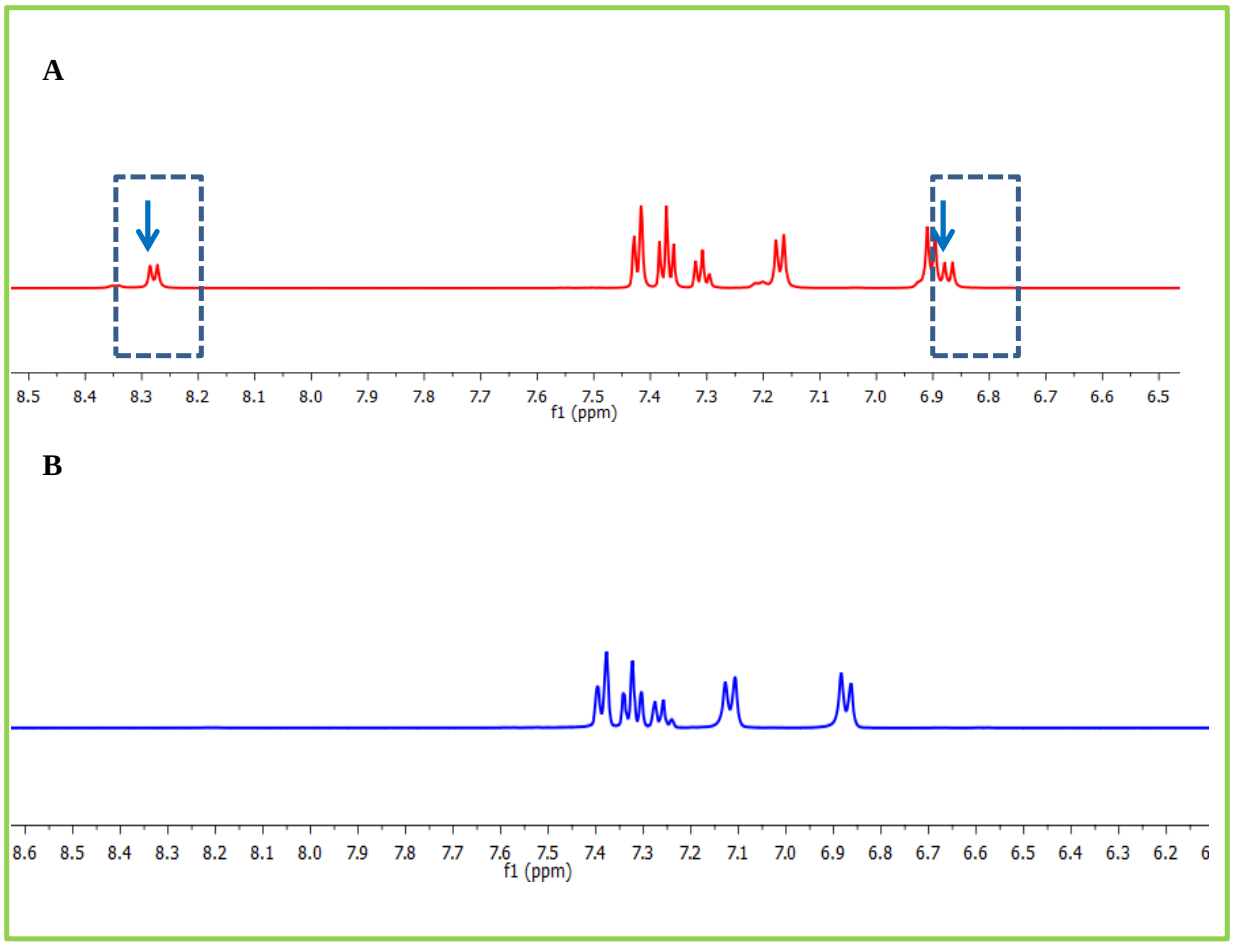

Figure 35. (A) Expanded form of ^{1}H-NMR of TBP1 in DMSO-d_6 (amide-NHs are marked). (B) Expanded form of ^{1}H-NMR ofTBP1 in MeOD solvent (amide-NHs are absent).

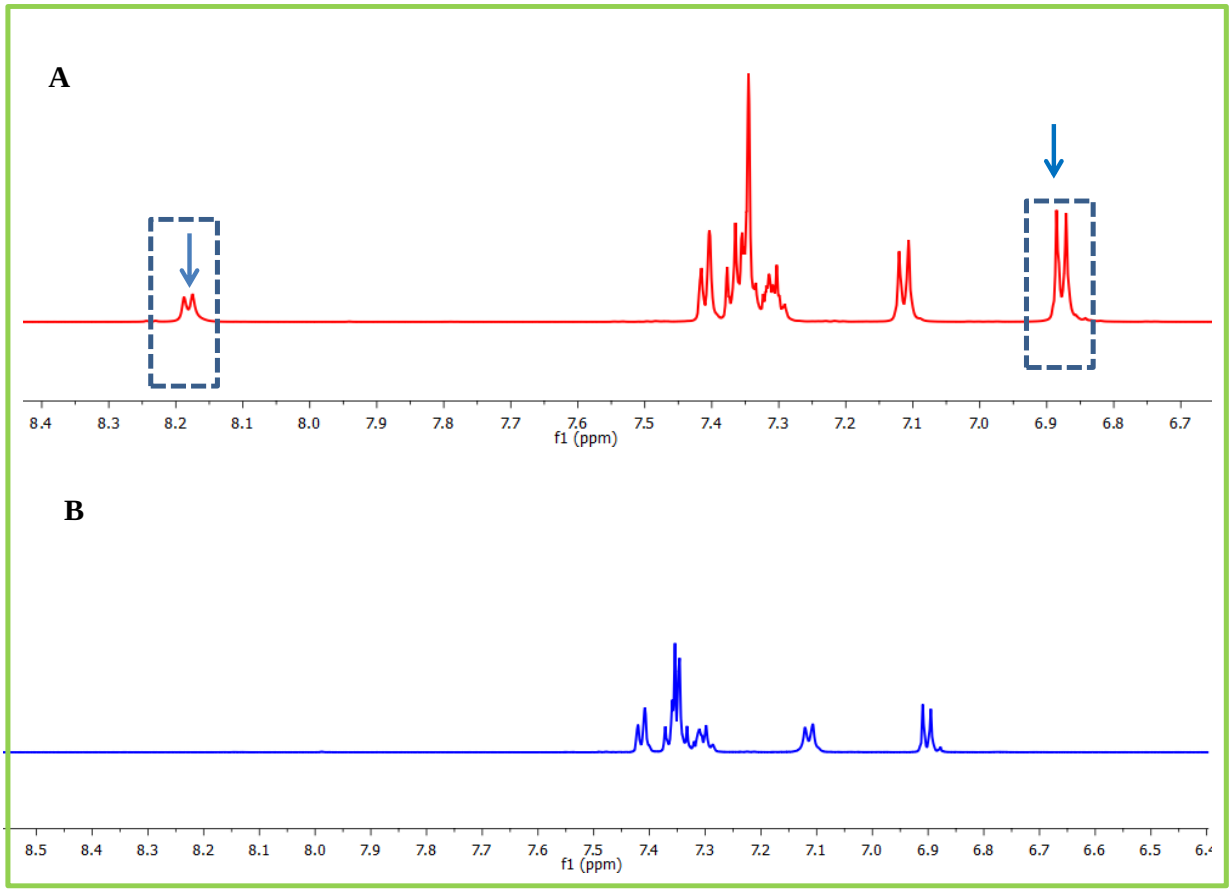

Figure 36. (A) Expanded form of ^{1}H-NMR of TBP2 in DMSO-d_6 (amide-NHs are marked). (B) Expanded form of ^{1}H-NMR of TBP2 in MeOD solvent (amide-NHs are absent).

3.5.8 calculated FT-IR spectra of the peptides in MeOH (transmittance vs. wavenumber plot)

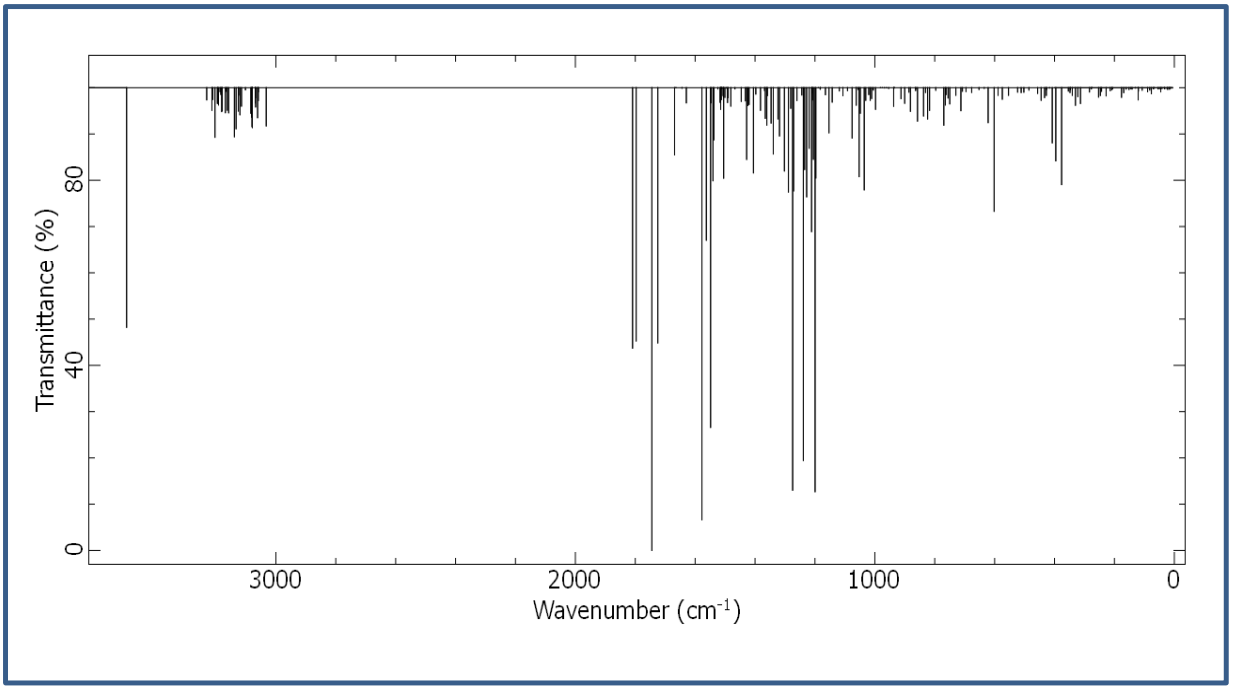

Figure 37: Full range of calculated FT-IR spectra of dipeptide TBP1 in methanol.

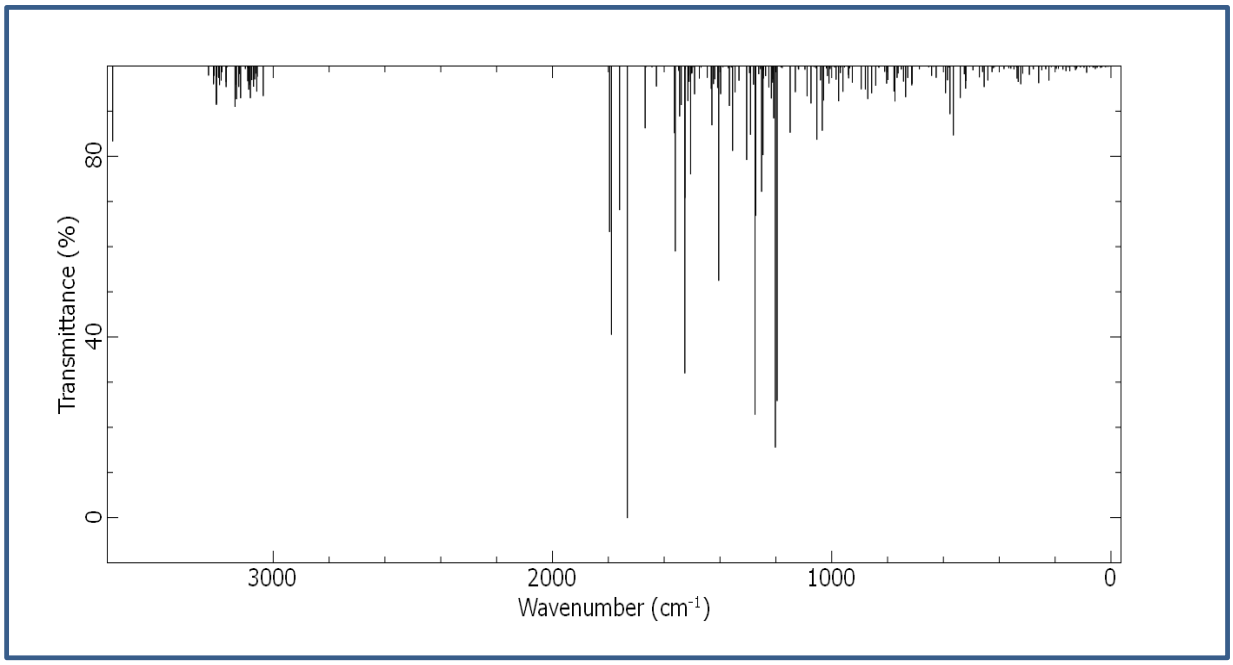

Figure 38: Full range of calculated FT-IR spectra of dipeptide TBP2 in methanol.

CHAPTER 4

ß-SHEET PROMOTED HELICAL STRUCURE PRODUCED BY SIDE CHAIN PROTECTED DI-TYROSINE DIPEPTIDE

4.1 Aim of the work

Short peptides are versatile class of organic building blocks which have shown great potential in wide range of biomedical applications. Self-assembled nanostructures obtained from peptide units display stability and a large variety of morphological architectures. In recent years, much has been discovered about phenyl-alanine self-assembly but less is known about the influence on aggregation by two aromatic amino acids, tyrosine and tryptophan. Tyrosine is an important amino acid in biological systems. In this present investigation, a side chain protected di-tyrosine based short peptide (TTP) was designed, synthesized and its conformation and self-assembly pattern were investigated through AFM, FE-SEM, NMR, IR, fluorescence study and single crystal X-Ray analysis. Surprisingly, this dipeptide showed unique morphology in different solvent conditions which was confirmed through AFM and FE-SEM study. Further to understand the key molecular forces responsible for the morphological pattern of this dipeptide, the single crystal X-ray analysis was carried out. The single crystal X-ray analysis of TTP confirmed that this peptide displayed in a parallel ß-sheet pattern which further self-assembled to form ß-sheet promoted helical architectures by various non-covalent interactions in the crystalline state. To best of our knowledge, this is the first crystallographic report of side chain protected di-tyrosine based short peptide adopting ß-sheet promoted helical structures. Therefore, spectroscopic studies, single crystal X-ray analysis, Hirshfeld surface analysis and DFT study revealed the unique ß-sheet promoted helical structure for this dipeptide TTP.

4.2 Introduction

In recent years, development of nanomaterial inspired drug delivery system has gained substantial research interest among the researcher community.[201] Investigation of these nanomaterials in the field of disease diagnosis, treatment and prevention, unlocks new entities designated as 'Nanomedicine'.[202] Nanomedicines containing liposome, niosome, metal nanoparticle, micelle and biodegradable polymeric nanoparticle have been reported to date.[203–208] In current days, peptide based nanoparticles are exploring in the field of nanomedicine. The advent of peptide based nanoparticle in terms of drug carrier lies on their unique physiochemical properties such as biocompatibility, biodegradability and the versatility in their structure.[209,210] Peptide derived nanoparticles including hydrogel nanocapsule and nanosphere have shown significant efficiency as nanomedicine.[19,211] Potent pharmaceuticals having poor absorbance, poor solubility has been administered along with the nanocapsule and nanosphere for exerting desirable activity to the target site. Various types of substance such as drugs, enzymes, genes are delivered via tagging with nanosphere to attain the desired consequence.[212] Nanoparticle with less than 200 nm size offers the best result in drug delivery to the targeted site.[213] To optimize this drug delivery system, development of peptide inspired novel nanoparticle with desirable size is very much needed. Apart from the drug carrier, peptide derived nanoparticle possess a broad spectrum of application such as sensors, tissue engineering, imaging tools, energy storage, bio-mineralization, surfactants etc.[213,214] Peptide inspired various nanostructures have been obtained through molecular self-assembly. Molecular self-assembly of the peptide molecule resulted well-ordered nano architectures.[38] Several physiochemical parameters and the molecular interactions triggering the orientation of the self-assembly and thus control the ultimate shape and the size of the assembly. To achieve novel peptide based nanostructures, better understanding of the molecular mechanism behind the

assembly formation is essential. To fulfil the requirement of better biomedical application, huge no. of peptide inspired self-assembled nanostructure has been reported to date, however the mechanistic details of those self-assembly is still an interesting area of research community.

One specific morphology that has been a breakthrough in the field of nanotechnology is fibrils specially ß-sheet type. Infact, ß- sheet forming peptides have been ever popular since its inception due to their crucial involvement in a variety of neurodegenerative disorders including Alzheimer's, Parkinson's disease, type II diabetes, prion disease etc.[215] These types of ß- sheet forming fibrils are also known as amyloid one. Therefore, in recent time's ß- sheet forming peptides captured attention of the scientists in the arena of nanotechnology and it is very important to understand the molecular mechanism involved in the generation of ß- sheet forming fibrils. Several group showed that the presence of aromatic amino acid residues generally contributes the activation energy along with the directionality required for ß-sheet type fibril formation through π-π stacking interactions.[216] Hence, extensive research work has been carried out on evaluating the formation and morphology of self-assembled structures of peptides, from a wide range of polypeptide to the simplest one in the family, i.e dipeptides. For example, in the year 2003, Reches and Gazit reported the self-assembled structure of diphenylalanine (L-Phe-L-Phe, FF) by diluting the dipeptide solution in HFIP (1,1,1,3,3,3-hexafluro-2-propanol) with water.[216]

According to their analysis, this dipeptide (FF) formed nanotubes of several micrometre lengths in solution. Later, this group investigated the self-assembled structure generated from another similar dipeptide with respect to diphenylalanine i.e. diphenyl glycine.[77] Surprisingly, diphenylglycine self-assembled in the form of closed cage nanostructures. Gorbitz in 2006 discovered that the nanotube formed from diphenylalanine is the core recognition motif of the alzheimer's ß- amyloid polypeptide. This work suggested that three

dimensional aromatic stacking arrangement plays the role of an adhesive between hydrogen bonded cylinders of peptide main chains and promotes fiber formation.[65] Based on these result, diphenylalanine (FF) has become a very common motif and particular interest in the field of nanobiomaterials. Subsequently, a large number of studies have focused on elucidating the structure and fibril formation mechanism involved in phenylalanine based peptides. In recent days research interest of several groups focused not only on natural amino acids, but also on modified amino acids (such as, involvement of protecting groups, side chain variation, substitution etc.) to understand their participation in self-assembly process.[78]

Like ß-sheet, another important secondary conformation of protein folding is α-helix. In biological systems, helicity takes part in a very significant manner for example- DNA double helical structure, the collagen triple helix etc. Therefore, designing of helix forming peptide moieties has become a powerful tool for biomedical and materials chemistry applications. Although, there is still remain difficulties in the design and development of single helical or double helical assembly through peptides or peptidomimetics.[216] Inspired and elicited from this approach, several investigations has been carried out such as- Gorbitz investigated a series of dipeptides which showed double helical strucrure generated from val-ala class.[217] Luis and co-workers found columnar helical self-assembled structure obtained from Val and Phe containing pseudopeptides.[218] Another interesting observation was found by Gazit et al. which demonstrated Pro-Phe-Phe- the most aggregation-prone tripeptide of natural amino acid self-assembled in a helical like sheet structure.[219] Dutt Konar et al. described the double helical structures obtained from model Aib (2-Aminoisobutyric acid) containing tripeptides and pyridine carboxamide contained tyrosine pseudopeptides.[220]

Due to the versatility in the structure associated with molecular self-assembly process of short peptides, several computer stimulations studies have been

performed both in all atom and coarse grained model. This computational based analysis opens a new avenue to gain insight about the mechanism and types of interactions involved during self-assembly process. Therefore, the fusion between both experimental and computational analysis of the self-assembly pattern generated by this peptides has become a new field of research interest in nanoscience.

In recent years, much attention was given to phenylalanine based self-assembly. However there were very few reports on tyrosine based self-assembled nanostructures. As a consequence of this, in order to get further insight into the nature of interaction and the self-assembly patterns of tyrosine based peptide moiety, in the present study, we, for the first time explored the molecular details of assembled structures, particularly ß-sheet induced helical structure formed by a novel di-tyrosine dipeptide. Tyrosine is an important amino acid playing significant role in living organism. It acts as a building block of proteins, a precursor of melanin and several neurotransmitters and hormones. Some tyrosine residues can participate equally in signal transduction processes in proteins and function as a receiver. Tyrosinemia is a genetic disorder characterized by disruptions in the multistep process that breaks down the amino acid- tyrosine. It falls into the category of amyloid like metabolic diseases. Alkaptonuria, a typical amyloidogenic disorder occurs due to the accumulation of metabolite tyrosine and homogentisic acid. Therefore, now a day's self-organization of tyrosine based peptides have gained significant research interest.

Inspired by this approach the present work represents here mainly focused on the dipeptide in which N-terminal was protected by tert-butoxy carbonyl (BOC) group and C-terminal protected by ester group. In addition, the side chain of each tyrosine residue was protected by benzyl group. We purposefully synthesized this O-benzyl protected tyrosine dipeptide to determine whether the substitution of tyrosine unit could alter the triggering force for molecular assembly and affect the ultimate self-assembled structure compared to that of other peptides. This novel dipeptide readily

underwent the formation of fibrillar network with ß-sheet induced helical pattern in solution. This is very rare in the literature. Consequently, Atomic force microscopy image and FE-SEM analyses have been employed to characterize the morphology of the assembled structure generated by this dipeptide in solution state. To find out the molecular forces responsible for this dipeptide assembly, NMR, Fourier transform infrared spectroscopy (FT-IR) have been performed. H/D exchange proton NMR study suggested the participation of amide hydrogens in intramolecular hydrogen bonding. This conclusion also corroborated with the result obtained from temperature dependent proton NMR analysis. In addition, Circular dichroism spectroscopy established the self-assembly phenomenon associated with this dipeptide. Moreover, the self-assembly pattern of this tyrosine based dipeptide was studied by using single-crystal-X-ray-crystallography, which provide information about inter and intra side chain non-covalent interactions. Two types of amide hydrogen bonding and π-π stacking interactions are involved to stabilize the structure. Another interesting T-shaped type of interactions is also involved in this crystal packing. If all the interactions including the ring systems can grow along C-axis, the crystal structure is stabilized through parallel ß-sheet type fashion. Most interestingly, in this peptide, C-H….π type of interaction present which can be realised from another orientation. These interactions facilitate the formation of ß-sheet induced helical structure which is quite rare in the literature present in short peptide. Thus this work may hold future promise in developing exotic nanomaterials for further improvement in this field.

4.3Results and discussion

The dipeptide was synthesized by conventional solution phase methodology. The N-terminus was protected through BOC (tert-butoxycarbonyl) group and C-terminus was protected though methyl ester. Coupling reaction was mediated using 1- ethyl-3,3-(dimethylamino) propyl carbodiimide hydrochloride (EDC.HCl) and hydroxybenzotriazole (HOBt). The molecular architecture is shown in scheme 1.

4.3.1 Synthesis of dipeptide TTP

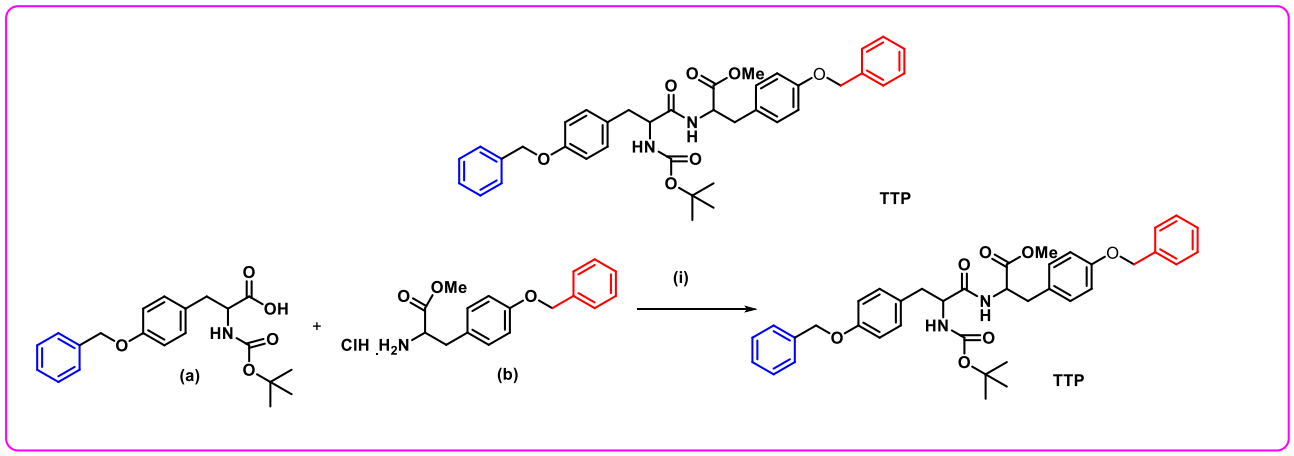

Scheme 1*. Structure and schematic presentation of the synthesis of peptide TTP.*
Substrates for the synthesis of TTP: (a) N-(tert-butoxycarbonyl)-O-benzyl-L-tyrosine (b) HCl salt of methyl ester of O-benzyl-L-tyrosine. (i) EDC.HCl, HOBt, 0^{o}C, RT,8h.

To a well-stirred solution of N-(tert-Butoxycarbonyl)-O-benzyl-L-tyrosine (a; 500 mg, 1.34 mmol) dissolved in N,N-dimethylformamide (8 mL),was added anhydrous hydroxybenzotriazole (HOBT; 218 mg, 1.6 mmol) followed by 1- ethyl-3,3-(dimethylamino) propyl carbodiimide hydrochloride (EDC•HCl; 387 mg, 2.01 mmol) under cold condition and nitrogen atmosphere. The stirring was continued for 10 min under ice-cooled condition and then triethylamine (TEA; 1 mL, 10 mmol) was added to this mixture along with methyl ester of O-benzyl-L-tyrosine (b; 518 mg, 1.6 mmol); subsequently, the reaction was further continued for 8 h at room temperature and completion of the reaction was monitored via thin-layer chromatography (TLC). The reaction mixture was then concentrated under reduced pressure, diluted with water and extracted with ethyl acetate from aqueous layer. The crude product was obtained after evaporation of the solvent and purified by column chromatography over silica gel (petroleum ether /ethyl acetate 60:40) to afford peptide "TTP" as white solid (yield = 75 %).

4.3.1 Self-assembly of the dipeptides in different solvents

AFM study

AFM images were obtained on Pico Plus 5500 AFM (Agilent Technologies, Inc., Santa Clara, CA, USA) with the piezo scanner range of 9 μm. The images (256 × 256 pixels) were captured with a scan size between 0.5 and 5 μm at the scan speed rate of 0.5 rpm. The images were processed through flattening via Pico view software (Molecular Imaging Inc., Ann Arbor, MI, USA). For this purpose, dipeptide TTP

solution incubated at room temperature for 24 h, and then the solution was applied to a mica foil, after drying the sample solution placed at mica foil, the specimen was observed through atomic force microscopy.

In the past few decades, several groups suggested that the aromatic amino acid residues present in short peptides played crucial role in generating the formation of fibrillar morphology through π-π stacking interactions. To gain further insight into the morphology of the self-assembled structures adapted by this dipeptide, Atomic Force Microscopy (AFM) and Field Emission Scanning Electron microscopy were performed in dilute solution of the dipeptide in different solvents. For this purpose, the dipeptide dissolved in ethyl acetate, dichloromethane (DCM), dimethylsulfoxide (DMSO) and DMSO-water separately, incubated for 24h, drop-casted on the mica sheet and the specimens were observed through different microscope after drying the sample. In all cases the dipeptide formed nanofibrillar assembly with twist in their self-assembled structure. First, the dipeptide dissolved in ethyl acetate and the final concentration of the peptide was 0.03 mM. Figure 1Aa showed a unique coil like morphology having no void space rather it was filled with interconnecting fibrillar network. If we take a close look on the coil structure as shown in Figure 1Ab and 1Ac, it was looking like a long fibril was spinning around to get this unique morphological

pattern. The width of the fiber was in 50-70 nm range. With increase in concentration to 0.3 mM the morphology diversified forming a chain like assembly where the coils were interconnected with fibrillar network (Figure 1Ad). Here the fiber was within 40-120 nm range. In DCM the dipeptide produced different morphological pattern, some of them were simple fibrils, and some were coils with or without void spaces represented in Figure 1Be. In this case we observed some coils were discrete and some of them were interconnected with fibrillar network. The width of the fiber varied in the range of 20-50 nm. The inner diameter of the void space of the coil was 30-110 nm. The width of the coil was 90-300 nm in range and it as formed due to the self-association of several mini fibers (Figure 1Be). At higher concentration (~ 0.3mM) as shown in figure 1BF this dipeptide again formed nanofibrillar assembly with some fibrillar clot in between. Moreover, the fibrils observed like nanofilaments. The width of the fibrils varied within the range of 30-80 nm. Then switching the solvent to DMSO (Figure 1Bg and 1Bh), slight helically twisted bent fibrils was observed of width 40-130 nm at low concentration. It was moreover looking like the root of a big tree. Highly cross linked dense fibrillar network was observed when the concentration in DMSO increased to 0.3 mM. However, in this case most of the fibrils were helical twisted fibrils as shown in Figure 1Ci and 1Cj. Therefore with increase in concentration single fibrils were connected to each other to give this dense fibrillar network. The widths of the fibers were 50-150 nm. In 1% DMSO-water mixture, helically twisted fibrils were observed of width 60-130 nm.(Figure 1Ck, 1Cl).

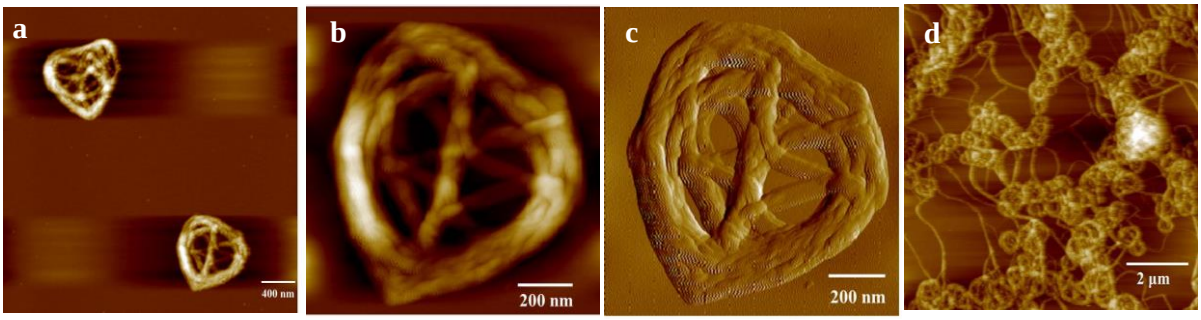

Figure 1A. *Atomic Force microscopy images of the aggregates produced from TTP in different solvents.(a) A unique fibrillar assembly obtained from TTP in ethyl acetate at 0.03 mM concentration after 24h incubation. (b) The enlarged portion of the area enclosed by white dotted line in (a). (c) The phase diagram image of (b). (d) represents the aggregates obtained from concentrated solution of TTP in ethyl acetate (0.3 mM).*

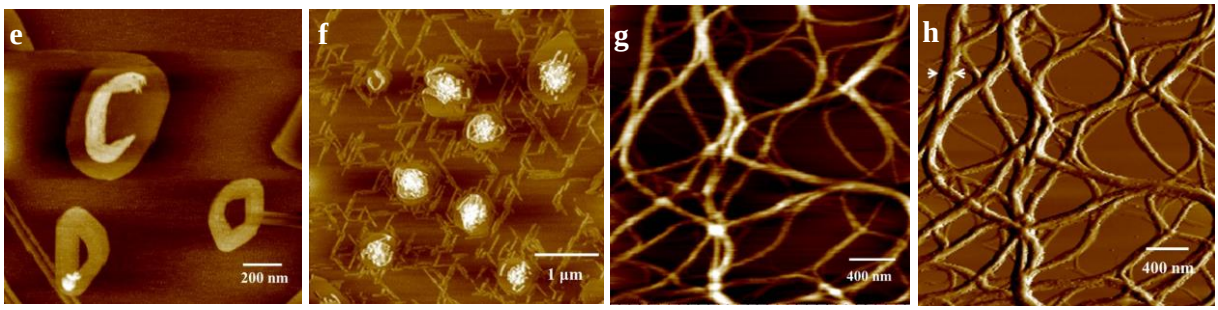

Figure 1B. *Atomic Force microscopy images of the aggregates produced from TTP in different solvents. (e) and (f) The fibrillar aggregates obtained from TTP in DCM at 0.03 and 0.3 mM concentration respectively. (g) Helically twisted along with bent fibers of width 40-130 nm obtained from TTP in DMSO at 0.03 mM concentration. (h) The phase diagram of the corresponding (g).*

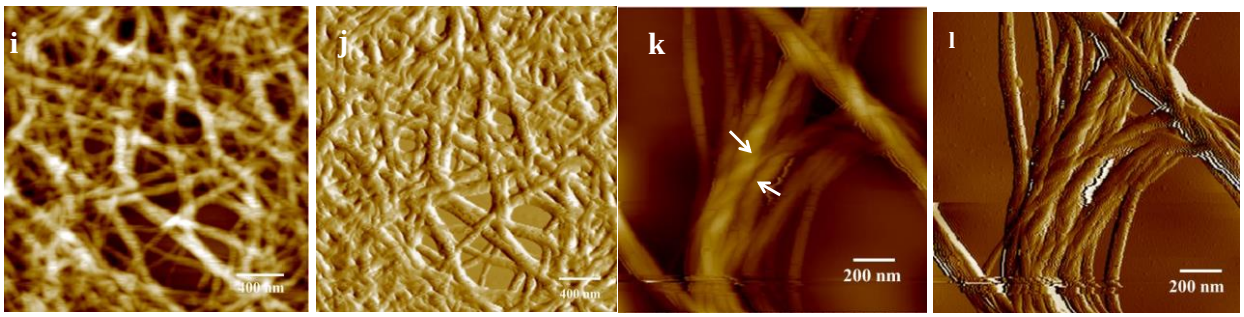

Figure 1C. *Atomic Force microscopy images of the aggregates produced from TTP in different solvents. (i) Highly cross linked fibrillar network obtained from concentrated solution of TTP in DMSO (0.3 mM) of width 50-150 nm. (j) The phase diagram image of the corresponding (i). (k) and (l) indicate helically twisted fibrillar network with width 60-130 nm obtained from TTP in 1% DMSO-water solution.*

FE-SEM Study:

Morphology of the self-assembled structure obtained from dipeptide solution in 1% DMSO-water using field emission scanning electron microscopy. For the FE-SEM study, dipeptide solution in 1% DMSO-water was dried and platinum coating was carried out. Then the micrographs were taken in an FE-SEM apparatus (ZEISS-SIGMA, Carl ZEISS Microscopy, Germany).

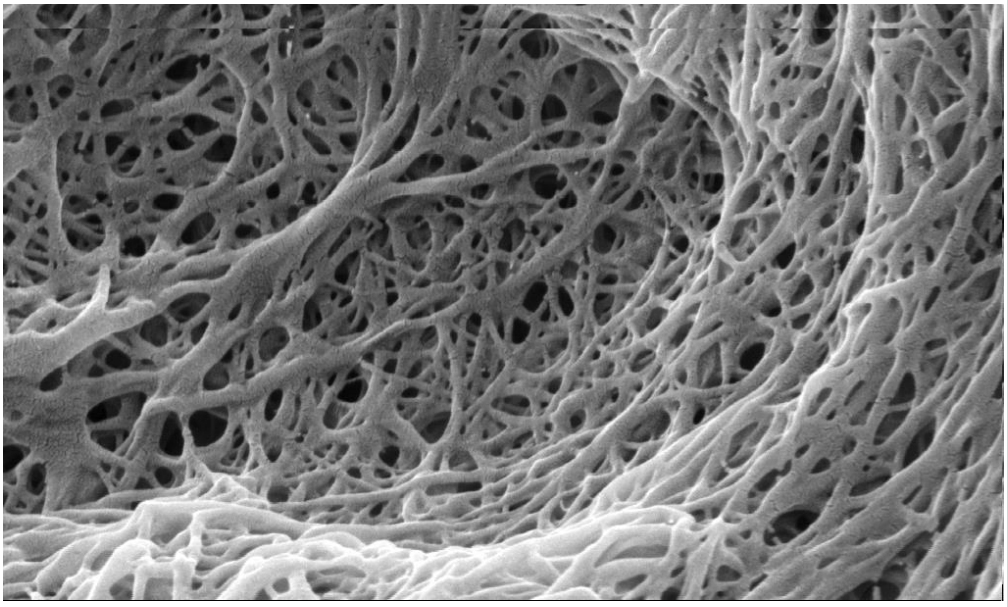

Figure 2. *FE-SEM images of the aggregates produced from TTP in 1% DMSO-water solvent after 24h incubation.*

Field - emission scanning electron microscopy (FE-SEM) experiments were carried out to understand the structure of the self-assembled aggregates produced from TTP in 1% DMSO-water solution. It was found that the dipeptide solution showed highly dense web like architechtures of numerous long nanofibers. Along with these nanofibers, some helically twisted fibers were also found. The average width of the fiber was 70-120 nm and the length was several microns, indicating porous nanostructures with high surface area. These fibers did not appear as discrete one rather each nanofibers were interconnected with other to form an inter woven network.

4.3.2 Solid state assembly of TTP

To understand the self-assembly property of TTP, single-crystal X-ray crystallography of the dipeptide can help by providing the information of inter and intra-side chain non-covalent interactions. In addition to this, the intricate structure of the peptide characterizations will also be confirmed. The crystal structure of TTP is shown in figure 3A. In the monoclinic crystal system, the molecule TTP crystallizes with $P2_1$ space group.

Two molecules of TTP (A; green and B; yellow) were present in the asymmetric unit of its crystal (Figure 3b). Here, they assembled in a parallel fashion (Figure 3b) using various supramolecular interactions. Strong intra- and intermolecular hydrogen bonding, π…π, C-H…π, and C-H…O=C interactions between A and B molecules were observed in this unit. There were two anti-parallel hydrogen bondings observed between 1) C=O5 of A and H-N2 of B (2.16 Å), and 2) H-N1 of A and C=O1 of B (2.15 Å). The C=O5 of A and the C-H beside the N2 involved in the carbon interactions. The phenyl rings the set of molecules are involved in the π…π staking interactions. The benzylic CH2 of R4 ring of B molecule show C-H…π interactions with R3 ring of A. Here, another interesting type of by T-shaped π-staking interaction was observed among the R2 and R4 set of rings of A and R2 of A and R4 of B. In this way, the flexibility of the terminal phenyl rings became somewhat restricted.

The aforesaid strong hydrogen bonding, carbon interactions, and ladder-like π…π stacking of R1 and R3 rings might have grown along the unit cell axis c to stabilize the parallel ß-sheet arrangement in this direction (Figure 3c). The terminal phenyl rings did not have continuous ladder-like π-stacking interactions as internal phenyl rings. Therefore, they might have some flexibility. Four such terminal rings construct an arrow-shape through T-shaped π stacking interactions (Figure 3d). The R2 ring of A interacts with R2 of B on one side and R4 of B on another side through intermolecular π-stacking to form an angle shape which

bisected by intramolecular pi-staking of R4 ring of A and make the arrow shape (Figure 3d).

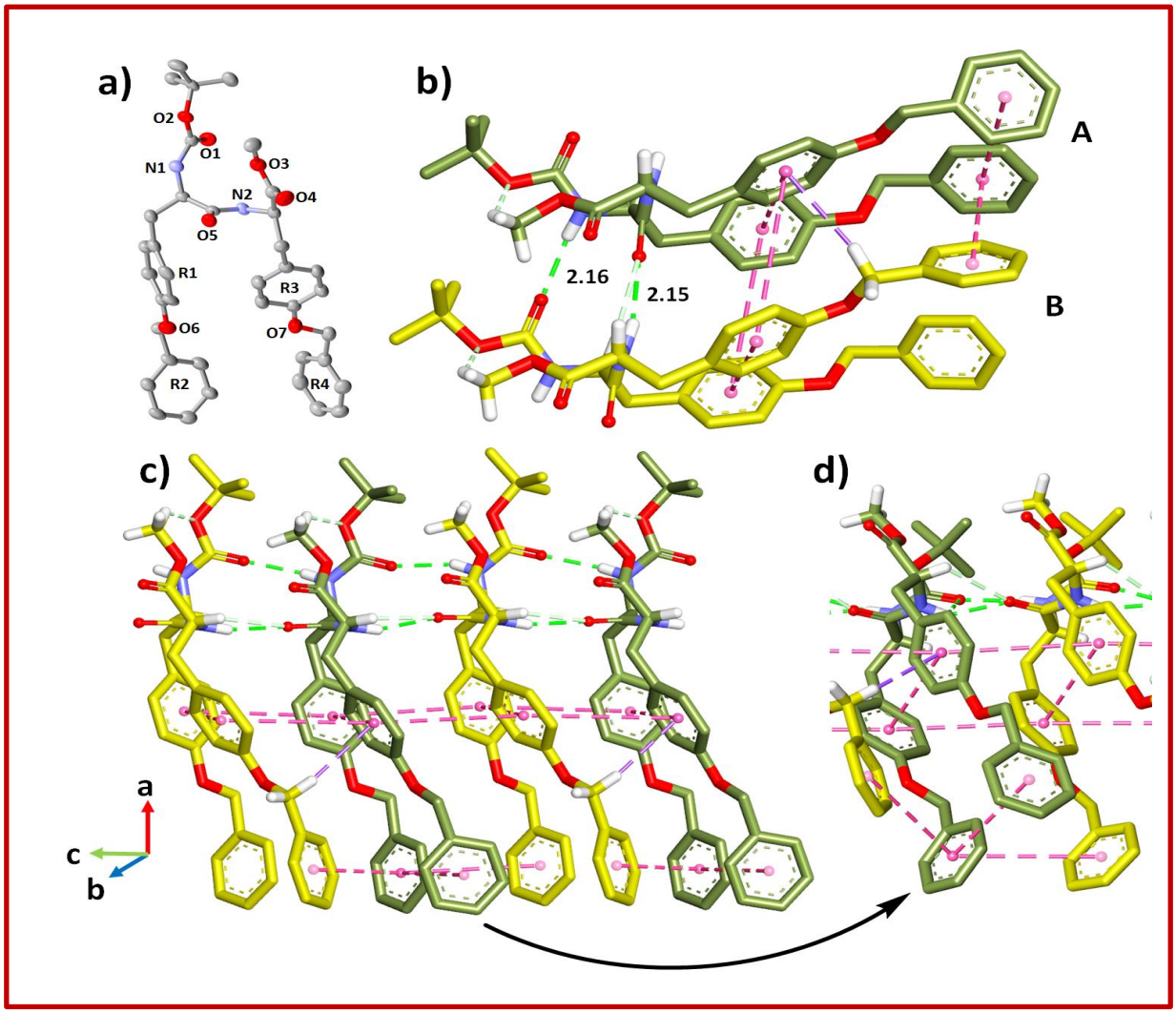

Figure 3. *(a) X-ray crystal structure of TTP (30% thermal probability of the ellipsoid). (b) Two molecules of TTP in the asymmetric unit of the crystal and non-covalent interactions involved in between them. (c) ß-sheet arrangement of the compound in solid state by with the help of various interactions (d) Zoomed picture of terminal part of ß-sheet arrangement of TTP. Most of the hydrogens are omitted for clarity.*

In the solid-state, two adjacent parallel ß-sheet units were anti-parallel which might be understood from the direction of tertiary butyl groups (Figure 4). Apart from the aforesaid π-stacking, another C-H... π interactions play a very interesting role in solid-state assembly. The C-H of the tertiary butyl group of one ß-sheet unit forms C-H…π interactions with the next anti-parallel ß-sheet unit. In this case, the slight flexibility of the terminal phenyl ring was utilized. Such inter ß-sheet units interactions along the unit cell axis b led to a helical structure formation (Figure 4). One methyl group of A molecule in one ß-sheet unit was connected with another B molecule of the nearest ß-sheet unit using C-H…π interactions and construct a helical structure (single-helix). It is interesting to note that various non-covalent interactions help to stabilize β-sheet-assembly which promote helical arrangements by C-H…π are rare in the literature.[221–224] This solid-state assembly pattern of TTP might help to understand the behaviour of this molecule during the self-assembly in solution phase.

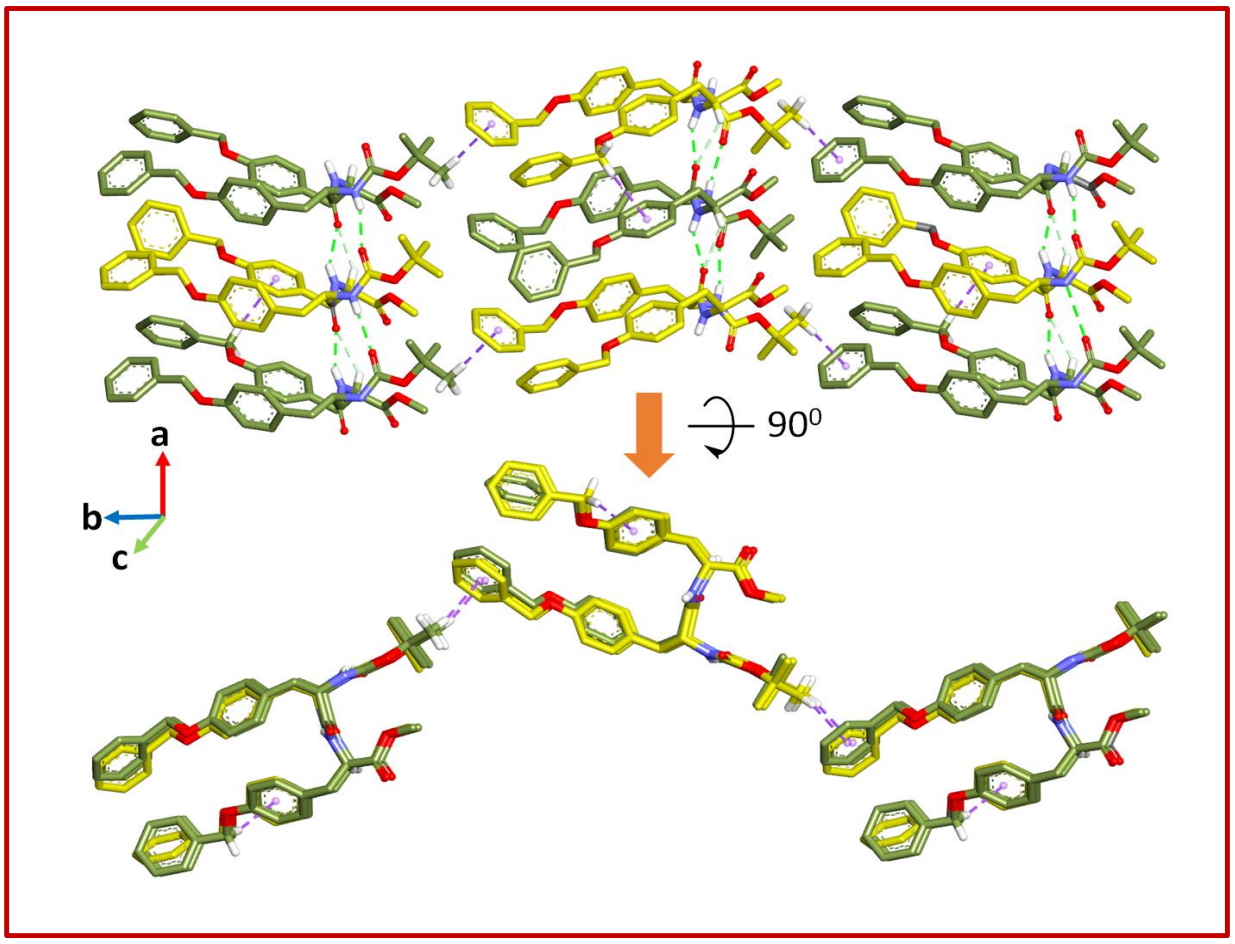

Figure 4. *β-Sheet promoted helix formation in the solid state assembly of TTP.*

4.3.3 Hirshfeld Surface Analysis of TTP

Hirshfeld Surface Analysis of TTP was performed with the help of Crystal Explorer 17.5.[225] The structure of the compound was optimized to get energy minimized structure Gaussian 09W was utilized.[186] The optimized structure of P1 was obtained by B3LYP/6-311 G level of theory in aqueous medium (CPCM model). The Frontier molecular orbital were depicted using GaussView 5.[226]

The Hirshfeld surfaces (HSs) and the 2D fingerprint of TTP were investigated to realize, in a crystalline environment, the packing modes, molecular local shape of the crystal, and the distribution of electron density of different molecular fragments in the crystal. It provides a quantitative intermolecular non-covalent interactions inside the crystal of a molecule.[227] The negative and positive

potentials are manifested by red and blue color coding, respectively. The Hirshfeld surfaces are mapped with the help of the normalized contact distance (d_{norm}) which is related to the internal and external distances, d_i and d_e, and the van der Waals radii of atoms (Figure 5a-c).

On the Hirshfeld surface, the bright red spots (on d_{norm}) indicate the respective donor and acceptor atoms for intermolecular hydrogen bonds. These are C=O5…H-N2 and C=O1…H-N1 (Figure 5a). The faint red spots are correspond to the C-H…π interactions. In the 2D fingerprint of TTP, it has been found that there are main three types of interactions to the formation of the crystal. The H…H interactions occupy the 60.0% region of the Hirshfeld surface which is highest in all types of interactions (Figure 5d and 5e). The concentration of these interactions is highest at $d_e = d_i$ ~0.9 Å. Interestingly, a faint red spot at the benzylic proton of R1 ring indicates a significant short range H…H contact. Two peaks at $d_e + d_i$ ~ 3.2 Å on this 2D fingerprint of C…H contact corresponds to the C-H…π interactions. These contacts bestow 24% of the total. Two thorn-like parts were appeared in the fingerprints in the area of $d_e + d_i$ ~2.2 Å that corresponds to the O…H hydrogen bonding. This type of interaction furnishes 15.1% of the total Hirshfeld area. These three types of interactions provide 99.1% of the total. Therefore, these interactions are most important among the atoms interacting in the crystal system. These results, hence, stipulate the importance of these interactions in the crystal packing disposition of the crystal structure. With the help of these results, a comprehensive model has been developed which helps to understand the significance of the different types of non-covalent interactions for the packing of TTP to construct a three-dimensional architecture of the molecule.

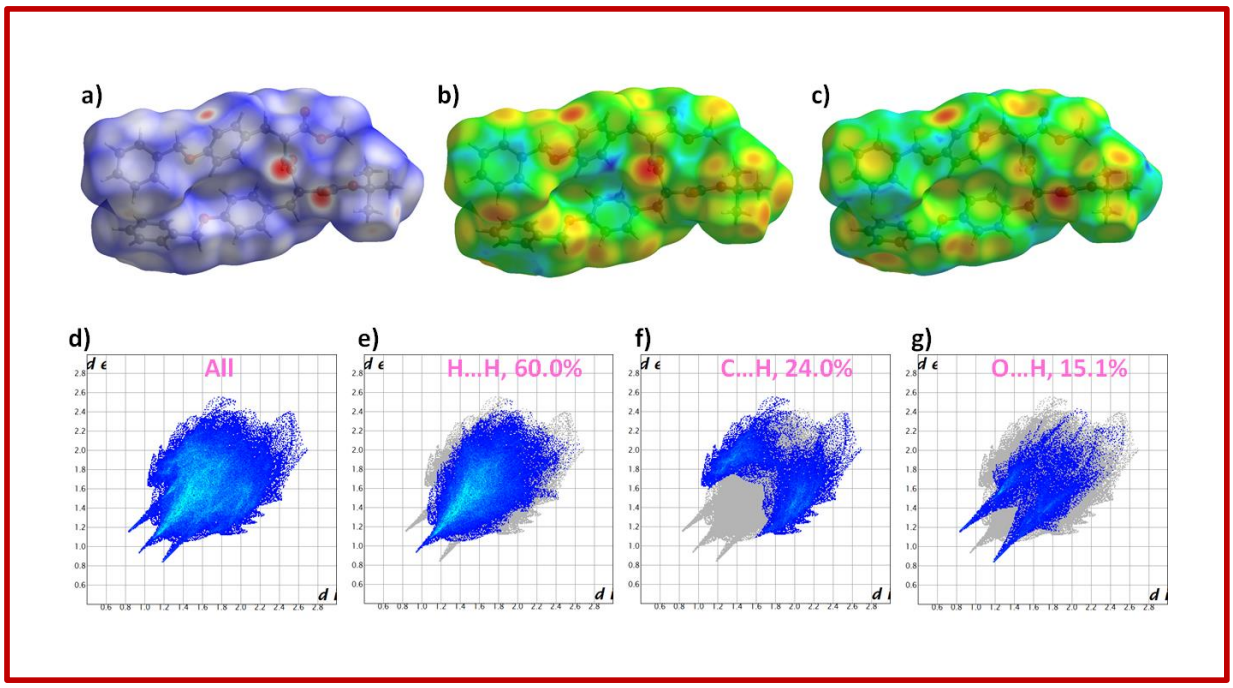

***Figure 5**. Hirshfeld surfaces of TTP on (a) d_{norm}, (b) d_e, (c) d_i, and 2D fingerprint of it showing contribution of (d) all, (e) H…H, (f) C…H, and (g) O…H interactions on the surface.*

4.3.4 NMR study

H/D exchange proton NMR analysis

Deuteratium (H/D) exchange proton NMR study the peptide TTP provided important insights about the hydrogen bonding patterns of two amide protons of their respective solution state. Figure 6 displays the proton NMR spectra of TTP in DMSO and in the presence of D_2O/DMSO (1:50 V/V) mixed solvent. In the absence of D_2O, two doublet peaks appeared around δ 8.25 and 6.79 ppm, respectively, for –NH proton of -CONH, and tert-butoxycarbonyl (BOC) group (Figure 6a). The other peaks appeared at δ 7.42-7.40 (4H), 7.38- 7.34 (4H), 7.32-7.29 (2H), and 6.91-6.88 (2H) were responsible for aromatic protons in TTP (Figure 6b). After adding D_2O to a 10 mM solution of TTP in DMSO-d_6, the intensity of the proton at δ 8.25 ppm decreased as time passed (Figure 6b, 6c and 6d). The intensity of proton signal appeared at δ 6.79 ppm decreased and slightly shifted from δ 6.79 to 6.72 ppm as shown in Figures 6b, 6c and 6d.The initial shifting of the proton in the NMR spectrum may be due to changing of the solvent condition (from pure DMSO to DMSO/D_2O mixure); In DMSO medium, the dipeptide (TTP) formed strong H-bonding with DMSO. The addition of D_2O, -NH of tert-butoxycarbonyl (BOC) group weakened and shifted towards higher shielding region. However subsequent changes in the intensity of NH protons were due to exchange of the N-H group with deuterium. Therefore, from this NMR study it can be concluded that both the N-H protons were solvent exposed and participated in intermolecular hydrogen bonding with them and with another dipeptide molecule.

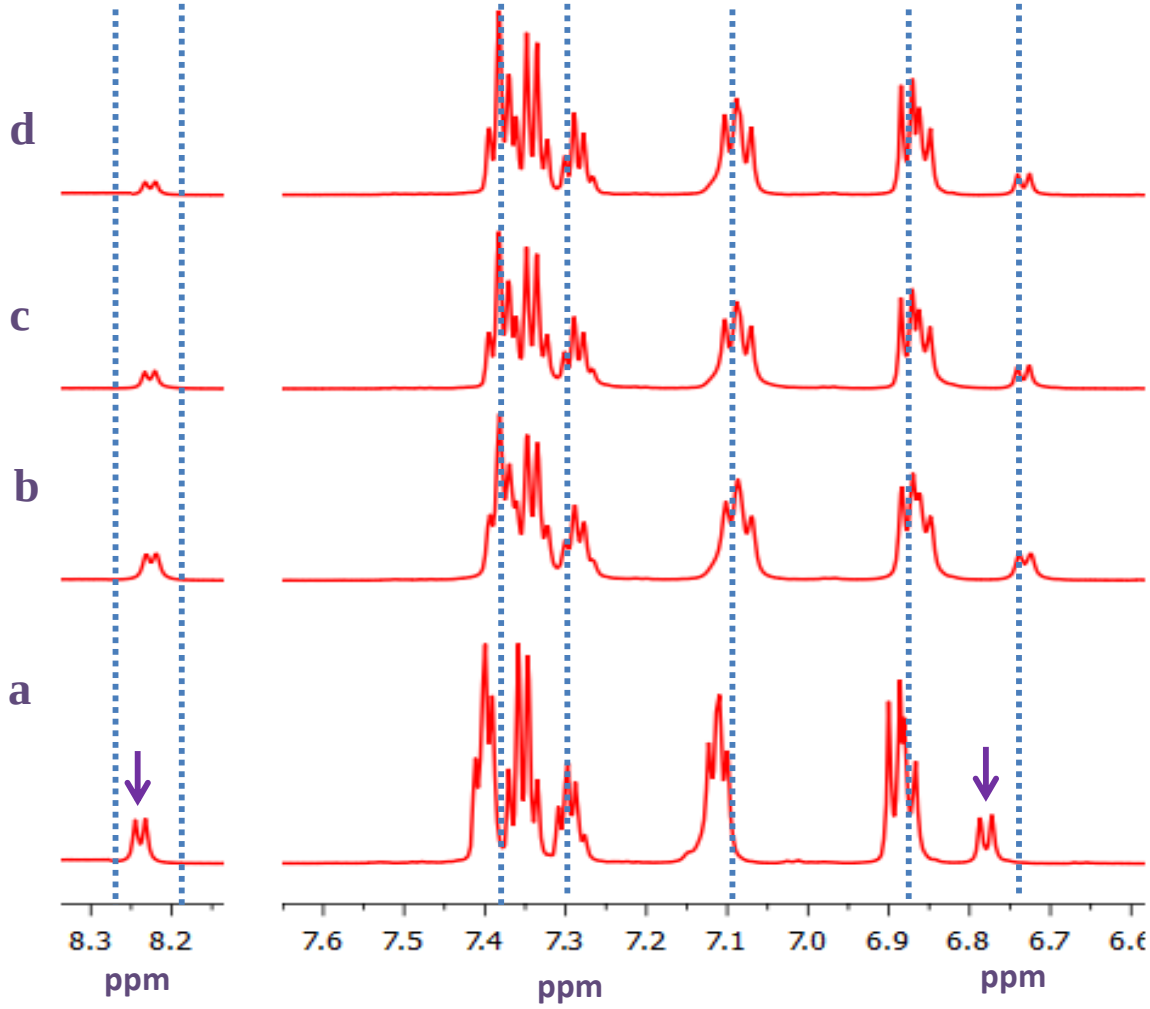

Figure 6: *H/D exchange NMR experiment on TTP (10 mM) in DMSO-d_6. (a) ^{1}H-NMR spectra of TTP in absence of D_2O in solution. Upper panels shows the perturbation of the spectra in presence of D_2O (D_2O: DMSO-d_6 = 1:50) at different point after addition of D_2O: (b) 0h, (c) 3h and (d) 6h. For presentation clarity only peak regions are shown and the bottom axis is broken. Dashed lines and arrows are to highlight the perturbation of the peak positions and intensities.*

Temperature dependent ^{1}H NMR study

Temperature dependence of peptide NH chemical shifts is widely used technique for the study of intra or inter molecular hydrogen bonded conformations of peptide in solution. For this experiment, first ^{1}H NMR spectrum of TTP was taken at 295 K/ 22 ^{0}C in DMSO (Figure 7a). Then ^{1}H NMR spectrum of TTP was taken at three different increased temperatures as shown in Figure 7b, 7c and 7d (313K/ 40 ^{o}C, 323K/ 50^{o}C and 333K/ 60^{o}C). At room temperature (295 K/ 22^{o}C) both –NH peaks for –CONH and tert-butoxycarbonyl (BOC) group appeared at δ 8.25 and 6.79 ppm respectively. The other peaks in the spectrum were appeared due to aromatic protons as mentioned earlier. With increase in temperature both –NH peaks were shielded to the upfield region. At highest temperature i.e 313K/ 60^{0}C the –NH peak of –CONH shielded to δ 8.04 ppm and –NH of tert-butoxycarbonyl (BOC) shielded to δ 6.54 ppm (Figure 7d). The shielding of the both –NH peaks to the upfield region indicated that both –NH peaks are involved in intermolecular H- bonding and there was no participation of these protons in intramolecular H- bonding. This observation was corroborated with the data obtained from H/D exchange proton NMR analysis.

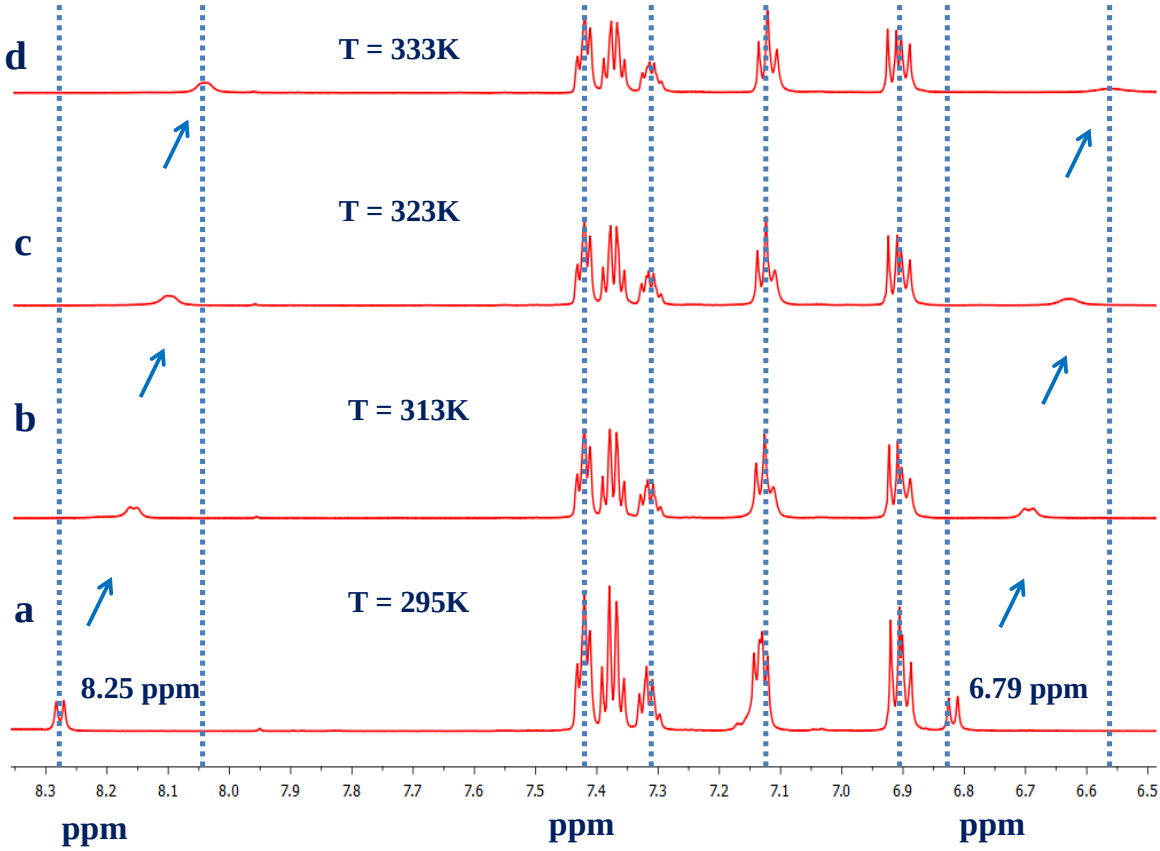

Figure 7. *Temperature dependent NMR experiment on TTP (10 mM) in DMSO-d_6. (a) ^{1}H-NMR spectra of TTP in DMSO-d_6 at temperature 295 K/ 22^{o}C. Upper panels indicate the ^{1}H-NMR spectra of TTP in DMSO-d_6 at different temperature (b) 313K/ 40^{o}C, (c) 323K/ 50^{o}C and (d) 333K/ 60^{o}C. For presentation clarity only peak regions are shown and the bottom axis is broken. Dashed lines and arrows are to highlight the perturbation of the peak positions and intensities.*

4.3.5 Circular dichroism (CD) study

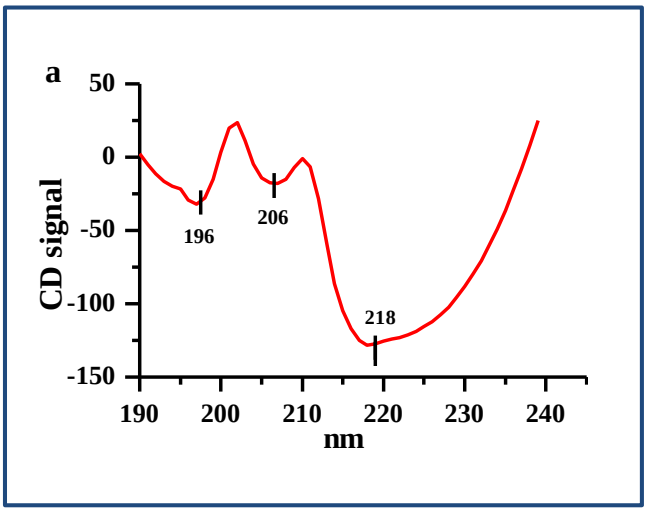

Figure 8*. (a) Circular dichroism spectra obtained from TTP at 1% DMSO-water mixture after 24h incubation.*

The CD spectrum of the tripeptide was recorded at JASCO-810 spectro polarimeter under constant nitrogen flow condition. Peptide dissolved in 1% DMSO/ water solution placed at 1 mm path length quartz cuvette was used for all the CD spectra measurements. All the CD measurements were performed at 25 ^{o}C with an accuracy of 0.1. The far-UV region was scanned between 190 to 250 nm using bandwidth of 1 nm. Each represented spectra was taken as the average of three individual scans. Experimental data obtained were analyzed using Origin Pro 8.0 SRO software (OriginLab Corporation).

Circular dichroism (CD) was performed to understand the conformations of the peptides in solution. For short peptides, the CD signal showed negative minima in between 218-230 nm which is thought to be representative of a ß-sheet conformation of the attached peptide. In this case we performed the CD analysis of the dipeptide in 1% DMSO-water solvent after 24h incubation as shown in Figure 8. The dipeptide showed broad negative band at 218 nm along with small intense

negative minima at 206 nm. This indicated the presence of both helical and ß-sheet rich conformation of the dipeptide in solution. This is due to the fact that secondary structure of such small sequences in solution might not be highly stable.

4.3.6 FT-IR analysis

The FT-IR spectra of the samples were recorded on a Bruker TENSOR27 spectrometer. The KBr disc technique was used to record the spectra of the solid sample. Solid sample was mixed with KBr in a clean glass pestle and compressed to obtain a pellet. Background spectra were obtained for KBr pellet for each sample. The spectra were scanned from 600 to 4000 cm^{-1}. Bruker software was used for data processing. Experimental data obtained were analyzed using Origin Pro 8.0 SRO software (OriginLab Corporation).

Fourier Transform Infrared (FT-IR) was used to characterize the secondary conformation of this dipeptide TTP in solid state. From solid state FT-IR spectrum, a wide range of vibrational bands were observed due to the presence of different functional groups for example -CONH, $-COOCH_3$, aromatic groups and aliphatic groups ($-CH_3$, $-CH_2$) etc. important band positions were marked in Figure 9a and the assignments of the band positions were provided in Table 1. Generally, in FT-IR spectrum, characteristic amide I, amide II and amide III bands are mainly originating from backbone vibrations appeared at 1600-1690 cm^{-1}, 1480-1580 cm^{-1} and 1230-1300 cm^{-1} respectively. The origin of amide I mode of vibration is due to CO stretching vibration and the amide II and amide III bands correspond to the coupling of C-N stretching and N-H in plane bending. For this dipeptide, the characteristic vibration bands appeared at 3326, 2927, 1743, 1685, 1656, 1517, 1447, 1375, 1296, 1240, 1170, 1015, 864 and 701 cm^{-1} respectively. TTP showed stretching of amide I mode of vibration at 1656 and 1685 cm^{-1}. The amide I band arises mainly due to the amide C=O stretching vibration, but there are some minor contributions come from out of phase C-N stretching motion, C-C-N deformation and N-H in plane bending motion also. The ester carbonyl stretching frequency

observed at 1743 cm^{-1}. The characteristic vibration bands at 1517, 1240 and 1296 cm^{-1} appeared due to amide II and amide III mode of vibration. There are many reports where it was mentioned that peptides having inclination towards ß-sheet conformation, give two characteristic bands between 1645-1656 cm^{-1} and the other one is between 1680-1700 cm-1 in the FT-IR region. In our case, the characteristic amide I band appeared at 1656 and 1685 cm^{-1} indicated the formation of ß-sheet through intermolecular hydrogen bonding. No bond was observed at 3400 cm^{-1} suggesting that all the –NH s were involved in intermolecular hydrogen bonding. All the characteristic peaks confirmed that the dipeptide existed ß-sheet like conformation in solid state.

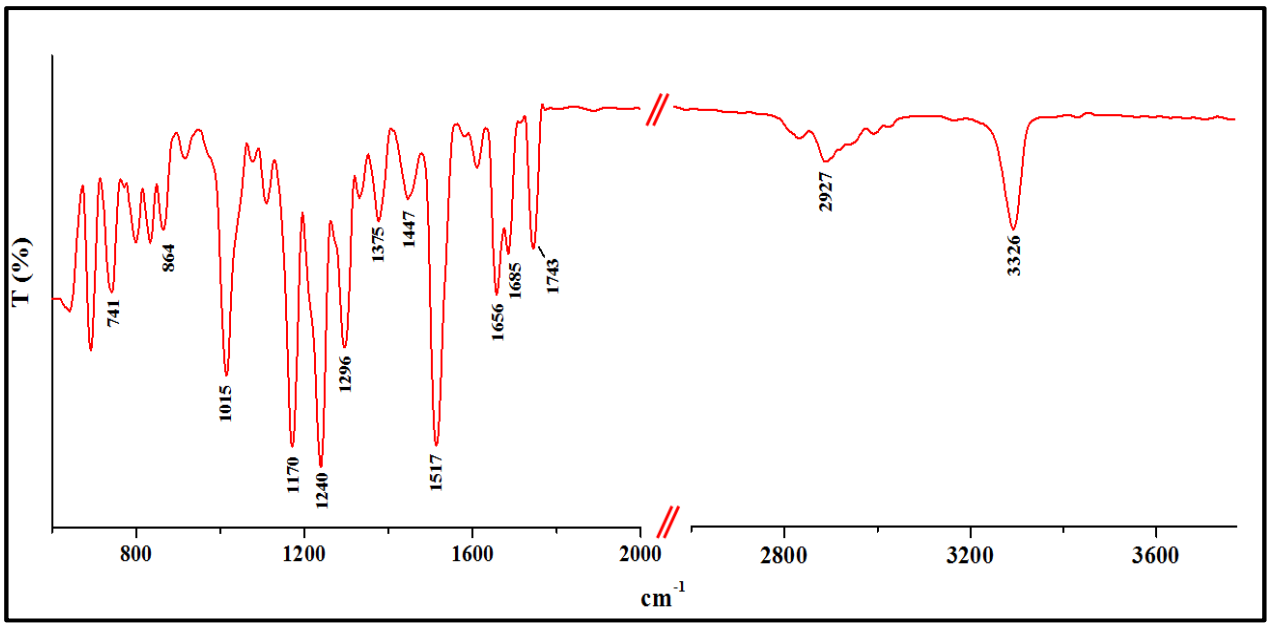

Figure 9: *(a) Fourier transform infrared (FT-IR) spectra of TTP in solid state*

Table 1: Assignment of the FT-IR bands of the dipeptide (TTP) at solid state

IR frequency (cm^{-1})	Vibration assignment	IR frequency (cm^{-1})	Vibration assignment
3326	Amide N-H symmetric stretching.	1375	CH_3 tertiary group symmetric bending.
2927	CH_2 antisymmetric stretching	1296	Amide III (N-H bend in plane and C-N stretch)
1743	C=O stretching of the ester	1240	Amide III (N-H bend in plane and C-N stretch)
1685	Amide I (amide C=O stretching)	1170	Ester C-O asymmetric stretch
1656	Amide I (amide C=O stretching)	1015	
1517	Amide II	864	
1447	CH_2 bending	741	Out of plane N-H bending

4.3.7 Thioflavin T (ThT) fluorescence assay

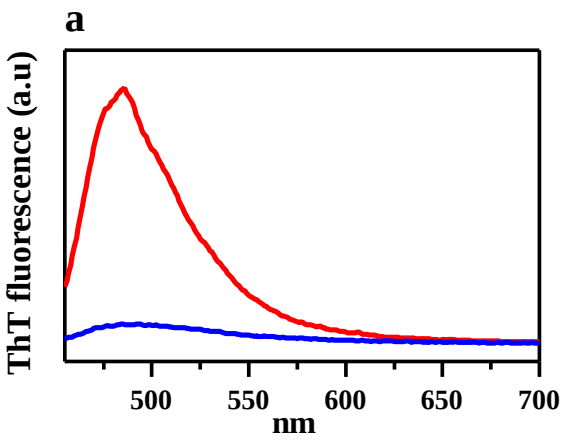

Figure 10. *(a) ThT fluorescence spectra spectrum in the absence and presence of peptides (~50 μM) in 1% DMSO-water solvent incubated for 24h at 25°C: blue trace, without any peptide; red trace, in the presence TTP.*

The self-assembly formation by TTP was examined by ThT fluorescence assay measurements. The peptide solution was prepared by dissolving the solid peptide in DMSO and incubated for 24h at ambient temperature. Experimental data are recorded on Cary Eclipse fluorescence Spectrophotometer of Agilent technology in a quartz cuvette of 1 cm path length. The excitation and emission slit widths were fixed at 5 nm each. A stock solution of (~50 μM) ThT was prepared in water. Before spectral measurement, a certain volume of peptide was added to 1 mL of ThT solution so that the final concentration of the peptide was~ 50 μM. The fluorescence emission spectra were recorded within the range 455-600 nm (excitation ~445 nm).

Thioflavin T (ThT) fluorescence study was used to measure the nature of the secondary structure present in peptide/ protein sample in solution. Mainly, ThT is a benzothiazole which emits a strong fluorescence signal upon binding to the cradle of β-sheet structures often found in fibrillary network produced from proteins/peptide. The more ThT fluorescence signal/intensity in presence of protein sample suggests higher amount of fibrils with ß- sheet conformation.

Figure 10a represented the ThT fluorescence spectra in presence of TTP (solution in 1% DMSO-water). It was observed that ThT fluorescence intensity was significantly higher in presence of TTP indicating the presence of fibrillary network with ß sheet conformation.

4.3.8 DFT-Study

DFT study of small organic molecules provides important insights into chemical reactivity and their related biological activities.[228,229] The Frontier molecular orbital of the dimeric form of TTP was calculated from its energy minimized structure. The hydrogen-bonded dimeric structure of TTP was optimized at the B3LYP/6-311 G level of theory. The electronic distribution and the energy of the HOMO and LUMO of TTP are shown in Figure 11a. The high HOMO and low LUMO energy of the molecule facilitate the non-covalent interactions through donation and acceptance of electrons, respectively. In the case of this molecule, the energy gap is very low (3.74 eV) which can facilitate its intermolecular interactions and chemical reactions. The electron density of HOMO orbitals is concentrated on R1 ring whereas in case of LUMO it is on the R2 and R4 rings.

Overlying the optimized (magenta) and crystal (green) structures of TTP (Figure 11b and 11c) can give an insight of structural features for self-aggregation. In the DFT optimized structure of TTP, the angles of intermolecular hydrogen bonds of amides, (**A**) C=O5…H-N2 (B) and (A) N1-H…O1=C (B) has appeared at 178.06^{o} and 164.01^{o}, respectively, where it was 147.13^{o} and 162.83^{o} in the crystal structure, respectively. The bond distance of these two hydrogen bonds is 1.824 and 1.871 Å in energy minimized structure whereas 2.100 and 2.154 Å in the crystal structure, respectively. Therefore, this improvement of bond distance and angle empowers the strength of these bonds in the experimental conditions. The R2 and R4 rings of molecules A and B of TTP have changed dihedral angles in optimized structure. It is to be noted that there is no huge abrupt change of TTP in

the X-ray and DFT optimized structure. Therefore, such structural change in energy minimized form of the compound may stabilize the ß-sheet-assembly and ß-sheet promote single strand helical arrangements of TTP as observed in solid-state, CD, and AFM experiments.

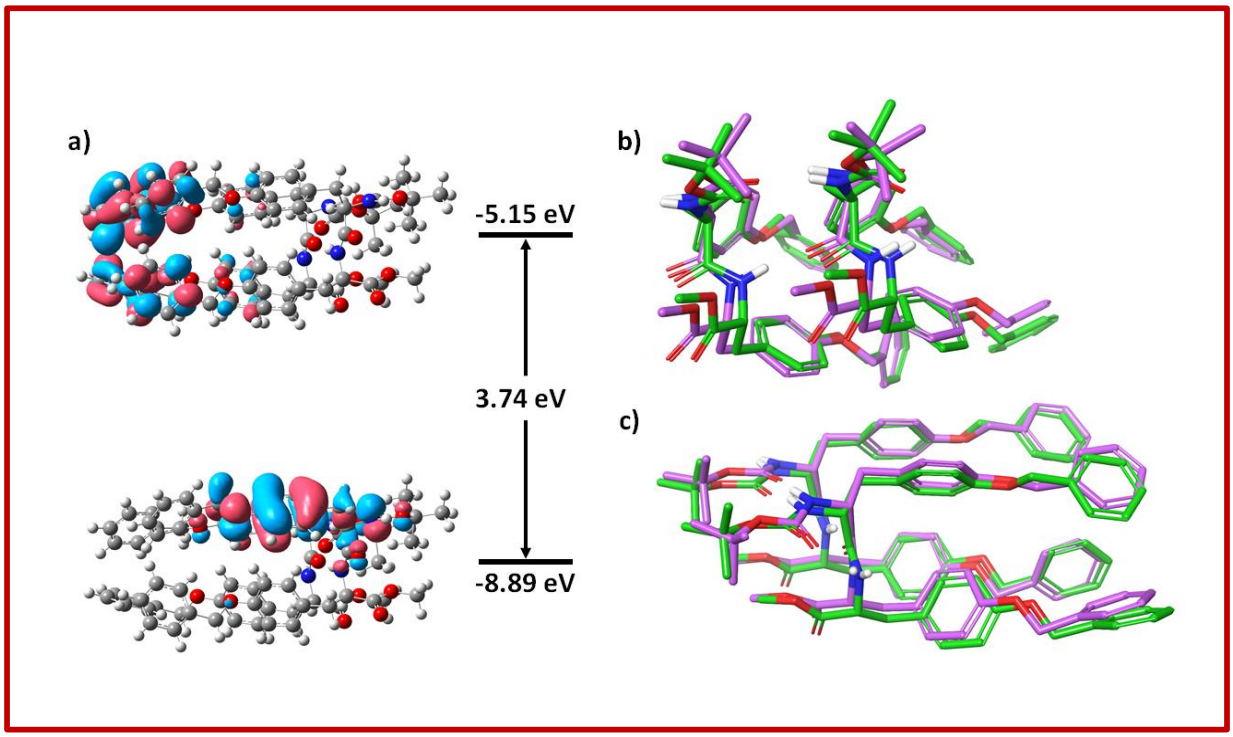

Figure 11. (a) HOMO, LUMO and their energy of TTP. Overly of X-ray (green) and DFT optimized (magenta) structure of the TTP at (b) peptide region and (c) total molecule.

4.4 Conclusion

In conclusion, we established the conformation and morphology of side chain protected tyrosine based peptide moiety. The solid state crystallographic analysis suggested thatTTP exhibited parallel ß-sheet structure in the crystalline state but it again self-assembled to form ß-sheet promoted helical architectures which is very rare in the literature. Both the structures were stabilized through several supramolecular interactions such as- intermolecular hydrogen bonding, π-π, C-H….π and C-H….O interactions. This C-H….π interaction is the main driving factor for the generation of ß-sheet promoted helical architectures. This peptide showed unique self-assembled fibrillar morphology under different solvent conditions which was confirmed through AFM anslysis. There was no intramolecular hydrogen bonding involved as suggested by H/D exchange proton NMR study and temperature dependent proton NMR measurement. Solid state FT-IR spectra and Thioflavin (ThT) fluorescence test helped to establish the presence of ß-sheet structure in their conformation. TTP exhibited both helix and ß-sheet like structure in solution state (1% DMSO-water) confirmed through CD-analysis. HIrshfeld surface analysis and DFT study help to visualize the types of interactions involved to stabilize the energy minimized structure of the molecule. The result from DFT study also corroborated with the result obtained from solid state X-ray, AFM and CD analyses. Thus the overall study on side chain protected tyrosine dipeptide gave a glimpse of different secondary structures adopted by small peptides. The improvisation of tuning factors like protecting the hydroxyl (-OH) group of tyrosine by benzylic group help to adopt ß-sheet structure and ß-sheet promoted helical architectures which is rare in the literature. Moreover, biocompatibility of peptide self-assembled nanoarchitechtures makes them valuable for applications as biosensors and in tissue engineering..

4.5 Supporting information

4.5.1 Characterization of the dipeptides:

i) ^{1}H and ^{13}C NMR spectroscopy of methyl 3-(4-(benzyloxy)phenyl)-2-(3-(4-(benzyloxy)phenyl)-2-((tert-butoxycarbonyl)amino)propanamido)propanoate (TT P):

^{1}H NMR (600 MHz, DMSO-d_6): δ (in ppm) 8.24 (1H, d, *J*= 6Hz, NH of amide), 7.42-7.40 (4H, m), 7.38-7.34 (4H, m), 7.32-7.29 (2H, m), 7.13-7.11 (4H, m,), 6.91-6.88 (4H, m), 6.79 (1H, d, *J*= 6Hz, NH of amide), 5.04 (4H, s), 4.45-4.41 (1H, m), 4.12-4.08 (1H, m), 3.56 (3H, s), 2.97-2.94 (1H, m), 2.90-2.86 (1H, m), 2.82-2.80 (1H, m), 2.62-2.58 (1H, m), 1.28 (9H, s).

^{13}C NMR (150 MHz, DMSO-d_6): δ (in ppm) 172.29, 157.55, 155.53, 137.66, 130.61, 128.82, 128.19, 128.03, 114.99, 114.72, 78.42, 69.54, 56.16, 54.14, 52.23, 28.55.

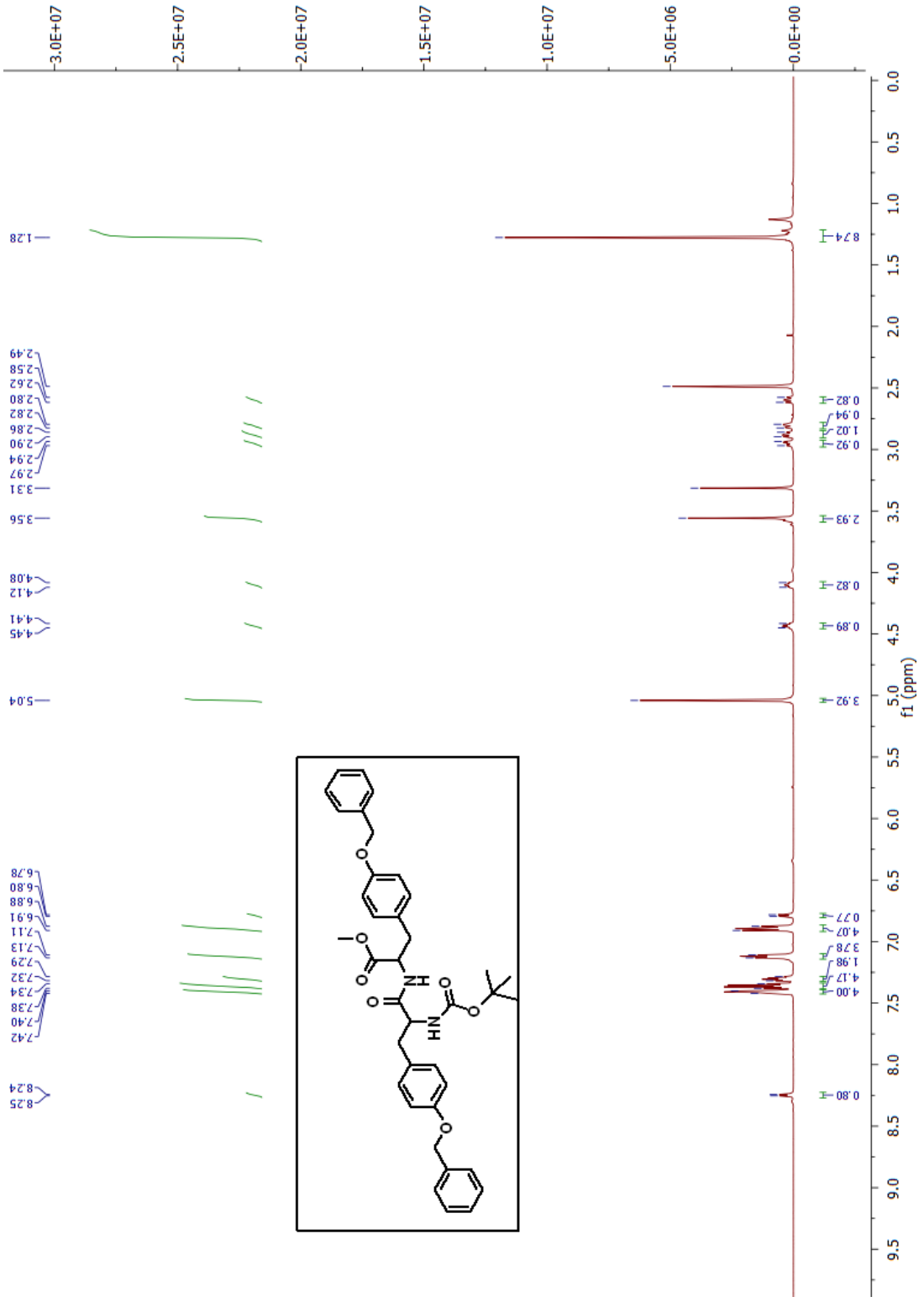

Figure 12. ^{1}H-NMR spectra of dipeptide TTP in DMSO-d_6.

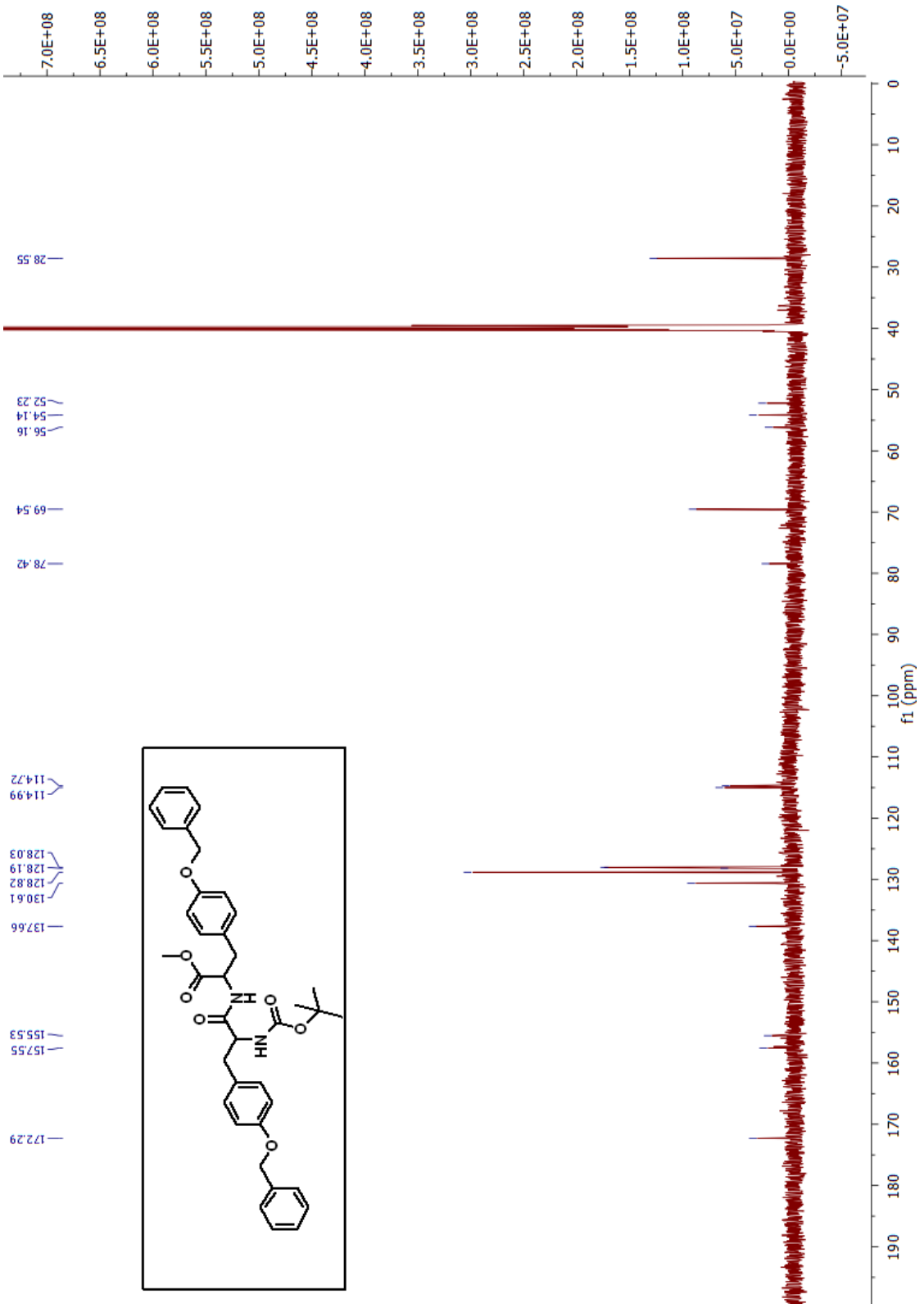

Figure 13. ^{13}C-NMR spectra of dipeptide TTP in DMSO-d_6

4.5.2. X-ray crystallographic information of dipeptide TTP:

Single crystal of dipeptide TTP was obtained through slow evaporation (at room temperature) of a solution in dichloromethane-petroleum ether. A single crystal of TTP was attached to a glass fiber with epoxy glue and transferred to an X-ray diffractometer, equipped with a graphite monochromator. Diffraction data of TTP with MoKα radiation (λ = 0.71073 Å) at 293 K. The structure was solved by direct methods using the SHELXS-97 program.[230] Refinements were carried out with a full matrix least squares method against *F*2 using SHELXL-97.[231] The non-hydrogen atoms were refined with anisotropic thermal parameters. The hydrogen atoms were included in geometric positions and given thermal parameters equivalent to 1.2 times those of the atom to which they were attached. Important crystal data of dipeptide TTP is given below.

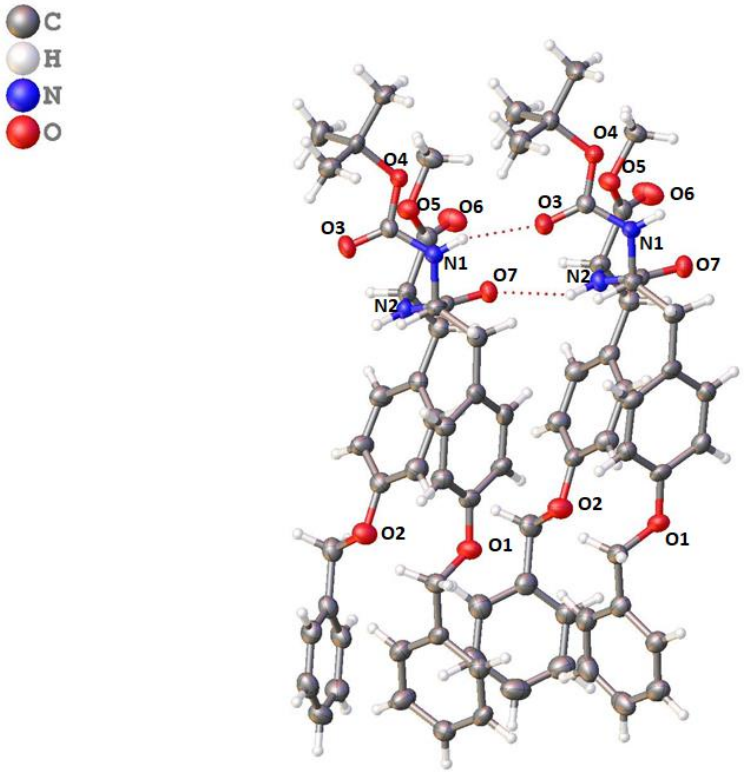

Figure 14. ORTEP diagram of peptide TTP

Table 1: Important crystal data of TTP	
Emperical Formula	$C_{38}H_{42}N_2O_7$
Formula weight	638.30
Temperature/K	120
Wave length	1.54178
Crystal system	Monoclinic
Space group	$P2_1$
Unit cell dimension	a = 9.7532(7)Å α = 90 b =33.475 (2)Å ß= 92.569(4) c = 10.2136 (7)Å γ = 90
Volume	3331.3(4) $Å^3$
Z	4
Density (calculated)	1.274 g/cm^3
Absorption coefficient (Mu)	0.711mm^{-1}
F(000)	1360.0
Theta range for data collection	4.333 to 67.096
Index ranges	$-11 \leq h \leq 11$, $-39 \leq k \leq 39$, $-10 \leq l \leq 12$
Reflection collected	11928
Completeness to theta	0.999
Absorption correction	multi-scan
Max. and Min. Transmission	0.986 and 0.975
Refinement method	Full-matrix least-squares on F2
Data/restraints/parameters	11752/1/856
Good of fit on (F^2)	1.099
Final R indices [I>=2σ (I)]	$R_1 = 0.0631$, $wR_2 = 0.1321$
R indices (all data)	$R_1 = 0.0691$, $wR_2 = 0.1356$
Largest diff. Peak and hole	0.230/-0.251e $^{-3}$ Å

References:

(1) Barber, D. J.; Freestone, I. C. An Investigation of the Origin of the Colour of the Lycurgus Cup by Analytical Transmission Electron Microscopy. *Archaeometry* **1990**, *32* (1), 33–45. https://doi.org/10.1111/j.1475-4754.1990.tb01079.x.

(2) Freestone, I.; Meeks, N.; Sax, M.; Higgitt, C. The Lycurgus Cup — A Roman Nanotechnology. *Gold Bull* **2007**, *40* (4), 270–277. https://doi.org/10.1007/BF03215599.

(3) Wagner, F. E.; Haslbeck, S.; Stievano, L.; Calogero, S.; Pankhurst, Q. A.; Martinek, K.-P. Before Striking Gold in Gold-Ruby Glass. *Nature* **2000**, *407* (6805), 691–692. https://doi.org/10.1038/35037661.

(4) Pradell, T.; Climent-Font, A.; Molera, J.; Zucchiatti, A.; Ynsa, M. D.; Roura, P.; Crespo, D. Metallic and Nonmetallic Shine in Luster: An Elastic Ion Backscattering Study. *Journal of Applied Physics* **2007**, *101* (10), 103518. https://doi.org/10.1063/1.2734944.

(5) Introduction to Nanotechnology | Wiley https://www.wiley.com/en-us/Introduction+to+Nanotechnology-p-9780471079354 (accessed 2021 -07 -26).

(6) Reibold, M.; Paufler, P.; Levin, A. A.; Kochmann, W.; Pätzke, N.; Meyer, D. C. Carbon Nanotubes in an Ancient Damascus Sabre. *Nature* **2006**, *444* (7117), 286–286. https://doi.org/10.1038/444286a.

(7) Faraday, M. X. The Bakerian Lecture. —Experimental Relations of Gold (and Other Metals) to Light. *Philosophical Transactions of the Royal Society of London* **1857**, *147*, 145–181. https://doi.org/10.1098/rstl.1857.0011.

(8) Feynman, R. P. There's Plenty of Room at the Bottom. *Engineering and Science* **1960**, *23* (5), 22–36.

(9) TANIGUCHI, N. On the Basic Concept of Nanotechnology. *Proceeding of the ICPE* **1974**.

(10) Mansoori, G. A.; Soelaiman, T. F. Nanotechnology — An Introduction for the Standards Community. *JAI* **2005**, *2* (6), 1–22. https://doi.org/10.1520/JAI13110.

(11) Lehn, J. M. Supramolecular Chemistry. *Science* **1993**, *260* (5115), 1762–1763. https://doi.org/10.1126/science.8511582.

(12) Iqbal, P.; Preece, J. A.; Mendes, P. M. Nanotechnology: The "Top-Down" and "Bottom-Up" Approaches. In *Supramolecular Chemistry*; American Cancer Society, 2012. https://doi.org/10.1002/9780470661345.smc195.

(13) Zhu, S.; Oberdörster, E.; Haasch, M. L. Toxicity of an Engineered Nanoparticle (Fullerene, C60) in Two Aquatic Species, Daphnia and Fathead Minnow. *Mar Environ Res* **2006**, *62 Suppl*, S5-9. https://doi.org/10.1016/j.marenvres.2006.04.059.

(14) Warheit, D. B.; Laurence, B. R.; Reed, K. L.; Roach, D. H.; Reynolds, G. a. M.; Webb, T. R. Comparative Pulmonary Toxicity Assessment of Single-Wall Carbon Nanotubes in Rats. *Toxicol Sci* **2004**, *77* (1), 117–125. https://doi.org/10.1093/toxsci/kfg228.

(15) Decandio, C. C.; Silva, E. R.; Hamley, I. W.; Castelletto, V.; Liberato, M. S.; Oliveira, V. X.; Oliveira, C. L. P.; Alves, W. A. Self-Assembly of a Designed Alternating Arginine/Phenylalanine Oligopeptide. *Langmuir* **2015**, *31* (15), 4513–4523. https://doi.org/10.1021/acs.langmuir.5b00253.

(16) Adler-Abramovich, L.; Gazit, E. The Physical Properties of Supramolecular Peptide Assemblies: From Building Block Association to Technological Applications. *Chem. Soc. Rev.* **2014**, *43* (20), 6881–6893. https://doi.org/10.1039/C4CS00164H.

(17) Singh, N.; P. Conte, M.; V. Ulijn, R.; F. Miravet, J.; Escuder, B. Insight into the Esterase like Activity Demonstrated by an Imidazole Appended Self-Assembling Hydrogelator. *Chemical Communications* **2015**, *51* (67), 13213–13216. https://doi.org/10.1039/C5CC04281J.

(18) Ghobril, C.; Charoen, K.; Rodriguez, E. K.; Nazarian, A.; Grinstaff, M. W. A Dendritic Thioester Hydrogel Based on Thiol–Thioester Exchange as a Dissolvable Sealant System for Wound Closure. *Angewandte Chemie International Edition* **2013**, *52* (52), 14070–14074. https://doi.org/10.1002/anie.201308007.

(19) Basu, K.; Baral, A.; Basak, S.; Dehsorkhi, A.; Nanda, J.; Bhunia, D.; Ghosh, S.; Castelletto, V.; W. Hamley, I.; Banerjee, A. Peptide Based Hydrogels for Cancer Drug Release: Modulation of Stiffness, Drug Release and Proteolytic Stability of Hydrogels by Incorporating d -Amino Acid Residue(s). *Chemical Communications* **2016**, *52* (28), 5045–5048. https://doi.org/10.1039/C6CC01744D.

(20) Bowerman, C. J.; Nilsson, B. L. Review Self-Assembly of Amphipathic β-Sheet Peptides: Insights and Applications. *Peptide Science* **2012**, *98* (3), 169–184. https://doi.org/10.1002/bip.22058.

(21) Baral, A.; Roy, S.; Dehsorkhi, A.; Hamley, I. W.; Mohapatra, S.; Ghosh, S.; Banerjee, A. Assembly of an Injectable Noncytotoxic Peptide-Based Hydrogelator for Sustained Release of Drugs. *Langmuir* **2014**, *30* (3), 929–936. https://doi.org/10.1021/la4043638.

(22) Altunbas, A.; Lee, S. J.; Rajasekaran, S. A.; Schneider, J. P.; Pochan, D. J. Encapsulation of Curcumin in Self-Assembling Peptide Hydrogels as Injectable Drug Delivery Vehicles. *Biomaterials* **2011**, *32* (25), 5906–5914. https://doi.org/10.1016/j.biomaterials.2011.04.069.

(23) Singh, M.; Kundu, S.; M, A. R.; Sreekanth, V.; Motiani, R. K.; Sengupta, S.; Srivastava, A.; Bajaj, A. Injectable Small Molecule Hydrogel as a Potential Nanocarrier for Localized and Sustained in Vivo Delivery of Doxorubicin. *Nanoscale* **2014**, *6* (21), 12849–12855. https://doi.org/10.1039/C4NR04064C.

(24) Kim, S. H.; Kaplan, J. A.; Sun, Y.; Shieh, A.; Sun, H.-L.; Croce, C. M.; Grinstaff, M. W.; Parquette, J. R. The Self-Assembly of Anticancer Camptothecin–Dipeptide Nanotubes: A Minimalistic and High Drug Loading Approach to Increased Efficacy. *Chemistry – A European Journal* **2015**, *21* (1), 101–105. https://doi.org/10.1002/chem.201404520.
(25) Zhou, M.; Smith, A. M.; Das, A. K.; Hodson, N. W.; Collins, R. F.; Ulijn, R. V.; Gough, J. E. Self-Assembled Peptide-Based Hydrogels as Scaffolds for Anchorage-Dependent Cells. *Biomaterials* **2009**, *30* (13), 2523–2530. https://doi.org/10.1016/j.biomaterials.2009.01.010.
(26) Marchesan, S.; Vargiu, A. V.; Styan, K. E. The Phe-Phe Motif for Peptide Self-Assembly in Nanomedicine. *Molecules* **2015**, *20* (11), 19775–19788. https://doi.org/10.3390/molecules201119658.
(27) Dehsorkhi, A.; M. Gouveia, R.; M. Smith, A.; W. Hamley, I.; Castelletto, V.; J. Connon, C.; Reza, M.; Ruokolainen, J. Self-Assembly of a Dual Functional Bioactive Peptide Amphiphile Incorporating Both Matrix Metalloprotease Substrate and Cell Adhesion Motifs. *Soft Matter* **2015**, *11* (16), 3115–3124. https://doi.org/10.1039/C5SM00459D.
(28) Lee, K. Y.; Mooney, D. J. Hydrogels for Tissue Engineering. *Chem. Rev.* **2001**, *101* (7), 1869–1880. https://doi.org/10.1021/cr000108x.
(29) Bhattacharya, S.; Krishnan-Ghosh, Y. First Report of Phase Selective Gelation of Oil from Oil/Water Mixtures. Possible Implications toward Containing Oil Spills. *Chem. Commun.* **2001**, No. 2, 185–186. https://doi.org/10.1039/B007848O.
(30) Whitesides, G. M.; Boncheva, M. Beyond Molecules: Self-Assembly of Mesoscopic and Macroscopic Components. *PNAS* **2002**, *99* (8), 4769–4774. https://doi.org/10.1073/pnas.082065899.
(31) Aizenberg, J.; Fratzl, P. Biological and Biomimetic Materials. *Advanced Materials* **2009**, *21* (4), 387–388. https://doi.org/10.1002/adma.200803699.
(32) Sanchez, C.; Arribart, H.; Giraud Guille, M. M. Biomimetism and Bioinspiration as Tools for the Design of Innovative Materials and Systems. *Nature Mater* **2005**, *4* (4), 277–288. https://doi.org/10.1038/nmat1339.
(33) Palmer, L. C.; Newcomb, C. J.; Kaltz, S. R.; Spoerke, E. D.; Stupp, S. I. Biomimetic Systems for Hydroxyapatite Mineralization Inspired By Bone and Enamel. *Chem. Rev.* **2008**, *108* (11), 4754–4783. https://doi.org/10.1021/cr8004422.
(34) Ariga, K.; Hill, J. P.; Lee, M. V.; Vinu, A.; Charvet, R.; Acharya, S. Challenges and Breakthroughs in Recent Research on Self-Assembly. *Science and Technology of Advanced Materials* **2008**, *9* (1), 014109. https://doi.org/10.1088/1468-6996/9/1/014109.
(35) Nie, Z.; Kumacheva, E. Patterning Surfaces with Functional Polymers. *Nature Mater* **2008**, *7* (4), 277–290. https://doi.org/10.1038/nmat2109.

(36) Ajayaghosh, A.; K. Praveen, V.; Vijayakumar, C. Organogels as Scaffolds for Excitation Energy Transfer and Light Harvesting. *Chemical Society Reviews* **2008**, *37* (1), 109–122. https://doi.org/10.1039/B704456A.
(37) He, Q.; Duan, L.; Qi, W.; Wang, K.; Cui, Y.; Yan, X.; Li, J. Microcapsules Containing a Biomolecular Motor for ATP Biosynthesis. *Advanced Materials* **2008**, *20* (15), 2933–2937. https://doi.org/10.1002/adma.200800622.
(38) Whitesides, G. M.; Mathias, J. P.; Seto, C. T. Molecular Self-Assembly and Nanochemistry: A Chemical Strategy for the Synthesis of Nanostructures. *Science* **1991**, *254* (5036), 1312–1319. https://doi.org/10.1126/science.1962191.
(39) Wang, J.; Liu, K.; Xing, R.; Yan, X. Peptide Self-Assembly: Thermodynamics and Kinetics. *Chemical Society Reviews* **2016**, *45* (20), 5589–5604. https://doi.org/10.1039/C6CS00176A.
(40) Steed, J. W.; Turner, D. R.; Wallace, K. *Core Concepts in Supramolecular Chemistry and Nanochemistry*; John Wiley & Sons, 2007.
(41) Zhang, S. Fabrication of Novel Biomaterials through Molecular Self-Assembly. *Nat Biotechnol* **2003**, *21* (10), 1171–1178. https://doi.org/10.1038/nbt874.
(42) Stupp, S. I. Self-Assembly and Biomaterials. *Nano Lett.* **2010**, *10* (12), 4783–4786. https://doi.org/10.1021/nl103567y.
(43) Gazit, E. Self-Assembled Peptide Nanostructures: The Design of Molecular Building Blocks and Their Technological Utilization. *Chem. Soc. Rev.* **2007**, *36* (8), 1263–1269. https://doi.org/10.1039/B605536M.
(44) Tao, K.; Levin, A.; Adler-Abramovich, L.; Gazit, E. Fmoc-Modified Amino Acids and Short Peptides: Simple Bio-Inspired Building Blocks for the Fabrication of Functional Materials. *Chem. Soc. Rev.* **2016**, *45* (14), 3935–3953. https://doi.org/10.1039/C5CS00889A.
(45) Santis, E. D.; Ryadnov, M. G. Peptide Self-Assembly for Nanomaterials: The Old New Kid on the Block. *Chem. Soc. Rev.* **2015**, *44* (22), 8288–8300. https://doi.org/10.1039/C5CS00470E.
(46) Tao, K.; Wang, J.; Zhou, P.; Wang, C.; Xu, H.; Zhao, X.; Lu, J. R. Self-Assembly of Short Aβ(16−22) Peptides: Effect of Terminal Capping and the Role of Electrostatic Interaction. *Langmuir* **2011**, *27* (6), 2723–2730. https://doi.org/10.1021/la1034273.
(47) Tian, F.; Cziferszky, M.; Jiao, D.; Wahlström, K.; Geng, J.; Scherman, O. A. Peptide Separation through a CB[8]-Mediated Supramolecular Trap-and-Release Process. *Langmuir* **2011**, *27* (4), 1387–1390. https://doi.org/10.1021/la104346k.
(48) Maity, S.; Jana, P.; Maity, S. K.; Haldar, D. Fabrication of Hollow Self-Assembled Peptide Microvesicles and Transition from Sphere-to-Rod Structure. *Langmuir* **2011**, *27* (7), 3835–3841. https://doi.org/10.1021/la104461m.

(49) Khazanovich, N.; Granja, J. R.; McRee, D. E.; Milligan, R. A.; Ghadiri, M. R. Nanoscale Tubular Ensembles with Specified Internal Diameters. Design of a Self-Assembled Nanotube with a 13-.ANG. Pore https://pubs.acs.org/doi/pdf/10.1021/ja00092a079 (accessed 2021 -07 -27). https://doi.org/10.1021/ja00092a079.
(50) Ghadiri, M. R.; Granja, J. R.; Milligan, R. A.; McRee, D. E.; Khazanovich, N. Self-Assembling Organic Nanotubes Based on a Cyclic Peptide Architecture. *Nature* **1993**, *366* (6453), 324–327. https://doi.org/10.1038/366324a0.
(51) Mandal, D.; Shirazi, A. N.; Parang, K. Self-Assembly of Peptides to Nanostructures. *Org. Biomol. Chem.* **2014**, *12* (22), 3544–3561. https://doi.org/10.1039/C4OB00447G.
(52) Hartgerink, J. D.; Beniash, E.; Stupp, S. I. Self-Assembly and Mineralization of Peptide-Amphiphile Nanofibers. *Science* **2001**, *294* (5547), 1684–1688. https://doi.org/10.1126/science.1063187.
(53) Gudlur, S.; Sukthankar, P.; Gao, J.; Avila, L. A.; Hiromasa, Y.; Chen, J.; Iwamoto, T.; Tomich, J. M. Peptide Nanovesicles Formed by the Self-Assembly of Branched Amphiphilic Peptides. *PLOS ONE* **2012**, *7* (9), e45374. https://doi.org/10.1371/journal.pone.0045374.
(54) Scanlon, S.; Aggeli, A. Self-Assembling Peptide Nanotubes. *Nano Today* **2008**, *3* (3), 22–30. https://doi.org/10.1016/S1748-0132(08)70041-0.
(55) Ranganathan, D.; Samant, M. P.; Karle, I. L. Self-Assembling, Cystine-Derived, Fused Nanotubes Based on Spirane Architecture: Design, Synthesis, and Crystal Structure of Cystinospiranes. *J. Am. Chem. Soc.* **2001**, *123* (24), 5619–5624. https://doi.org/10.1021/ja0101734.
(56) Santoso, S.; Hwang, W.; Hartman, H.; Zhang, S. Self-Assembly of Surfactant-like Peptides with Variable Glycine Tails to Form Nanotubes and Nanovesicles. *Nano Lett.* **2002**, *2* (7), 687–691. https://doi.org/10.1021/nl025563i.
(57) Lakshmanan, A.; Zhang, S.; Hauser, C. A. E. Short Self-Assembling Peptides as Building Blocks for Modern Nanodevices. *Trends Biotechnol* **2012**, *30* (3), 155–165. https://doi.org/10.1016/j.tibtech.2011.11.001.
(58) Rajagopal, K.; Schneider, J. P. Self-Assembling Peptides and Proteins for Nanotechnological Applications. *Curr Opin Struct Biol* **2004**, *14* (4), 480–486. https://doi.org/10.1016/j.sbi.2004.06.006.
(59) Aggeli, A.; Nyrkova, I. A.; Bell, M.; Harding, R.; Carrick, L.; McLeish, T. C. B.; Semenov, A. N.; Boden, N. Hierarchical Self-Assembly of Chiral Rod-like Molecules as a Model for Peptide β-Sheet Tapes, Ribbons, Fibrils, and Fibers. *PNAS* **2001**, *98* (21), 11857–11862. https://doi.org/10.1073/pnas.191250198.
(60) Marini, D. M.; Hwang, W.; Lauffenburger, D. A.; Zhang, S.; Kamm, R. D. Left-Handed Helical Ribbon Intermediates in the Self-Assembly of a β-

Sheet Peptide. *Nano Lett.* **2002**, *2* (4), 295–299. https://doi.org/10.1021/nl015697g.
(61) Lu, K.; Jacob, J.; Thiyagarajan, P.; Conticello, V. P.; Lynn, D. G. Exploiting Amyloid Fibril Lamination for Nanotube Self-Assembly. *J. Am. Chem. Soc.* **2003**, *125* (21), 6391–6393. https://doi.org/10.1021/ja0341642.
(62) Xu, G.; Wang, W.; Groves, J. T.; Hecht, M. H. Self-Assembled Monolayers from a Designed Combinatorial Library of de Novo β-Sheet Proteins. *PNAS* **2001**, *98* (7), 3652–3657. https://doi.org/10.1073/pnas.071400098.
(63) Veiga, A. S.; Sinthuvanich, C.; Gaspar, D.; Franquelim, H. G.; Castanho, M. A. R. B.; Schneider, J. P. Arginine-Rich Self-Assembling Peptides as Potent Antibacterial Gels. *Biomaterials* **2012**, *33* (35), 8907–8916. https://doi.org/10.1016/j.biomaterials.2012.08.046.
(64) Chen, C.; Pan, F.; Zhang, S.; Hu, J.; Cao, M.; Wang, J.; Xu, H.; Zhao, X.; Lu, J. R. Antibacterial Activities of Short Designer Peptides: A Link between Propensity for Nanostructuring and Capacity for Membrane Destabilization. *Biomacromolecules* **2010**, *11* (2), 402–411. https://doi.org/10.1021/bm901130u.
(65) Görbitz, C. H. The Structure of Nanotubes Formed by Diphenylalanine, the Core Recognition Motif of Alzheimer's β-Amyloid Polypeptide. *Chem. Commun.* **2006**, No. 22, 2332–2334. https://doi.org/10.1039/B603080G.
(66) Adler-Abramovich, L.; Aronov, D.; Beker, P.; Yevnin, M.; Stempler, S.; Buzhansky, L.; Rosenman, G.; Gazit, E. Self-Assembled Arrays of Peptide Nanotubes by Vapour Deposition. *Nature Nanotech* **2009**, *4* (12), 849–854. https://doi.org/10.1038/nnano.2009.298.
(67) Wang, M.; Du, L.; Wu, X.; Xiong, S.; Chu, P. K. Charged Diphenylalanine Nanotubes and Controlled Hierarchical Self-Assembly. *ACS Nano* **2011**, *5* (6), 4448–4454. https://doi.org/10.1021/nn2016524.
(68) Zhu, P.; Yan, X.; Su, Y.; Yang, Y.; Li, J. Solvent-Induced Structural Transition of Self-Assembled Dipeptide: From Organogels to Microcrystals. *Chemistry – A European Journal* **2010**, *16* (10), 3176–3183. https://doi.org/10.1002/chem.200902139.
(69) Ryu, J.; Park, C. B. High-Temperature Self-Assembly of Peptides into Vertically Well-Aligned Nanowires by Aniline Vapor. *Advanced Materials* **2008**, *20* (19), 3754–3758. https://doi.org/10.1002/adma.200800364.
(70) Li, Z.; Liu, C.; Ma, S.; Zhang, D.; Yamaguchi, Y. Analysis of the Inhibition of Nucleic Acid Dyes on Polymerase Chain Reaction by Capillary Electrophoresis. *Anal. Methods* **2016**, *8* (11), 2330–2334. https://doi.org/10.1039/C5AY02705E.
(71) Kim, J.; Han, T. H.; Kim, Y.-I.; Park, J. S.; Choi, J.; Churchill, D. G.; Kim, S. O.; Ihee, H. Role of Water in Directing Diphenylalanine Assembly into Nanotubes and Nanowires. *Adv Mater* **2010**, *22* (5), 583–587. https://doi.org/10.1002/adma.200901973.

(72) Hendler, N.; Sidelman, N.; Reches, M.; Gazit, E.; Rosenberg, Y.; Richter, S. Formation of Well-Organized Self-Assembled Films from Peptide Nanotubes. *Advanced Materials* **2007**, *19* (11), 1485–1488. https://doi.org/10.1002/adma.200602265.
(73) Caroline, M. L.; Kumaresan, S.; Aravindan, P. G.; Mohamed, M. P.; Mani, G. Crystal Structure of L-Tryptophan–Fumaric Acid–Water (1/1/1). *Acta Cryst E* **2015**, *71* (9), o661–o662. https://doi.org/10.1107/S205698901501484X.
(74) Görbitz, C. H. Nanotubes from Hydrophobic Dipeptides: Pore Size Regulation through Side Chain Substitution. *New J. Chem.* **2003**, *27* (12), 1789–1793. https://doi.org/10.1039/B305984G.
(75) Görbitz, C. H. Nanotube Formation by Hydrophobic Dipeptides. *Chemistry – A European Journal* **2001**, *7* (23), 5153–5159. https://doi.org/10.1002/1521-3765(20011203)7:23<5153::AID-CHEM5153>3.0.CO;2-N.
(76) Görbitz, C. H. An Exceptionally Stable Peptide Nanotube System with Flexible Pores. *Acta Cryst B* **2002**, *58* (5), 849–854. https://doi.org/10.1107/S0108768102012314.
(77) Reches, M.; Gazit, E. Formation of Closed-Cage Nanostructures by Self-Assembly of Aromatic Dipeptides. *Nano Lett.* **2004**, *4* (4), 581–585. https://doi.org/10.1021/nl035159z.
(78) Reches, M.; Gazit, E. Designed Aromatic Homo-Dipeptides: Formation of Ordered Nanostructures and Potential Nanotechnological Applications. *Phys. Biol.* **2006**, *3* (1), S10–S19. https://doi.org/10.1088/1478-3975/3/1/S02.
(79) Yemini, M.; Reches, M.; Rishpon, J.; Gazit, E. Novel Electrochemical Biosensing Platform Using Self-Assembled Peptide Nanotubes. *Nano Lett.* **2005**, *5* (1), 183–186. https://doi.org/10.1021/nl0484189.
(80) Yemini, M.; Reches, M.; Gazit, E.; Rishpon, J. Peptide Nanotube-Modified Electrodes for Enzyme−Biosensor Applications. *Anal. Chem.* **2005**, *77* (16), 5155–5159. https://doi.org/10.1021/ac050414g.
(81) Amdursky, N.; Koren, I.; Gazit, E.; Rosenman, G. Adjustable Photoluminescence of Peptide Nanotubes Coatings. *Journal of Nanoscience and Nanotechnology* **2011**, *11* (10), 9282–9286. https://doi.org/10.1166/jnn.2011.4278.
(82) Amdursky, N.; Molotskii, M.; Aronov, D.; Adler-Abramovich, L.; Gazit, E.; Rosenman, G. Blue Luminescence Based on Quantum Confinement at Peptide Nanotubes. *Nano Lett.* **2009**, *9* (9), 3111–3115. https://doi.org/10.1021/nl9008265.
(83) Adler-Abramovich, L.; Badihi-Mossberg, M.; Gazit, E.; Rishpon, J. Characterization of Peptide-Nanostructure-Modified Electrodes and Their Application for Ultrasensitive Environmental Monitoring. *Small* **2010**, *6* (7), 825–831. https://doi.org/10.1002/smll.200902186.

(84) Orbach, R.; Adler-Abramovich, L.; Zigerson, S.; Mironi-Harpaz, I.; Seliktar, D.; Gazit, E. Self-Assembled Fmoc-Peptides as a Platform for the Formation of Nanostructures and Hydrogels. *Biomacromolecules* **2009**, *10* (9), 2646–2651. https://doi.org/10.1021/bm900584m.
(85) Mahler, A.; Reches, M.; Rechter, M.; Cohen, S.; Gazit, E. Rigid, Self-Assembled Hydrogel Composed of a Modified Aromatic Dipeptide. *Advanced Materials* **2006**, *18* (11), 1365–1370. https://doi.org/10.1002/adma.200501765.
(86) Guha, S.; Drew, M. G. B.; Banerjee, A. Dipeptide Nanotubes, with N-Terminally Located ω-Amino Acid Residues, That Are Stable Proteolytically, Thermally, and Over a Wide Range of PH. *Chem. Mater.* **2008**, *20* (6), 2282–2290. https://doi.org/10.1021/cm703159b.
(87) Guha, S.; Drew, M. G. B.; Banerjee, A. Construction of Helical Nanofibers from Self-Assembling Pseudopeptide Building Blocks: Modulating the Handedness and Breaking the Helicity. *Small* **2008**, *4* (11), 1993–2005. https://doi.org/10.1002/smll.200800002.
(88) Reches, M.; Gazit, E. Self-Assembly of Peptide Nanotubes and Amyloid-like Structures by Charged-Termini-Capped Diphenylalanine Peptide Analogues. *Israel Journal of Chemistry* **2005**, *45* (3), 363–371. https://doi.org/10.1560/5MC0-V3DX-KE0B-YF3J.
(89) Liebmann, T.; Rydholm, S.; Akpe, V.; Brismar, H. Self-Assembling Fmoc Dipeptide Hydrogel for in Situ 3D Cell Culturing. *BMC Biotechnology* **2007**, *7* (1), 88. https://doi.org/10.1186/1472-6750-7-88.
(90) Jayawarna, V.; Ali, M.; Jowitt, T. A.; Miller, A. F.; Saiani, A.; Gough, J. E.; Ulijn, R. V. Nanostructured Hydrogels for Three-Dimensional Cell Culture Through Self-Assembly of Fluorenylmethoxycarbonyl–Dipeptides. *Advanced Materials* **2006**, *18* (5), 611–614. https://doi.org/10.1002/adma.200501522.
(91) Jayawarna, V.; Smith, A.; Gough, J. E.; Ulijn, R. V. Three-Dimensional Cell Culture of Chondrocytes on Modified Di-Phenylalanine Scaffolds. *Biochemical Society Transactions* **2007**, *35* (3), 535–537. https://doi.org/10.1042/BST0350535.
(92) Yang, Z.; Liang, G.; Xu, B. Supramolecular Hydrogels Based on β-Amino Acid Derivatives. *Chem. Commun.* **2006**, No. 7, 738–740. https://doi.org/10.1039/B516133A.
(93) Liang, G.; Yang, Z.; Zhang, R.; Li, L.; Fan, Y.; Kuang, Y.; Gao, Y.; Wang, T.; Lu, W. W.; Xu, B. Supramolecular Hydrogel of a D-Amino Acid Dipeptide for Controlled Drug Release in Vivo. *Langmuir* **2009**, *25* (15), 8419–8422. https://doi.org/10.1021/la804271d.
(94) Yang, Z.; Gu, H.; Zhang, Y.; Wang, L.; Xu, B. Small Molecule Hydrogels Based on a Class of Antiinflammatory Agents. *Chem. Commun.* **2004**, No. 2, 208–209. https://doi.org/10.1039/B310574A.

(95) Johnson, E. K.; Adams, D. J.; Cameron, P. J. Directed Self-Assembly of Dipeptides to Form Ultrathin Hydrogel Membranes. *J. Am. Chem. Soc.* **2010**, *132* (14), 5130–5136. https://doi.org/10.1021/ja909579p.
(96) Song, Y.; Challa, S. R.; Medforth, C. J.; Qiu, Y.; Watt, R. K.; Peña, D.; Miller, J. E.; Swol, F. van; Shelnutt, J. A. Synthesis of Peptide-Nanotube Platinum-Nanoparticle Composites. *Chem. Commun.* **2004**, No. 9, 1044–1045. https://doi.org/10.1039/B402126F.
(97) Krysmann, M. J.; Castelletto, V.; Kelarakis, A.; Hamley, I. W.; Hule, R. A.; Pochan, D. J. Self-Assembly and Hydrogelation of an Amyloid Peptide Fragment. *Biochemistry* **2008**, *47* (16), 4597–4605. https://doi.org/10.1021/bi8000616.
(98) Reches, M.; Porat, Y.; Gazit, E. Amyloid Fibril Formation by Pentapeptide and Tetrapeptide Fragments of Human Calcitonin *. *Journal of Biological Chemistry* **2002**, *277* (38), 35475–35480. https://doi.org/10.1074/jbc.M206039200.
(99) Santis, P. D.; Forni, E.; Rizzo, R. Conformational analysis of DNA–basic polypeptide complexes: Possible models of nucleoprotamines and nucleohistones. *Biopolymers* **1974**, *13* (2), 313–326. https://doi.org/10.1002/bip.1974.360130207.
(100) Chapman, R.; Danial, M.; Liang Koh, M.; A. Jolliffe, K.; Perrier, S. Design and Properties of Functional Nanotubes from the Self-Assembly of Cyclic Peptide Templates. *Chemical Society Reviews* **2012**, *41* (18), 6023–6041. https://doi.org/10.1039/C2CS35172B.
(101) Fernandez-Lopez, S.; Kim, H.-S.; Choi, E. C.; Delgado, M.; Granja, J. R.; Khasanov, A.; Kraehenbuehl, K.; Long, G.; Weinberger, D. A.; Wilcoxen, K. M.; Ghadiri, M. R. Antibacterial Agents Based on the Cyclic d,l -α-Peptide Architecture. *Nature* **2001**, *412* (6845), 452–455. https://doi.org/10.1038/35086601.
(102) Tu, R. S.; Tirrell, M. Bottom-up Design of Biomimetic Assemblies. *Advanced Drug Delivery Reviews* **2004**, *56* (11), 1537–1563. https://doi.org/10.1016/j.addr.2003.10.047.
(103) Gore, T.; Dori, Y.; Talmon, Y.; Tirrell, M.; Bianco-Peled, H. Self-Assembly of Model Collagen Peptide Amphiphiles. *Langmuir* **2001**, *17* (17), 5352–5360. https://doi.org/10.1021/la010223i.
(104) Liu, L.; Busuttil, K.; Zhang, S.; Yang, Y.; Wang, C.; Besenbacher, F.; Dong, M. The Role of Self-Assembling Polypeptides in Building Nanomaterials. *Phys. Chem. Chem. Phys.* **2011**, *13* (39), 17435–17444. https://doi.org/10.1039/C1Cß1338E.
(105) Vauthey, S.; Santoso, S.; Gong, H.; Watson, N.; Zhang, S. Molecular Self-Assembly of Surfactant-like Peptides to Form Nanotubes and Nanovesicles. *PNAS* **2002**, *99* (8), 5355–5360. https://doi.org/10.1073/pnas.072089599.
(106) Hamley, I. W. Peptide Fibrillization. *Angewandte Chemie International Edition* **2007**, *46* (43), 8128–8147. https://doi.org/10.1002/anie.200700861.

(107) Castelletto, V.; Cheng, G.; Hamley, I. W. Amyloid Peptides Incorporating a Core Sequence from the Amyloid Beta Peptide and Gamma Amino Acids: Relating Bioactivity to Self-Assembly. *Chem. Commun.* **2011**, *47* (46), 12470–12472. https://doi.org/10.1039/C1CC15493A.
(108) Lagadec, C. A.; Smith, D. K. Structure–Activity Effects in Peptide Self-Assembly and Gelation – Dendritic versus Linear Architectures. *Chem. Commun.* **2012**, *48* (63), 7817–7819. https://doi.org/10.1039/C2CC32921B.
(109) Raeburn, J.; McDonald, T. O.; Adams, D. J. Dipeptide Hydrogelation Triggered via Ultraviolet Light. *Chem. Commun.* **2012**, *48* (75), 9355–9357. https://doi.org/10.1039/C2CC34677J.
(110) Sangeetha, N. M.; Maitra, U. Supramolecular Gels: Functions and Uses. *Chem. Soc. Rev.* **2005**, *34* (10), 821–836. https://doi.org/10.1039/B417081B.
(111) Hirst, A. R.; Escuder, B.; Miravet, J. F.; Smith, D. K. High-Tech Applications of Self-Assembling Supramolecular Nanostructured Gel-Phase Materials: From Regenerative Medicine to Electronic Devices. *Angewandte Chemie International Edition* **2008**, *47* (42), 8002–8018. https://doi.org/10.1002/anie.200800022.
(112) Bhattacharya, S.; Srivastava, A.; Pal, A. Modulation of Viscoelastic Properties of Physical Gels by Nanoparticle Doping: Influence of the Nanoparticle Capping Agent. *Angewandte Chemie* **2006**, *118* (18), 3000–3003. https://doi.org/10.1002/ange.200504461.
(113) Pal, A.; Chhikara, B. S.; Govindaraj, A.; Bhattacharya, S.; Rao, C. N. R. Synthesis and Properties of Novel Nanocomposites Made of Single-Walled Carbon Nanotubes and Low Molecular Mass Organogels and Their Thermo-Responsive Behavior Triggered by near IR Radiation. *J. Mater. Chem.* **2008**, *18* (22), 2593–2600. https://doi.org/10.1039/B719432C.
(114) Suzuki, M.; Sakakibara, Y.; Kobayashi, S.; Kimura, M.; Shirai, H.; Hanabusa, K. Preparation of Porous Polymers by ” in Situ Precipitation” Using Low Molecular Weight Gelators. *Polym J* **2002**, *34* (6), 474–477. https://doi.org/10.1295/polymj.34.474.
(115) Hafkamp, R. J. H.; Kokke, B. P. A.; Danke, I. M.; Geurts, H. P. M.; Rowan, A. E.; Feiters, M. C.; Nolte, R. J. M. Organogel Formation and Molecular Imprinting by Functionalized Gluconamides and Their Metal Complexes. *Chemical Communications* **1997**, *0* (6), 545–546. https://doi.org/10.1039/A608266A.
(116) Ono, Y.; Nakashima, K.; Sano, M.; Kanekiyo, Y.; Inoue, K.; Shinkai, S.; Sano, M.; Hojo, J. Organic Gels Are Useful as a Template for the Preparation of Hollow Fiber Silica. *Chem. Commun.* **1998**, No. 14, 1477–1478. https://doi.org/10.1039/A802829J.
(117) Jung, J. H.; Kobayashi, H.; Masuda, M.; Shimizu, T.; Shinkai, S. Helical Ribbon Aggregate Composed of a Crown-Appended Cholesterol Derivative Which Acts as an Amphiphilic Gelator of Organic Solvents and as a

Template for Chiral Silica Transcription. *J. Am. Chem. Soc.* **2001**, *123* (36), 8785–8789. https://doi.org/10.1021/ja010508h.
(118) Sone, E. D.; Zubarev, E. R.; Stupp, S. I. Semiconductor Nanohelices Templated by Supramolecular Ribbons. *Angewandte Chemie International Edition* **2002**, *41* (10), 1705–1709. https://doi.org/10.1002/1521-3773(20020517)41:10<1705::AID-ANIE1705>3.0.CO;2-M.
(119) Wang, D.; Hao, J. Self-Assembly Fibrillar Network Gels of Simple Surfactants in Organic Solvents. *Langmuir* **2011**, *27* (5), 1713–1717. https://doi.org/10.1021/la104333x.
(120) Debnath, S.; Shome, A.; Dutta, S.; Das, P. K. Dipeptide-Based Low-Molecular-Weight Efficient Organogelators and Their Application in Water Purification. *Chemistry – A European Journal* **2008**, *14* (23), 6870–6881. https://doi.org/10.1002/chem.200800731.
(121) Plank, T. N.; Skala, L. P.; Davis, J. T. Supramolecular Hydrogels for Environmental Remediation: G4-Quartet Gels That Selectively Absorb Anionic Dyes from Water. *Chem. Commun.* **2017**, *53* (46), 6235–6238. https://doi.org/10.1039/C7CC03118A.
(122) Yoshii, T.; Onogi, S.; Shigemitsu, H.; Hamachi, I. Chemically Reactive Supramolecular Hydrogel Coupled with a Signal Amplification System for Enhanced Analyte Sensitivity. *J. Am. Chem. Soc.* **2015**, *137* (9), 3360–3365. https://doi.org/10.1021/ja5131534.
(123) George, M.; Weiss, R. G. Molecular Organogels. Soft Matter Comprised of Low-Molecular-Mass Organic Gelators and Organic Liquids. *Acc. Chem. Res.* **2006**, *39* (8), 489–497. https://doi.org/10.1021/ar0500923.
(124) Esch, J. H. van; Feringa, B. L. New Functional Materials Based on Self-Assembling Organogels: From Serendipity towards Design. *Angewandte Chemie International Edition* **2000**, *39* (13), 2263–2266. https://doi.org/10.1002/1521-3773(20000703)39:13<2263::AID-ANIE2263>3.0.CO;2-V.
(125) Mohmeyer, N.; Schmidt, H.-W. A New Class of Low-Molecular-Weight Amphiphilic Gelators. *Chemistry – A European Journal* **2005**, *11* (3), 863–872. https://doi.org/10.1002/chem.200400716.
(126) Suzuki, M.; Nanbu, M.; Yumoto, M.; Shirai, H.; Hanabusa, K. Novel Dumbbell-Form Low-Molecular-Weight Gelators Based on L-Lysine: Their Hydrogelation and Organogelation Properties. *New J. Chem.* **2005**, *29* (11), 1439–1444. https://doi.org/10.1039/B511158G.
(127) Yang, H.; Yi, T.; Zhou, Z.; Zhou, Y.; Wu, J.; Xu, M.; Li, F.; Huang, C. Switchable Fluorescent Organogels and Mesomorphic Superstructure Based on Naphthalene Derivatives. *Langmuir* **2007**, *23* (15), 8224–8230. https://doi.org/10.1021/la7005919.
(128) Mohmeyer, N.; Schmidt, H.-W. Synthesis and Structure–Property Relationships of Amphiphilic Organogelators. *Chemistry – A European*

Journal **2007**, *13* (16), 4499–4509. https://doi.org/10.1002/chem.200601154.
(129) Suzuki, M.; Nakajima, Y.; Yumoto, M.; Kimura, M.; Shirai, H.; Hanabusa, K. In Situ Organogelation at Room Temperature: Direct Synthesis of Gelators in Organic Solvents. *Org. Biomol. Chem.* **2004**, *2* (8), 1155–1159. https://doi.org/10.1039/B401683A.
(130) Schmidt, R.; Schmutz, M.; Michel, M.; Decher, G.; Mésini, P. J. Organogelation Properties of a Series of Oligoamides. *Langmuir* **2002**, *18* (15), 5668–5672. https://doi.org/10.1021/la011549u.
(131) Loos, M. de; Friggeri, A.; Esch, J. van; M. Kellogg, R.; L. Feringa, B. Cyclohexane Bis-Urea Compounds for the Gelation of Water and Aqueous Solutions. *Organic & Biomolecular Chemistry* **2005**, *3* (9), 1631–1639. https://doi.org/10.1039/B500837A.
(132) Kastler, M.; Pisula, W.; Wasserfallen, D.; Pakula, T.; Müllen, K. Influence of Alkyl Substituents on the Solution- and Surface-Organization of Hexa-Peri-Hexabenzocoronenes. *J. Am. Chem. Soc.* **2005**, *127* (12), 4286–4296. https://doi.org/10.1021/ja0430696.
(133) Banerjee, S.; Das, R. K.; Maitra, U. Supramolecular Gels 'in Action.' *J. Mater. Chem.* **2009**, *19* (37), 6649–6687. https://doi.org/10.1039/B819218A.
(134) Skilling, K. J.; Citossi, F.; Bradshaw, T. D.; Ashford, M.; Kellam, B.; Marlow, M. Insights into Low Molecular Mass Organic Gelators: A Focus on Drug Delivery and Tissue Engineering Applications. *Soft Matter* **2013**, *10* (2), 237–256. https://doi.org/10.1039/C3SM52244J.
(135) Wu, Y.; Xu, M.; Chen, X.; Yang, S.; Wu, H.; Pan, J.; Xiong, X. CTAB-Assisted Synthesis of Novel Ultrathin MoSe 2 Nanosheets Perpendicular to Graphene for the Adsorption and Photodegradation of Organic Dyes under Visible Light. *Nanoscale* **2016**, *8* (1), 440–450. https://doi.org/10.1039/C5NR05748E.
(136) Konicki, W.; Aleksandrzak, M.; Moszyński, D.; Mijowska, E. Adsorption of Anionic Azo-Dyes from Aqueous Solutions onto Graphene Oxide: Equilibrium, Kinetic and Thermodynamic Studies. *Journal of Colloid and Interface Science* **2017**, *496*, 188–200. https://doi.org/10.1016/j.jcis.2017.02.031.
(137) Zhang, J.; Shafiul Azam, M.; Shi, C.; Huang, J.; Yan, B.; Liu, Q.; Zeng, H. Poly(Acrylic Acid) Functionalized Magnetic Graphene Oxide Nanocomposite for Removal of Methylene Blue. *RSC Advances* **2015**, *5* (41), 32272–32282. https://doi.org/10.1039/C5RA01815C.
(138) Qi, Y.; Yang, M.; Xu, W.; He, S.; Men, Y. Natural Polysaccharides-Modified Graphene Oxide for Adsorption of Organic Dyes from Aqueous Solutions. *Journal of Colloid and Interface Science* **2017**, *486*, 84–96. https://doi.org/10.1016/j.jcis.2016.09.058.

(139) Gong, Y.; Zhao, X.; Cai, Z.; O'Reilly, S. E.; Hao, X.; Zhao, D. A Review of Oil, Dispersed Oil and Sediment Interactions in the Aquatic Environment: Influence on the Fate, Transport and Remediation of Oil Spills. *Marine Pollution Bulletin* **2014**, *79* (1), 16–33. https://doi.org/10.1016/j.marpolbul.2013.12.024.
(140) Shen, Z. M.; Wu, D.; Yang, J.; Yuan, T.; Wang, W. H.; Jia, J. P. Methods to Improve Electrochemical Treatment Effect of Dye Wastewater. *Journal of Hazardous Materials* **2006**, *131* (1), 90–97. https://doi.org/10.1016/j.jhazmat.2005.09.010.
(141) Tripathi, P. K.; Liu, M.; Zhao, Y.; Ma, X.; Gan, L.; Noonan, O.; Yu, C. Enlargement of Uniform Micropores in Hierarchically Ordered Micro–Mesoporous Carbon for High Level Decontamination of Bisphenol A. *J. Mater. Chem. A* **2014**, *2* (22), 8534–8544. https://doi.org/10.1039/C4TA00578C.
(142) Eccles, H. Treatment of Metal-Contaminated Wastes: Why Select a Biological Process? *Trends in Biotechnology* **1999**, *17* (12), 462–465. https://doi.org/10.1016/S0167-7799(99)01381-5.
(143) Banerji, B.; Chatterjee, M.; Pal, U.; Maiti, N. C. Formation of Annular Protofibrillar Assembly by Cysteine Tripeptide: Unraveling the Interactions with NMR, FTIR, and Molecular Dynamics. *J. Phys. Chem. B* **2017**, *121* (26), 6367–6379. https://doi.org/10.1021/acs.jpcb.7b04373.
(144) Banerji, B.; Chatterjee, M.; Prodhan, C.; Chaudhuri, K. Tripeptide Consisting of Benzyl Protected Di-Cysteine and Phenylalanine Forms Spherical Assembly and Induces Cytotoxicity in Cancer Cells via Apoptosis. *RSC Adv.* **2016**, *6* (113), 112667–112676. https://doi.org/10.1039/C6RA23911K.
(145) Suzuki, M.; Nakajima, Y.; Yumoto, M.; Kimura, M.; Shirai, H.; Hanabusa, K. Effects of Hydrogen Bonding and van Der Waals Interactions on Organogelation Using Designed Low-Molecular-Weight Gelators and Gel Formation at Room Temperature. *Langmuir* **2003**, *19* (21), 8622–8624. https://doi.org/10.1021/la034772v.
(146) Zhang, Y.-Z.; Roder, H.; Paterson, Y. Rapid Amide Proton Exchange Rates in Peptides and Proteins Measured by Solvent Quenching and Two-Dimensional NMR. *Protein Science* **1995**, *4* (4), 804–814. https://doi.org/10.1002/pro.5560040420.
(147) Abraham, R. J.; Byrne, J. J.; Griffiths, L.; Perez, M. 1H Chemical Shifts in NMR: Part 23, the Effect of Dimethyl Sulphoxide versus Chloroform Solvent on 1H Chemical Shifts. *Magnetic Resonance in Chemistry* **2006**, *44* (5), 491–509. https://doi.org/10.1002/mrc.1747.
(148) Barth, A. Infrared Spectroscopy of Proteins. *Biochimica et Biophysica Acta (BBA) - Bioenergetics* **2007**, *1767* (9), 1073–1101. https://doi.org/10.1016/j.bbabio.2007.06.004.

(149) Balbach, J. J.; Ishii, Y.; Antzutkin, O. N.; Leapman, R. D.; Rizzo, N. W.; Dyda, F.; Reed, J.; Tycko, R. Amyloid Fibril Formation by Aβ16-22, a Seven-Residue Fragment of the Alzheimer's β-Amyloid Peptide, and Structural Characterization by Solid State NMR. *Biochemistry* **2000**, *39* (45), 13748–13759. https://doi.org/10.1021/bi0011330.
(150) Fleming, S.; Ulijn, R. V. Design of Nanostructures Based on Aromatic Peptide Amphiphiles. *Chem. Soc. Rev.* **2014**, *43* (23), 8150–8177. https://doi.org/10.1039/C4CS00247D.
(151) EANES, E. D.; GLENNER, G. G. X-RAY DIFFRACTION STUDIES ON AMYLOID FILAMENTS. *J Histochem Cytochem.* **1968**, *16* (11), 673–677. https://doi.org/10.1177/16.11.673.
(152) Hughes, M.; Frederix, P. W. J. M.; Raeburn, J.; Birchall, L. S.; Sadownik, J.; Coomer, F. C.; Lin, I.-H.; Cussen, E. J.; Hunt, N. T.; Tuttle, T.; Webb, S. J.; Adams, D. J.; Ulijn, R. V. Sequence/Structure Relationships in Aromatic Dipeptide Hydrogels Formed under Thermodynamic Control by Enzyme-Assisted Self-Assembly. *Soft Matter* **2012**, *8* (20), 5595–5602. https://doi.org/10.1039/C2SM25224D.
(153) Mu, X.; Eckes, K. M.; Nguyen, M. M.; Suggs, L. J.; Ren, P. Experimental and Computational Studies Reveal an Alternative Supramolecular Structure for Fmoc-Dipeptide Self-Assembly. *Biomacromolecules* **2012**, *13* (11), 3562–3571. https://doi.org/10.1021/bm301007r.
(154) Ryan, D. M.; Anderson, S. B.; Senguen, F. T.; Youngman, R. E.; Nilsson, B. L. Self-Assembly and Hydrogelation Promoted by F5-Phenylalanine. *Soft Matter* **2010**, *6* (3), 475–479. https://doi.org/10.1039/B916738B.
(155) Singh, P.; Brar, S. K.; Bajaj, M.; Narang, N.; Mithu, V. S.; Katare, O. P.; Wangoo, N.; Sharma, R. K. Self-Assembly of Aromatic α-Amino Acids into Amyloid Inspired Nano/Micro Scaled Architects. *Materials Science and Engineering: C* **2017**, *72*, 590–600. https://doi.org/10.1016/j.msec.2016.11.117.
(156) Wang, Y.; Chang, Y.; Yin, L.; Xue, Y.; Li, Z.; Xue, C. A Novel Technological Process of Extracting L-Tyrosine with Low Fluorine Content from Defatted Antarctic Krill (Euphausia Superba) By-Product by Enzymatic Hydrolysis. *Food Bioprocess Technol* **2016**, *9* (4), 621–627. https://doi.org/10.1007/s11947-015-1658-x.
(157) Katyal, N.; Deep, S. A Computational Approach to Get Insights into Multiple Faces of Additives in Modulation of Protein Aggregation Pathways. *Phys. Chem. Chem. Phys.* **2019**, *21* (44), 24269–24285. https://doi.org/10.1039/C9CP03763B.
(158) Li, L.-L.; Qi, G.-B.; Yu, F.; Liu, S.-J.; Wang, H. An Adaptive Biointerface from Self-Assembled Functional Peptides for Tissue Engineering. *Advanced Materials* **2015**, *27* (20), 3181–3188. https://doi.org/10.1002/adma.201500658.

(159) Lian, M.; Chen, X.; Lu, Y.; Yang, W. Self-Assembled Peptide Hydrogel as a Smart Biointerface for Enzyme-Based Electrochemical Biosensing and Cell Monitoring. *ACS Appl. Mater. Interfaces* **2016**, *8* (38), 25036–25042. https://doi.org/10.1021/acsami.6b05409.
(160) Schneider, A.; Garlick, J. A.; Egles, C. Self-Assembling Peptide Nanofiber Scaffolds Accelerate Wound Healing. *PLOS ONE* **2008**, *3* (1), e1410. https://doi.org/10.1371/journal.pone.0001410.
(161) Gao, X.; Matsui, H. Peptide-Based Nanotubes and Their Applications in Bionanotechnology. *Advanced Materials* **2005**, *17* (17), 2037–2050. https://doi.org/10.1002/adma.200401849.
(162) Dickerson, M. B.; Sandhage, K. H.; Naik, R. R. Protein- and Peptide-Directed Syntheses of Inorganic Materials. *Chem. Rev.* **2008**, *108* (11), 4935–4978. https://doi.org/10.1021/cr8002328.
(163) Paramonov, S. E.; Jun, H.-W.; Hartgerink, J. D. Self-Assembly of Peptide−Amphiphile Nanofibers: The Roles of Hydrogen Bonding and Amphiphilic Packing. *J. Am. Chem. Soc.* **2006**, *128* (22), 7291–7298. https://doi.org/10.1021/ja060573x.
(164) Diehl, M. R.; Yaliraki, S. N.; Beckman, R. A.; Barahona, M.; Heath, J. R. Self-Assembled, Deterministic Carbon Nanotube Wiring Networks. *Angewandte Chemie* **2002**, *114* (2), 363–366. https://doi.org/10.1002/1521-3757(20020118)114:2<363::AID-ANGE363>3.0.CO;2-I.
(165) Collins, P. G.; Arnold, M. S.; Avouris, P. Engineering Carbon Nanotubes and Nanotube Circuits Using Electrical Breakdown. *Science* **2001**, *292* (5517), 706–709. https://doi.org/10.1126/science.1058782.
(166) Lv, C.; Xue, Q.; Shan, M.; Jing, N.; Ling, C.; Zhou, X.; Jiao, Z.; Xing, W.; Yan, Z. Self-Assembly of Double Helical Nanostructures inside Carbon Nanotubes. *Nanoscale* **2013**, *5* (10), 4191–4199. https://doi.org/10.1039/C2NR33157H.
(167) Colombo, G.; Soto, P.; Gazit, E. Peptide Self-Assembly at the Nanoscale: A Challenging Target for Computational and Experimental Biotechnology. *Trends in Biotechnology* **2007**, *25* (5), 211–218. https://doi.org/10.1016/j.tibtech.2007.03.004.
(168) Mann, S. Self-Assembly and Transformation of Hybrid Nano-Objects and Nanostructures under Equilibrium and Non-Equilibrium Conditions. *Nature Materials* **2009**, *8* (10), 781–792. https://doi.org/10.1038/nmat2496.
(169) Davis, V. A.; Parra-Vasquez, A. N. G.; Green, M. J.; Rai, P. K.; Behabtu, N.; Prieto, V.; Booker, R. D.; Schmidt, J.; Kesselman, E.; Zhou, W.; Fan, H.; Adams, W. W.; Hauge, R. H.; Fischer, J. E.; Cohen, Y.; Talmon, Y.; Smalley, R. E.; Pasquali, M. True Solutions of Single-Walled Carbon Nanotubes for Assembly into Macroscopic Materials. *Nature Nanotechnology* **2009**, *4* (12), 830–834. https://doi.org/10.1038/nnano.2009.302.

(170) Rica, R. de la; Matsui, H. Applications of Peptide and Protein-Based Materials in Bionanotechnology. *Chem. Soc. Rev.* **2010**, *39* (9), 3499–3509. https://doi.org/10.1039/B917574C.
(171) Woolfson, D. N.; Mahmoud, Z. N. More than Just Bare Scaffolds: Towards Multi-Component and Decorated Fibrous Biomaterials. *Chem. Soc. Rev.* **2010**, *39* (9), 3464–3479. https://doi.org/10.1039/C0CS00032A.
(172) Tan, S. J.; Campolongo, M. J.; Luo, D.; Cheng, W. Building Plasmonic Nanostructures with DNA. *Nature Nanotechnology* **2011**, *6* (5), 268–276. https://doi.org/10.1038/nnano.2011.49.
(173) Banerji, B.; Kumar Pramanik, S.; Mandal, S.; Chandra Maiti, N.; Chaudhuri, K. Synthesis, Characterization and Cytotoxicity Study of Magnetic (Fe 3 O 4) Nanoparticles and Their Drug Conjugate. *RSC Advances* **2012**, *2* (6), 2493–2497. https://doi.org/10.1039/C2RA01118B.
(174) Huang, R.; Qi, W.; Su, R.; Zhao, J.; He, Z. Solvent and Surface Controlled Self-Assembly of Diphenylalanine Peptide: From Microtubes to Nanofibers. *Soft Matter* **2011**, *7* (14), 6418–6421. https://doi.org/10.1039/C1SM05752A.
(175) Chen, Y.; Gan, H. X.; Tong, Y. W. PH-Controlled Hierarchical Self-Assembly of Peptide Amphiphile. *Macromolecules* **2015**, *48* (8), 2647–2653. https://doi.org/10.1021/ma502572w.
(176) Abelein, A.; Jarvet, J.; Barth, A.; Gräslund, A.; Danielsson, J. Ionic Strength Modulation of the Free Energy Landscape of Aβ40 Peptide Fibril Formation. *J. Am. Chem. Soc.* **2016**, *138* (21), 6893–6902. https://doi.org/10.1021/jacs.6b04511.
(177) Li, R.; Horgan, C. C.; Long, B.; Rodriguez, A. L.; Mather, L.; Barrow, C. J.; Nisbet, D. R.; Williams, R. J. Tuning the Mechanical and Morphological Properties of Self-Assembled Peptide Hydrogels via Control over the Gelation Mechanism through Regulation of Ionic Strength and the Rate of PH Change. *RSC Adv.* **2014**, *5* (1), 301–307. https://doi.org/10.1039/C4RA13266A.
(178) M. Doran, T.; M. Ryan, D.; L. Nilsson, B. Reversible Photocontrol of Self-Assembled Peptide Hydrogel Viscoelasticity. *Polymer Chemistry* **2014**, *5* (1), 241–248. https://doi.org/10.1039/C3PY00903C.
(179) Huang, R.; Wang, Y.; Qi, W.; Su, R.; He, Z. Temperature-Induced Reversible Self-Assembly of Diphenylalanine Peptide and the Structural Transition from Organogel to Crystalline Nanowires. *Nanoscale Research Letters* **2014**, *9* (1), 653. https://doi.org/10.1186/1556-276X-9-653.
(180) Wang, J.-X.; Lei, Q.; Luo, G.-F.; Cai, T.-T.; Li, J.-L.; Cheng, S.-X.; Zhuo, R.-X.; Zhang, X.-Z. Controlled Arrays of Self-Assembled Peptide Nanostructures in Solution and at Interface. *Langmuir* **2013**, *29* (23), 6996–7004. https://doi.org/10.1021/la4010714.
(181) Rissanou, A. N.; Georgilis, E.; Kasotakis, E.; Mitraki, A.; Harmandaris, V. Effect of Solvent on the Self-Assembly of Dialanine and Diphenylalanine

Peptides. *J. Phys. Chem. B* **2013**, *117* (15), 3962–3975. https://doi.org/10.1021/jp311795b.
(182) Mayans, E.; Casanovas, J.; Gil, A. M.; Jiménez, A. I.; Cativiela, C.; Puiggalí, J.; Alemán, C. Diversity and Hierarchy in Supramolecular Assemblies of Triphenylalanine: From Laminated Helical Ribbons to Toroids. *Langmuir* **2017**, *33* (16), 4036–4048. https://doi.org/10.1021/acs.langmuir.7b00622.
(183) Zhao, Y.; Deng, L.; Wang, J.; Xu, H.; Lu, J. R. Solvent Controlled Structural Transition of KI4K Self-Assemblies: From Nanotubes to Nanofibrils. *Langmuir* **2015**, *31* (47), 12975–12983. https://doi.org/10.1021/acs.langmuir.5b02303.
(184) Banerji, B.; Pramanik, S. K.; Pal, U.; Maiti, N. C. Dipeptide Derived from Benzylcystine Forms Unbranched Nanotubes in Aqueous Solution. *J Nanostruct Chem* **2013**, *3* (1), 12. https://doi.org/10.1186/2193-8865-3-12.
(185) Naskar, J.; Banerjee, A. Concentration Dependent Transformation of Oligopeptide Based Nanovesicles to Nanotubes and an Application of Nanovesicles. *Chemistry – An Asian Journal* **2009**, *4* (12), 1817–1823. https://doi.org/10.1002/asia.200900274.
(186) Gaussian ~09 Revision D.01 – ScienceOpen https://www.scienceopen.com/document?vid=839f33cc-9114-4a55-8f1a-3f1520324ef5 (accessed 2021 -05 -13).
(187) Becke, A. D. Density-functional Thermochemistry. III. The Role of Exact Exchange. *J. Chem. Phys.* **1993**, *98* (7), 5648–5652. https://doi.org/10.1063/1.464913.
(188) Lee, C.; Yang, W.; Parr, R. G. Development of the Colle-Salvetti Correlation-Energy Formula into a Functional of the Electron Density. *Phys. Rev. B* **1988**, *37* (2), 785–789. https://doi.org/10.1103/PhysRevB.37.785.
(189) Hariharan, P. C.; Pople, J. A. The Influence of Polarization Functions on Molecular Orbital Hydrogenation Energies. *Theoret. Chim. Acta* **1973**, *28* (3), 213–222. https://doi.org/10.1007/BF00533485.
(190) Brown, G. J.; Ellis, M. J.; Martin, T. D.; McCunn, L. R. Vibrational Bands of the 2-Butyn-1-Yl Radical. *J. Phys. Chem. A* **2020**, *124* (20), 4081–4086. https://doi.org/10.1021/acs.jpca.0c02218.
(191) Miertuš, S.; Scrocco, E.; Tomasi, J. Electrostatic Interaction of a Solute with a Continuum. A Direct Utilizaion of AB Initio Molecular Potentials for the Prevision of Solvent Effects. *Chemical Physics* **1981**, *55* (1), 117–129. https://doi.org/10.1016/0301-0104(81)85090-2.
(192) Jarmelo, S.; Maiti, N.; Anderson, V.; Carey, P. R.; Fausto, R. Cα−H Bond-Stretching Frequency in Alcohols as a Probe of Hydrogen-Bonding Strength: A Combined Vibrational Spectroscopic and Theoretical Study of n-[1-D]Propanol. *J. Phys. Chem. A* **2005**, *109* (10), 2069–2077. https://doi.org/10.1021/jp046683c.

(193) Das, S.; Pal, U.; Chatterjee, M.; Pramanik, S. K.; Banerji, B.; Maiti, N. C. Envisaging Structural Insight of a Terminally Protected Proline Dipeptide by Raman Spectroscopy and Density Functional Theory Analyses. *J. Phys. Chem. A* **2016**, *120* (49), 9829–9840. https://doi.org/10.1021/acs.jpca.6b10017.
(194) Biancalana, M.; Koide, S. Molecular Mechanism of Thioflavin-T Binding to Amyloid Fibrils. *Biochimica et Biophysica Acta (BBA) - Proteins and Proteomics* **2010**, *1804* (7), 1405–1412. https://doi.org/10.1016/j.bbapap.2010.04.001.
(195) Bera, K.; Mondal, A.; Pal, U.; Maiti, N. C. Porphyrin-Armored Gold Nanospheres Modulate the Secondary Structure of α-Synuclein and Arrest Its Fibrillation. *J. Phys. Chem. C* **2020**, *124* (11), 6418–6434. https://doi.org/10.1021/acs.jpcc.9b11503.
(196) Borba, A.; Gómez-Zavaglia, A.; Simões, P. N. N. L.; Fausto, R. Matrix-Isolation FT-IR Spectra and Theoretical Study of Dimethyl Sulfate. *Spectrochimica Acta Part A: Molecular and Biomolecular Spectroscopy* **2005**, *61* (7), 1461–1470. https://doi.org/10.1016/j.saa.2004.10.050.
(197) Ji, Y.; Yang, X.; Ji, Z.; Zhu, L.; Ma, N.; Chen, D.; Jia, X.; Tang, J.; Cao, Y. DFT-Calculated IR Spectrum Amide I, II, and III Band Contributions of N-Methylacetamide Fine Components. *ACS Omega* **2020**, *5* (15), 8572–8578. https://doi.org/10.1021/acsomega.9b04421.
(198) Gellman, S. H.; Dado, G. P.; Liang, G. B.; Adams, B. R. Conformation-directing effects of a single intramolecular amide-amide hydrogen bond: variable-temperature NMR and IR studies on a homologous diamide series https://pubs.acs.org/doi/pdf/10.1021/ja00004a016 (accessed 2021 -05 -05). https://doi.org/10.1021/ja00004a016.
(199) Naskar, J.; Palui, G.; Banerjee, A. Tetrapeptide-Based Hydrogels: For Encapsulation and Slow Release of an Anticancer Drug at Physiological PH. *J. Phys. Chem. B* **2009**, *113* (35), 11787–11792. https://doi.org/10.1021/jp904251j.
(200) Bhowmik, D.; Mote, K. R.; MacLaughlin, C. M.; Biswas, N.; Chandra, B.; Basu, J. K.; Walker, G. C.; Madhu, P. K.; Maiti, S. Cell-Membrane-Mimicking Lipid-Coated Nanoparticles Confer Raman Enhancement to Membrane Proteins and Reveal Membrane-Attached Amyloid-β Conformation. *ACS Nano* **2015**, *9* (9), 9070–9077. https://doi.org/10.1021/acsnano.5b03175.
(201) Suri, S. S.; Fenniri, H.; Singh, B. Nanotechnology-Based Drug Delivery Systems. *J Occup Med Toxicol* **2007**, *2* (1), 16. https://doi.org/10.1186/1745-6673-2-16.
(202) Mansoori, G. A.; Mohazzabi, P.; McCormack, P.; Jabbari, S. Nanotechnology in Cancer Prevention, Detection and Treatment: Bright Future Lies Ahead. *World Review of Science, Technology and Sustainable*

Development **2007**, *4* (2–3), 226–257. https://doi.org/10.1504/WRSTSD.2007.013584.
(203) Liu, Y.; Miyoshi, H.; Nakamura, M. Nanomedicine for Drug Delivery and Imaging: A Promising Avenue for Cancer Therapy and Diagnosis Using Targeted Functional Nanoparticles. *International Journal of Cancer* **2007**, *120* (12), 2527–2537. https://doi.org/10.1002/ijc.22709.
(204) Langner, M.; Kral, T. E. Liposome-Based Drug Delivery Systems. *Pol J Pharmacol* **1999**, *51* (3), 211–222.
(205) Kazi, K. M.; Mandal, A. S.; Biswas, N.; Guha, A.; Chatterjee, S.; Behera, M.; Kuotsu, K. Niosome: A Future of Targeted Drug Delivery Systems. *J Adv Pharm Technol Res* **2010**, *1* (4), 374–380. https://doi.org/10.4103/0110-5558.76435.
(206) McBain, S. C.; Yiu, H. H.; Dobson, J. Magnetic Nanoparticles for Gene and Drug Delivery. *Int J Nanomedicine* **2008**, *3* (2), 169–180.
(207) Kedar, U.; Phutane, P.; Shidhaye, S.; Kadam, V. Advances in Polymeric Micelles for Drug Delivery and Tumor Targeting. *Nanomedicine: Nanotechnology, Biology and Medicine* **2010**, *6* (6), 714–729. https://doi.org/10.1016/j.nano.2010.05.005.
(208) Soppimath, K. S.; Aminabhavi, T. M.; Kulkarni, A. R.; Rudzinski, W. E. Biodegradable Polymeric Nanoparticles as Drug Delivery Devices. *Journal of Controlled Release* **2001**, *70* (1), 1–20. https://doi.org/10.1016/S0168-3659(00)00339-4.
(209) Crombez, L.; Morris, M. C.; Deshayes, S.; Heitz, F.; Divita, G. Peptide-Based Nanoparticle for Ex Vivo and In Vivo Dug Delivery. *Current Pharmaceutical Design* **2008**, *14* (34), 3656–3665.
(210) Bawa, R.; Fung, S.-Y.; Shiozaki, A.; Yang, H.; Zheng, G.; Keshavjee, S.; Liu, M. Self-Assembling Peptide-Based Nanoparticles Enhance Cellular Delivery of the Hydrophobic Anticancer Drug Ellipticine through Caveolae-Dependent Endocytosis. *Nanomedicine: Nanotechnology, Biology and Medicine* **2012**, *8* (5), 647–654. https://doi.org/10.1016/j.nano.2011.08.007.
(211) Carino, G. P.; Jacob, J. S.; Mathiowitz, E. Nanosphere Based Oral Insulin Delivery. *Journal of Controlled Release* **2000**, *65* (1), 261–269. https://doi.org/10.1016/S0168-3659(99)00247-3.
(212) Singh, R.; Lillard, J. W. Nanoparticle-Based Targeted Drug Delivery. *Experimental and Molecular Pathology* **2009**, *86* (3), 215–223. https://doi.org/10.1016/j.yexmp.2008.12.004.
(213) Gungormus, M.; Branco, M.; Fong, H.; Schneider, J. P.; Tamerler, C.; Sarikaya, M. Self Assembled Bi-Functional Peptide Hydrogels with Biomineralization-Directing Peptides. *Biomaterials* **2010**, *31* (28), 7266–7274. https://doi.org/10.1016/j.biomaterials.2010.06.010.

(214) Zhao, X. Design of Self-Assembling Surfactant-like Peptides and Their Applications. *Current Opinion in Colloid & Interface Science* **2009**, *14* (5), 340–348. https://doi.org/10.1016/j.cocis.2009.07.002.
(215) Knowles, T. P. J.; Vendruscolo, M.; Dobson, C. M. The Amyloid State and Its Association with Protein Misfolding Diseases. *Nat Rev Mol Cell Biol* **2014**, *15* (6), 384–396. https://doi.org/10.1038/nrm3810.
(216) Mondal, S.; Gazit, E. The Self-Assembly of Helical Peptide Building Blocks. *ChemNanoMat* **2016**, *2* (5), 323–332. https://doi.org/10.1002/cnma.201600048.
(217) Görbitz, C. H. Microporous Organic Materials from Hydrophobic Dipeptides. *Chemistry – A European Journal* **2007**, *13* (4), 1022–1031. https://doi.org/10.1002/chem.200601427.
(218) Gorla, L.; Martí-Centelles, V.; Altava, B.; Burguete, M. I.; Luis, S. V. The Role of the Side Chain in the Conformational and Self-Assembly Patterns of C2-Symmetric Val and Phe Pseudopeptidic Derivatives. *CrystEngComm* **2019**, *21* (14), 2398–2408. https://doi.org/10.1039/C8CE02088D.
(219) Bera, S.; Mondal, S.; Xue, B.; Shimon, L. J. W.; Cao, Y.; Gazit, E. Rigid Helical-like Assemblies from a Self-Aggregating Tripeptide. *Nat. Mater.* **2019**, *18* (5), 503–509. https://doi.org/10.1038/s41563-019-0343-2.
(220) Sharma, A.; Tiwari, P.; Dutt Konar, A. The Dominant Role of Side Chains in Supramolecular Double Helical Organisation in Synthetic Tripeptides. *Journal of Molecular Structure* **2018**, *1161*, 44–54. https://doi.org/10.1016/j.molstruc.2018.01.018.
(221) Misra, S.; Singh, P.; Mahata, R. N.; Brandão, P.; Roy, S.; Mahapatra, A. K.; Nanda, J. Supramolecular Antiparallel β-Sheet Formation by Tetrapeptides Based on Amyloid Sequence. *The Journal of Physical Chemistry B* **2021**, *125* (17), 4274–4285. https://doi.org/10.1021/acs.jpcb.0c10920.
(222) Guha, S.; Drew, M. G. B.; Banerjee, A. A New Molecular Scaffold for the Formation of Supramolecular Peptide Double Helices: The Crystallographic Insight. *Organic Letters* **2007**, *9* (7), 1347–1350. https://doi.org/10.1021/ol0701870.
(223) Giri, R. S.; Mandal, B. Formation of Supramolecular Single and Double Helix-like Structures from Designed Tripeptides. *CrystEngComm* **2019**, *21* (37), 5618–5625. https://doi.org/10.1039/C9CE01168D.
(224) Hema, K.; Sureshan, K. M. B-Sheet to Helical-Sheet Evolution Induced by Topochemical Polymerization: Cross-α-Amyloid-like Packing in a Pseudoprotein with Gly-Phe-Gly Repeats. *Angewandte Chemie International Edition* **2020**, *59* (23), 8854–8859. https://doi.org/10.1002/anie.201914975.
(225) Spackman, P. R.; Turner, M. J.; McKinnon, J. J.; Wolff, S. K.; Grimwood, D. J.; Jayatilaka, D.; Spackman, M. A. CrystalExplorer: A Program for Hirshfeld Surface Analysis, Visualization and Quantitative Analysis of

Molecular Crystals. *J Appl Cryst* **2021**, *54* (3), 1006–1011. https://doi.org/10.1107/S1600576721002910.
(226) GaussView, V. 5, Wallingford, CT, Gaussian. Inc 2009.
(227) Al-Wahaibi, L. H.; Joubert, J.; Blacque, O.; Al-Shaalan, N. H.; El-Emam, A. A. Crystal Structure, Hirshfeld Surface Analysis and DFT Studies of 5-(Adamantan-1-Yl)-3-[(4-Chlorobenzyl)Sulfanyl]-4-Methyl-4H-1,2,4-Triazole, a Potential 11β-HSD1 Inhibitor. *Scientific Reports* **2019**, *9* (1), 19745. https://doi.org/10.1038/s41598-019-56331-z.
(228) Sepay, N.; Saha, P. C.; Shahzadi, Z.; Chakraborty, A.; Halder, U. C. A Crystallography-Based Investigation of Weak Interactions for Drug Design against COVID-19. *Physical Chemistry Chemical Physics* **2021**, *23* (12), 7261–7270. https://doi.org/10.1039/D0CP05714B.
(229) Ali, A.; Sepay, N.; Afzal, M.; Sepay, N.; Alarifi, A.; Shahid, M.; Ahmad, M. Molecular Designing, Crystal Structure Determination and in Silico Screening of Copper(II) Complexes Bearing 8-Hydroxyquinoline Derivatives as Anti-COVID-19. *Bioorganic Chemistry* **2021**, *110*, 104772. https://doi.org/10.1016/j.bioorg.2021.104772.
(230) Sheldrick, G. M. Phase Annealing in SHELX-90: Direct Methods for Larger Structures. *Acta Cryst A* **1990**, *46* (6), 467–473. https://doi.org/10.1107/S0108767390000277.
(231) SHELDRICK, G. M. SHELXL-97. *Program for crystal-structure refinement* **1997**.

List of Publications:

1. Majumder, L., Chatterjee, M., Bera, K., Maiti, N.C. and Banerji, B., 2019. Solvent-assisted tyrosine-based dipeptide forms low-molecular weight gel: preparation and its potential use in dye removal and oil spillage separation from water. *ACS omega*, *4*(11), pp.14411-14419.

2. Banerji, B., **Majumder, L**. and Adhikary, S., 2018. A Metal-Free Oxidative Carboannulation Approach towards Synthesis of 2, 3-Diarylindenones and Its Regioisomers. *ChemistrySelect*, *3*(5), pp.1381-1384.

3. Banerji, B., Adhikary, S., **Majumder, L**. and Ghosh, S., 2019. A Green Synthetic Approach towards Polyarylated Oxazoles via Iodine-Catalyzed One-Pot sp3 C− H Functionalization in Water: From Natural Product Synthesis To Photophysical Studies. *Asian Journal of Organic Chemistry*, *8*(4), pp.514-525.

4. Banerji, B., Chatterjee, S., Chandrasekhar, K., Bera, S., **Majumder, L**., Prodhan, C. and Chaudhuri, K., 2017. Expedient synthesis of a phenanthro-imidazo-pyridine fused heteropolynuclear framework via CDC coupling: a new class of luminophores. *Organic & biomolecular chemistry*, *15*(19), pp.4130-4134.

5. Adhikary, S**., Majumder, L**., Pakrashy, S., Srinath, R., Mukherjee, K., Mandal, C. and Banerji, B., 2020. Polysubstituted Imidazoles as LysoTracker Molecules: Their Synthesis via Iodine/H_2O and Cell-Imaging Studies. *ACS omega*, *5*(24), pp.14394-14407.

6. NMR and Vibrational Spectroscopic Studies on the Structure and Self-Assembly of Two de novo Dipeptides in Methanol. **Leena Majumder**, Kaushik Bera, Krishnendu Khamaru, Uttam Pal, Nakul C. Maiti and Biswadip Banerji. (in communication)

ACS OMEGA

Article

Cite This: ACS Omega 2019, 4, 14411−14419

http://pubs.acs.org/journal/acsodf

Solvent-Assisted Tyrosine-Based Dipeptide Forms Low-Molecular Weight Gel: Preparation and Its Potential Use in Dye Removal and Oil Spillage Separation from Water

Leena Majumder,[†] Moumita Chatterjee,[†] Kaushik Bera,[§] Nakul Chandra Maiti,[§] and Biswadip Banerji*[,†,‡]

[†]Organic and Medicinal Chemistry Division, [‡]Academy of Science and Industrial Research, and [§]Structural Biology and Bioinformatics Division, CSIR—Indian Institute of Chemical Biology, Jadavpur, Kolkata 700032, India

Supporting Information

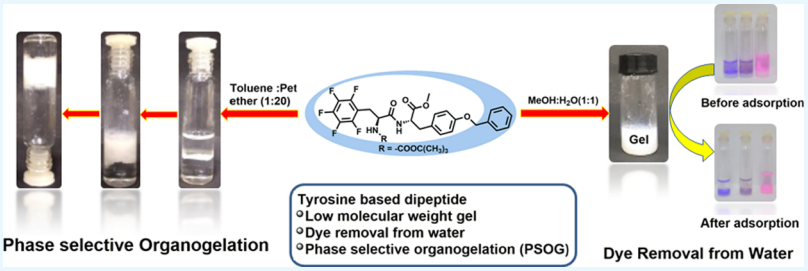

ABSTRACT: Low-molecular weight gelators (supramolecular, or simply molecular gels) are highly important molecular frameworks because of their potential application in drug delivery, catalysis, pollutant removal, sensing materials, and so forth. Herein, a small dipeptide composed of *N*-(*tert*-butoxycarbonyl)pentafluoro-L-phenylalanine and O-benzyl-L-tyrosine methyl ester was synthesized, and its gelation ability was investigated in different solvent systems. It was found that the dipeptide was unable to form gel with a single solvent, but a mixture of solvent systems was found to be suitable for the gelation of this dipeptide. Interestingly, water was found to be essential for gelation with the polar protic solvent, and long-chain hydrocarbon units such as, petroleum ether, kerosene, and diesel, were important for gelation with aromatic solvents. The structural insights of these gels were characterized by field-emission scanning electronic microscopy, atomic force microscopy, Fourier transform infrared analysis, and X-ray diffraction studies, and their mechanical strengths were characterized by rheological experiments. Both of the gels obtained from these two solvent systems were thermoreversible in nature, and these translucent gels had potential application for the treatment of waste water. The gel obtained from dipeptides with methanol−water was used to remove toxic dyes (crystal violet, Eriochrome Black T, and rhodamine B) from water. Furthermore, the gel obtained from dipeptide with assistance from toluene−petroleum ether was used as a phase-selective gelator for oil-spill recovery.

INTRODUCTION

The peptide and amino acid-derived supramolecular gels are currently an important class of materials which have attracted significant interest because of their potential applications in advance material science, pharmaceutical preparation, drug delivery, oil-spill recovery, and as environmental pollutant-removing agents.[1−14] Gels can be defined as soft materials in which solvent molecules self-assemble into one-dimensional structure that entraps and cross links to constitute a network.[15−17] This has the ability to immobilize a particular solvent. In other words, gels are formed under suitable conditions where solvent molecules are trapped into a three-dimensional architecture.[18−20] Most of the gels are polymeric materials and hyper-branched dendritic molecules. However, low-molecular weight gels or supramolecular gels are another fascinating class of materials because of their unique applications.[21−23] These gelator molecules were formed via various noncovalent interactions such as-hydrogen bonds, van der Waals forces, $\pi-\pi$ stacking, dipole−dipole, charge-transfer coordination interactions, and solvophobic effects.[24−33] Among the abovementioned interactions, hydrogen bonding and/or $\pi-\pi$ interactions are responsible for their gelatinous nature. In recent era, low-molecular weight gelators in organic and aqueous solvents were explored, having ample applications in nanomedicine, catalysis, light-harvesting, tissue engineering, sensing, templating, and nanoelectronics.[21−23]

With the development and industrialization of human civilization, there has been acute shortage of clean and hygienic water throughout the world.[34,35] The degradation and contamination of water by harmful chemicals has made our natural resources (rivers, lakes, oceans, etc.) a great threat to us.[34,36] Nowadays, water purification has become a matter of utmost importance in contemporary environmental research. The exclusive characteristics of supramolecular gels, that is,

Received: May 6, 2019
Accepted: June 27, 2019
Published: August 27, 2019

DOI: 10.1021/acsomega.9b01301
ACS Omega 2019, 4, 14411−14419

ChemPubSoc Europe

DOI: 10.1002/slct.201702843

Chemistry SELECT Full Papers

Catalysis

A Metal-Free Oxidative Carboannulation Approach towards Synthesis of 2,3-Diarylindenones and Its Regioisomers

Biswadip Banerji,*[a, b] Leena Majumder,[a] and Saswati Adhikary[a]

A metal free, PIDA (Iodosobenzene diacetate) mediated radical oxidative annulation of aromatic aldehydes with 1,2-diphenylethyne was developed, resulting an array of 2,3-diaryl indenones in moderate to good yields. This methodology requires no preactivation of the aldehyde groups and involves activation of the C(sp)-C(sp) bond of the internal alkyne by in situ generated acyl radical under metal free condition. This procedure is applicable to a large variety of functionalized substrates specially heterocyclic aldehydes and ortho hydroxyl aromatic aldehydes to give 2,3-diaryl indenones. Interestingly, meta substituted aromatic aldehyde provided two regioisomers in 1:1 ratio when they were subjected to the experimental condition. These two regioisomers were isolated by column chromatography and their colour, spectral data and crystal structures were investigated.

Introduction

Transition metal catalyzed organic synthesis had been ever popular since its inception.[1] However slowly metal-free organic reactions have gained attention in both industry and academia because these are environmentally benign, cost and step-economical.[2] Annulation reaction is one which creates carbocycles very efficiently.[3] More than one carbocycles can be stitched together simultaneously forming several new bonds through annulations process. Hence this step economical process would certainly reduce the chances of many by-products. Indenone is a privileged heterocycle that represents an important class of building blocks.[4] It was found to have broad application in synthetic chemistry, material chemistry and medicinal chemistry.[4b,5] It exists in a considerable number in many naturally occurring and biologically active molecules. Such as stem bark of *vaticapaucifora* contains paucifloral F and stem of *cissusquadragularis* consists of quadraguarin A, which have indenone moiety and act as an inhibitors for cancer growth.[4b,6] Considering their importance, a number of synthetic methods are available in the literature to access diverse indenone skeleton. Among them, several transition metal catalyzed methodologies were reported in the literature. For example Kuninobu and Takai described rhenium catalyzed trimerization of the aryl aldehyde for the synthesis of indenone moiety.[7] Chatani et al reported a Rh-catalyzedreaction of alkynes with 2-bromophenylboronic acids involving carbonylative cyclization to produce indenones[8] (Scheme 1). Larock et al showed a carbopalladation of 2-iodoarenennitrilemethodology using alkyne substrates to generate 2,3-diaryl indnones[9] (Scheme 1). However annulation of alkynes with ortho-bifuc-

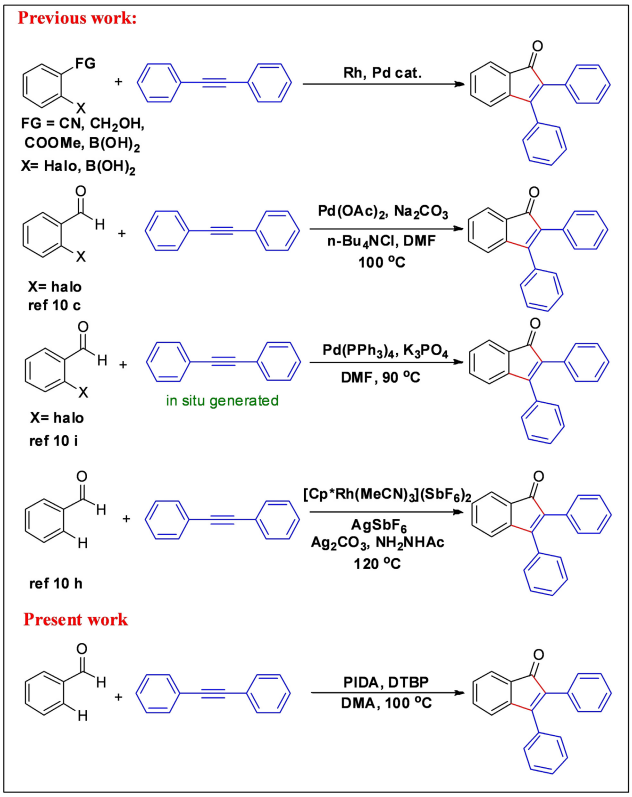

Scheme 1. Indenone Synthesis.

[a] *Dr. B. Banerji, L. Majumder, S. Adhikary*
Organic & Medicinal Chemistry Division
Indian Institute of Chemical Biology
CSIR-IICB
4, Raja S. C. Mullick Road, Jadavpur, Kolkata-700032, India
E-mail: biswadip.banerji@gmail.com
biswadip@iicb.res.in

[b] *Dr. B. Banerji*
Academy of Council of Scientific & Industrial Research (AcSiR)
CSIR-IICB
Kolkata, India

Supporting information for this article is available on the WWW under https://doi.org/10.1002/slct.201702843

A Green Synthetic Approach Towards Polyarylated Oxazoles Via Iodine Catalyzed One Pot sp^3 C-H Functionalization In Water : From Natural Product Synthesis To Photophysical Studies

Biswadip Banerji,* [a,b] Saswati Adhikary[a], Leena Majumder[a] and Saswati Ghosh[a]

Abstract: A 'green' methodology for the convenient synthesis of specific regioisomer of polysubstituted oxazoles through iodine catalyzed, water-mediated, aerobic oxidative C(sp^3)–H functionalization of primary amines was developed. This domino procedure is a toxic peroxide, transition-metal and organic solvent free, mild and regioselective. The versatility of this methodology was demonstrated by preparing a natural product, texaline. It is also scalable and having wide of substrate scope. This methodology opens up a new, simple avenue for the synthesis of polyarylated oxazole moiety from various readily available amines as well as 1,2-diketones and acyloins (alpha hydroxyl ketones) in moderate to excellent yields. Furthermore, these highly substituted oxazole molecules showed excellent fluorescence properties and thus have enormous potential to be a new type of fluorescent probe for the use in medicinal as well as material science.

Introduction

Recently, sp^3 C-H bond functionalization has gained great interests. Organic reactions carried out under metal-free conditions have become popular due to the drawbacks of expensive, toxic, and air-sensitive metals or organometallics. Iodine serves as an alternative catalyst for transition metals in many reactions [1]. Studies show that molecular iodine has the capability to functionalize carbon-hydrogen bonds to form new carbon-carbon and carbon-hetero bonds as well[2]. Iodine is insensitive to air and moisture and can also be removed from the reaction mixture by simple washing with reducing agents. Till now, an enormous number of organic synthesis have been successfully carried out in aqueous medium[3]. Water is non-flammable, non-toxic, non-hazardous, inexpensive environmentally benign as well as readily obtainable solvent in nature.

Scheme 1: Biologically active molecules having oxazole scaffold.

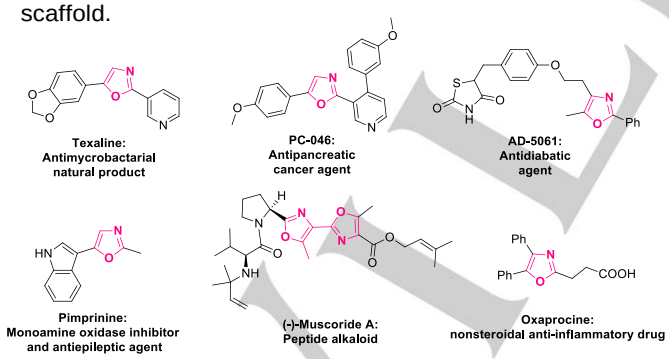

Scheme 2: Synthetic strategies for synthesis of oxazoles from 1,2-diketones and alpha hydroxy ketone.

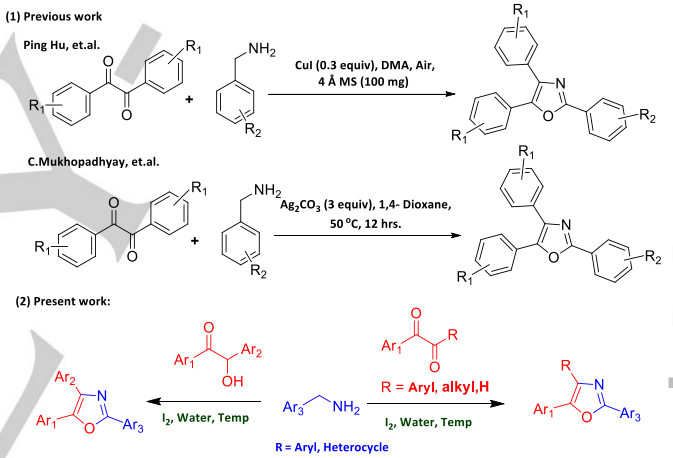

In organic synthesis, cascade reaction is an efficient and atom-economical methodology as it offers several advantages like avoiding multiple steps, long time duration and purification of the intermediates. Oxazole framework belongs to one of the most widely occurring scaffolds found in many pharmaceutically active compounds, and natural products which exhibit attractive biological activities[4]. For instance antimycobacterial natural product texaline[5], non-steroidal anti-inflammatory drug oxaprozin[6] and aristoxazole[7], anti-pancreatic cancer agent PC-046[8] contain oxazole in their framework[9] (**Scheme 1**). Oxazole scaffolds also have important application in fluorescence dyes[10], polymers[11] and are also essential building blocks in synthetic organic chemistry[12]. Due to numerous importance of this scaffold, several synthetic methodologies were developed to construct fully functionalized oxazoles[13].

Very recently easily accessible 1,2-diketone (benzil) were exploited for the synthesis of fully substituted oxazole [4d, 14]**(Scheme 2)**. Regardless of their applicability and broad substrate scope, these methods suffer from limitations of transition metal reagent and organic solvents. Therefore environmentally benign chemical processes are still in high demand. From these points, the progress of synthetically more

[a] Dr. B. Banerji, S. Adhikary, L. Majumder & S. Ghosh *Organic and Medicinal Chemistry Division, Indian Institute Of Chemical Biology (CSIR-IICB), 4 Raja S. C. Mullick Road, Kolkata, 700032, India.*

[b] Dr. B. Banerji *Academy of Scientific and Innovative Research (AcSIR), Indian Institute of Chemical Biology (CSIR-IICB), 4 Raja S. C. Mullick Road, Kolkata, 700032, India Corresponding Author Email Address: biswadip.banerji@gmail.com, biswadip@iicb.res.in; Fax: +91 33 24735197, +91 33 24723967 ; Tel : + 91 33 24995709*

Supporting information for this article is given via a link at the end of the document.

ACS OMEGA

http://pubs.acs.org/journal/acsodf

Article

Polysubstituted Imidazoles as LysoTracker Molecules: Their Synthesis via Iodine/H_2O and Cell-Imaging Studies

Saswati Adhikary, Leena Majumder, Sourav Pakrashy, Ravuri Srinath, Kaustuv Mukherjee, Chitra Mandal, and Biswadip Banerji*

Cite This: *ACS Omega* 2020, 5, 14394−14407

Read Online

ACCESS | Metrics & More | Article Recommendations | Supporting Information

ABSTRACT: An iodine-catalyzed, environmentally benign one-pot methodology has been developed for the synthesis of diverse substituted imidazoles. This transition-metal-free, aerobic, water-mediated cyclization reaction is operationally simple and works well with different amines or aldehydes by multiple C−N bond formations with satisfactory yield. The methodology is regioselective as well as scalable. These imidazole derivatives show excellent fluorescence properties both in the solid and solution phase, which is further extended to live-cell imaging. Due to the suitable fluorescence properties of these scaffolds, lysosome-directing groups are incorporated in two of these derivatized imidazoles to track intracellular lysosomes. Successfully, those molecules show bright blue fluorescence while detecting lysosomes in human or murine cells and can be considered to be rapid lysosome-staining probes.

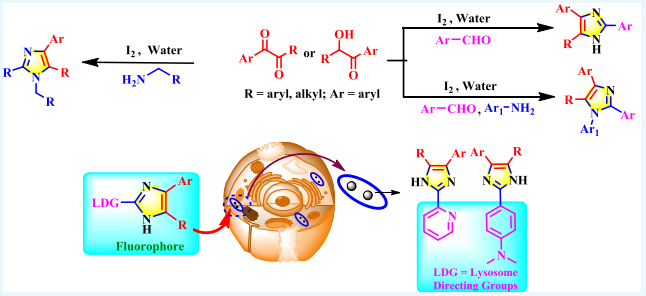

INTRODUCTION

Imidazoles are the most important privileged nitrogen-containing heterocyclic scaffolds present in many natural products and pharmaceutical drugs (Figure 1).[1−5] They are known to exhibit a broad range of biological activities, such as anticancer, antimicrobial, antihypertensive, and protein kinase inhibitor properties.[6−10] Apart from these activities, imidazole-containing molecules are also reported to exhibit fluorescence properties. These properties are further utilized in metal sensing, biological imaging applications, and organic light-emitting diodes (OLEDs).[11−15] A lysosome is an important organelle in eukaryotic cells that is involved in the degradation of foreign internalized particles. Lysosomes also play an active role in autophagy, cellular metabolism and recycling. Thus, it becomes an important candidate for immunological research, where the resolution of infection is often dependent on lysosome-mediated degradation of engulfed pathogens by phagocytic immune cells, such as macrophages and neutrophils. Lysosome-dependent processing of pathogens is also related to antigen display and antibody production.[16] These organelles are involved in many cellular signaling functions, including intracellular transport, cell antigen processing, and the initiation of apoptosis.[17,18] Lysosomes are acidic, membrane-bound organelles (pH ≤5) present in cells. Dysfunctions of lysosomes have been implicated in several diseases, such as tumour generation and neurodegenerative diseases.[16] Selective probing of these organelles with small fluorescent molecules has been reported recently, and further, these probes are useful to reveal the underlying mechanism behind the cause of diseases.[19]

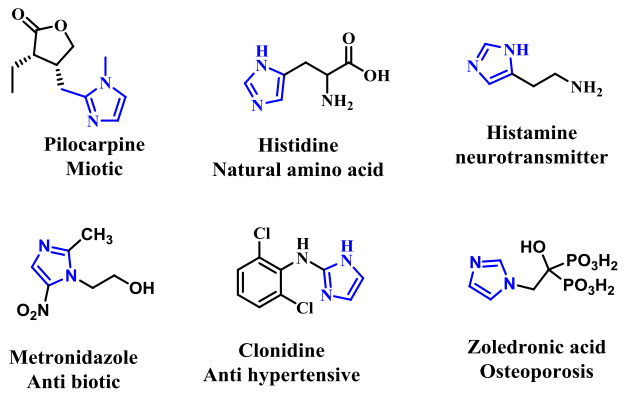

Figure 1. Some of the important imidazole-containing natural products and drugs.

In the previous literature, these imidazole molecules were synthesized using transition-metal-catalyzed approaches, with transition metals such as copper, palladium, silver, etc., but these synthetic approaches practically have several drawbacks,

Received: March 2, 2020
Accepted: March 31, 2020
Published: June 11, 2020

https://dx.doi.org/10.1021/acsomega.0c00934
ACS Omega 2020, 5, 14394−14407

Organic & Biomolecular Chemistry

PAPER

View Article Online
View Journal | View Issue

Cite this: *Org. Biomol. Chem.*, 2017, **15**, 4130

Expedient synthesis of a phenanthro-imidazo-pyridine fused heteropolynuclear framework *via* CDC coupling: a new class of luminophores†

Biswadip Banerji,*[a,b] Satadru Chatterjee,[a] K. Chandrasekhar,[a] Suvankar Bera,[a] Leena Majumder,[a] Chandraday Prodhan[c] and Keya Chaudhuri[c]

Received 6th March 2017,
Accepted 16th March 2017

DOI: 10.1039/c7ob00564d

rsc.li/obc

We herein report the design and synthesis of a group of fused phenanthro-imidazo[1,2-*a*]pyridine derivatives as a new class of luminescent materials through a Pd(II) catalyzed intramolecular CDC (cross dehydrogenative coupling) reaction. This method thus unlocked a convenient & expedient way for the synthesis of a new molecular framework containing π-extended fused heteropolycycles. The heteropolycycles showed very good fluorescence properties both in solid and solution phases which were further utilized in live cell imaging. These kinds of molecules have potential to be used as therapeutic probes and also their solid state luminescence properties can be further utilized for making optoelectronic devices.

Introduction

In recent years, different fused aromatic motifs have attracted considerable interest due to their enormous applications in different fields. Among different fused motifs, N-fused heterocycles dominate due to their significant biological importance[1,2] and presence in a wide class of natural products and functional materials.[3–6] The construction of new heteropolycycles through C–H bond functionalization is highly challenging. It has always been a challenge to synthesize versatile fused heteropolycycles by a simple, convenient, and high yielding method. Serious research efforts are ongoing to construct a new class of fused heteropolycycles using a transition metal catalyzed C–H bond functionalization procedure[7,8] which is atom economical and cost efficient. C–C bond formation through direct dehydrogenative cross coupling is one of the most used methods to construct fused heteropolycycles.[9–12] Recently, arylation of different heterocycles like pyrroles,[13] azoles,[14,15] phenanthroimidazoles,[16,17] polyfluoroarenes,[18,19] benzo[*h*]quinolines,[20,21] *etc.* through direct dehydrogenative cross coupling reactions using various transition metals as catalysts has been reported. It was observed that among different transition metals, palladium is widely used due to its catalytic and synthetic efficiencies. Recently, different functionalized imidazo[1,2-*a*]pyridines[22] are in the limelight due to their appealing and vast applications. Imidazo[1,2-*a*]pyridine is an important pharmacophore found in various natural products as well as in some marketed drugs like zolimidine (antiulcer), alpidem (anxiolytic), zolpidem (hypnotic), *etc.*[23–28] Some of these classes of molecules have also made great contributions in the field of materials science (Fig. 1).[29]

In the present study, we have synthesized a new class of imidazo[1,2-*a*]pyridine heteropolycycles using dehydrogenative cross coupling as a key step (Fig. 2). An optimized reaction condition was established for synthesizing these new heteropolycycles and thereafter their photophysical properties were examined thoroughly.

Due to the extended conjugation through π-expansion, the synthesized molecules have shown interesting fluorescence properties both in the solution and solid phases which were further applied in live cell imaging studies. Our studies there-

[a]*Organic & Medicinal Chemistry Division, Indian Institute of Chemical Biology (CSIR-IICB), 4 Raja S. C. Mullick Road, Kolkata, 700032, India*
[b]*Academy of Scientific and Innovative Research (AcSIR), Indian Institute of Chemical Biology (CSIR-IICB), 4 Raja S. C. Mullick Road, Kolkata, 700032, India.*
E-mail: biswadip.banerji@gmail.com, biswadip@iicb.res.in; Fax: +91 33 24735197, +91 33 24723967; Tel: +91 33 24995709
[c]*Molecular Genetics, Indian Institute of Chemical Biology (CSIR-IICB), 4 Raja S. C. Mullick Road, Kolkata, 700032, India*

†Electronic supplementary information (ESI) available. CCDC 1515438. For ESI and crystallographic data in CIF or other electronic format see DOI: 10.1039/c7ob00564d

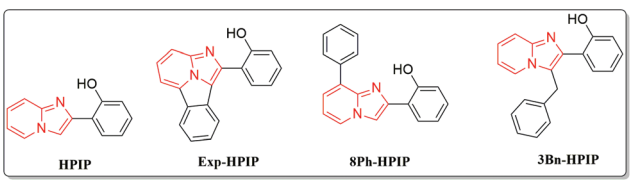

Fig. 1 Some reported imidazo[1,2-*a*]pyridine derivatives[29] having very distinct optical properties, and exhibiting excited state intramolecular proton transfer (ESIPT).